Università degli Studi di Parma

Dottorato di ricerca in Scienze Chimiche

XXII Ciclo

Anni accademici 2007-2009

Synthesis and Properties of Calix[n]arene Receptors for the Preparation of "Active" Organic-Inorganic Hybrid Materials

Tutors:
Dr. Andrea Secchi
Prof. Andrea Pochini

Dottorando:
Luca Pescatori

2010

A M D G

Contents

Chapter 1:
The role of Supramolecular Chemistry in the Nanosciences

Chapter 1. The role of Supramolecular Chemistry in the Nanosciences

1.1 A brief introduction to Nanosciences

Nanotechnology and *Nanosciences*[1] are two terms nowadays very often associated and interchanged.[2] The term *Nanotechnology* well describes the technological development of devices and materials having nanometric size, which are assuming an increasing relevance in important areas such as healthcare, information and communication technology (ICT) and energy storage. The term *Nanosciences* more properly describes all the scientific disciplines investigating the relationship between properties and the structure of the matter at the namometric scale (from 1 to 1000 nm). This "matter" indeed is endowed with properties that are different and very often more enticing than those associated with the macroscopic world.

Many kinds of nanomaterials and nanodevices have been developed in the last twenty years as inorganic-organic *hybrid materials*,[3] which are constituted by an ensemble of organic and inorganic components. Hybrid materials are endowed with an intrinsic positive characteristic: they generally show superior properties compared with their pure counterparts. Two principles are employed in the synthesis of hybrid materials: the self-assembly of the building blocks that constitute the hybrid material and the use of templates that can self-assemble and give a shape to the functional hybrid material. Very interesting examples of

1. For a series of introductory books on Nanosciences, Nanotechnology and Nanochemistry see e. g.: (a) C. P. Poole Jr, F. J. Owens, *Introduction to Nanotechnology*, John Wiley & Sons, Hoboken New Jersey, 2003; (b) *Nanoscale Materials in Chemistry*, Ed. K. J. Klabunde, John Wiley & Sons, New York, 2001; (c) *Handbook of Nanoscience, Engineering, and Technology*, Eds. W. A. Goddard, III, D. W. Brenner, S. E. Lyshevski, G. J. Iafrate, CRC Press, Boca raton, 2003; (d) *The Chemistry of Nanomaterials*, Eds: C. N. R. Rao, A. Müller, A. K. Cheetham, WILEY-VCH, Weinheim, 2004; (e) G. A. Ozin, A. C. Arsenault, L. Cademartiri, *Nanochemistry*, 2nd Ed, RSC Publishing, Cambridge, 2009.
2. The term "Nanotechnology" was used for the first time in 1986 by Kim Eric Drexler in his book *Engines of Creation: The Coming Era of Nanotechnology* (1986); nevertheless the first widely accepted "birth of nanotechnology" is found in the plenary lecture gave by Richard Feynman in 1959 at the annual meeting of the American Physical Society held at the California Institute of Technology (Caltech). In this famous lecture entitled "There's plenty of room at the bottom", Feynman evidenced that for the construction of very small dispositives the contribute of the force of gravity become less important, while the contribute of the Van der Waals interaction and surface tension between atoms and molecules, become foundamental. The lecture was first published in the February 1960 issue (Volume XXIII, No. 5, pp. 22–36) of Caltech's Engineering and Science. Its full transcript can be read at the following URL: http://www.zyvex.com/nanotech/feynman.html
3. See e. g.: (a) *Funtional Hybid Materials*, Eds.: P. Gomez-Romero, C. Sanchez,Wiley-VCH, Weinheim, 2004; (b) *Hybrid Materials. Synthesis, Characterization, and Applications*, Ed.: G. Kickelbick, Wiley-VCH, Weinheim, 2007.

hybrid materials are those obtained either by covering metal surfaces and metal nanoparticles (or nanorods) with an organic stabilizing shell (see Figure 1.1).

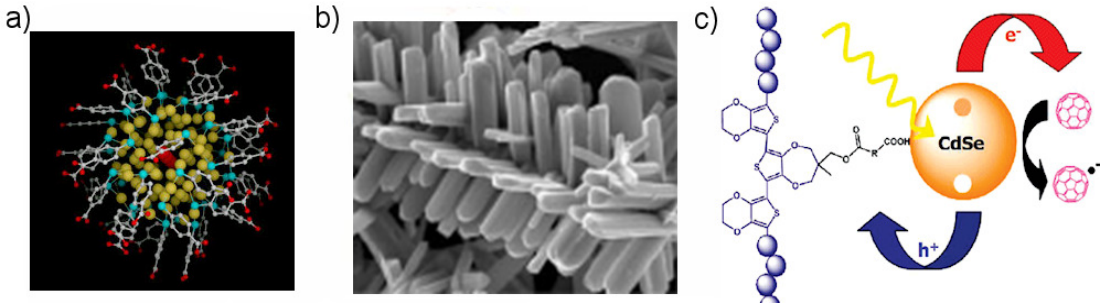

Figure 1.1 Organic-inorganic hybrid materials: a) Au MPCs; b) Au nanorods and c) CdSe quantum dosts.

In the first case we have 2D self assembled monolayers (2D SAMs),[4] while in the second monolayer protected clusters (MPCs or 3D SAMs).[5] The enticing aspect of these systems is that the nature of both the metal and the organic layer can address the properties of the resulting hybrid material. As an example, the functionalization of 2D and 3D SAM with receptors molecules, chromophores, catalysts etc could transform them in hybrid materials embedded with specific functions.

1.2 Nanosciences and Supramolecular Chemistry: what is the link?

The realization of a new functional nanomaterial or nonodevice is currently pursued by the "top-down approach". This approach, which leads physicists and engineers to manipulate progressively smaller pieces of matter by photolithography and related techniques, has operated in an outstanding way up until this time. It is becoming increasingly apparent, however, that the top-down approach is subject to drastic limitations for dimensions smaller than 100 nm.[6] An alternative and most promising strategy to exploit science and technology at the nanometer scale is offered by the "bottom-up approach", which starts from nano or subnanoscale objects (namely, atoms or molecules, see infra) to build up nanostructures endowed with specific functions. [7] The bottom-up approach can in principle benefit of the principles and methods devised by Supramolecular Chemistry, an interdisciplinary science devoted to the study of the weak intermolecular interactions occurring between ions and

4. (a) S. A. Di Benedetto, A. Facchetti, M. A. Ratner, T. J. Marks, *Adv. Mat.*, **2009**, *21*, 1407; (b) D. Zacher, O. Shekhah, C. Woell, R. A. Fischer, *Chem. Soc. Rev.*, **2009**, *38*, 1418.
5. See e. g.: *Nanoparticles – Building blocks for nanotechnology*, Ed.: V. M. Rotello, Kluwer Academic / Plenum Publisher, New York, 2004.
6. R. F. Service, *Science* **2001**, *293*, 785.
7. V. Balzani, A. Credi, M. Venturi, *Molecular Devices and Machines. A Journey into the Nanoworld*, VCH-Wiley, Weinheim, 2003.

molecules.[8] During last decade it became clear that supramolecular chemistry, through the application of the "bottom-up approach" opens virtually unlimited possibilities regarding the design of nanomaterials and nanoscale objects. The application of these principles allows for example the preparation of molecular devices of growing complexity through the self-assembly of simpler molecular components that are capable of performing specific functions upon stimulation with external energy inputs. A striking example of the application of these principles is represented by the artificial molecular nanorotor called "Sunny" (see Figure 1.2) developed by Balzani and co-workers,[9] that is able to rotate with a frequency of 60'000 cycle/minute through the application of light external stimuli.

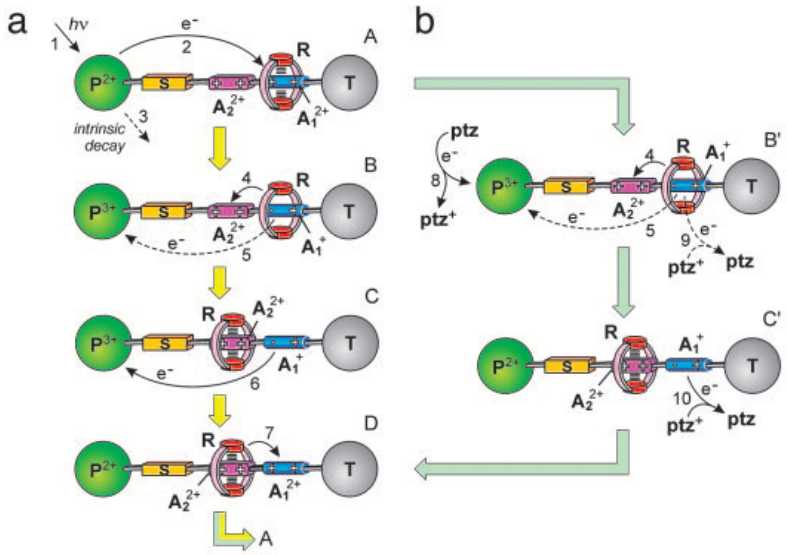

Figure 1.2 A prototype of molecular rotor that works through light external stimuli (by gently concession of PNAS, http://www.pnas.org/content/103/5/1178.full.pdf+html?sid=9e1ea2fc-fdda-44b1-9c94-fb0e7b919f83).

Among the several macrocyclic synthetic hosts that have been used ar receptors in Supramolecular Chemistry, Calix[n]arenes have been widely used as molecular platforms, on which a large variety of binding sites can be inserted and oriented in space, or as tridimensional receptors able to include into their aromatic cavities either neutral or charged species (see Chapter 2).[10] The results of the investigations carried out by our research group in the recent past have demonstrated that preorganized calix[4]arenes derivatives functionalized

8. J. W. Steed, D. R. Turner, K. J. Wallace, *Core Concepts in Supramolecular Chemistry and Nanochemistry*, John Wiley & Sons, Chichester, 2007.
9. V. Balzani, M. Clemente-Leon, A. Credi, B. Ferrer, M. Venturi, A. H. Flood, J. F. Stoddart, *PNAS*, **2006**, *106*, 1178.
10. (a) C. D. Gutsche, *Calixarenes Revisited, Monographs in Supramolecular Chemistry*, Ed.: J. F. Stoddart, Royal Society of Chemistry: Cambridge, U.K., 1998; (b) *Calixarenes in Action*, Eds.: L. Mandolini, R. Ungaro, Imperial College Press: London, 2000; (c) *Calixarenes 2001*, Eds.: Z. Asfari, V. Böhmer, J. Harrowfield, J. Vicens, Kluwer Academic: Dordrecht, 2001.

with hydrogen bond donor groups are potent receptors for ion pairs in low polar solvents,[11] while the corresponding calix[6]arene derivatives can be used as active components for the preparation of molecular machines prototypes.[11] We soon envisioned the potentiality of these compounds as "functional" stabilizers for 2D and 3D SAM. Indeed, a remarkable effort has been accomplished by our research group to transfer the unique binding abilities of calix[n]arene derivatives to the preparation of calixarene-based gold nanoparticles[12] and CdSe–ZnS core–shell quantum dots.[13]

Starting form these studies, in this thesis we deepen our knowledge on the synthesis and purification of calix[n]arene-based 2D and 3D SAM. The more challenging part it has been the study of their chemical characteristics and the evaluation of their self-assembly properties both in solution (3D SAM) and at the interface (2D SAM). The several arguments tackled during this thesis have been organized in chapters here briefly described:

Chapter 2 - **Calix[n]arenes as receptors.**

In this chapter are reported the recognition properties in solution and at the solid state of a series of calix[4]arene monotopic and heteroditopic receptors toward pyridinum-based ion pair. The study is then extended to the synthesis of ditopic bis-calix[4]arene "semitubes".

Chapter 3 - **Calix[4]arene-protected gold nanoparticles and MPCs.**

In this chapter is described the preparation and the characterization of a series of calix[4]arene-protected gold MPCs. The role played by the "sulphur denticity" of the calix[4]arene thiolated ligand as size control element for the MPC synthesis is also discussed. The last part of the chapter presents our studies on the formation in solution of low polar solvents of 3D networks of self-assembled Au MPCs driven by the complexation of proper difunctional guests.

Chapter 4 - **Calix[n]arene-based 2D Self-Assembled Monolayers.**

In the last chapter of thesis is described the synthesis of a series of calix[n]arene derivatives as protecting layer for the formation of 2D SAM on Si(100) and polycrystalline copper. The characterization and the complexing properties at solid-liquid interface of these novel functional 2D SAM are also described.

---

11. A. Arduini, A. Secchi, A. Pochini *Molecular Machines and Nanodevices - An ion-pair approach* in *Calixarenes in the Nanoworld*, Eds.: J. Vicens, J. Harrowfield, Springer, The Netherlands, 2007, pp. 63-88.
12. (a) T. R. Tshikhudo, D. Demuru, Z. Wang, M. Brust, A. Secchi, A. Arduini, A. Pochini, *Angew. Chem. Int. Ed.*, **2005**, *44*, 2913; (b) A. Arduini, D. Demuru, A. Pochini, A. Secchi, *Chem. Comm.*, **2005**, 645.
13. B. Gadenne, I. Yildiz, M. Amelia, F. Ciesa, A. Secchi, A. Arduini, A. Credi, F. M. Raymo, *J. of Mat. Chem.,* **2008**, *18*, 2022.

Chapter 2:

Calix[n]arenes as receptors

Chapter 2. Calix[n]arenes as Receptors

2.1 A brief history of Calixarenes

2.1.1 Synthesis

Among the several classes of synthetic macrocyclic compounds currently used as receptors (hosts) in supramolecular chemistry, the calix[n]arenes[1] have assumed a key role due to their synthetic accessibility and versatility. Calix[n]arenes belong to the class of $[1_n]$-metacyclophanes[2] and are cyclic oligomers having para-alkylphenolic units linked by methylene bridges (see figure 2.1). These compunds are obtained in very high yield through a one-step condensation of formaldehyde with p-*tert*-butyl phenol in basic conditions. Depending on the reaction conditions and the nature of the base employed, it is possible to synthesize macrocycles that contain from four to eight phenol units in the annulus, even though the most used ones are the calix[4]- and calix[6]arenes.

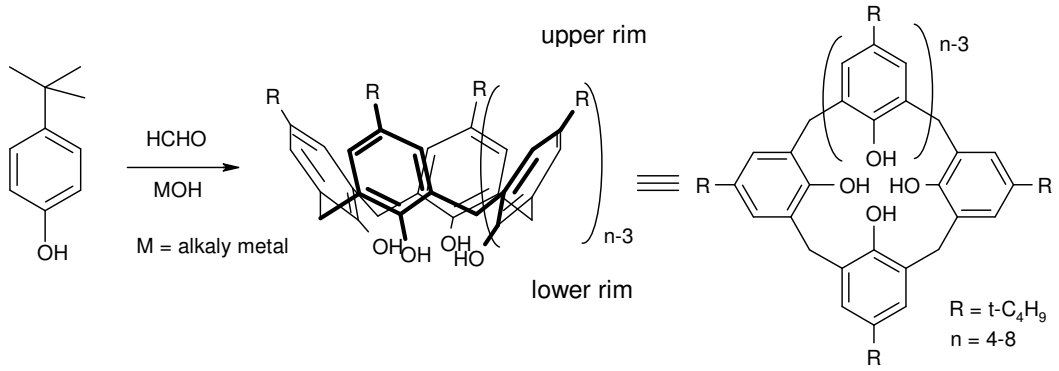

Figure 2.1 Synthesis of p-*tert*-butyl-calix[n]arene compounds (n= 4, 6 and 8).

The insertion of new functional groups on both "rims" (upper and lower see Fig. 2.1) of the macrocycle can be easily accomplished using common reactions typical of the organic chemistry. Such functionalization reactions allow, as an example, either the insertions of ancillary binding sites or the extension of the hosts aromatic cavity. For this reason

1. (a) C. D. Gutsche, *Calixarenes, Monographs in Supramolecular Chemistry*, Ed.: J. F. Stoddart, Royal Society of Chemistry: Cambridge, U.K., 1989; (b) C. D. Gutsche, *Calixarenes Revisited, Monographs in Supramolecular Chemistry*, Ed.: J. F. Stoddart, Royal Society of Chemistry: Cambridge, U.K., 1998; (c) *Calixarenes in Action*, Eds.: L. Mandolini, R. Ungaro, Imperial College Press: London, 2000; (d) *Calixarenes 2001*, Eds.: Z. Asfari, V. Böhmer, J. Harrowfield, J. Vicens, Kluwer Academic: Dordrecht, 2001; (e) C. D. Gutsche, *Calixarenes, An Introduction*, *Monographs in Supramolecular Chemistry*, Ed.: J. F. Stoddart, Royal Society of Chemistry: Cambridge, U.K., 2008
2. See *e. g.* F. Diederich, *Cyclophanes, Monographs in Supramolecular Chemistry*, Ed.: J. F. Stoddart, Royal Society of Chemistry: Cambridge, U.K., 1991.

calix[n]arenes can be considered as useful building block for the synthesis of new advanced receptors.[1]

2.1.2 Nomenclature and conventions

In the current nomenclature, the bracketed number (*i. e.* p-*tert*-butylcalix[4]arene) indicates the number of phenol units present in the macrocycle. The prefix "p-*tert*-butyl" defines the type of para alkylated phenol used during the synthesis. The nomenclature devised by the IUPAC for this class of macrocyles is too complicated for an ordinary use (the IUPAC name for p-*tert*-butyl calix[4]arene is 5,11,17,23-tetrakis(1,1-dimethylethyl)pentacyclo [19.3.1.1.1.1]octaosa 1(25),3,5,7(28),9,11,13(27),15,17,19(26),21,23-dodecaene-25,26,27,28-tetraol) and led Gutsche to introduce an unofficial but simpler nomenclature nowaday universally accepted. With this nomenclature, the macrocyles are numbered following the schemes gathered in figure 2.2.

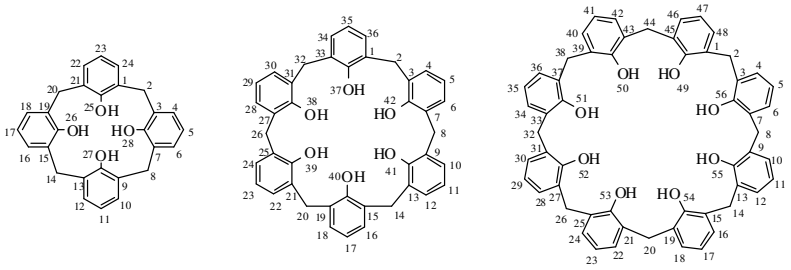

Figure 2.2 Conventional nomenclature of calixarenes devised by Gutsche.

2.1.3 Conformations of calixarenes

Calix[n]arenes are not rigid compounds and if not properly functionalized may adopt several conformations both in solution and in the solid state. These conformations are generated by the free rotation experienced by each aromatic ring with respect the others. The conformational behaviour of calix[4]arenes has been extensively studied. The most important conformation adopted by these compounds is called *cone* conformation. In this conformation all the phenolic nuclei are oriented in the same direction and a π-rich aromatic cavity is well defined (see Figure 2.3). The *cone* conformation is stabilized by the formation of four hydrogen bonds between the proximal phenolic groups (homodromic H-bond) and it is dominant at the solid state. The Brownian motion occurring in solution reduce the stability of this conformation at room temperature. As a consequence each phenolic ring can rotate through the annulus and thus the macrocycle can interconvert between the two limiting *cone* conformations depicted in Figure 2.3.

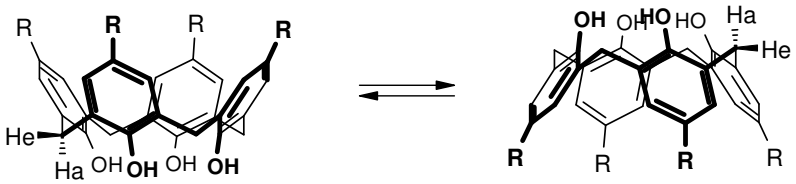

Figure 2.3 Typical interconversion between two limiting *cone* conformations of calix[4]arene in solution.

The annulus of the calix[4]arene is quite small and the rotation of the rings can occur only with the OH: the rate of conformational interconversion mainly depends on the nature of the solvent: the lowest $\Delta G^{\neq}$ value (13.7 Kcal mol^{-1}) has been found in pyridine, thus confirming that role played by hydrogen bonding in stabilizing the cone conformers.

It is important to observe that the two protons of each metylene "bridge" of calix[4]arenes blocked in *cone* conformation, are located in a different position with respect the aromatic nuclei (see figure 2.3). The protons that are almost perpendicular to the aromatic nuclei are named *equatorials*, while the other almost parallel are called *axial*. At the NMR, such protons experience a different magnetic environment giving rise to an AX system of two doublets coupled with a typical geminal coupling constant *J* of 13-16 Hz. The equatorials protons are "shielded" by the aromatic rings and thus they are upfield shifted with respect their common chemical shift, while those axials experience the opposite effect and hence are downfielded shifted.

Tetramethoxy and tetraethoxycalix[4]arenes are also conformationally mobile but the introduction at the lower rim of calix[4]arenes of alkyl group bulkier than ethyl, blocks the ring inversion process thus producing compounds with different stereochemistry, depending on the orientation of each aryl group which can project upward (*u*) or downward (*d*) relative to an average plane defined by the methylene bridges. The four different possible conformations have been named by Gutsche as *cone* (u, u, u, u), partial *cone* (u, u, u, d), 1,3-*alternate* (u, d, u, d) and 1,2-*alternate* (u, u, d, d) (see Figure 2.4).

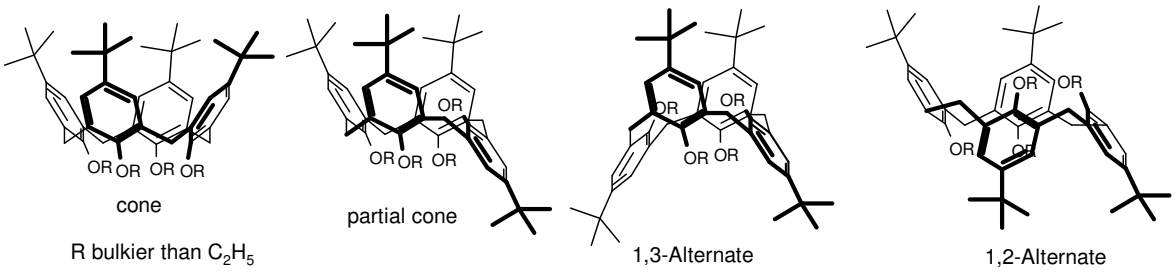

Figure 2.4 The four possible conformations of calix[4]arenes.

The conformational behaviour in solution of calix[6] and calix[8]arenes has been certainly less studied. These macrocycles experience a larger conformational mobility in

solution than calix[4]arenes since thay are endowed by a large annulus that allows the rotation of the phenolic rings from both the OH group and the para position of the aromatic ring. For this reason, any type of functionalization carried out on both rims of calix[6] and calix[8]arene derivatives cannot prevent these interconversion motions.

2.1.4 Functionalization of the calixarene macrocycle

Lower rim functionalization.

The functionalization of the phenolic hydroxy groups of calixarenes has been performed using a variety of alkylating and acylating agents. Most of the studies have been accomplished on the lower homologue of this class, that is the calix[4]arene, because the particular acidity properties of its OH groups can be exploited to address the regiochemistry of the functionalization reaction.[3] The partial functionalization of the lower rim of calix[4]arene in proximal 1,2 or distal 1,3 postion has been also accomplished by acting on the nature of the base employed during the alkylation reaction. Using a weak base, like the carbonate salts in dipolar aprotic solvents (acetone, acetonitrile), the distal dialykation is usually obtained in very high yields. Using a strong base like NaH in DMF, polyanions are obtained and the following alkylation reaction with an excess of alkylating agent usually afford tetralkylated calix[4]arenes in cone conformation.[1a,b,4]

Upper rim functionalization.

The facile removal of the *tert*-butyl groups present in the *para* position of the phenolic rings[5] with $AlCl_3$ allows the introduction on the upper rim of calix[n]arenes of several functional groups such as iodo, bromo, cyano, nitro, formyl, keto and hydroxy groups.[1] FGI reactions on these groups can be then accomplished to further extend the aromatic cavity of the macrocycle or to insert proper binding sites on the aromatic rings (see infra).

2.1.5 Complexing properties

Historically, calix[n]arenes have played an important role in *Supramolecular Chemistry* as receptors for neutral and charged species in solution, in the gas-phase and in the solid state.

---

3. A few efforts have been also made to address the problem of the regiochemical functionalization of the calix[6]arene lower rim see *e. g.*: A. Casnati, L. Domiano, A. Pochini, R. Ungaro, M. Carramolino, J. O. Magrans, P. M. Nieto, J. López-Prados, P. Prados, J. de Mendoza; R. G. Janssen; W. Verboon, D. N. Reinhoudt, *Tetrahedron*, **1995**, *51*, 12699.
4. See *e. g.* J.D. van Loon, A. Arduini, L. Coppi, W. Verboom, A. Pochini, R. Ungaro, S. Harkema, D.N. Reinhoudt, *J. Org. Chem.,* **1990**, *55*, 5639 and reference therein.
5. (a) C. D. Gutsche, J. A. Levine, *J. Am. Chem. Soc.,* **1982**, *104*, 2652; (b) C. D. Gutsche, J. A. Levine, P. K. Sujeeth, *J. Org. Chem.,* **1985**, *50*, 5802.

Several applications of calixarenes as sensors regard their employment as a molecular platform, that is, a scaffold on which few binding sites can be arranged to specifically recognize a guest species. As an striking example, the introduction of ester, amide or ketone functional groups through the proper functionalization of the lower rim phenolic groups has generated a plethora of efficient and selective receptors for positively charged species spanning from alkaline and alkaline-earth cations to lantanides and actinides.[1c,d]

The exploiting of the π-rich aromatic cavity of calixarenes as receptor site for the recognition of neutral molecules requires a high degree of preorganization of the macrocycle skeleton. Indeed, the recognition processes occurring between calixarene derivatives and neutral species are driven by weak intermolecular interactions, such as π-π and CH/π interactions,[6] which are maximized when the receptor (host) must not change its geometrical arrangement to interact with the substrate (guest). Owing to their large conformational flexibility, calix[6] and calix[8]arene derivatives have found only very few applications as receptors for neutral molecules (see infra). In the mid '90 several scientists operating in the field of *host-guest chemistry* were frustrated by the unexpected poor complexing behaviour showed in solution of low polar solvents by tetralkoxy calix[4]arenes blocked in the *cone* conformation. Variable temperature NMR experiments finally disclosed that *cone* tetralkoxy calix[4]arene derivatives experience a residual conformational mobility at room temperature. Indeed, they continuosly interchange between two limiting "flattened" (or "pinched") cone conformations having a C_{2v} symmetry (see figure 2.5).[7]

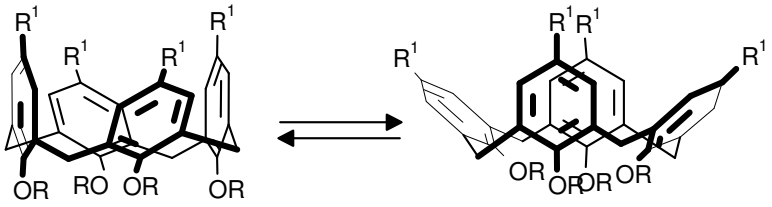

Figure 2.5 Interconversion in solution of tetraalkoxy calix[4]arene derivatives

Such motion obviously changes the effective shape of the π-rich aromatic cavity and prevents the onset of the weak CH/π intermolecular interactions. This problem was finally tackled through the intramolecular linkage of the macrocycle phenolic OHs with two short

6. See *e.g.*: (a) H. Takahashi, S. Tsuboyama, Y. Umezawa, K. Honda, M. Nishio, *Tetrahedron* **2000**, *56*, 6185; (b) S. Tsuzuki and A. Fujii, *Phys. Chem. Chem. Phys.*, **2008**, *10*, 2584; (c) M. Nishio and Y. Umezawa in *Topics in Stereochemistry*, Eds.: S. E. Denmark and J. S. Siegel, John Wiley & Sons, Hoboken, NJ, 2006, vol. 25, pp. 255-302; (d) M. Nishio, *Crystengcomm*, **2004**, 6, 130 and references therein
7. A. Arduini, M. Fabbi, M. Mantovani, L. Mirone, A. Pochini, A. Secchi, R. Ungaro, *J. Org. Chem.* **1995**, *60*, 1454.

alkyl chains in 1,2 and 3,4 position giving rise to class of calix[4]arene derivatives named biscrown-3-calix[4]arenes (see Figure 2.6).[7]

The short chains present on the lower rim of the macrocycle prevent the flattening of the cavity that assumes a pseudo C_4 symmetry. A similar cavity preorganization degree was obtained by reacting the OH groups with wolframium(VI) salts to yield wolframium-oxo hosts.[8] Finally it has been shown that also partially alkylated lower rim calix[4]arenes are highly preorganized in solution.[9] In the latter case, the preorganization was ascribed to the formation of strong hydrogen bonds between the non alkylated phenol groups with those alkylated. The aromatic cavity of calix[4]arenes preorganized and rigidified using these strategies has been successfully employed as binding site for *i.e.* neutral molecules containing relatively acidic C-H moieties (halogenated small molecules, ketones, *N*-methyl amides, nitriles and nitrometane) both in solution and in the solid state.[10]

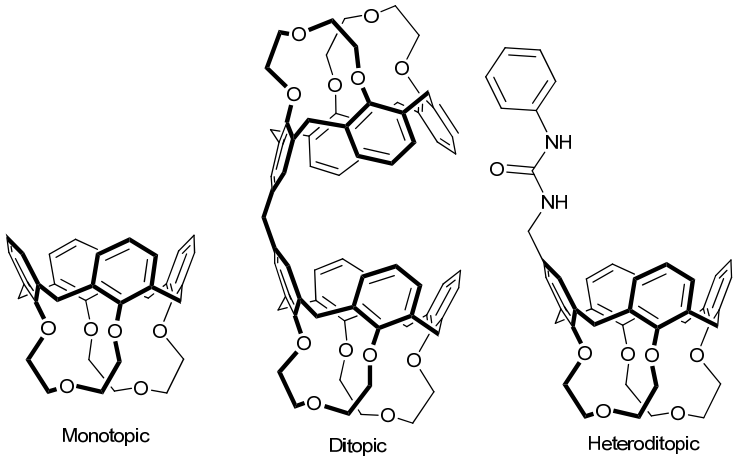

Figure 2.6 Structural representation of monotopic, ditopic and heteroditopic receptors for QUATS based on calix[4]arene derivatives.

Also calix[6]arenes have been employed as receptors for neutral species. For example, the poly-ammonium-calix[6]arene obtained through the protonation of the corresponding calix[6]aza-cryptand,[11] behaves as remarkable endo-receptors for small polar neutral molecules such as acetonitrile, DMSO and DMF. The self-assembled ion-paired caps close

8. See *e.g.* :(a) F. Corazza, C. Floriani, A. Chiesi-Villa, C. Rizzoli, *Inorg. Chem.*, **1991**, *30*, 4465; (b) B. Xu, Y.-J. Miao, T. M. Swager, *J. Org. Chem.*, **1998**, *63*, 8356; (c) A. Vigalok, Z. Zhu, T. M. Swager, *J. Am. Chem. Soc.*, **2001**, *123*, 7917; (d) A. Vigalok, T. M. Swager, *Adv. Mater.*, **2002**, *14*, 368.
9. W.Abraham, *J. Inclusion Phenom.*, **2002**, *43*, 159 and references therein.
10. (a) A. Arduini, W. M. McGregor, D. Paganuzzi, A. Pochini, A. Secchi, F. Ugozzoli, R. Ungaro, *J. Chem. Soc. Perkin Trans. 2*, **1996**, 839; (b) A. Arduini, G. Giorgi, A. Pochini, A. Secchi, F. Ugozzoli, *Tetrahedron*, **2001**, *57*, 2411; (c) G. Arena, A. Contino, A. Magri, D. Sciotto, A. Arduini, A. Pochini, A. Secchi, *Supramolecular Chemistry*, **2001**, *13*, 379; (d) A. Arduini, C. Massera, A. Pochini, A. Secchi, F. Ugozzoli, *New J. Chem.*, **2006**, *30*, 952.
11. U. Darbost, X. Zeng, M. Giorgi, I. Jabin, *J. Org. Chem.* **2005**, *70*, 10552.

the cavity, freeze the calixarene core in a cone conformation and stabilize the guests through hydrogen bonding and charge-dipole interactions.

In the last two decades calix[n]arenes have played an important role also as hosts for the complexation of organic salts in low polar solvents.[12] In these media, the organic salts are present as "tight" ion pairs and the π-rich aromatic cavity of calix[4]- and calix[6]arenes can be employed as a "soft" binding site for the cation by exploiting weak intramolecular interactions called cation/π interactions.[13] In this context, we have reported that calix[4]arene derivatives functionalized on the macrocycle upper rim with hydrogen bond donor groups can be used as receptors for ion-pairs. In the calix[4]arene series, the binding abilities of the aromatic cavities present in monotopic (one binding site),[10a,14] ditopic (two identical binding sites)[14] and heteroditopic (two different binding domains)[15] calix[4]arene derivatives (see Figure 2.6) were investigated toward a series of tetramethylammonium (TMA) ion pairs characterized by counteranions of different coordination strengths. In these studies, the positive cooperative action of two complementary binding domains on ion-pair recognition was evidenced.[15]

2.1.6 Calix[6]arene-based Pseudorotaxane and Rotaxane Structures

As seen in the introductory chapter, the recent developments of Supramolecular Chemistry[16] have extended the concept of machines and devices down to the molecular level. A *molecular machine* is defined as *an assembly of a number of molecular components that makes mechanical movements, designed to perform machine-like motions in response to appropriate external stimuli (chemical, photonics electrochemical etc.).*[17] Several molecular components have been successfully used to devise molecular machines. Among them, those

---

12. (a) D. E. Gross, F. P. Schmidtchen, W. Antonius, P. A. Gale, V. M. Lynch, J. L. Sessler, *Chem.Eur. J.*, **2008**, 14, 7822; (b) M. Hamon, M. Menand, S. Le Gac, M. Luhmer, V. Dalla and I. Jabin, *J. Org. Chem.*, **2008**, *73*, 7067; (c) M. D. Lankshear, I. M. Dudley, K. M. Chan, A. R. Cowley, S. M. Santos, V. Felix, P. D. Beer *Chem. Eur. J.*, **2008**, *14*, 2248; (d) S. Le Gac, I. Jabin *Chem. Eur. J.*, **2008**, *14*, 548; (e) M. D. Lankshear, N. H. Evans, S. R. Bayly, P. D. Beer *Chem. Eur. J.*, **2007**, *13*, 3861; (f) M. Cametti, M. Nissinen, A. Dalla Cort, L. Mandolini, K. Rissanen *J. Am. Chem. Soc.*, **2007**, *129*, 3641 and references therein.
13. See *e.g.*: (a) N. Zacarias, D. A. Dougherty, *Trends Pharmacol Sci* **2002**, *23*, 281; (b) J. P. Gallivan and D. A. Dougherty, *Proc. Natl. Acad. Sci. U.S.A.*, **1999**, *96*, 9459; (c) J. C. Ma and D. A. Dougherty, *Chem. Rev.*, **1997**, *97*, 1303 and references therein.
14. A. Arduini, A. Pochini, A. Secchi, *Eur. J. Org. Chem.*, **2000**, 2325.
15. (a) A. Arduini, G. Giorgi, A. Pochini, A. Secchi, F. Ugozzoli *J. Org. Chem.*, **2001**, *66*, 8302; (b) A. Arduini, E. Brindani, G. Giorgi, A. Pochini, A. Secchi *J. Org. Chem.*, **2002**, *67*, 6188;
16. J. W. Steed, D. R. Turner, K. J. Wallace, *Core Concepts in Supramolecular Chemistry and Nanochemistry*, John Wiley & Sons, Chichester, 2007
17. V. Balzani, A. Credi, M. Venturi, *Molecular devices and machines - A journey into the nano world* ,Wiley-VCH, Germany, **2003**.

belonging to the classes of *rotaxanes* and *pseudorotaxanes* seem to offer a wider potentiality.[18] In simple instances, a rotaxane is a mechanically-interlocked molecular architecture consisting of a dumbbell-shaped district that is threaded through a macrocycle or a ring-like component (see Figure 2.7). The two components are kinetically trapped as the two end-groups of the dumbbell (the stoppers) are larger than the internal diameter of the ring, thus preventing the dissociation (dethreading) of the components since this would require significant distortion or cleavage of covalent bonds. When the thread bears only one or no stopper, the system is a supramolecular complex the thermodynamic stability of which is dictated by the magnitude and nature of the non covalent intermolecular interactions that take place upon complex formation. This latter type of supramolecular complex is termed a pseudorotaxane.[18]

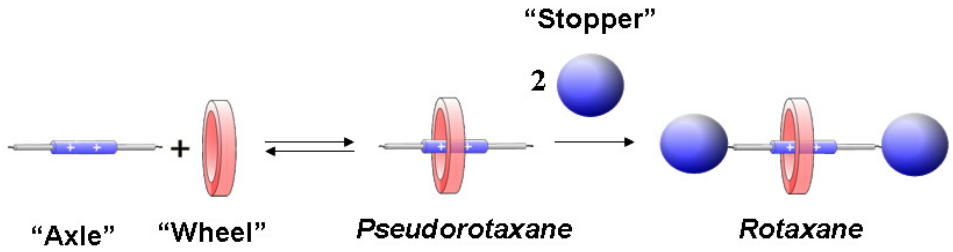

Figure 2.7 Schematic representation of pseudorotaxane and rotaxane.

In the recent years our research group has extensively used a triphenyluriedo calix[6]arene derivative as a wheel for the synthesis of rotaxanes and pseudorotaxanes[19] (see Figure 2.8a) with axles based on derivatives of 4,4'-bipyridinium salt (viologens). Calix[6]arene derivatives such as the one depicted in figure 2.9a have as important peculiarity, a truncated cone structure where an axle could, in principle, enter form the narrower or wider side, giving rise to oriented pseudorotaxanes or rotaxanes characterized by the univocal orientation of the wheel side with respect to the two termini of the axial component. Our research group has shown that it is possible to govern the threading process from the macrocycle upper rim using monostoppered asymmetrical axle to yield oriented

18. See e. g.: (a) P. R. Ashton, I. Baxter, M. C. T. Fyles, F. M. Raymo, J. F. Stoddart, A. J. P. White, D. J. Williams, *J. Am. Chem. Soc.*, **1988**, *120*, 2297; (b) M. Asakawa, P. R. Ashton. R. Ballardini, V. Balzani, M. Belohradsky, M. T. Gandolfi, O. Kocian, L. Prodi, F. M. Raymo, J. F. Stoddart, M. Venturi, *J. Am. Chem. Soc.*, **1997**, *119*, 302; (c) F. M. Raymo, J. F. Stoddart, *Chem. Rev.*, **1999**, *99*, 1643; (d) J.-P. Sauvage, C. O. Dietrich-Buchecker, Molecular Catenanes, Rotaxanes and Knots, Wiley-VCH, Weinheim, **1999**.
19. (a) A. Arduini, A. Credi, G. Faimani, C. Massera, A. Pochini, A. Secchi, M. Semeraro, S. Silvi, F. Ugozzoli, *Chem. Eur. J.*, **2008**, *14*, 98; (b) A. Credi, S. Dumas, S. Silvi, M. Venturi, A. Arduini, A. Pochini, A. Secchi, *J. Org. Chem.*, **2004**, *69*, 5881; (c) A. Arduini, F. Calzavacca, A. Pochini, A. Secchi, *Chem. Eur. J.*, **2003**, *9*, 793; (d) A. Arduini, R. Ferdani, A. Pochini, A. Secchi, F. Ugozzoli, *Angew. Chem. Int. Ed.*, **2000**, *39*, 3453.

pseudorotaxanes and rotaxanes.[19c] This behaviour was explained on the basis of the following observations: i) in low polar media the bipyridinium-based axles are present as tight ion pairs that cannot enter into the calix[6]arene cavity; ii) in low polar media the access of the axle into the cavity from the lower rim is prevented for sterical reasons by the inward orientation of the three methoxy groups present on the rim; iii) the access of the axle from the upper rim is favoured by the presence of three hydrogen bond donor ureido groups that are able to separate the ion-pair, thus pivoting the entrance of the bipyridinium axle into the cavity (see Figure 2.8b).

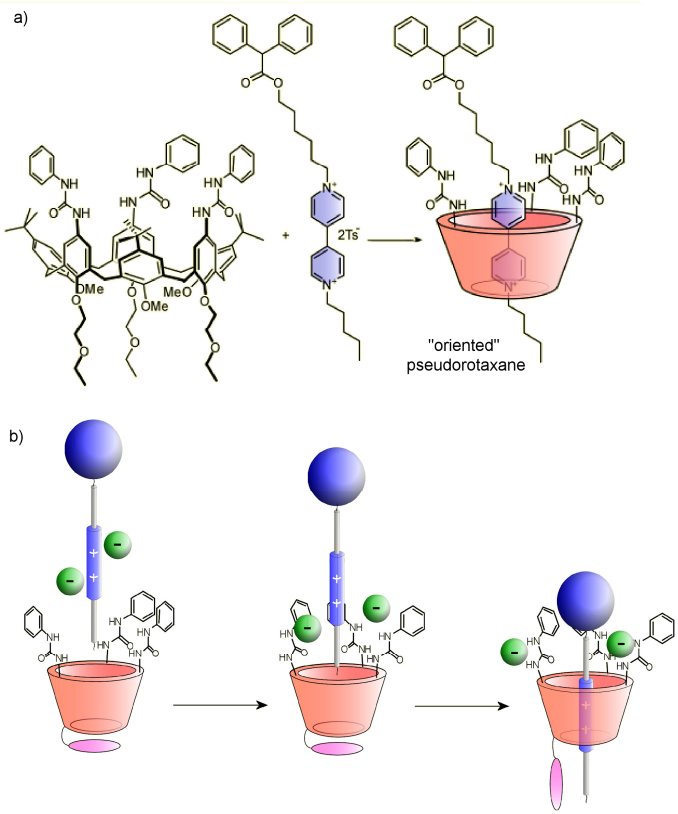

Figure 2.8 a) Formation of oriented "pseudorotaxanes" form tri-phenylureido-calix[6]arene-based "wheel" and monostoppered viologen-based "axle"; b) schematic representation of the selective threading process (the violet oval represents the three methoxy groups present onto the macrocycle lower rim).

The access to the cavity can be also controlled varying the polarity of the media where the threading process is carried out. In more polar media like acetonitrile, the threading process occurs also from the lower rim and it is thus possible to obtained almost equimolar mixture of the two different oriented pseudorotaxanes that can than be converted after the stopping reaction in the respectively mixture of the two oriented rotaxanes.[20]

20. A. Arduini, F. Ciesa, M. Fragassi, A. Pochini, A. Secchi, *Angew. Chem. Int. Ed.* **2005**, *44*, 278.

2.2 Calix[4]arene as receptors for pyridinium and viologen ion pairs[21]

As seen in Chapter 1 there is currently considerable interest to govern non covalent interactions among molecular level components for the construction of new functional materials through the bottom up approach. By adopting the principles and methods of supramolecular chemistry, remarkable examples exist where, through the insertion of the proper structural and chemical information within the components, the (non covalent) self-organisation of either neutral or charged species or a combination of both has been achieved.[22] As seen in the previous paragraph, calix[n]arenes derivatives have been extensively employed as receptors. Nevertheless, they have also found an important role as platforms for the construction of capsules[23] and higher order aggregates.[24] In this latter perspective, both anionic *p*-sulfonato calix[4]arenes[25] and thiacalix[4]arenes[26] have clearly demonstrated the ability to form fascinating extended superstructure.

Relatively less explored is the possibility to use neutral calixarene hosts for the construction of supramolecular architectures through ion pair recognition in which the calixarene cavity itself acts as binding site. Recent studies of our research group have shown that the presence of a phenylurea hydrogen bond donor sidearm on the upper rim of highly preorganized calix[4]arene strongly enhances the ability of the calixarene cavity to act as endo-cavity receptor site toward tetramethylammonium salts (see also paragraph 2.1.5).

The transfer of the chemical information stored in this system for the development of more complex switchable functional devices, such as supramolecular polymers and intelligent

---

21. This study has been published in: L. Pescatori, A. Arduini, A. Pochini, A. Secchi, C. Massera, F. Ugozzoli *Cryst. Eng. Comm.*, **2009**, *11*, 239; (b) L. Pescatori, A. Arduini, A. Pochini, A. Secchi, C. Massera, F. Ugozzoli *Org. Biomol. Chem.*, **2009**, *7*, 3698.
22. See for example: (a) J. D. Wuest *Chem. Commun*., **2005**, 5830; (b) M. Barboiu, G. Vaughanl, A. van der Lee *Org. Lett.*, **2003**, *5*, 3073; (c) L. Brunsveld, B. J. B. Folmer, E. W. Meijer, R. P. Sijbesma *Chem. Rev.*, **2001**, *101*, 4071.
23. (a) I. Vatsouro, E. Alt, M. Vysotsky, V. Böhmer *Org. Biomol. Chem.*, **2008**, *6*, 998; (b) I. Vatsouro, V. Rudzevich, V. Böhmer *Org. Lett.*, **2007**, *9*, 1375; (c) T. Amaya, J. Rebek *J. Am. Chem. Soc.*, **2004**, *126*, 14149; (d) A. M. Rincon, P. Prados, J. de Mendoza *Eur. J. Org. Chem.*, **2002**, 640; (e) J. J. Gonzalez, R. Ferdani, E. Albertini, J. M. Blasco, A. Arduini, A. Pochini, P. Prados, J. de Mendoza, *Chem. Eur. J.*, **2000**, *6*, 73; f) A. Arduini, L. Domiano, L. Ogliosi, A. Pochini, A. Secchi, R. Ungaro *J. Org. Chem.*, **1997**, *62*, 7866.
24. A. Casnati, F. Sansone, R. Ungaro *Acc. Chem. Res.*, **2003**, *36*, 246.
25. (a) Y. Liu, D.-S. Guo, H.-Y. Zhang, F. Ding, K. Chen, H.-B. Song *Chem. Eur. J.*, **2007**, *13*, 466; (b) S. J. Dalgarno, P. K. Thallapally, L. J. Barbour, J. L. Atwood *Chem. Soc. Rev.*, **2007**, *36*, 236; (c) C. B. Smith, L. J. Barbour, M. Makha, C. L. Raston, A. N. Sobolev *Chem. Commun.*, **2006**, 950; (d) G. W. Orr, L. J. Barbour, J. L. Atwood, *Science*, **1999**, *285*, 1049.
26. J. Martza, E. Grafa, M. W. Hosseini, A. De Ciana, N. Kyritsakas-Gruber, *C. R. Chimie*, **2002**, *5*, 481.

materials, [27,28] should be based on a deeper understanding of the supramolecular interactions that stabilise these complexes. This aspect is particularly important in those cases where either the cation or the anion does not have isotropic charge distribution, thus adding a further control element to the system.

On this premise, in this paragraph, is reported a systematic investigation we carried out on the parameters that affect the recognition of *N*-methylpyridinium and *N*,*N*'-dimethylviologen salts by monotopic (**1** and **2**) and heteroditopic (**3**-**4**) calix[4]arene-based receptors (see Fig. 2.9) in solution of low polar solvents[29] and in the solid state, by looking at both the structure of the host (preorganization and binding topicity) and the nature of the guest (charge effect and anion coordinating strength).

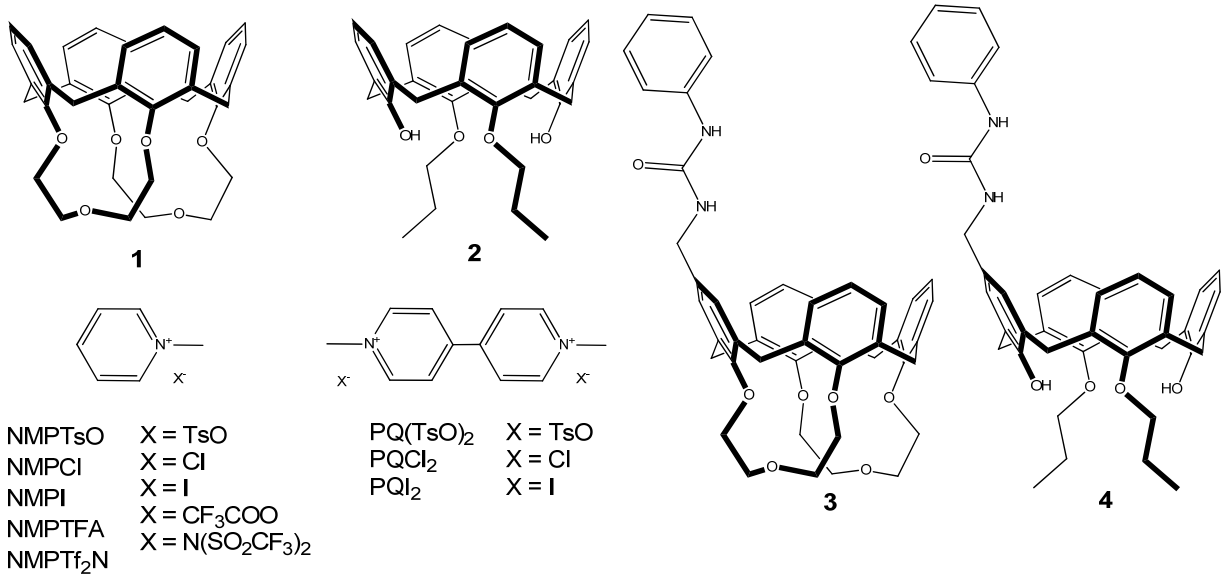

Figure 2.9 Structural formulae of the calix[4]arene-based receptors (**1**-**4**) and of the *N*-methyl pyridinium and *N*,*N*'-dimethyl viologen salts.

27. *Intelligent Materials*, eds. M. Shahinpoor and H.-J. Schneider, Royal Society of Chemistry, Cambridge, 2007;
28. *Supramolecular Polymers*, ed. A. Ciferri, Marcel-Dekker, New York, 2000; (c) C. Rao, *Supramolecular Organization and Materials Design*, Cambridge University Press, 2001.
29. For the recognition of *N*-alkyl pyridinium and *N*,*N*'-dialkyl dipyridinium salts by calix[n]arene derivatives in aqueous media see e.g.: (a) R. Kaliappan, Y. Ling, A. E. Kaifer, V. Ramamurthy, *Langmuir*, **2009**, *25*, 8982; (b) D.-S. Guo, K. Wang, Y. Lu, *J. Incl. Phenom. Macrocycl. Chem.*, **2008**, *62*, 1; (c) C. Gaeta, T. Caruso, M. Mincolelli, F. Troisi, E. Vasca, P. Neri, *Tetrahedron*, **2008**, *64*, 5370; (d) N. Korbakov, P. Timmerman, N. Lidich, B. Urbach, A. Sa′ar, S. Yitzchaik, *Langmuir*, **2008**, *24*, 2580; e) D.-S Guo, L.-H. Wang, Y. Liu, *J. Org. Chem.*, **2007**, *72*, 7775; (f) T. R. Tshikhudo, D. Demuru, Z. Wang, M. Brust, A. Secchi, A. Arduini, A. Pochini, *Angew. Chem. Int. Ed.*, **2005**, *44*, 2913.

2.2.1 Recognition of *N*-methyl pyridinium ion pairs (NMPX)

Binding Studies in solution

The binding properties of monotopic calix[4]arenes **1**–**2** were investigated by ^{1}H NMR spectroscopy in $CDCl_3$ solution at 300 K toward the series of *N*-methyl pyridinium salts (NMPX) depicted in Figure 2.9. The set of salts was selected on the basis of the different coordinating character of the anion X. In a typical ^{1}H NMR titration experiment, increasing amounts of a solution of the calix[4]arene receptor (usually c = 1.5×10^{-2} M) were added to a solution of the NMPX salt (usually c = 1.5×10^{-3} M). After each addition, the variation of chemical shift experienced by the proton signals of the *N*-methyl pyridinium (NMP) cation was monitored and plotted versus the receptor-salt concentrations ratio. The ^{1}H NMR titration experiment, carried out using the monotopic receptors **1** and **2**, always showed time-averaged signals for the free and complexed species.

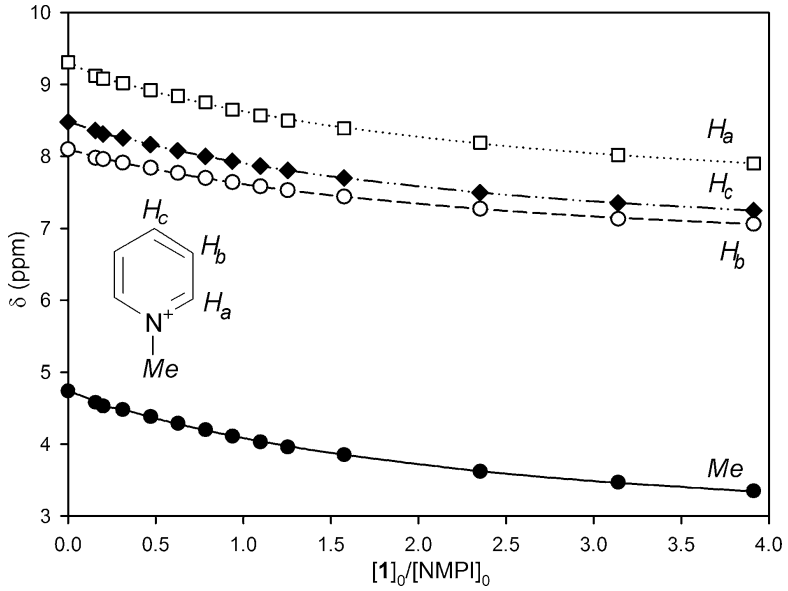

Figure 2.10 Binding isotherms for the complexation of NMPI (c = 1.3×10^{-3} M) with **1** (c = 10^{-2} M) in $CDCl_3$. Symbols ●, □, ○ and ♦ show the chemical shift variation of protons *Me*, H_a, H_b and H_c, respectively, (*Reproduced by permission of The RSC* http://www.rsc.org/Publishing/Journals/OB/article.asp?doi=b906409e).

As a typical example, in Figure 2.10 have been reported the binding isotherms obtained during the titration of NMPI with **1**. The plots show that the aromatic cavity of **1** exerts an anisotropic shielding effect on the protons of the NMP cation resulting in an extensive upfield shift of the corresponding resonances. After having verified the formation of 1:1 receptor-salt adducts through the application of continuous variation methods (Job's plot),[30] the apparent binding constants (log*K*) and the limiting upfield shifts ($\Delta\delta_\infty$, ppm) were calculated through

30. K. A. Connors, *Binding Constants*, Wiley, New York, 1987.

the non-linear fitting[31] of the chemical shift variation experienced, upon complexation, by the NMP resonances.

The log*K* gathered in Table 2.1 shows that the binding efficiency of **1** increases as the coordinating strength of the anion decreases (see also Figure 2.11a). The less coordinating bistriflimide (Tf_2N) and trifluoroacetate (TFA) counteranions afforded the highest log*K* value, while the more coordinating p-toluensulfonate (TsO) yielded the lowest log*K*. With NMPI and NMPCl ion pairs, the inverse correlation between binding efficiency and coordinating strength of the anion was satisfied only when the log*K* was calculated considering the chemical shift variation of the NMP methyl group. In particular with NMPCl a significant deviation from this general trend was observed (see Figure 2.11a). Such a behaviour can be tentatively explained considering that 1:1 binding stoichiometry could be affected by other factors.

Table 2.1 Binding constants (log*K*) and limiting upfield shifts ($\Delta\delta_\infty$, ppm) for the formation of 1:1 adducts of *N*-methylpyridinium salts with monotopic calix[4]arene receptors 1 and 2.[a,b]

		NMPTsO		NMPCl		NMPI		NMPTFA		$NMPTf_2N$	
Receptor	Resonance[c]	log*K*	$-\Delta\delta_\infty$	log*K*	$-\Delta\delta_\infty$	log*K*	$-\Delta\delta_\infty$	log*K*	$-\Delta\delta_\infty$	log*K*	$-\Delta\delta_\infty$
1	*Me*	2.06(2)	1.8	2.38(5)	1.9	2.62(2)	2.5	2.75(1)	1.8	2.94(3)	2.7
	H_a	2.06(3)	2.3	2.53(8)	2.1	2.71(5)	2.3	2.72(1)	2.2	2.95(1)	2.2
	H_b	1.99(3)	2.2	2.79(5)	1.5	2.55(3)	2.1	2.73(1)	2	2.92(1)	1.7
	H_c	2.00(4)	2.8	2.74(4)	1.9	2.56(3)	2.4	2.69(1)	2.4	2.93(1)	2
2	*Me*	2.11(9)	1.8	2.99(1)	1.1	3.35(4)	1.1	3.08(4)	1.1	3.02(1)	1.4
	H_a	2.48(1)	2.7	2.99(7)	2.4	3.44(6)	2.1	3.02(3)	2.2	2.98(1)	2.5
	H_b	2.34(5)	3.2	3.05(1)	2.4	3.33(5)	2.2	3.03(4)	2.4	3.02(2)	2.4
	H_c	2.54(5)	3	[d]	[d]	[d]	[d]	[d]	[d]	2.95(2)	3.1

[a] Determined by ^{1}H NMR spectroscopic titrations at T = 300 K in $CDCl_3$ (standard deviations in parenthesis); [b] $\Delta\delta_\infty = \delta_\infty - \delta_{free}$ where δ_{free} (ppm): **NMPTsO**, 4.63 (Me), 9.21 (Ha), 7.97 (Hb), 8.36 (Hc); **NMPCl**, 4.83 (Me), 9.53 (Ha), 8.06 (Hb), 8.44 (Hc); **NMPI**, 4.74 (Me), 9.31 (Ha), 8.10 (Hb), 8.48 (Hc); **NMPTFA**, 4.68 (Me), 9.29 (Ha), 8.04 (Hb), 8.42 (Hc); **$NMPTf_2N$**, 4.52 (Me), 8.77 (Ha), 8.07 (Hb), 8.49 (Hc); [c] resonance of the NMP cation used for the non-linear fitting (see Figure 2.2.3 for labelling); [d] extensive overlapping of the resonances.

The analysis of the calculated limiting upfield shifts (see $-\Delta\delta_\infty$ values in Table 2.1) reveals that the binding mode of **1** is significantly affected by the strength of the ion pair. Indeed, the rigid "pseudo cone" aromatic cavity of this receptor is able to recognise the NMPX ion pair either through the methyl group (*Me*) or the aromatic protons H_b and H_c of the NMP cation. However, $NMPTf_2N$, being the more "loose" ion pair among those investigated,

31. C. S. Wilcox, in *Frontiers of Supramolecular Organic Chemistry and Photochemistry*, eds. H.-J. Schneider and H. Dürr, VCH, Weinheim, 1991, pp. 123-143.

is preferentially recognised through the acidic methyl group of its NMP cation ($-\Delta\delta_\infty$ for *Me* and H_c is 2.7 and 2 ppm, respectively), while the "tight" and more sterically demanding NMPTsO is likely bound through the electron poor aromatic moiety of its cation ($-\Delta\delta_\infty$ for *Me* and H_c is 1.8 and 2.8 ppm, respectively).

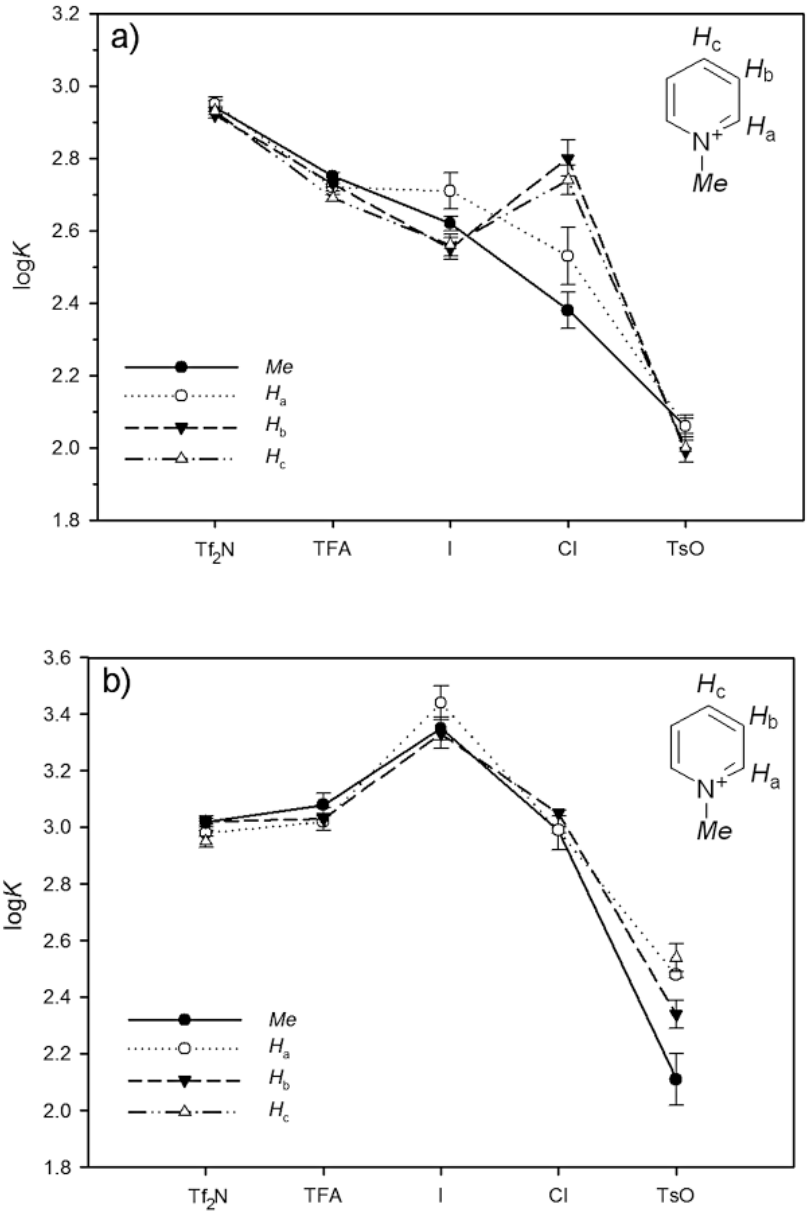

Figure 2.11 Diagrams showing the log*K* calculated through the non-linear fitting of the chemical shift variation endured by each NMP resonance upon complexation with receptors a) **1** and b) **2** respectively, (*Reproduced by permission of The RSC*, http://www.rsc.org/Publishing/Journals/OB/article.asp?doi=b906409e).

Receptor **2** is always a more efficient receptor than **1**, however its binding efficiency cannot be correlated with the coordinating strength of the counteranion (see Figure 2.11b). This receptor experiences its largest affinity for NMPI, that represents the ion pair characterised by the more polarisable anion. With the exception of NMPTsO, the log*K*

calculated for the other salts were all similar (see Table 2.1). The titration experiments involving **2** evidenced an extensive upfield shifts of the aromatic protons (H_a–H_c) of the NMP cation. The $-\Delta\delta_\infty$ values calculated for these resonances were always larger than those calculated for the methyl group (see Table 2.1). These findings suggest that **2**, whose aromatic cavity can adopt a "flattened cone" conformation, recognises preferentially the electron poor aromatic portion of the NMP cation probably via π-π stacking interactions.[32] The higher binding efficiency observed for **2** with respect to **1** can be thus reasonably ascribed to the better conformational adaptability of its aromatic cavity that can maximise the interactions with the NMP cation regardless of the steric requirements imposed by the nature of the counteranion.

The binding properties of the heteroditopic receptors **3** and **4** (see Figure 2.9), were initially investigated through ^{1}H NMR spectroscopic titrations. However, upon complexation, it was observed an extensive upfield shift and broadening of the resonances of the NMP cation. Similarly, the resonances of the phenylurea NH protons of the calixarene receptor endured a large downfield shift. Both findings suggested that, as found in the solid state, ion-pair binding mainly occurs through the cooperation of a "soft" cation/π and a "hard" H-bond interaction. The former of these interactions occurs between the NMP cation and the π-rich aromatic cavity of the calixarene scaffold, while the stronger H-bond operates between the phenylurea group and the anion. The broadening of the NMP resonances was unfortunately observed at the initial stages of the titrations. Such phenomenon, that could be consistent either with binding saturation or slow binding equilibria, usually prevents the determination of reliable binding constants via NMR measurements. Therefore, the binding properties of **3** and **4** were investigated using more diluted solution of NMPX salts by UV/vis spectroscopy. In a typical titration experiment increasing amounts of a 10^{-3} M solution of the receptor in $CHCl_3$ were added to a 10^{-4} M solution of the investigated NMPX salt in the same solvent. The titration of NMPI offered the most interesting results since the addition of the solution of **3** or **4** induced a blue shift of the two low energy charge-transfer (C.T.) bands, centred at λ = 294 and 367 nm, that are characteristic for the solutions of this salt in halogenated solvents.[33] The hypsochromic shift of the NMPI bands generates an isosbestic point at λ = 293 nm (see Figure 2.12) and at λ = 305 nm with **3** and **4**, respectively.

32. See *e. g.* S. Grimme, *Angew. Chem. Int. Ed.*, **2008**, *47*, 3430 and references therein.
33. J. S. Brinen, J. G. Koren, H. D. Olmstead, R. C. Hirt, *J. Phys. Chem.*, **1965**, *69*, 3791.

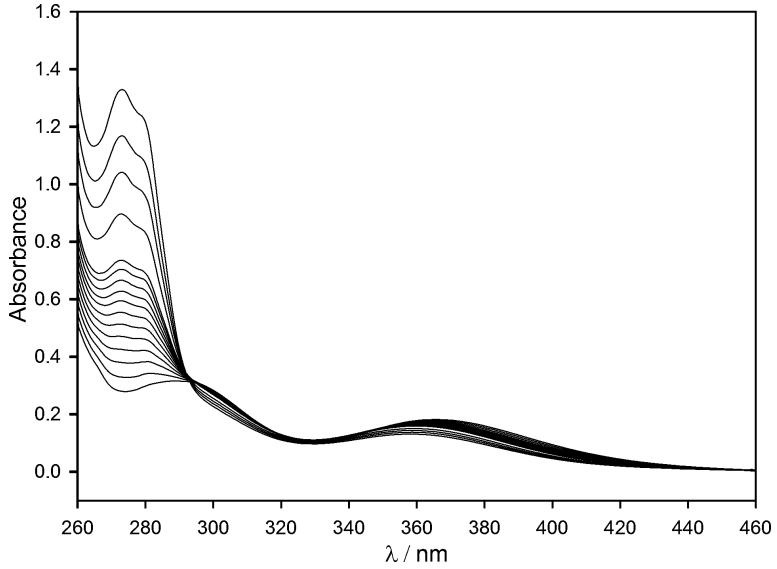

Figure 2.12 UV/vis spectral titration of NMPI (c = 1×10^{-4} M) with **3** (c = 1×10^{-3} M) in $CHCl_3$, (*Reproduced by permission of Royal Society of Chemistry*, see: http://www.rsc.org/Publishing/Journals/OB/article.asp?doi=b906409e).

These shifts were reasonably ascribed to a reduction of the charge transfer process within the ion pair as a consequence of complex formation. This phenomenon was not monitored during the titrations of the other NMPX salts because in chloroform solution their C.T. bands are completely hidden by the strong absorption band of the pyridinium cation centred at λ = 260 nm. The families of spectra collected during the titrations were analysed with the Specfit/32 software.[34] The application of a 1:1 binding stoichiometry to the non-linear fitting of the spectral data yielded binding constants (log*K*) characterised by satisfactory standard deviations (see Table 2.2).

Table 2.2 Binding constants (log*K*) for the formation in $CHCl_3$ (T=300 K) of 1:1 adducts between *N*-methylpyridinium salts (NMPX) and calix[4]arene receptors **3** and **4**.[a,b]

Receptor	NMPTsO	NMPCl	NMPI	NMPTFA	$NMPTf_2N$
3	4.1(0.1)	5.5(0.2)	5.0(0.1)	5.0(0.1)	3.8(0.1)
4	4.75(0.07)	4.8(0.1)	5.0(0.2)	4.9(0.1)	3.5(0.1)

[a] Measured with UV/vis titrations (standard deviations in parenthesis); [b] spectral data λ_{max} (nm) and ε ($\times10^3$ mol^{-1} L cm^{-1}) for the NMPX salts: 260, 4.1 (TsO); 260, 2.5 (Cl); 294, 2.9 and 376, 1.9 (I); 260, 4.1 (TFA); 260, 4.5 (Tf2N); and for the free receptors: 273, 4.4 (3); 282, 7.8 (4).

The comparison of the binding constants calculated for **3** and **4** with those calculated for the corresponding monotopic receptors **1** and **2** (see Table 2.2), shows that the introduction of the ancillary anion binding site on the calix[4]arene cavity increases the affinity for the NMPX salts up to two orders of magnitude. Such binding enhancement has been tentatively

34. SPECFIT/32™ Global Analysis System for Windows.

evaluated in terms of *cooperative heteroditopic effect*.[35] The latter was expressed as the ratio between the binding constants calculated for each couple of heteroditopic and monotopic receptors having the same calix[4]arene skeleton. For the couple of biscrown-3-based receptors **3** and **1** the approximated ratios were 100 (TsO), 1300 (Cl), 240 (I), 170 (TFA), and 6 (Tf_2N). The highest increment was observed for NMPCl. The cooperative effect calculated for the couple of 1,3-dipropoxy calix[4]arene-based receptors **2** and **4** was 440 (TsO), 65 (Cl), 45 (I), 90 (TFA), and 2.5 (Tf_2N). For these more flexible receptors the largest binding enhancement was recorded with the tight NMPTsO ion pair. The binding data also show that, differently from the monotopic receptors, the binding efficiency of **3** and **4** cannot be directly correlated with the coordinating strength of the anion. In particular, the log*K* values calculated for **4** were, within the experimental errors, almost identical with the exception of the poorly recognised NMPTf_2N "loose" ion pair. The more rigid and preorganised cavity of **3** determines a better binding selectivity. This receptor indeed maximises its recognition properties toward NMPCl (log*K* =5.5), while its efficiency substantially drops (more than an order of magnitude) with the ion pairs of the series having the strongest (TsO) and the weakest (Tf_2N) coordinating anion. This behaviour can be rationalised neglecting, in first approximation, any entropic effect and assuming that the maximum recognition efficiency would mainly derive by the balance of two opposing effects: a) an energetic gain achieved by the interaction of the two ions with the two binding sites, and b) an energetic loss due to the stereochemical requirements associated with the recognition of tight ion pairs. In particular, specific steric requirements are involved in the pyridinium-anion and urea-anion interaction and the latter is strongly dependent on the receptor structure. On this premise, the low efficiency recorded with NMPTsO by **4** (log*K* = 4.75) and in larger proportion by **3** (log*K* = 4.1), that is more rigid, can be ascribed to the latter adverse effect. On the other hand, the poor coordinating character of the Tf_2N anion should reduce the establishment of energetic H-bonding interactions with the phenylurea group of the receptors (effect a). The good affinity observed between NMPCl and **3** can be mainly ascribed to the small spherical anion that improves the fitting between the ion pair and the geometrical arrangement of the two binding sites present in **3**.

35. For recent examples of positive allosteric effect on ion-pair binding see *e. g.*: a) K. Zhu, S. Li, F. Wang, F. Huang *J. Org. Chem.*, **2009**, *74*, 1322; b) C. M. G. dos Santos, T. McCabe, G. W. Watson, P. E. Kruger, T. Gunnlaugsson, *J. Org. Chem.*, **2008**, *73*, 9235; c) L. Kovbasyuk, R. Kramer, *Chem. Rev.*, **2004**, *104*, 3161.

NMR structural studies

The structure of the complexes in solution was inferred using 2D NMR techniques. A 2:1 mixture of **1** and NMPI was submitted to NOESY experiment. Two intense NOE cross-peaks in the spectrum evidenced the close proximity of the NMP methyl group with the aromatic protons H_m and H_p of the calix[4]arene skeleton (see Figure 2.13). Weak cross-peaks are also present between the proton H_a of NMP and the protons H_m and H_p of **1**, thus confirming that, as seen through the comparison of $\Delta\delta_\infty$ of Table 2.2, the NMP guest can interact with the cavity of the receptor also through its aromatic moiety. Similar NOE correlations were present in the 2D NOESY spectrum of the mixture between **3** and NMPCl. Rather intense NOE cross-peaks arising between the aromatic protons H_b of the pyridinium ring and protons *2* and *3* of the phenylurea moiety (see Figure 2.14) were also found, suggesting the proximity of these two aromatic rings.

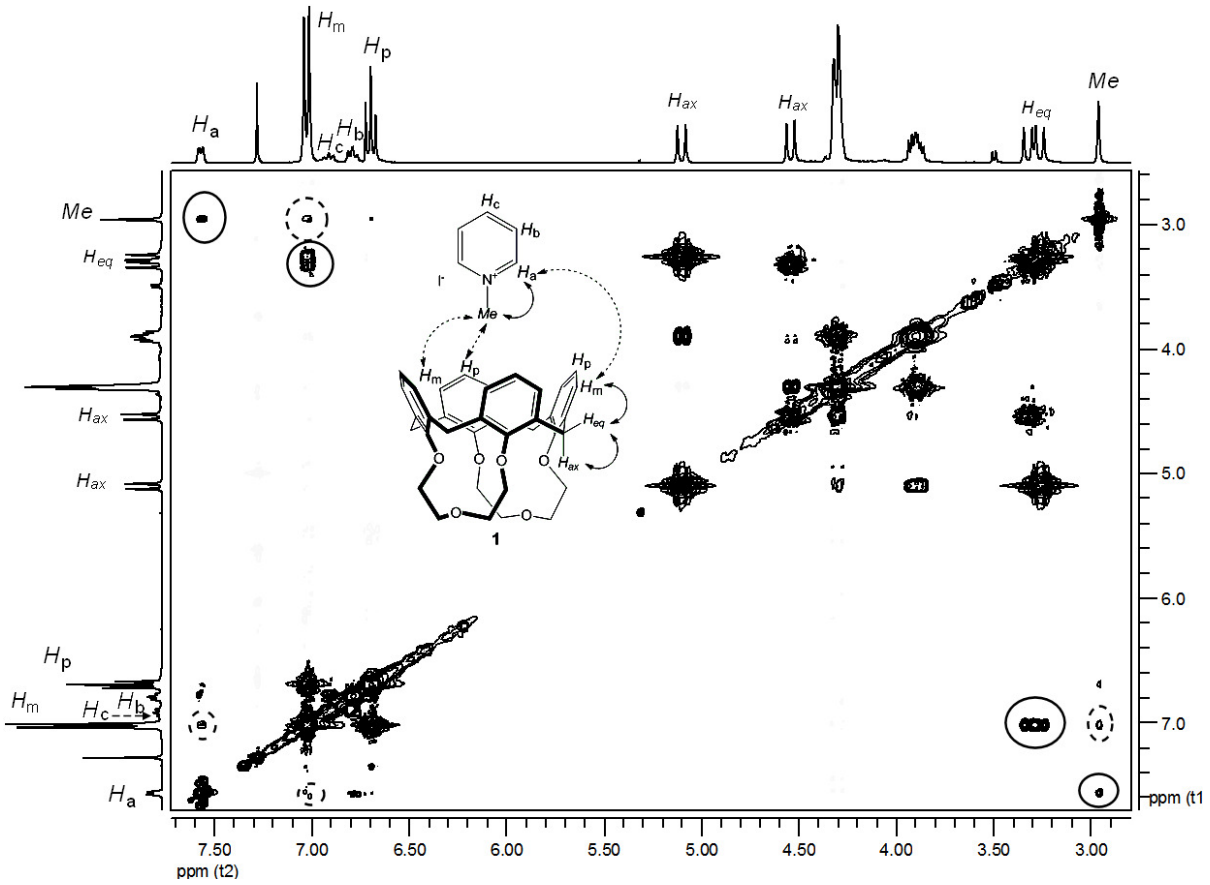

Figure 2.13 2D NOESY spectrum ($CDCl_3$, *T*=300 K, mixing time = 0.4 ms) of the 2:1 mixture of **1** and NMPI. The most representative NOE cross-peaks have been evidenced in the spectrum with dashed lines. The relative intermolecular connections have been indicated in the schematic representation of the complex (not scaled) with dashed arrows.

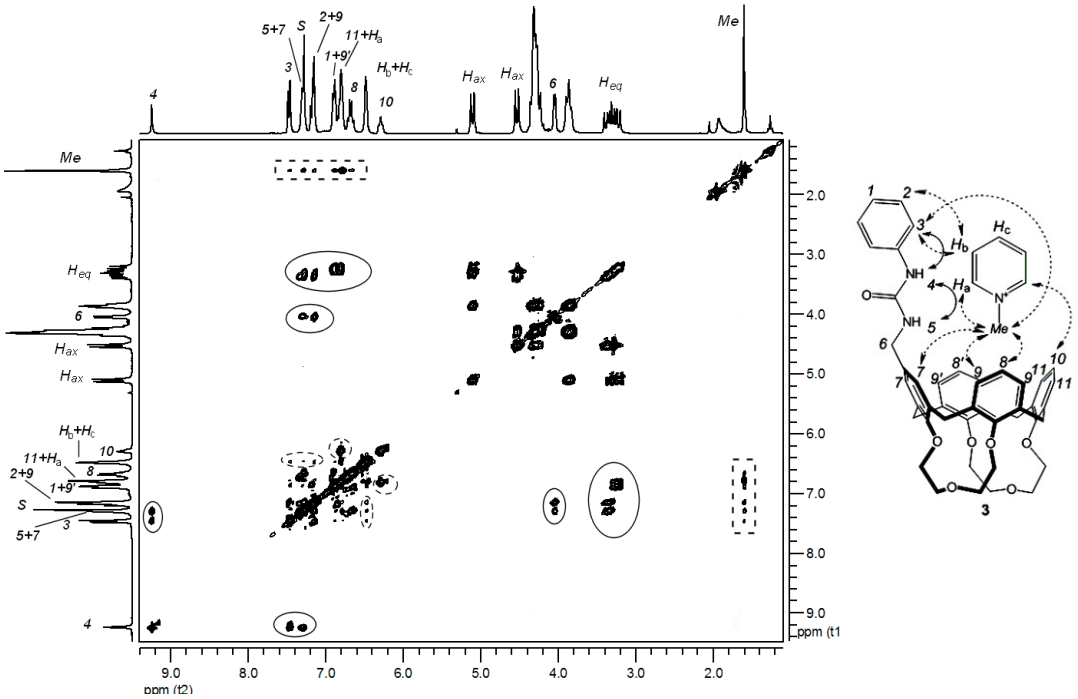

Figure 2.14. 2D NOESY spectrum ($CDCl_3$, *T*=300 K, mixing time = 0.4 ms) of a 1:1 mixture of **3** and NMPCl. Intra- and intermolecular NOE cross-peaks are represented with continuous and dashed lines.

Solid State Studies

Crystals suitable for X-ray analysis were obtained from the evaporation of an equimolar mixture of **1** and NMPI in chloroform. The crystal structure revealed the formation in the solid state of an inclusion complex (**1**⊃NMPI) in which the cavity of **1** is filled with the methyl group of the NMP cation (see Figure 2.15a). The aromatic cavity, which usually adopts a pseudo C_4 symmetry,[36] is forced by the complexation in a pseudo C_2 elliptical *cone* conformation, as shown by the conformational parameters ϕ and χ (see experimental section).[37] The attraction between the CH_3 group and the three aromatic rings A, D and C of **1** is driven by three CH/π interactions. The geometrical parameters of these interactions (see Table 2.3) show that the strongest attractions occur with the two opposite phenolic rings A and C, which show the shortest C···Ct (centroid) distances, whereas the interaction with the phenolic ring D is weaker due to the higher value of its δ angle (opposed rings D and B diverge more than A and C).

36. G. Arena, A. Contino, E. Longo, G. Spoto, A. Arduini, A. Pochini, A. Secchi, C. Massera, F. Ugozzoli, *New J. Chem*., **2004**, *28*, 56.
37. F. Ugozzoli, G. D. Andreetti, *J. Incl. Phenom. and Mol Rec. in Chem*., **1992**, *13*, 337.

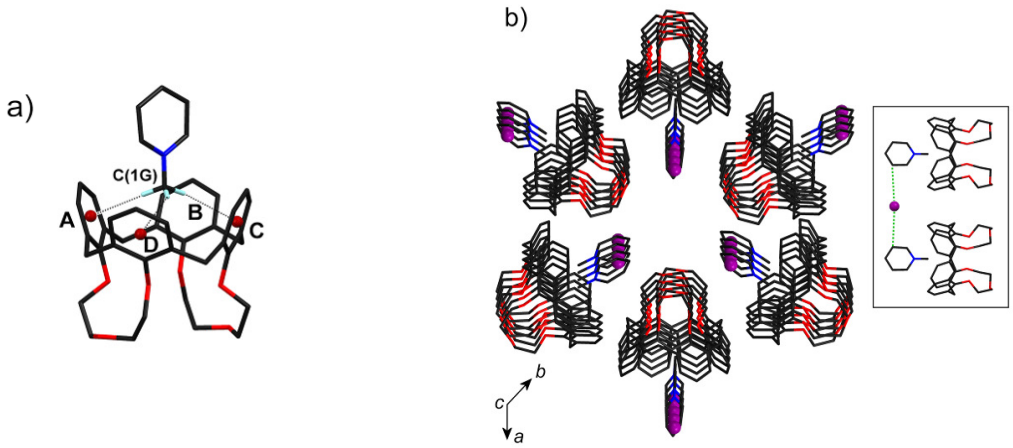

Figure 2.15 Perspective view of a) the X-ray structure of **1**⊃NMP cationic complex and b) of the self-assembled **1**⊃NMPI complexes along the *c* axis (inset: the superstructure is viewed orthogonally to the *c* axis). (*Reproduced by permission of The RSC*, http://www.rsc.org/Publishing/Journals/OB/article.asp?doi=b906409e).

The iodide ion is segregated outside the cavity of **1** and shielded from strong interactions with the NMP cation: the shortest I···CNMP distance is 3.97 Å and it is close to the sum of the van der Waals radii of C (1.7 Å) and I– (2.2 Å).[38] In the symmetry-extended structure, the **1**⊃NMP cationic complexes and the I^- anions self-assemble in clusters of six **1**⊃NMPI units in a columnar arrangement, running along the crystallographic c axis, with a three-fold symmetry. The I^- anions are interdigitated between the cationic complexes along the same crystallographic axis (see Figure 2.15b). The crystalline structure of **1**⊃NMPI is thus the result of the cooperation between weak and strong intermolecular interactions: the weak, but directional, CH/π interactions are responsible of the complexation of the NMP cation within the calixarene cavity, and the strong, but not directional, electrostatic interactions are the structure-directing factor for the self-assembly of the cationic complexes **1**⊃NMP^+ and the I^- anions in the crystal lattice.

Table 2.3 Geometrical parameters relative to the CH/π and hydrogen bond interactions found in the **1**⊃NMPI complex.[a]

Entry	Interaction	Distance (Å)		Angle (°)
	Donor(*D*)–H···Acceptor(*A*)	H···*A*	*D*···*A*	*D*–H···*A*
1	C(1G)-H·· Ct(A)	2.44	3.44(1)	174
2	C(1G)-H·· Ct(C)	2.72	3.35(1)	122
3	C(1G)-H·· Ct(D)	2.82	3.70(1)	156

[a] Ct indicates the centroids of the calix[4]arene aromatic rings.

38. *Hanbook of Chemistry and Physics*, 76th edition, CRP press, 1996.

From the slow evaporation of a mixture of **3** and NMPCl in chloroform and ethanol we also succeded in the isolation of crystals suitable for X-ray analysis. The diffraction analysis revealed that in the solid state two calix[4]arene units of **3** encapsulate the NMP cation in a "cage-like" structure characterised by a C_i symmetry (**1**$_2$⊃NMPCl, see Figure 2.16). The conformation of the each calix[4]arene unit is unequivocally described by the conformational parameters ϕ and χ (see experimental section). The inversion centre of the complex (on the barycentre of the NMP) coincides with a crystallographic inversion centre: the NMP cation is thus statistically disordered over two different orientations with the methyl group alternatively oriented up or down in the cage (see Figure 2.16a and 2.16b).

The NMP cation is held in the cavity by two CH/π interactions involving the hydrogens of its methyl group and the two aromatic rings A and B (in the alternative orientations of the methyl group, the two CH/π interactions involve the aromatic rings A' and B').

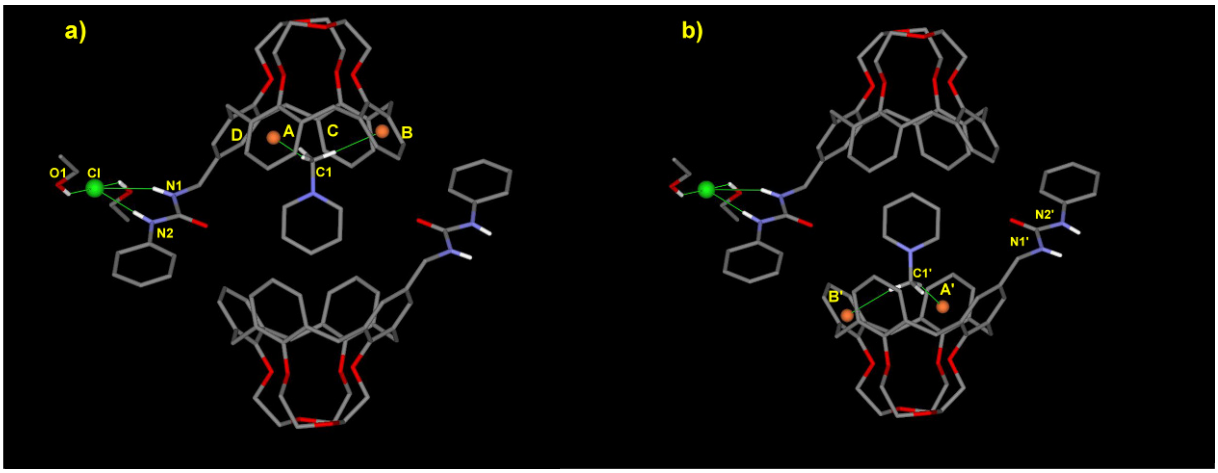

Figure 2.16 Perspective view of the **3**$_2$⊃NMPCl complex showing the two statistically disordered orientations of the methyl group of the pyridinium cation (NMP) inside the "cage-like" structure defined by the two calix[4]arenes. The primed atoms are related to the unprimed ones through the symmetry operation: 1-x, 1-y, -z. The short contacts (H-bonds and CH/π interactions) have been depicted with green lines (*Reproduced by permission of The RSC*, http://www.rsc.org/Publishing/Journals/CE/article.asp?doi=b816490h).

The two equilibrium distances C···Ct (centroid) are indicative that the guest is stabilised by strong CH···π interactions (see Table 2.4). The C1–H···Ct(A) interaction is particularly strong due to the short C···Ct separation (3.20 Å, see entry 4, Table 2.4) and by the high value (163°) of the C–H···Ct angle. Both C···Ct distances are shorter than those calculated at high level of theory for methane-benzene12[39] (3.8 Å) and chloroform-benzene (3.6 Å) dimers.[40]

39. S. Tzuzuki, K. Honda, T. Uchimaru, M. Mikami, K. Tanabe, *J. Am. Chem. Soc*., **2000**, *122*, 3746.
40. S. Tzuzuki, K. Honda, T. Uchimaru, M. Mikami, K. Tanabe, *J. Phys. Chem. A.*, **2002**, *106*, 4423.

Table 2.4 Geometrical parameters for CH/π and H-bond interactions found in $\mathbf{1}_2$⊃NMPCl.[a]

Entry	Interaction	Distance (Å)		Dihedral (°)
	Donor–H···Acceptor	H···A	D···A	D–H···A
1	N1–H···Cl	2.54	3.34	156
2	N2–H···Cl	2.41	3.24	161
3	O1–H···Cl	2.81	3.50	143
4	C1–H···Ct(A)	2.27	3.20	163
5	C1–H···Ct(B)	2.71	3.54	145

[a]Ct indicates the centroid of the calix[4]arene aromatic rings.

In the solid state, the NMPCl guest is a ligand separated ion pair. The chloride ion is indeed segregated outside the calix[4]arene cage and shielded from strong interaction with its counterion, through the formation of four hydrogen bonds: two strong with the urea hydrogens N1 and N2 (see entries 1 and 2, Table 2.4) and further two with two ethanol molecules of the crystallization solvent (see entry 3, Table 2.4).

a)

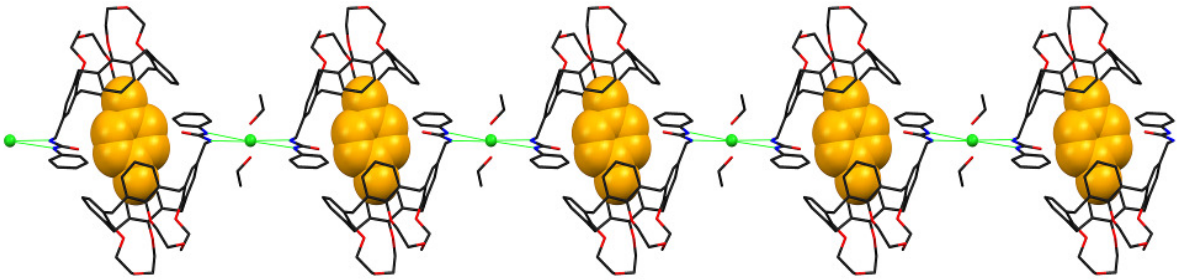

b)

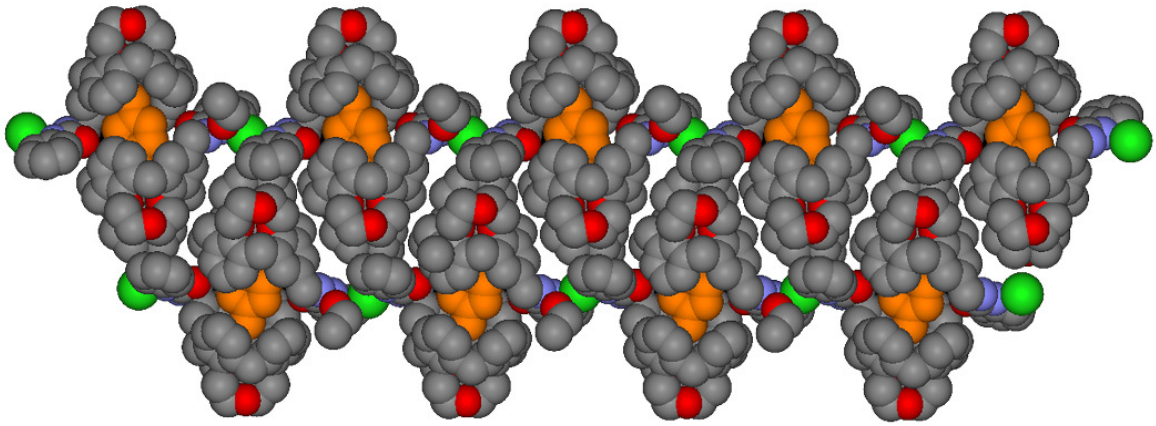

Figure 2.17 a) Partial view of one infinite hydrogen-bonded 1D polymeric chain of self-assembled 2:1 complexes between heteroditopic calix[4]arene **3** and *N*-methyl pyridinium choloride ion pairs (the disordered cationic guest is represented with CPK spheres, hydrogen atoms were omitted for clarity), (*Reproduced by permission of The RSC*, http://www.rsc.org/Publishing/Journals/OB/article.asp?doi=b906409e); b) CPK view of the interdigitation mode of two 1D infinite polymeric chains (hydrogen atoms were omitted for clarity).

The chloride also lies on a centre of symmetry, independent from that of the cage. In the symmetry expanded structure, it acts as a bridge between adjacent $\mathbf{1}_2\supset NMP^+$ cationic complexes giving rise to the infinite 1D hydrogen-bonded polymeric chains illustrated in Figure 2.17. The "pitch" along the 1D hydrogen-bonded polymeric chain, taken as $Cl^-\cdots Cl^-$ separation, is 18.647(9) Å corresponding to the double of the $Cl^-\cdots$Ct(NMP) distance, where Ct(NMP) is the centroid of the guest aromatic ring. As a "secondary structure", in the crystal lattice the 1D polymeric chains are interdigitated with the adjacent ones as shown in Figure 2.17b. Each 1D polymeric chain is shifted of one half of the "pitch" with respect of the adjacent ones. The $Cl^-\cdots$Ct(NMP) separation between the chlorine ion of one 1D chain and the Ct(NMP) of the interdigitated 1D chain is 13.349(9) Å.

2.2.2 Recognition of Paraquat ion pairs (PQX_2)

Gas-phase binding studies

The binding properties of the heteroditopic receptors **3** and **4** were also investigated toward a series of dimethyl viologen (paraquat) salts.[41] Due to the very low solubility of paraquat salts in halogenated solvents, preliminary binding studies were accomplished in the gas phase using ESI mass spectrometry.[42] Samples for mass analysis were prepared by suspending an excess of the solid paraquat salt PQX_2 (X = TsO, Cl, and I) in a refluxing $CHCl_3$ solution of the receptor (~10^{-3} M). After filtration and dilution with methanol (see experimental), the resulting mixtures were submitted to ESI-MS in the positive mode. Figure 2.18a shows the mass spectrum of the mixture of **3** with $PQ(TsO)_2$. The peak at m/z = 806.0 was ascribed to a doubly charged species in which two calix[4]arene units are associated with a paraquat dication: $[\mathbf{3}_2\supset PQ^{2+}]$. Such a supramolecular adduct also gives rise to a weak singly charged ion $[\mathbf{3}_2\supset PQ(TsO)^+]$ at m/z = 1783.2 in which a tosylate anion has been retained. The spectrum also shows two intense peaks at m/z = 449.3 and 1069.5 that correspond to the doubly $[\mathbf{3}\supset PQ^{2+}]$ and singly $[\mathbf{3}_2\supset PQ(TsO)^+]$ charged 1:1 adducts. A similar distribution of ionised species was identified in the mass spectrum of the mixture containing receptor **4** and $PQ(TsO)_2$ (see Fig. 2.18b).

41. P. M. Monk, *The Viologens*, John Wiley & Sons, Chichester, 1998.
42. For a review on the use of mass technique for the evaluation of binding in the gas-phase see: M. Kogey, C. A. Schalley in *Analytical Methods in Supramolecular Chemistry*, ed. C. A. Schalley, Wiley-VCH, Weinheim, 2007, pp. 104-162.

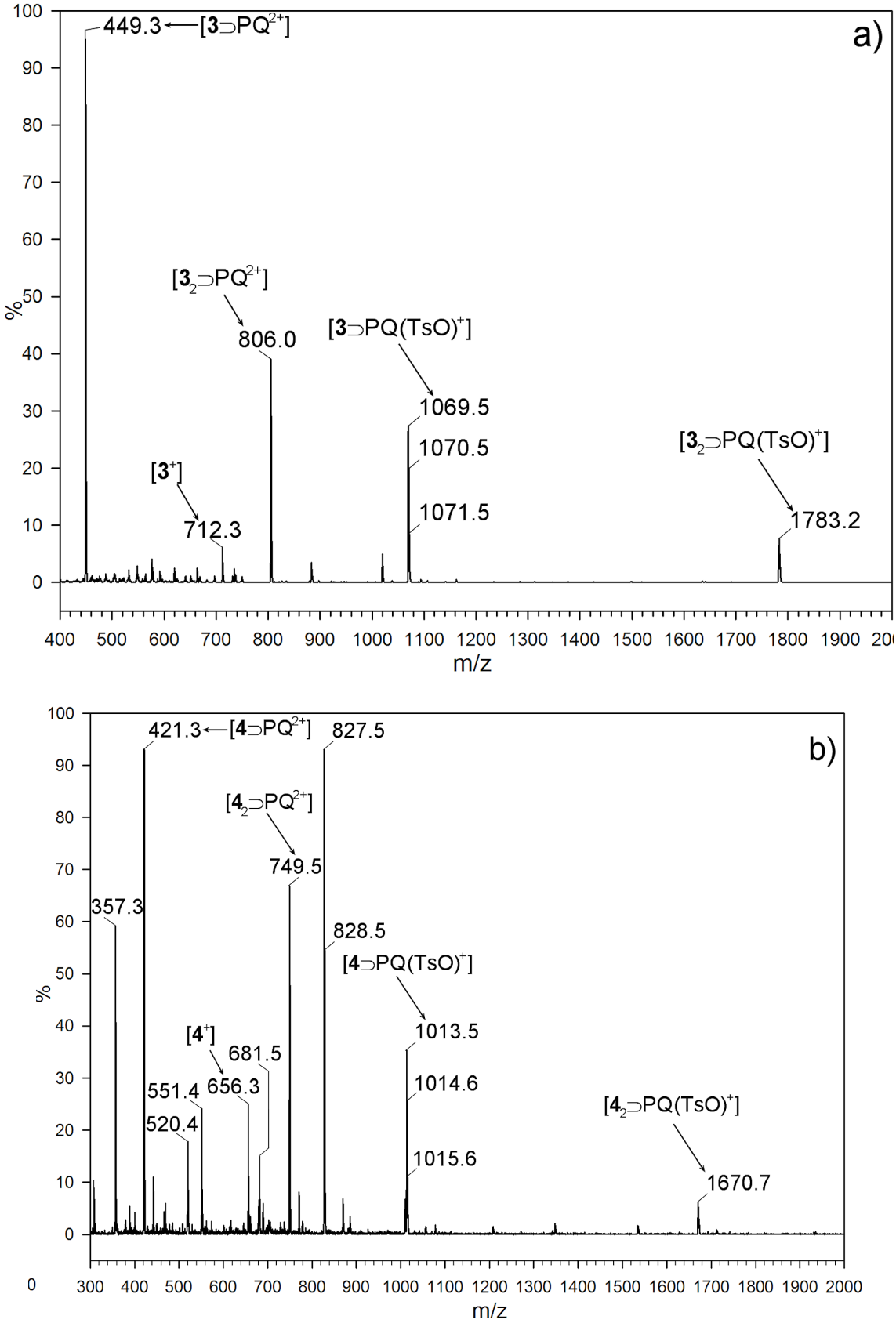

Figure 2.18 ESI-MS spectra obtained from the 9:1 $CHCl_3$:MeOH solutions of a) **3** and b) **4** with $PQ(TsO)_2$ (cone voltage: 25-40 V; desolvation temperature: 120 °C) (*Reproduced by permission of The RSC*, http://www.rsc.org/Publishing/Journals/OB/article.asp?doi=b906409e).

The 2:1 adduct yields peaks at m/z = 749.5 and 1670.7 corresponding to the doubly [$\mathbf{4}_2 \supset PQ^{2+}$] and singly [$\mathbf{4}_2 \supset PQ(TsO)^+$] charged species, respectively. The 1:1 adduct is recognisable for the intense peaks at m/z = 421.3 [$\mathbf{4} \supset PQ^{2+}$] and 1013.5 [$\mathbf{4} \supset PQ(TsO)^+$]. The two spectra of figure 2.2.7 also revealed the presence in the gas-phase of the free receptor (m/z = 712.3 and 656.3 for **3** and **4**, respectively). The analysis of the mass spectra recorded in the same experimental conditions from the samples derived by the suspension of $PQCl_2$ and PQI_2 in the solutions of **3** and **4** did not reveal any appreciable formation of supramolecular adduct in the gas-phase.

Solution binding studies

The formation of the supramolecular adducts between $PQ(TsO)_2$ and receptors **3** and **4** has been studied also in solution of low polar solvents using both NMR and UV/vis spectroscopy. Samples appropriate for NMR analysis were obtained by suspending for 30 min an excess of the solid $PQ(TsO)_2$ in a refluxing $CDCl_3$ solution of each receptor (~2×10^{-2} M). The ^1H NMR spectra of the pale yellow solutions obtained after the filtration of the undissolved material showed that both receptors were able to dissolve the paraquat salt in chloroform. The stack plot of figure 2.19 shows that, upon complexation, the resonances of **4** underwent a significant rearrangement (see Figure 2.19a). In particular, the large downfield shift (up to 2.6 ppm) experienced by the NH protons of the phenylurea group (cfr. Figure 2.19b) is in agreement with a complexation reaction that involved hydrogen bonding with the two tosylate anions. 2D HH COSY and 2D HC HMQC correlation experiments (see Figures 2.20 and 2.21) assigned the doublets resonating at δ = 6.65 (♥) and 8.35 (●) ppm to the protons in the ortho e meta position of the pyridinic rings, respectively. The former of these doublets is noticeably upfield shifted (~2.3 ppm) with respect to its usual chemical shift in D_2O. An even more marked upfield shift (~3.8 ppm) was observed for the six viologen methyl protons (♦) which resonate, as a singlet, at δ = 0.57 ppm. Considering that the signal integration yields a 2:1 ratio between **4** and $PQ(TsO)_2$, these upfield shifts are likely due to the complexation of the bypyridinium dication within an extended aromatic cavity created by the cooperation of two self-assembled cavities of **4**. 2D ROESY experiments (fig 2.22) finally confirmed the spatial close proximity between the methyl protons of the viologen unit with the aromatic protons present on the upper rim of the calix[4]arene macrocycle. The solid-liquid extraction experiment carried out using the more rigid receptor **3** afforded very similar results.

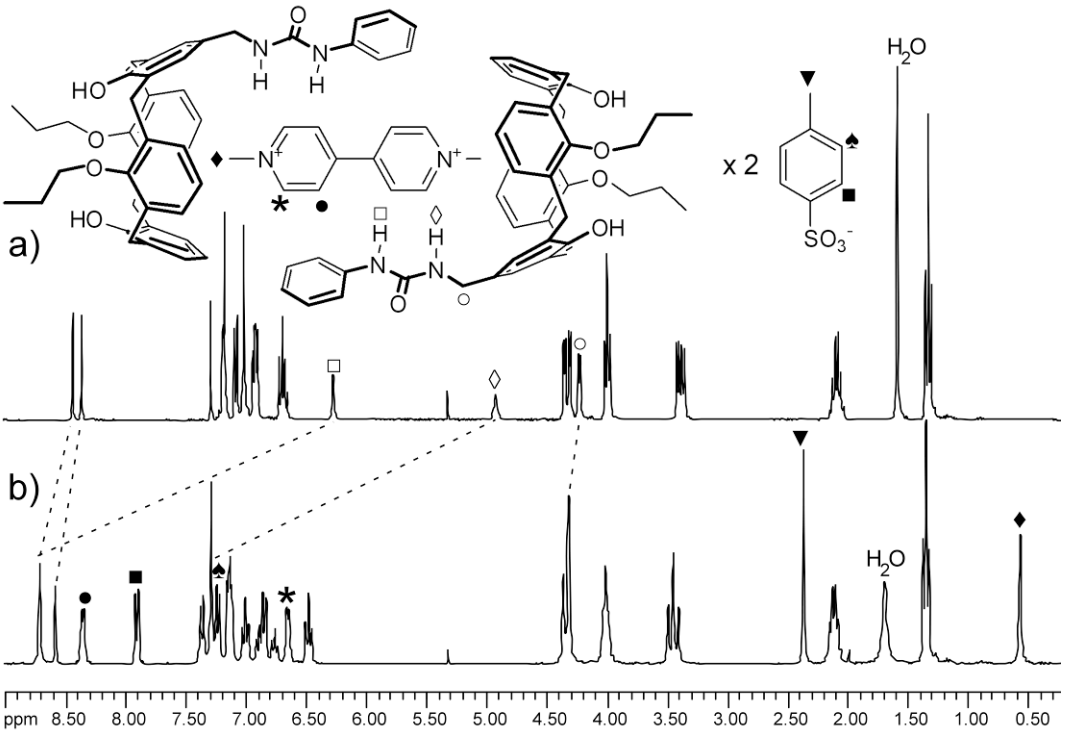

Figure 2.19 ^{1}H NMR spectra (300 MHz, $CDCl_3$) of a) **4** and b) its 2:1 complex with $PQ(TsO)_2$. The most representative resonances are indicated with symbols (see sketch), (*Reproduced by permission of The Royal Society of Chemistry*, http://www.rsc.org/Publishing/Journals/OB/article.asp?doi=b906409e)..

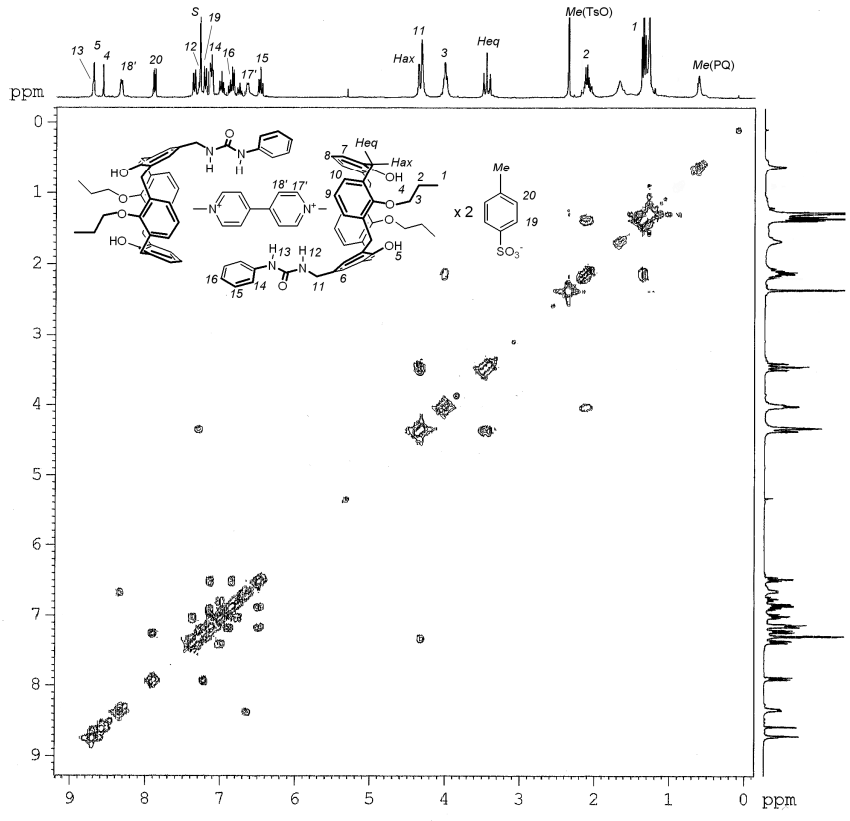

Figure 2.20. 2D COSY spectrum ($CDCl_3$, *T*=300 K) of the 2:1 mixture of **4** and $PQ(TsO)_2$.

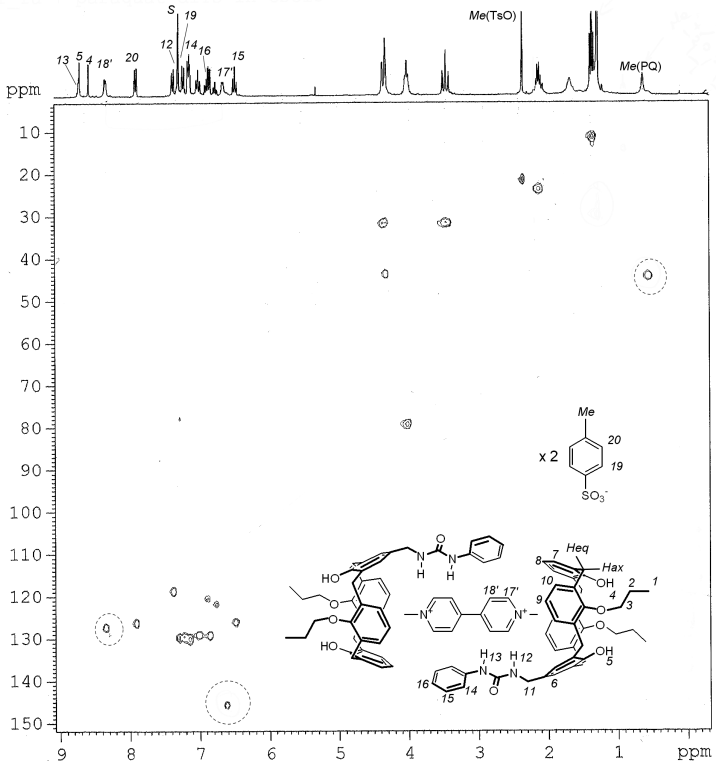

Figure 2.21 2D HMQC spectrum ($CDCl_3$, *T*=300 K) of the 2:1 mixture of **4** and $PQ(TsO)_2$.

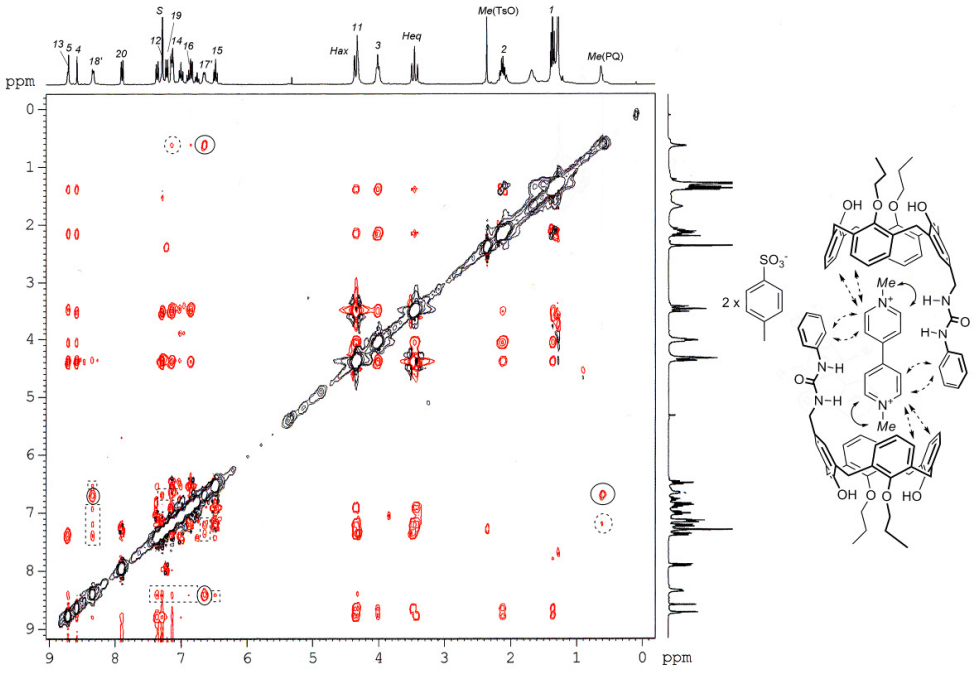

Fig. 2.22 2D ROESY spectrum ($CDCl_3$, *T*=300 K, spin lock = 200 ms) of the 2:1 mixture of **4** and $PQ(TsO)_2$.The most representative NOE cross-peaks and the corresponding intra- and intermolecular connections have been evidenced in the spectrum with continuous and dashed lines and in the schematic representation of the complex with continuous and dashed arrows, respectively.

NMR diffusion experiments (DOSY)[43,44] were successively carried out to provide further information on the composition of the $CDCl_3$ solution containing the $\mathbf{4}_2 \supset PQ(TsO)_2$ complex (see experimental section). The linear fitting of the attenuation profiles of all the resonances of the spectrum reported in figure 2.19b yielded a mean diffusion coefficient D=4.7±0.1×10^{-6} cm^2 s^{-1}. For reference, the diffusion experiment was also performed on the solution of **4**. The calculated diffusion coefficient for the free receptor was D = 6.8±0.2×10^{-6} cm^2 s^{-1}. This confirms, as expected, that the cumbersome 2:1 supramolecular adduct is a slower diffusing species in solution than the free receptor. The application of the Stoke-Einstein equation $D = k_B T/(c\pi\eta r_H)$, where k_B is the Boltzmann constant, T is the temperature, c is a numerical factor correlated with the size of the diffusing species, and η is the solvent viscosity, yielded, assuming a spherical shape of the diffusing species and using the slip conditions (c = 4), a hydrodynamic radius r_H of ~1.2 and ~0.8 nm for the 2:1 complex and the free **4**, respectively.

The $PQ(TsO)_2$ salt experiences sufficient solubility in neat chloroform to allow a determination through UV/vis spectroscopy of the thermodynamic stability of these 2:1 adducts. Typically, a solution of $PQ(TsO)_2$ salt (1×10^{-5} M) in $CHCl_3$ was titrated with a solution of the receptors (1×10^{-4} M) in $CHCl_3$. The free $PQ(TsO)_2$ yields a main absorption band centred at λ=272 nm (ε= 2.01×104 mol^{-1} L cm^{-1}) that upon complexation with either **3** or **4** experiences a weak bathochromic shift. The collected spectra were fitted with Specfit/32[30] using the following binding modes:

$$R + PQ \underset{}{\overset{K_{11}}{\rightleftharpoons}} R \supset PQ \qquad (1)$$

$$R \supset PQ + R \underset{}{\overset{K_{21}}{\rightleftharpoons}} R_2 \supset PQ \qquad (2)$$

$$2R + PQ \underset{}{\overset{\beta_{21}}{\rightleftharpoons}} R_2 \supset PQ \qquad (3)$$

where R is the calix[4]arene receptor and PQ is the viologen ion pair. Good fittings were obtained by applying a 2:1 binding mode (equation 3) yielding a logβ_{21} of 10.2±0.2 and 10.7±0.5 for **3** and **4**, respectively. The UV/vis studies did not reveal the presence in solution of concomitant 1:1 and 2:1 adducts (equation 1 and 2).

43. C. S. Johnson, *Prog. Nucl. Magn. Reson. Spectrosc.*, **1999**, *34*, 203 and references therein.
44. For a general review on the application of DOSY in supramolecular chemistry please see: Y. Cohen, L. Avram, L. Frish, *Angew. Chem. Int. Ed.*, **2005**, *44*, 520.

Solid State Studies

We were able to separate from the chloroform solution crystals of $\mathbf{4}_2\supset PQ(TsO)_2$ suitable for X-ray analysis. The complex is effectively characterised by a "cage" structure with the PQ dication encapsulated within the intramolecular cavity created by the two calix[4]arene units of **4** (see Figure 2.23). The mutual attraction between the calixarene cage and the PQ dication occurs through four CH/π interactions involving the hydrogen atoms of the two PQ methyl groups and the four aromatic rings of the calix[4]arene cage (see Table 2.5 for the geometrical parameters of the CH/π interactions).

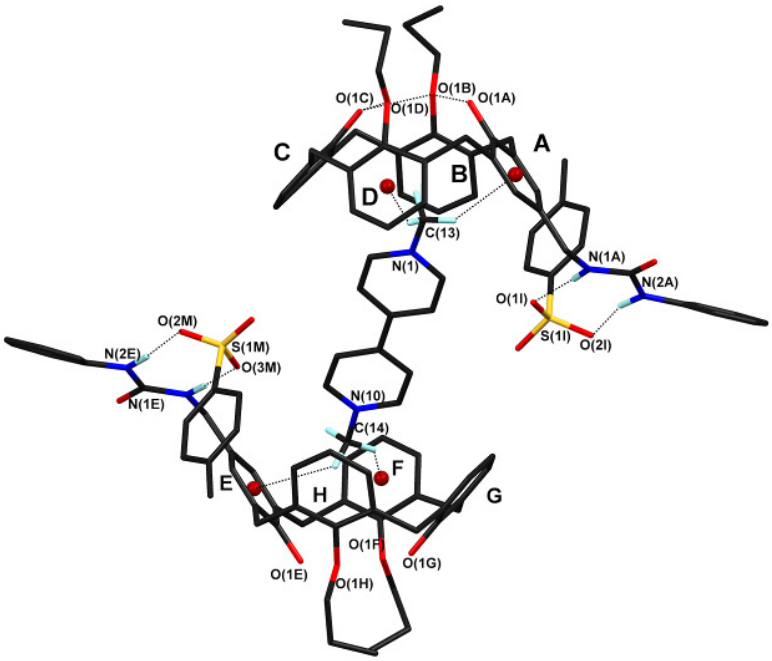

Figure 2.23 Perspective stick view of the 2:1 complex $\mathbf{4}_2\supset PQ(TsO)_2$. Several atoms not involved in intermolecular interactions have been omitted for clarity, (*Reproduced by permission of The Royal Society of Chemistry*, http://www.rsc.org/Publishing/Journals/OB/article.asp?doi=b906409e).

The conformation of the two calixarene units is quite different one from the other as shown by the conformational parameters ϕ and χ (see experimental section). Such conformation is indiced by intramolecular hydrogen bonding O···O contacts between the following phenolic oxygens: O(1A)···O(1D) 2.718(6), O(1C)···O(1D) 2.672(6), O(1C)···O(1B) 2.967(6) Å in the ABCD calixarene, and O(1E)···O(1H) 2.702(6), O(1F)···O(1G) 2.642(6), O(1G)···O(1H) 2.950(6) Å in the EFGH calixarene. In this complex, the strength of the four CH/π interactions is close to the one observed in the $\mathbf{3}_2\supset$NMPCl complex (the C···Ct separations range from 3.164(7) to 3.419(7) Å in $\mathbf{4}_2\supset PQ(TsO)_2$ and from 3.204(1) to 3.535(1) Å in $\mathbf{3}_2\supset$NMPCl). The two tosylate counteranions are located on the border of the cage in close proximity of the PQ dication. Each of them is linked to the urea

chain of a calixarene through two strong hydrogen bonds (see Table 2.5). In such a way all the complex is stabilised by the simultaneous cooperation of three different types of interactions: the coulombic forces (strong but not directional and thus not selective) between the two tosylate anions and the PQ dication; the four hydrogen bonds (directional and selective) which link the two anions to the calixarene cage; the four CH/π interactions (directional and thus selective) which stabilizes the PQ dication within the cage.

Table 2.5 Geometrical parameters relative to the CH/π and hydrogen bonds interactions found in the $\mathbf{4}_2 \supset PQ(TsO)_2$ complex.[a]

Entry	Interaction	Distance (Å)		Angle (°)
	Donor–H···Acceptor	H···A	D···A	D–H···A
1	N(1A)-H···O(1I)	2.953	2.014(6)	166
2	N(2A)-H···O(2I)	2.940	2.018(5)	161
3	N(1E)-H···O(3M)	2.936	1.977(5)	177
4	N(2E)-H···O(2M)	3.055	2.104(6)	170
5	C(13)-H·· Ct(A)	2.530	3.419(7)	155
6	C(13)-H·· Ct(D)	2.584	3.363(6)	128
7	C(14)-H·· Ct(E)	2.814	3.164(7)	127
8	C(14)-H·· Ct(F)	2.485	2.014(6)	166

[a] Ct indicates the centroids of the calix[4]arene aromatic rings.

In summary, the present study shows that, in low polar media, the binding efficiency of synthetic monotopic calix[4]arene receptors **1** and **2** toward *N*-methylpyridinium salts is strongly dependent on the nature of the anion. In particular, ion-pair binding is prompted by low coordinating anions such as triflimide. On the other hand the ancillary H-bond donor group present on the calixarene scaffold of the heteroditopic receptors **3** and **4** induces a general enhancement of the binding efficiency. The binding data also evidence that the structure of the ion pairs having an anisotropic charge distribution strongly affects the recognition process in particular with the heteroditopic receptors. For **3**, the observed self-assembly of cations, anions and neutral molecules in the crystal lattice, is the result of the simultaneous cooperation between the strong, long-range (but not directional) electrostatic interactions between charges species, and the weak, short-range and directional hydrogen bond interactions. Although the binding energy involved in the hydrogen bonds are lower when compared with the Coulombic energy of the ionic bond, it is the directionality of the hydrogen bond itself that play the dominant role in the formation of the infinite 1D polymeric

chains. Thus, it is the hydrogen bond and not the ionic bond which becomes the structure directing factor for the self-assembly. A systematic investigation on the factors that govern these self-assembly processes are undergoing in our laboratories.

The large affinity evidenced by the heteroditopic receptors **3** and **4** for the pyridinium ring was exploited for the complexation of dimethylviologen salts (paraquat). Differently from the *N*-methyl pyridinium cation, the paraquat dication (PQ^{2+}) benefits of peculiar redox properties and its salts may be potentially exploited as an electrochemical switchable "supramolecular bridge" between two calix[4]arene units. The formation of the 2:1 host-guest complexes could be seen as the starting point for the preparation of self-assembled superstructures switchable through external electrochemical stimuli.

2.3 Self-assembly of calix[4]arene-based semitubes in solution

In the previous chapter it has been shown how *N*-alkylpyridinium and viologen salts can be complexed by calix[4]arene hosts giving rise to the formation of 1:1 and 2:1 host:guest adducts. It is also known that *N*-alkylpyridinium and in particular viologens salts are endowed with interesting redox properties.

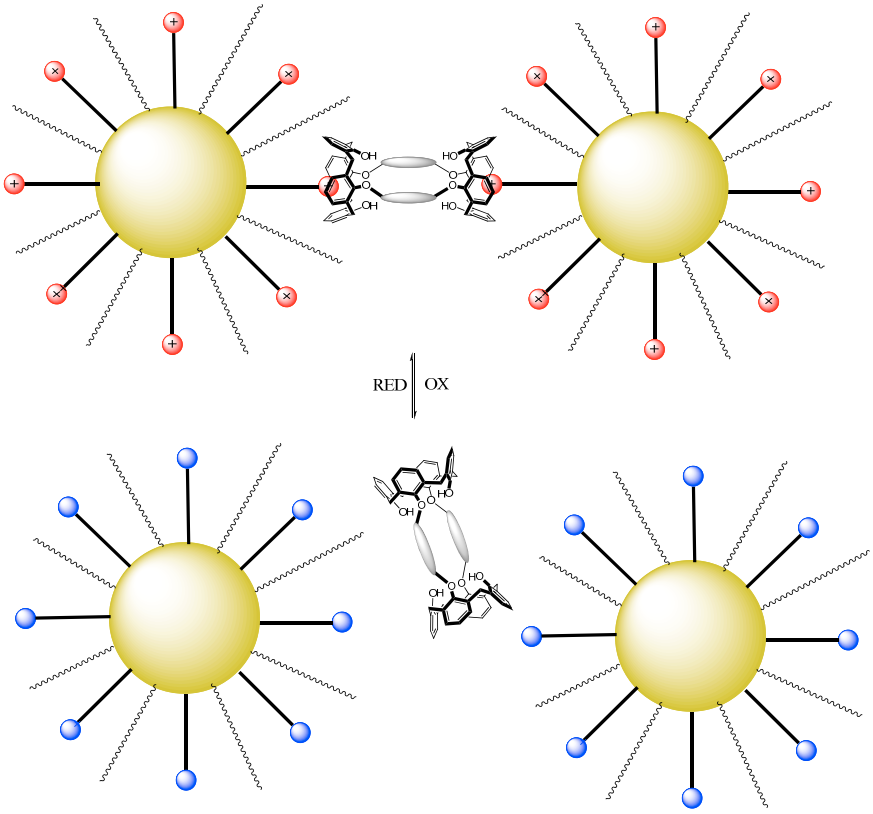

Figure 2.24 Schematic representation of a self-assembled 3D network obtained through the complexation of ditopic hosts with nanoclusters functionalized with alkyl pyridinium-based guest.

This suggested us the possibility to use calix[4]arene-based ditopic hosts as "supramolecular bridges" that promote the reversible self-assembly of nanostructures (2D or 3D SAM) properly functionalized on their surfaces with *N*-alkylpyridinium or viologen salts (see Figure 2.24).

Synthesis of the ditopic hosts

The design of the calix[4]arene ditopic hosts was based on previous studies reporting the synthesis of bis-calix[4]arene hosts covalently linked through their lower rim. Beer[45] named these calix[4]arene hosts as "tubes" when they are characterized by the presence of four "bridging spacers" connecting the two calix[4]arene sub-units (see Figure 2.25a), and calix[4]arene "semitubes" when only two bridges are present in 1,3-distal position of the lower rim (see Figure 2.25b). In both cases, the bis-calix[4]arenes maintain the two aromatic binding sites exposed to the bulk and thus they can be classified as ditopic hosts.

The synthesis of calix[4]arene tubes and semitubes is usually accomplished through the covalent linking of the phenolic groups present on the lower rim of each calix[4]arene unit. Such "bridging" procedure is not trivial and only few examples of synthesis are present in the literature that are based on two different approaches: a) synthesis step by step and b) one-pot synthesis. In the synthesis step by step,[45,46] the first step involves the functionalization of the calixarene phenolic groups with "spacers" having the general formula "X-spacer-Y". X is usually a good leaving group, such as a tosylate, and Y is either a worse leaving group, such as a bromide, or a functional group that can be transformed in a good leaving group before the second step. In the one-pot synthesis,[47] the calixarenes are mixed with spacers of formula X-spacer-X characterized by two identical leaving groups X. In both the approaches, the spacers can be either flexible alkyl chains of variable length or rigid aromatic mojeties. The step by step approach reduces the formation of intramolecular side-products but it is usually characterized by an overall low reaction yield due to the formation of several undesired oligomers. The one-pot synthesis is in contrast very often affected by the formation of appreciable amounts of intramolecular side-products especially when long alkyl chains are used as spacers.

45. R. A. Philip, W. Beer, P. Beer, *Dalton Trans.*, **2003**, 2249.
46. (a) P. Schmitt, P. D. Beer, M. G. B. Drew ,P. D. Sheen, *Angew. Chem., Int. Ed. Engl.*, **1997**, *36*, 1840; (b) S. E. Matthews, P. Schmitt, V. Felix, M. G. B. Drew, P. D. Beer, *J. Am. Chem. Soc.*, **2002**, *124*, 1341; (c) P. R. A. Webber, A. Cowley, M. G. B. Drew, P. D. Beer, *Chem. Eur. J.*, **2003**, *9*, 2439.
47. (a) K. Tantrakarn, C. Ratanatawanate, T. Pinsuk, O. Chailapakul and T. Tuntulani, *Tetrahedron Lett.*, **2003**, *44*, 33; (b) C. M. Jin, C. Ye, B. Twamley, J. M. Shreeve, *Synthesis*, **2006**, *17*, 2903; (c) P. R. A. Webber, P. D. Beer, G. Z. Chen, V. Felix, M. G. B. Drew, *J. Am. Chem. Soc.*, **2003**, *125*, 5774; (d) T. Nabeshima, T. Saiki, K. Sumimoto, S. Akine, *Tetraedron Lett.*, **2004**, *45*, 4719.

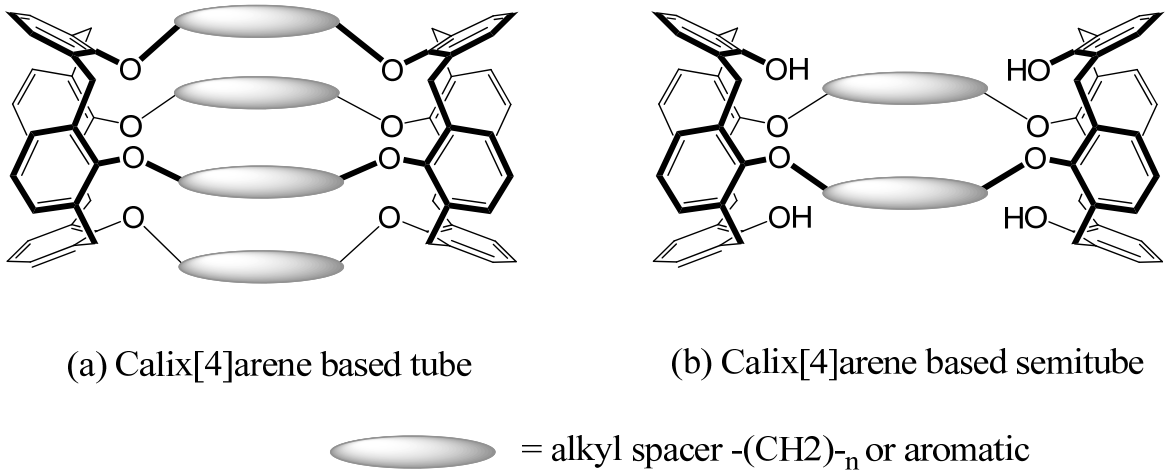

Figure 2.25 Calix[4]arene-based a) tubes and b) semitubes as ditopic receptors.

During the thesis we planned to synthetize only calix[4]arene semitubes because, as seen in 2.1, to the partial alkylation of the calix[4]arene sub-units should correspond a good degree of preorganization of the aromatic cavities. In order to evaluate the effect of the length of the spacers on the complexation properties of these ditopic hosts, we designed the synthesis of the bis-calix[4]arenes **6a** and **6b** (see Scheme 2.1), which are characterized by the presence of two spacers of three and six carbon atoms, respectively. The synthesis was accomplished following the one-pot strategy,[47b] by refluxing the calix[4]arene (**5**) in acetonitrile with two equivalents of the alkylating agent and of the base (K_2CO_3). As alkylating agents, we used the ditosylates of 1,3-propanediol and of 1,6-hexanediol.

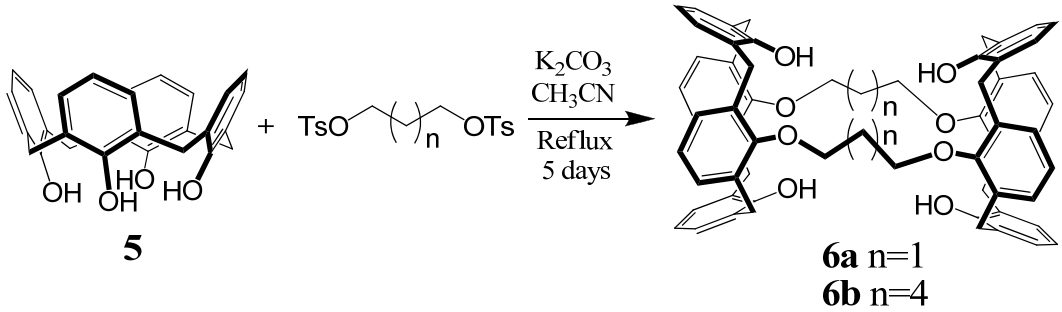

Scheme 2.1 Synthesis of the calix[4]semitube **6a** and **6b**.

The bis-calix[4]arene **6a** was obtained in high yields (60%) after refluxing the mixture for 5 days. **6a** is sparingly soluble in halogenated solvents especially in $CHCl_3$ and this propery was exploited for its purification. **6a** was indeed recovered by filtration after the treatment of the reaction residue with hot $CHCl_3$. **6b** is more soluble than **6a** in halogenated solvents and it has been isolated in 20% yield from the reaction mixture by column chromatography purification.

Both compounds have been characterized using NMR spectroscopy, elemental analysis and mass spectrometry. In the ^{1}H NMR spectrum of **6a** (see Figure 2.26) in CD_2Cl_2 is well visibile at very low fields (δ = 8.89 ppm) a singlet for 4 protons ascribable to the protons of the not alkylated phenolic groups. At δ ~ 7.1 ppm are present two overlapped doublets while at δ = 6.89 and 6.65 ppm are visible two separated triplets. These signals correspond to the meta and para protons of the aromatic nuclei, respectively. The separation of the two triplets suggests that the two calix[4]arene sub-units adopt a "flattened cone" conformation. The axial and equatorials protons of the methylene bridges of each calix[4]arene sub-unit give rise to a typical AX system (see paragraph 2.1.3) of two doublets (δ = 4.46 and 3.50 ppm). At δ = 4.39 ppm it is also present a triplet for 8 protons of the four methylene groups (α) of the two alkyl bridging units. Finally, at higher fields (δ = 3.16 ppm) is found a multiplet of 4 protons that corresponds to the two central methylene groups (β) of the chains.

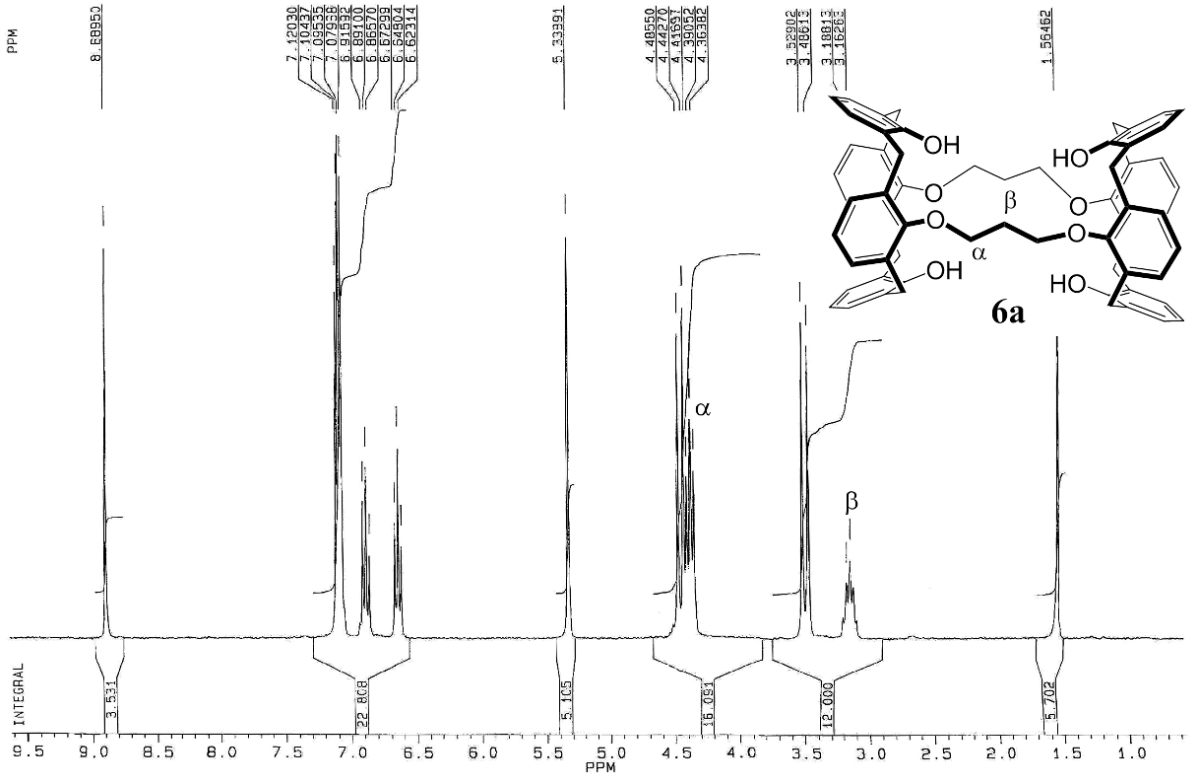

Figure 2.26 ^{1}H NMR spectrum of bis-calix[4]arene **6a** in CD_2Cl_2 (300 MHz)

The ^{1}H NMR spectrum of **6b** was taken in $CDCl_3$ (see Figure 2.27). It features are similar to those found in the spectrum of **6a** except the presence of two broad signals at δ = 1.9 and 2.3 ppm which were assigned to the methylene protons β and γ of the bridging alkyl chains.

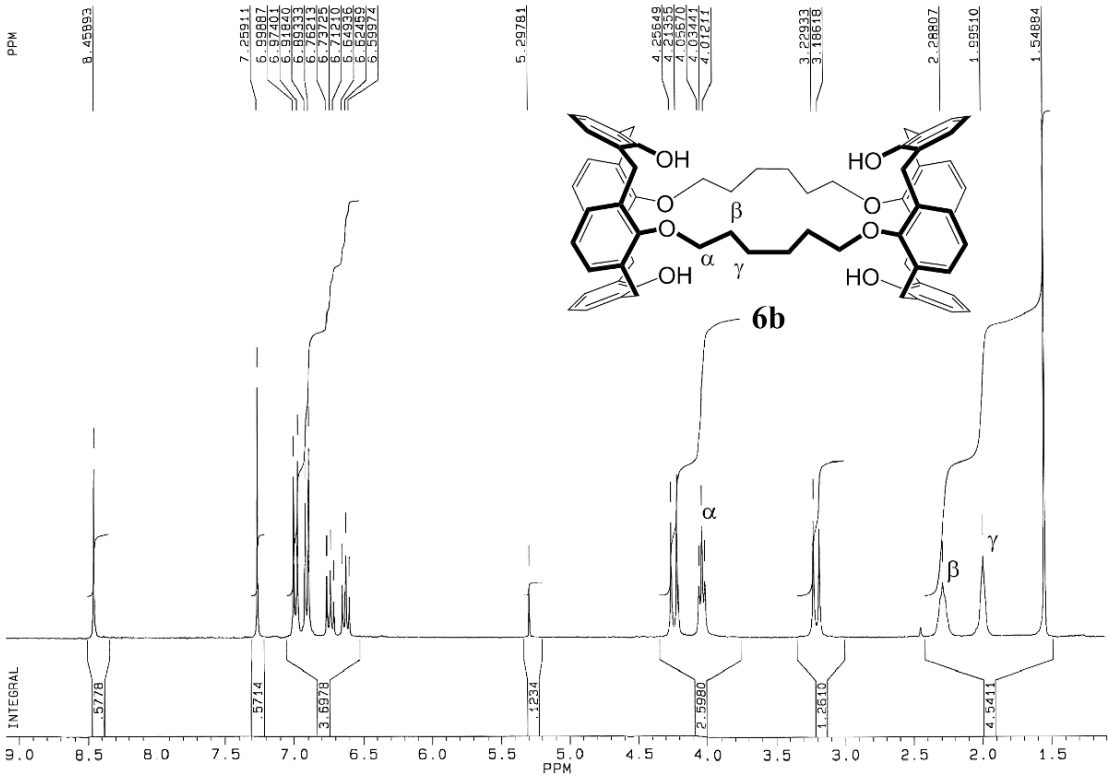

Figure 2.27 ^{1}H NMR spectrum of bis-calix[4]arene **6b** in $CDCl_3$

From the slow evaporation of a chloroform solution were obtained crystals of the bis-calix[4]arene **6b** that were analysed through XRD spectroscopy (see experimental section). The X-ray analysis confirms the hypothesized structure of **6b** (see figure 2.28). In the unit cell are present also two molecules of chloroform. **6b** forms an inclusion complex with one of these two molecules, which is embedded in a hydrophobic pocket defined by two aromatic rings belonging to different calix[4]arene sub-units and the two hexyl bridging chains. This result is not unexpected since it is known that the aromatic cavity of calix[4]arene derivatives is not wide enough to host the cumberson chloform molecule.

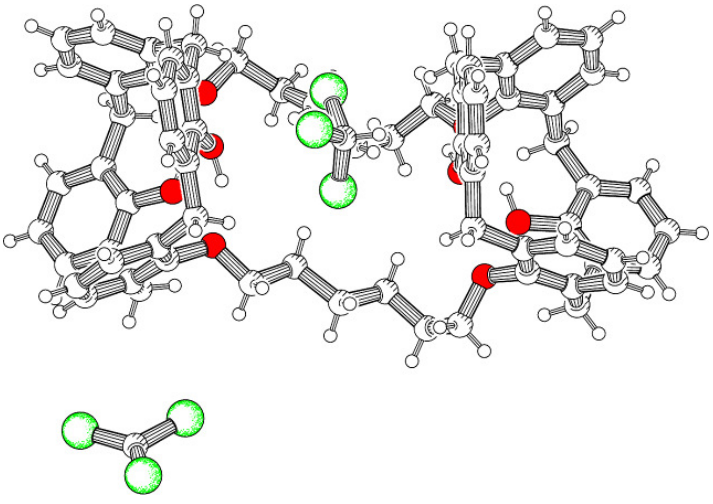

Figure 2.28 X-ray structure of bis-calix[4]arene **6b**.

Solution studies

In order to determine whether the aromatic cavities of the ditopic hosts **6a** and **6b** are capable to recognize simultaneously two pyridinum units in low polar solvents, we chosen and synthesized (see experimental part) the *N*-octyl pyridium iodide (**7**×2I) (see Figure 2.29) as lipophilic ion pair. We carried out preliminary ^{1}H NMR binding experiments in $CDCl_3$ solution. We chosen ^{1}H NMR spectroscopy as investigation tool because this technique can return very important information on the structure of the possible complexes formed in solution. The NMR study was unfortunately limited to **6b** because we observed that the solubility of the more rigid host **6a** in chloroform is far beyond the solubility limit (~5×10^{-3} M) allowed in order to obtain reliable binding results.

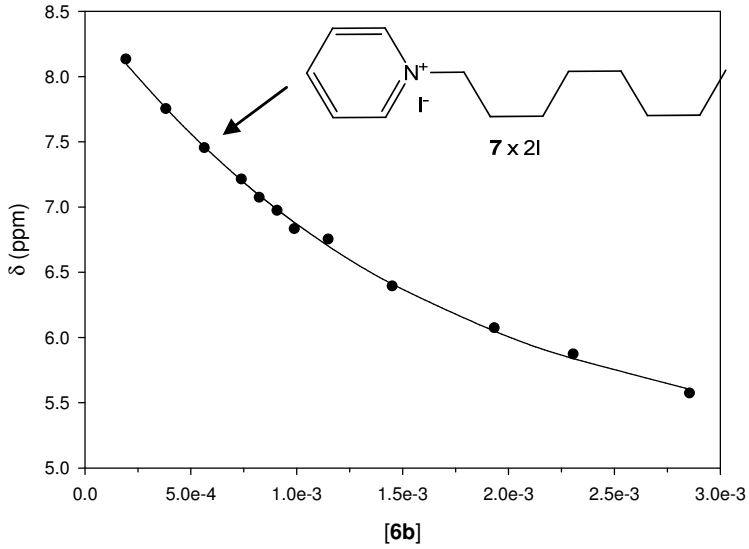

Figure 2.29 ^{1}H NMR binding isotherm obtained by the complexation of **7** with **6b** in $CDCl_3$ (T= 300 K) by monitoring the chemical shift experienced by the guest proton in para position.

In a typical ^{1}H NMR titration experiment (see also experimental part), increasing amounts of a solution of **6b** (c = 10^{-2} M) were added to a solution of **7** (c = 10^{-3} M). For reference, the binding experiment has been also carried out using **2** that represent the monotopic equivalent of **6b**. The binding process was faster than the NMR timescale and upon addition of **6b** the resonances of the pyridium ring of **7** were substantially upfield shifted (see Figure 2.29). This means that **7** was recognized by the aromatic cavities of **6b** and **2** through its π-poor pyridine ring. The binding costant (log$K$) and the limiting upfield shift ($\Delta\delta_\infty$) were thus calculated through the non-linear fitting[27] of the chemical shift variation experienced by the resonances of the pyridinium ring and gathered in Table 2.6.

Table 2.6. Binding constants ($\log K_{11}$) and limiting upfield shifts ($\Delta\delta_\infty$, ppm) for the formation of 1:1 adducts between *N*-octylpyridinium iodide (**7**) and ditopic and monotopic calix[4]arene-based hosts **6b** and **2**.[a]

Host	Resonance	$\log K_{11}$	δ_∞ (ppm)	$-\Delta\delta_\infty$ (ppm)[b]
6b	H_{ortho}	3.07±0.02	6.85±0.04	2.5
	H_{meta}	3.12±0.04	5.38±0.08	2.7
	H_{para}	3.00±0.03	4.38±0.11	4.2
2	H_{ortho}	3.07±0.02	6.85±0.04	2.5
	H_{meta}	2.9±0.2	6.33±0.26	1.8
	H_{para}	2.9±0.1	5.91±0.34	2.6

[a]Determined by ^{1}H NMR spectroscopic titrations at T = 300 K in $CDCl_3$ (standard deviations in parenthesis); initial concentration of the guest [**7**] = 10^{-3} M, concentration of the titrant [**6b**] = 10^{-2} M; [b] $\Delta\delta_\infty = \delta_\infty - \delta_{free}$ where δ_{free} (ppm): 9.33 (ortho), 8.13 (meta), 8.53 (para).

The binding data gathered in Table 2.6 show that: a) the log*K* are almost independent from the pyridine resonance used for their determination, and b) the binding efficiencies of the ditopic host **6b** and of the monotopic one **2** are very similar. Latter result is quite unexpected considering that **6b** could, in principle, recognize two ion pairs. On the other hand, it should be observed that for fast exchange conditions, the NMR titrations allow the determination of binding constants for complexation process having a pure 1:1 stoichiometry. The log*K* calculated for **6b** could be reasonably approximated. To verify these findings, the stoichiometry of binding between **6b** and **7** was assesed using continuos variation methods (see experimental part).

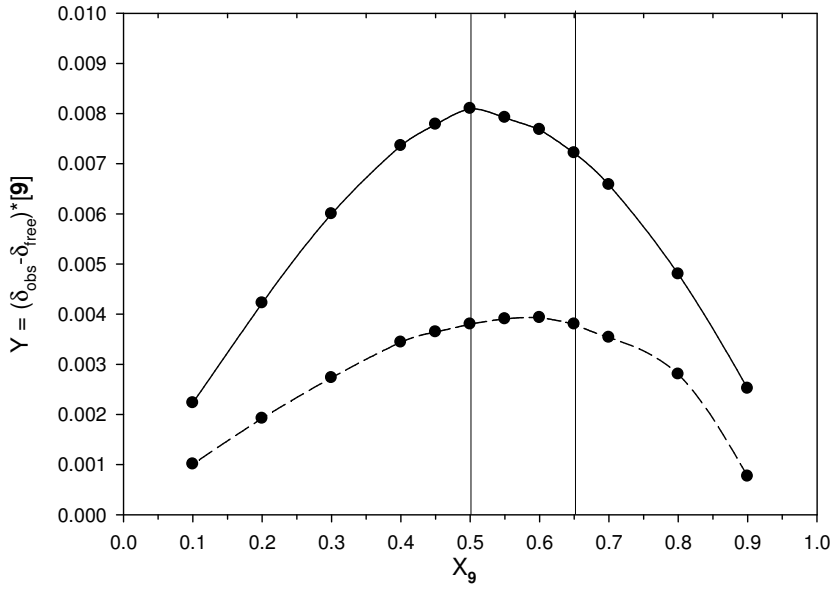

Figure 2.30 Job's plots for the complexation of **7** with **6b** in $CDCl_3$. The dashed and the continuos line represent the plots obtained using $n_{tot} = 2.5\times10^{-6}$ (dashed line) and 5×10^{-6} (continuos line); δ_{obs} is the chemical shift of the ortho proton of the aromatic ring of **7**.

The two plots of Figure 2.30 were determined using increasing amounts of the interacting species present in solution. When the total number of moles, expressed as $n_{tot}= n_{\mathbf{6b}} + n_{\mathbf{9}}$, is 2.5×10^{-6} , the value of the amount Y, proportional to the complex formed in solution, reaches its maximum for a molar fraction of X = 0.6. This value is slightly lower than the theoretic value of 0.66 that should correspond to a "pure" Host:Guest stoichiometry of 1:2.

Doubling n_{tot} (5×10^{-6}), the plot becomes sharper, but unexpectedly it reaches its maximum for a molar fraction of 0.5. From these results thus it appears that the two binding processes described by equilibria (1) and (2) are coexistent for lower concentration of **7**, while a pure 1:1 stoichiometry (1) is dominating when the concentration of **7** increased.

$$\text{H-H} + \text{G} \overset{K_{11}}{\rightleftharpoons} \text{H-H} \supset \text{G} \qquad (1)$$

$$\text{H-H} \supset \text{G} + \text{G} \overset{K_{12}}{\rightleftharpoons} \text{G} \subset \text{H-H} \supset \text{G} \qquad (2)$$

$$2\text{H-H} + 2\text{G} \overset{K'_{11}}{\rightleftharpoons} \text{H-H} \supset \text{G--G} \subset \text{H-H} \qquad (3)$$

The trend here observed is contrary to what reasonably expected and it could be tentatively explained only considering that, in low polar solvents, **7** is likely present as an aggregate of ion pairs. As a consequence the maximum of Y observed for a molar fraction of 0.5 could be arised for complexation processes having higher stoichiometry (2:2, 3:3 etc.), in which **7** is complexed *i.e.* as a dimer (see equation (3)). On the other hand the fast exchange conditions observed in the ^{1}H NMR titration experiments do not help to disclose the nature of this possible aggregation. To disclose the problem, we carried out dilution experiments on **7** using a "fast" investigation tool suche as UV/Vis spectroscopy. In Figure 2.31 it has been reported a collection of spectra of **7** recorded in $CHCl_3$ at different concentration. It is easily recognized that the position of the absorbing bands changes appreciably with the concentration of the salt. In particular we observed that the band present at λ~360 nm in the 10^{-2} M solution, undergoes a red shift on dilution. In the 5×10^{-4} M solution this band is no longer visible, while becomes appreciable the presence of a band denoted with an asterisk, that in the more concentrated solutions of **7** was barely recognized as a shoulder of more intense absorptions.

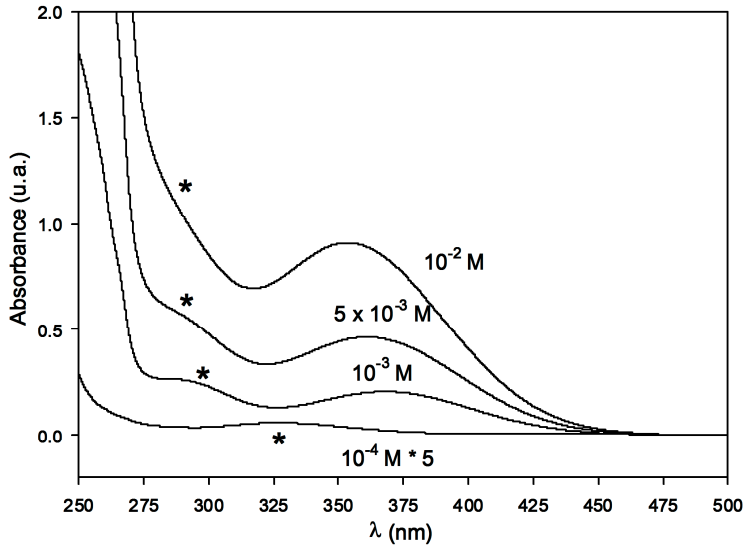

Figure 2.31 Absorbance of 10^{-2}, 5×10^{-3}, 10^{-3} and 10^{-4} M (multiplied five times) solutions of **7** in $CHCl_3$.

The first of the two bands was ascribed to a charge transfer (C.T.) process between the iodide and the positevely charged pyridinium ring. The red shift observed on dilution has been thus explained in terms of a loosening of the ion pair that occurs at low concentration of the salt. These results indirectly confirmed that the binding stoichiometry between **6b** and **7** is negatively affected by the aggregation of the ion pair. The only way to reduce this undesired phenomenon is to evaluate the binding process in solutions more diluted than those used in the previous NMR titration experiments (~10^{-3} M). A new optical titration experiment was hence devised, where a 10^{-4} M solution of **7** in $CHCl_3$ was titrated with a 10^{-3} M solution of **6b** in the same solvent. UV/vis spectroscopy was adopted as investigation tool because, differently from NMR, the collection of spectra obtained from a titration can be handled with analysis software such as Specfit/32[34] in order to evaluate the presence of more equilibria competing in solution.

The collection of spectra depicted in Figure 2.32 shows that the main effect determine by the addition of **6b** to the solution of **7** is an intensity reduction of the main CT band at λ ~325 nm and the formation of a new weak one at λ ~ 470 nm. The presence of an isosbestic point at λ = 435 nm suggests that at least two species are present in solution. The absorbption data were fitted using the binding models illustrated in equations (1) – (3) and the most reliable results were obtained considering the coexistent equilibria (1) and (2). The calculated binding constants were: $\log K_{11} = 4.0 \pm 0.1$; $\log \beta_{12} = 9.3 \pm 0.2$ and $\log K_{12} = 5.3 \pm 0.1$. From these results it also appears that at this concentration a positive allosteric effect is operating since the $\log K_{12}$ is slightly higher than the $\log K_{11}$.

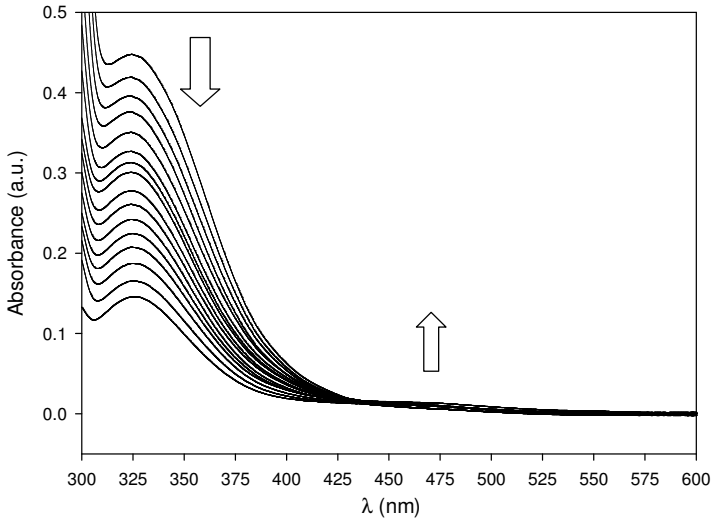

Figure 2.32 Collection of spectra obtaine during the UV/Vis titration of **7** with **6b** in chloroform solution (initial concentration of the guest [**7**] = 10^{-4} M, initial concentration of the titrant [**6b**] = 10^{-3} M). Only the spectral region 300-600 nm has been visualized because **6b** give rise to a strong absorbition band centred at λ = 285 nm.

2.4 Experimental section

2.4.1 Materials and instrumentation

All reactions were carried out under nitrogen; all solvents were freshly distilled under nitrogen and stored over molecular sieves for at least 3h prior to use. ^{1}H and ^{13}C NMR spectra were recorded on instrument operating at 300 and 75 MHZ, respectively. Chemical shift reported are referred either to the tetramethylsilane (TMS) or residual solved resonances. ESI-MS spectra were recorded with Infusion Waters Acquity Ultra Performance LC instrument. UV-Visible spectra were recorded with a Lambda Bio 20 instrument. Melting points are uncorrected, and were recorded with Electrothermal instrument. Silica gel layers (SiO2, MERCK 60 F254) were used for thin layer chromatography (TLC). 60 Å silica gel (MERCK, 0.04-0.063 mm, 230-240 mesh) were used for column chromatography. Compounds **1**,[7] **2**,[24] **3**,[48] **4**,[49] **5**,[50] *N*-methyl pyridinium triflimide[51] (NMPTf$_2$N), ditosylate of propan-1,3-diol[52] and ditosylate of hexane-1,6-diol[53] were synthesised according to reported procedures. All other reagents were of reagent grade quality as obtained from commercial suppliers and were used without further purification.

---

48. A. Arduini, A. Secchi, A. Pochini, *J. Org. Chem.*, **2000**, *65*, 9085.
49. A. Arduini, E. Brindani, G. Giorgi, A. Pochini, A. Secchi, *Tetrahedron*, **2003**, *59*, 7587.
50. A. Arduini, A. Casnati in *Macrocycle Synthesis, A Practical Approach,* Ed.*:* D. Parker, OUP, Oxford, 1996, pp. 145-172.
51. Y. Nakamura, T. Maki, X. Wang, K. Ishihara, H. Yamamoto *Adv. Synth. Catal.*, **2006**, *348*, 1505.
52. M. Nakamura, H. Yokono, K. Tomita, M. Ouchi, M. Miki, R. Dohno, *J. Org. Chem.*, **2002**, *67*, 3533.
53 (a) F. Drahowzal, D. Klamann, *Monatshefte fuer Chemie*, **1951**, *82*, 460; (b) V. Pejanovic, *Eur. J. Med. Chem.*, **2006**, *41*, 503.

2.4.2 Synthesis

General procedure for the synthesis of NMPX salts

Pyridine (2.3 g, 29 mmol) and the proper amount of methylating agent CH_3X (24 mmol) were dissolved in acetonitrile (150 ml). The resulting homogeneous solution was refluxed for 24h. After cooling to room temperature, 150 mL of ethyl acetate were slowly added to the reaction mixture until a crystalline solid precipitated from the solution. The solid was recovered by suction filtration, washed with ethyl acetate (3 × 25 ml) and dried under vacuum. The recovered salt did not required further purification.

***N*-methyl pyridinium tosylate (NMPTsO)**: toluene-4-sulfonic acid methyl ester (4.5 g) was used as methylating agent to afford 5.9 g of NMPTsO as a white solid (92%). M.p.: 138-139 °C; lit: 138-139 °C.[54]

***N*-methyl pyridinium iodide (NMPI)**: iodomethane (3.4 g) was used as methylating agent to afford 5.1 g of NMPI as a white solid (96%). M.p.: 117-119 °C; lit: 116-118 °C.[55]

***N*-methyl-pyridinium chloride (NMPCl)**: The salt was obtained from the corresponding tosylate (NMPTsO) by anion exchange on a 'Dowex' 1-X8 (Cl) 100-200 mesh standard grade resin. The resin (10 g) was initially activated with a solution of HCl (100 ml, 10% w/v in water), treated with a saturated solution of NaCl in water (100 ml), and washed with 200 ml of water. A solution of NMPTsO (2 g, 7.5 mmol) in 10 ml of water was eluted trough the resin. The exchanged product was recovered by washing the resin with 150 ml of water. The solution was dried under vacuum to obtain 0.95 g of NMPCl as a white hygroscopic solid (97 %). M.p.: 149-150 °C; lit: 149.5±0.5 °C.[56]

***N*-methyl pyridinium trifluoroacetate (NMPTFA)**: a 0.3 M solution of silver trifluoroacetate in water (50 ml) were added to a stirred solution of NMPI (3.3 g, 15 mmol) in 50 ml of water. The resulting solution was filtered off to remove the precipitate of AgI and evaporated to dryness under reduced pressure to afford 2.9 g of NMPTFA as a colourless viscous oil (96 %). ^{1}H NMR (DMSO-d_6, 300 MHz) δ (ppm) 9.13 (bd, 2 H, J = 6 Hz), 8.59 (bt,

54. C. S. Marvel, E. W. Scott, K. L. Amstutz, *J. Am. Chem. Soc.,* **1929**, *51*, 3638.
55. J. R. Ames, *J. Pharm. Sci.*, **1991**, *80*, 293.
56. D. S. Newman, D. P. Morgan, R. T. Tiliack, *J. Chem. Eng. Data,* **1976**, *21*, 279.

1 H, *J* = 6 Hz), 8.14 (bt, 2 H, *J* = 6 Hz), 4.42 (s, 3 H); ^{13}C NMR (DMSO-d_6, 75 MHz) δ (ppm) 158.3 (q, CF_3C=O, *J* = 30 Hz), 145.5, 144.8, 127.4, 117.1 (q, CF_3, *J* = 300 Hz), 47.5. Elemental analysis calculated for $C_8H_8F_3NO_2$: C, 46.38; H, 3.89; N, 6.76 %; found: C, 46.43; H, 3.99; N, 6.54%.

General procedure for the synthesis of PQX_2 salts

4,4'-bipyridine (2.5 g, 16 mmol) and the proper amount of methylating agent CH_3X (40 mmol) were dissolved in acetonitrile (150 ml). The resulting homogeneous solution was refluxed for 24h. After cooling to room temperature, 150 ml of ethyl acetate were slowly added to the reaction mixture until a crystalline solid precipitated from the solution. The solid was recovered by suction filtration, washed with ethyl acetate (3 × 25 ml) and dried under vacuum. The recovered salt did not required further purification.

***N,N'*-dimethyl viologen ditosylate ($PQ(TsO)_2$):** toluene-4-sulfonic acid methyl ester (7.4 g) was used as methylating agent to afford 7.5 g of $PQ(TsO)_2$ as a yellow solid (94 %). M.p.: 222-223 °C; ^{1}H NMR (D_2O, 300 MHz) δ (ppm) 8.93 (d, 4 H, *J* = 6 Hz), 8.35 (d, 4 H, *J* = 6 Hz), 7.56 (d, 4 H, *J* = 6 Hz), 7.24 (d, 4 H, *J* = 6 Hz), 4.43 (s, 6 H), 2.30 (s, 6 H); ^{13}C NMR (D_2O, 75 MHz) δ (ppm) 152.5, 149.4, 145.5, 142.8, 132.6, 129.7, 128.6, 51.5, 23.7. Elemental analysis calculated for $C_{26}H_{28}N_2O_6S_2$: C, 59.07; H, 5.34; N, 5.30; S, 12.13; found: C 59.14 %, H 5.40 %, N 5.31 %, S 12.22%.

***N,N'*-dimethyl viologen diiodide (PQI_2):** iodomethane (5.7 g) was used as methylating agent to afford 6.2 g of PQI_2 as a red solid (95 %). M.p.: 325-326 °C; lit: 325 °C.[57]

Bis-calix[4]arene 6a: a solution of calix[4]arene **5** (3 g, 7.1 mmol) and K_2CO_3 (2 g, 14.2 mmol) in CH_3CN (150 ml) was refluxed under vigorous stirring for 10 minutes. After this period, ditosylate of propan-1,3-diol (5.4 g, 14.2 mmol) was added. The resulting mixture was refluxed for further 3 days, cooled to room temperature and evaporated to dryness under reduced pressure. The residue was taken up with 50ml of a 10% v/v solution of HCl and dicloromethane (200 ml). The separated organic phase was was washed with distilled water (3x25ml), dried with Na_2SO_4, and evaporated to dryness under reduced pressare. The crude

57. J. H. Ross, R. I. Krieger, *J. Agric. Food Chem.*, **1980**, *28*, 1026.

residue was purified by trituration with chloroform followed by suction filtration. Calix[4]arene **6a** was isolated as a white solid in 60% yield.
^{1}H NMR (CD_2Cl_2, 300 MHz) δ (ppm): 8.90 (s, 4H, -OH); 7.11 (d, 8H, J = 7.5 Hz, ArH); 7.09 (d, 8H, J = 7.4 Hz, ArH); 6.89 (t, 4H, J = 7.5 Hz, ArH); 6.65 (t, 4H, J = 7.4 Hz, ArH); 4.46 (d, 8H, J = 12.8 Hz, Ar-CH_2-Ar ax.); 4.39 (t, 8H, J = 8 Hz, O-CH_2-CH_2-); 3.51 (d, 8H, J = 12.8 Hz, Ar-CH_2-Ar eq.); 3.16 (p, 4H, J = 8 Hz, O-CH_2-CH_2-CH_2); ^{13}C NMR (CD_2Cl_2, 75 MHz): δ (ppm) 153.6; 151.9; 134.9; 129.6; 129.0; 129.0; 126.1; 120.0; 73.0; 32.2; 31.2; ESI-MS : m/z = 951 $[M+Na]^+$; m.p.> 300 °C; elemental analysis for $C_{62}H_{56}O_8$, calcd.: C 80.17, H 6.03; obs.: C 80.35, H 6.28.

Bis-calix[4]arene 6b: a solution of calix[4]arene **5** (1 g, 2.4 mmol) and K_2CO_3 (0.6 g, 5 mmol) in CH_3CN (50 ml) was refluxed under vigiuros stirring for 10 minutes. After this period, ditosylate of hexane-1,6-diol (2 g, 4.7 mmol) was added. The resulting mixture was refluxed for further 3 days, cooled to room temperature and evaporated to dryness under reduced pressure. The residue was taken up with 20 ml of a 10% v/v solution of HCl and dicloromethane (50 ml). The separated organic phase was was washed with distilled water (3x25ml), dried with Na_2SO_4, and evaporated to dryness under reduced pressare. The crude residue was purified by column chromatography using a 7:3 dicholoromethane : n-hexane mixture as eluent. Calix[4]arene **6b** was isolated as a white solid in 30% yield.
^{1}H NMR ($CDCl_3$, 300 MHz): δ (ppm) 8.45 (s, 4H, -OH); 6.99 (d, 8H, J = 7.5 Hz, ArH); 6.91 (d, 8H, J = 7.5 Hz, ArH); 6.74 (t, 4H, J = 7.5 Hz, ArH); 6.62 (t, 4H, J = 7.4 Hz, ArH); 4.23 (d, 8H, J = 12.9 Hz, Ar-CH_2-Ar ax.); 4.03 (t, 8H, J = 6.7 Hz, O-CH_2-CH_2-); 3.21 (d, 8H, J = 12.9 Hz, Ar-CH_2-Ar eq.); 2.9-2.8 (m, 8H, O-CH_2-CH_2-CH_2); 2.0-1.9 (m, 8H, O-CH_2-CH_2-CH_2). ^{13}C NMR ($CDCl_3$, 75 MHz): δ (ppm) 153.3; 151.7; 133.6; 128.8; 128.4; 128.0; 125.3; 118.8; 75.9; 31.2; 30.1; 24.9; ESI-MS : m/z = 1035 $[M+Na]^+$; m/z = 1052 $[M+K]^+$; m.p. > 300 °C; elemental analysis for $C_{68}H_{68}O_8$: calc. C 80.63, H 6.72; obs. C 80.91, H 7.13.

***N*-octyl pyridinium iodide (7×2I):** pyridine (3.9 g, 50 mmol) and 1-iodooctane (4 g, 16.5 mmol) were dissolved in acetonitrile (100 ml). The resulting homogeneous solution was refluxed for 24h. After cooling to room temperature, solvent was removed under reduced pressure. The oily orange residue was taken up with 150 ml of ethyl acetate. The solution was refrigerated at -20°C until a yellow precipitate formed. The precipitate was recovered by suction filtration, washed with ethyl acetate (3 × 25 ml) and dried under vacuum to obtain the

pure **7**×2I as a very hygroscopic low melting yellow solid in 86% yield. ^{1}H NMR (D_2O, 300 MHz) :δ (ppm) 8.86 (d, 2H, J = 6.2 Hz, Ar-H); 8.55 (t, 1H, J = 7.8 Hz, Ar-H); 8.1-8.0 (m, 2H, Ar-H); 4.62 (t, 2H, J = 7.3 Hz, N-CH_2-CH_2-); 2.1-2.0 (m, 2H, N-CH_2-CH_2-); 1.3-1.2 (m, 10H, -CH_2-CH_2-CH_2-CH_2-CH_2-CH_3); 0.85 (t, 3H, J = 6.5 Hz, -CH_2-CH_3). ^{13}C NMR (D_2O, 75 MHz): δ (ppm) 149.0; 147.6; 131.6; 65.1; 34.6; 34.2; 31.8; 31.7; 28.8; 25.5; 17.0. ESI-MS: m/z = 192 $[M-I]^+$; elemental analysis for $C_{13}H_{22}NI$: calc. C 48.91, H 6.95, N 4.39; obs. C 48.65, H 7.15, N 4.28.

2.4.3 Binding studies

^{1}H NMR continuous variation methods (Job's plot)

Aliquots of stock solutions in $CDCl_3$ of the calix[4]arene host and of the corresponding *N*–alkyl pyridinium organic salt were added to several 5mm NMR tubes in different ratios maintaining the total molar concentration constant. In this way were prepared 12-14 samples in which the mole fraction (x) of the interacting species was continuously varied from 0.1 to 1. A ^{1}H NMR spectrum was recorded for each sample. The corresponding Job plot was obtained plotting a property proportional to the complex concentration, in this case $(\delta_{obs}-\delta_{free}) \times [guest]_0$, versus the mole fraction of the salt. δ_{obs} and δ_{free} represent the chemical shift (ppm) of a resonance of the pyridinium cation in the complex and in the free salt, respectively. The stoichiometry of binding is obtained from the value of the mole fraction in abscissa that yields the maximum of the plot. For x = 0.5, the stoichiometry of binding is 1:; for x = 0.66 the stoichiometry of binding is H:G = 1:2

^{1}H NMR titrations

Solutions (500 μl) in $CDCl_3$ of the organic salt (usually c = 10^{-3} M) were prepared in a 5 mm NMR tube and small aliquots of a tenfold concentrated solution of the calix[4]arene host (usually c= 10^{-2} M) in $CDCl_3$ were added. A ^{1}H NMR spectrum was recorded after each addition. Considering a 1:1 host-guest binding equilibrium, the apparent binding constant is expressed by the following equation:

$$R + S \underset{}{\overset{K}{\rightleftharpoons}} RS \; ; \; K = \frac{[RS]}{[R][S]}$$

where [R], [S], and [RS] are the concentrations of the calix[4]arene receptor, of the organic salt and of the complex at the equilibrium, respectively. The binding constants *K* were

calculated through the non-linear fitting of the chemical shift variation of the protons of the organic salt using the equation devised by Wilcox:[27]

$$\delta_{obs} = \delta_S + \frac{\Delta\delta}{2[S]_0}\left[\frac{1}{K} + [R]_0 + [S]_0 - \sqrt{\left(\frac{1}{K} + [R]_0 + [S]_0\right)^2 - 4[R]_0[S]_0}\right]$$

$$\Delta\delta = \delta_{RS} - \delta_S$$

where δ_{obs}, δ_S, δ_{RS}, $[R]_0$, and $[S]_0$ are the observed chemical shift of the proton under investigation in fast exchange condition, the chemical shift of same proton in the free salt and in the complex (guessed), the initial concentration of the guest and of the host, respectively. The conditions of the Weber parameter *p* ([conc. of the complex]/[maximum possible conc. of the complex]) were verified for each titration experiment according to the calculated binding constant.[27] If necessary the concentrations of the two reactants were adjusted and the NMR titration experiment repeated to explore the proper *p* range (0.2–0.8).

UV/vis titrations

Optical spectroscopic titrations were carried out in a quartz cuvette (path length = 1 cm), maintained at 300 K through an external thermostat, by adding small aliquots of a chloroform solution ($c = 2 \times 10^{-4}$ M) of the calix[4]arene host to a chloroform solution ($c = 2 \times 10^{-5}$ M) of the organic salt. The spectral data were collected in the 265–650 nm wavelength range. The binding constants were calculated selecting different binding models with the Specfit/32 software.[34] The fitting of the spectral data was carried out considering the optical variation in the sampled wavelength range. As for the NMR titrations, the Weber parameter *p* was checked against the calculated binding constant.

ESI-MS Measurements

In all the cases samples were prepared using the proper amount of host and guest in a chloroform : methanol 9 : 1 solution. Only for sample containing PQX_2 the preparation was executed by suspending a large excess of the solid paraquat salt PQX_2 (X = TsO, Cl, and I) in a 10^{-3} M solution of each receptor (**3** and **4**) in $CHCl_3$. The resulting heterogeneous mixtures were refluxed for at least half an hour, then cooled at room temperature and filtered to remove the undissolved solid material. The recovered homogeneous solutions were then diluted with a tenth part of methanol and analysed. All the samples were submitted to ESI-MS analysis in the positive mode with a Waters Acquity SQD equipment (cone voltage range: 25-40 V; desolvation temperature: 120 °C).

NMR diffusion experiments:

DOSY experiments were carried out in $CDCl_3$ at 300 K on a Bruker Avance 300 Spectrometer using a stimulated echo sequence with bipolar gradients (STEbp).[58] The diffusion coefficient *D* of the species present in solution was determined by monitoring the intensity decay of at least six resonances present in the NMR spectrum of the sample as a function of gradient strength applied to the sample. The fitting of the attenuation profiles was carried out using the equation:

$$I = I_0 e^{-D\gamma^2 g^2 \delta^2 (\Delta - \delta/3 - \tau/2)}$$

where *I* is the intensity of the observed resonance (attenuated), I_0 the intensity of the reference resonance (unattenuated), *D* the diffusion coefficient, γ the gyromagnetic ratio, *g* the gradient strength, δ the gradient pulse length, Δ the diffusion time, and τ the dephasing and rephasing correction time. For each sample 16 experiments were carried out, in which the gradient strength *g* was varied from 5 to 95 % of the maximum gradient intensity (5.35 G/mm).

X-ray crystallographic analysis

Crystallographic data for **1**⊃NMPI, $\mathbf{3}_2$⊃NMPCl, $\mathbf{4}_2$⊃$PQ(TsO)_2$ and **6b** are summarised in Table 2.7. Intensity data were collected on a Enraf-Nonius CAD4 diffractometer (**1**⊃NMPI, $\mathbf{4}_2$⊃$PQ(TsO)_2$) equipped with a CuKα radiation source (λ = 1.54178 Å), on a Bruker SMART diffractometer ($\mathbf{3}_2$⊃NMPCl) equipped with graphite monochromated MoKa radiation source (λ = 0.71073 Å) and CCD detector, and on a SiemensAED diffractometer (**6b**) using graphite monochromated CuKα radiation. The intensities were corrected for Lorentz, polarization and absorption effects. The structures were solved by direct methods using SIR2004[59] and refined on F^2 by full-matrix least-squares methods, using SHELXL-97.[60] All the non-hydrogen atoms were refined with anisotropic atomic displacements. For the **1**⊃NMPI structure, the hydrogen atoms were included in the refinement at idealised geometries and refined "riding" on the corresponding parent atoms with common isotropic atomic displacements 1.2 times those of their parent atoms. For the $\mathbf{4}_2$⊃$PQ(TsO)_2$ structure, the hydrogen atoms were placed at their calculated positions with the geometrical constraint C-H 0.96 Å and refined "riding" on their corresponding carbon atoms with relative isotropic atomic displacements.

58. D. Wu, A. Chen, C. S. Johnson, Jr., *J. Magn. Reson.*, **1995**, *A115*, 123.
59. SIR2004, M. C. Burla, R. Caliandro, M. Camalli, B. Carrozzini, G. L. Cascarano, L. De Caro, C. Giacovazzo, G. Polidori and R. Spagna, *J. Appl. Cryst.*, **2005**, 38, 381.
60. G. M. Sheldrick, *SHELXL97*, program for crystal structure refinement, University of Göttingen, Germany, **1997**, http://shelx.uni-ac.gwdg.de/shelx/index.html

Table 2.7 Crystal data for **1**⊃NMPI, $\mathbf{3}_2$⊃NMPCl, $\mathbf{4}_2$ ⊃$PQ(TsO)_2$ and **6b**.

	1⊃NMPI	$\mathbf{3}_2$⊃NMPCl	$\mathbf{4}_2$⊃$PQ(TsO)_2$	**6b**
Empirical formula	$C_{36}H_{36}O_6$•C_6H_8NI	$2C_{44}H_{44}N_2O_7$•C_6H_7NCl•$2C_2H_5OH$	$2C_{42}H_{44}N_2O_5$•$C_{12}H_{14}N_2$•$2C_7H_7SO_3$	$C_{33}H_{68}O_8$•$2CHCl_3$
Formula weight	785.717	1646.4	1842.277	1252.036
Crystal system	Trigonal	Monoclinic	Monoclinic	Triclinic
Space group	$P3_1$ (n. 144)	$P2_1/n$	$P2_1$ (n. 4)	*P -1*
a (Å)	18.564(1)	10.2410(8)	11.284(5)	15.114(1)
b (Å)	18.564(1)	25.067(2)	14.758(5)	19.254(1)
c (Å)	10.127(1)	17.916(1)	29.067(5)	12.036(1)
α (°)	90	90	90	103.11(1)
β (°)	90	102.30(1)	91.04(2)	104.06(1)
γ (°)	120	90	90	102.42(1)
V (Å^3)	3022.4(2)	4493.6(6)	4840(3)	3170.8(5)
Z	3	2	2	2
D_{calc} (g/cm^{-3})	1.295	1.217	1.264	1.311
F(000)	1212	1750	1956	1312
		Data collection		
Temperature (K)	293	293	293	293
θ Range (°)	3.0, 70.0	2.0, 23.28	3.0, 70.0	3.0, 70.0
Index ranges	-22 ≤*h*≤ 22 -22 ≤*k*≤ 20 -5 ≤*l*≤ 12	-11 ≤*h*≤ 11 -27 ≤*k*≤ 27 -19 ≤*l*≤ 19	-13≤ *h* ≤ 13 -15 ≤ *k* 17 -27 ≤ *l* ≤ 35	-12 ≤ *h* ≤ 8 -18 ≤ *k* ≤ 23 -14 ≤ *l* ≤ 14
Refl. measured	6301	36563	9717	12648
Indep. Refl.	4635 (R_{int}= 0.069)	6450 (Rint = 0.0535)	9527 (R_{int} = 0.0409)	12024 ($R_{int.}$ = 0.015)
Obs. Refl. [Fo > 4 σ(Fo)]	2719	3304	3432	6167
Data/ Restr./Param.	2719/ 14/ 452	6450/ 8/ 521	3432/ 33/ 1077	12024 / 761
		Structure refinement		
Final R indices[a] (obs. data)	*R1*=0.0584 *wR2*=0.092	*R1*=0.104 *wR2*=0.322	*R1* = 0.073 *wR2* = 0.2062	*R1* = 0.114 *wR2* = 0.372
Goodness of Fit *S*[b]	0.925	1.005	0.95	1.204
Min. and max. Residual ρ(e/Å^3)	0.34, -0.54	0.82, -0.41-	0.32, -0.25	1.12, -1.01

[a] $R1 = \Sigma \,||\, Fo| - |\, Fc|| / \Sigma \,|\, Fo|$, $wR2 = [\Sigma\, w(Fo^2\text{-}Fc^2)^2 / \Sigma wFo^4]^{1/2}$. [b] Goodness-of-fit $S = [\Sigma\, w(Fo^2\text{-}Fc^2)^2 / (n\text{-}p)]^{1/2}$, where *n* is the number of reflections and *p* the number of parameters.

For **6b** the structure contains two $CHCl_3$ solvent molecules for each bis-calix[4]arene unit. All the non-hydrogen atoms were refined with anisotropic atomic displacements. The hydrogen atoms were included in the last cycles of the refinement at idealized geometry (C-H and O-H

0.96 Å) and refined in the "riding" model with isotropic atomic displacements 1.2 times their Ueq their parent atoms. Geometric calculations were performed with the PARST97.[61]

Table 2.8. Conformational parameters[62] ϕ and χ and dihedral angles δ for the structures: **1**⊃NMPI (see Figure 2.15), $\mathbf{3}_2$⊃NMPCl (see Figure 2.16) and $\mathbf{4}_2$⊃PQ(TsO)$_2$ (see Figure 2.23)

	ϕ (°)	χ (°)		δ (°)
		1⊃NMPI		
A-B	70.3(8)	-85.3(7)	A-*R*	107.3(7)
B-C	88.8(7)	-72.7(8)	B-*R*	123.4(8)
C-D	70.8(7)	-85.5(7)	C-*R*	107.8(7)
D-A	87.3(8)	-72.5(8)	D-*R*	123.2(8)
		$\mathbf{3}_2$⊃NMPCl		
A-B	76.0(3)	-86.5(3)		
B-C	82.7(4)	-70.0(4)		
C-D	73.7(3)	-94.6(4)		
D-A	91.0(3)	-74.3(4)		
		$\mathbf{4}_2$⊃PQ(TsO)$_2$		
A-B	96.0(4)	-84.3(5)		
B-C	71.9(4)	-97.7(5)		
C-D	103.4(5)	-81.0(4)		
D-A	65.3(4)	-77.7(5)		
E-F	80.2(4)	-73.3(4)		
F-G	89.2(5)	-107.3(5)		
G-H	93.7(4)	-74.9(4)		
H-A	87.7(5)	-92.6(4)		

δ represent the dihedral angles between the least-squares planes through the phenolic rings and the molecular reference plane *R* (the least-squares plane through the four CH_2 bridging groups) according to the standard rules for calixarenes.[63]

61. M. Nardelli, *J. Appl. Crystallogr.*, **1996**, 29, 296-300.
62. F. Ugozzoli, G.D. Andreetti, *J. Incl. Phen. and Mol Rec. in Chem.*, **1992**, *13*, 337.
63. M. Perrin, D. Oehler in *Calixarenes 2001*, Eds. Z. Asfari,V. Böhmer, J. Harrowfield, J Vicens, Kluwer Academic Publisher, Dordrecht, 2001, pp. 65-85.

Chapter 3:
Calix[n]arene-protected Gold Nanoparticles and MPCs

Chapter 3. Calix[n]arene-protected gold nanoparticles and MPCs

3.1 Introduction to gold monolayer protected clusters (Au MPCs)

"Monolayer Protected Clusters" (MPCs),[1] also known as 3D Self-Assembled Monolayers (3D-SAM), represent an emerging class of organic–inorganic hybrid materials. Differently from colloids,[2] MPCs are constituted by a discrete aggregate of metal atoms (called inorganic core) stabilized by a shell of organic molecules (arranged like a monolayer around the metal surface), that maintain them stable in solution and prevent aggregation effect (see Figure 3.1). The MPCs characterized by a core of gold atoms (Au MPCs) are those that historically have attracted the largest interest of the scientific community,[3] even though in the literature it is possible to find increasing number of examples of MPCs characterized by cores of other noble metals such as silver,[4] palladium,[5] and copper.[6]

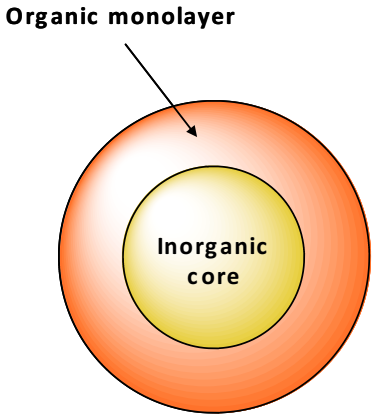

Figure 3.1 Schematic representation of a monolayer protected cluster (MPC)

1. For reviews on monolayer protected clusters see *e.g.*: (a) D. Astruc, M. C. Daniel, *Chem. Rev*. **2004**, *104*, 293; (b) A. C. Templeton, M. P. Wuelfing, R. W. Murray, *Acc. Chem. Res.*, **2000**, *33*, 27.
2. For book ands reviews on nobel metals nanoparticles see *e.g.* : (a) *Nanoparticles – Building blocks for nanotechnology*, Ed.: V. M. Rotello, Kluwer Academic / Plenum Publisher, New York, 2004; (b) *Nanoparticles: Synthesis, Stabilization, Passivation, and Functionalization*, Eds.: R. Nagarajan, T. A. Hatton, OUP, 2008; (c) *Nanoparticles, From Theory to Application,* Ed.: G. Schmid; Wiley-VCH, Weinheim, 2004.
3. For reviews on gold MPCs see: (a) R. Sardar, A. M. Funston, P. Mulvaney, R. W. Murray, *Langmuir*, **2009**, *25*, 13840; (b) E. Boisselier, D. Astruc, *Chem. Soc. Rev*., **2009**, *38*, 1759; (c) R. A. Sperling, G. P. Rivera, F. Zhang, M. Zanella, W. J. Parak, *Chem. Soc. Rev*., **2008**, *37*, 1896; (d) J. C. Love, L. A. Estroff, J. K. Kriebel, R. G. Nuzzo, G. M. Whitesides, *Chem. Rev.*, **2005**, *105*, 1103.
4. See *e.g.*:A. Brian, A. Korgel, D. Fitzmaurice, *Adv. Mater.* **1998**, *10*, 661 and references therein.
5. See *e.g.*: S. Chen, K. Huang, J. A. Stearns, *Chem. Mater.* **2000**, 12, 540 and references therein.
6. See *e.g.*: T. P. Ang, T. S. A. Wee, W. S. Chin, *J. Phys. Chem. B.* , **2004**, *108*, 11001 and references therein.

The stability and synthetic versatility of these compounds, together with their potential and fascinating properties correlated with the quantum confinement, have assured them an important role in the Nanosciences. The exploitment of these properties in discipline such as biology and medicine has been already documented.[1-3]

3.1.1 Synthesis of Au MPCs

The important role assumed nowadays by Au MPCs is, however, strictly derived from the more ancient studies on gold colloids. The first study dates back to 1857, when Faraday reported on the formation of deep red solutions of colloidal gold by reduction of an aqueous solution of chloroaurate ($AuCl_4^-$) using phosphorus in CS_2.[7] The reduction of $HAuCl_4$ with sodium citrate has been for the long time the most used method to prepare water soluble nanoparticles. This method was introduced by Turkevitch in 1951 and it leads to nanoparticles stabilized with citrate ions with a mean diameter of ca. 20 nm.[8] Successively, Frens et al.[9] and more recently Yonezawa et. al.[10] reported efforts aimed to obtain gold nanoparticles of chosen size by varying the ratio between the reducing or stabilizing agents and gold. The stabilization of gold nanoparticles with alkanethiols was first reported in 1993 by Mulvaney and Giersig, who showed the possibility of using thiols of different chain lengths and their analysis.[11].The first versatile and reproducible method for the synthesis of lipophilic Au MPCs was reported by Brust and Schiffrin in 1994 (see Figure 3.2).[12] This method allowed the synthesis gold nanoparticles (ranging in diameter between 1.5 and 5 nm) stabilized with n-dodecanthiol chains, which were thermally and air-stable. The Au MPC prepared with this method could be repeatedly isolated and redissolved in most organic solvents without irreversible aggregation or decomposition. Moreover, they could be analyzed with conventional characterization techniques such as NMR, IR, and UV-Vis. This new materials could be easily handled and functionalized just as stable organic and molecular compounds. The method is inspired by the Faraday's two-phase system[7] and it employs thiolated ligands as stabilizers of the gold surface due to the "soft" Lewis character of both Au and S.

$$AuCl_4^- (aq) + N(C_8H_{17})_4^+ (org) \rightarrow N(C_8H_{17})_4^+ AuCl_4^- (org)$$

$$AuCl_4^- (org) + nC_{12}H_{25}SH (org) + 3m\ e^- \rightarrow 4m\ Cl^- (aq) + [Au_m(C_{12}H_{25}SH)_n] (org)$$

---

7. M. Faraday, *Philos. Trans.*, **1857**, *147*, 145.
8. J. Turkevitch, P. C. Stevenson, J. Hillier, *Discuss. Faraday Soc*., **1951**, *11*, 55.
9. G. Frens, *Nature: Phys. Sci.*, **1973**, *241*, 20.
10. T. Yonezawa, T. Kunitake, Colloids Surf. A: Physicochemical. Eng. Asp., **1999**, 149, 193.
11. M. Giersig, P. Mulvaney, *Langmuir*, **1993**, *9*, 3408.
12. M. Brust, M. Walker, D. Bethell, D. J. Schiffrin, R, Whyman, *J. Chem. Soc., Chem. Commun.* **1994**, 801.

The aurate $AuCl_4^-$ is initially transferred to the toluene phase using tetraoctylammonium bromide as phase-transfer catalyst and reduced in situ by $NaBH_4$, previously dissolved in water, in the presence of dodecanethiol. During this step the organic phase changes its colour from orange to deep brown within a few seconds upon addition of $NaBH_4$ (see Figure 3.2).

Figure 3.2 Colour changes of the two-phase system during the synthesis of Au MPCS with the Brust-Schiffrin method: a) before the addition of tetraoctylammonium bromide the water solution containing the aurate (down) is yellow; b) after the addition of tetraoctylammonium bromide the aurate is transferred in toluene (up); after the addition of $NaBH_4$ the organic solution becomes black colored (gold reduction).

Murray et al. have later shown that large thiol/gold molar ratios give smaller average core sizes.[13] Following this author, indeed, the MPC synthesis reaction in the organic phase (toluene) is a two-step process here summarized:

$$AuCl_4^- \text{ (toluene)} + RSH \rightarrow (-Au^{I}SR-)_n \text{(polymer)} \quad (1)$$

$$(-Au^{I}SR-)_n + BH_4^- \rightarrow Au_x(SR)_y \quad (2)$$

In the first step, the aurate is reduced to Au^I by the thiols and inserted in a polymeric structure where the Au^I species are coordinated by two sulphur groups. During the second step, this polymeric structure is reduced by the hydride with the formation of the nanocluster. Steps (1) and (2) are consistent with a "nucleation – growth – passivation process" and large thiol/gold mole ratios, fast addition of $NaBH_4$ and short reaction times produce Au MPCs characterized by very small core sizes (<2 nm). The same authors have shown that a high abundance of very small clusters is obtained also using bulky ligands.[14] Brust et al. have then devised to a single phase system method for the preparation of *p*-mercaptophenol-stabilized Au MPCs.[15] The introduction of the single phase system method has allowed the synthesis of Au MPCs stabilized by a variety of functional thiol ligands.[16]

---

13. (a) M. J. Hostetler, J. E. Wingate, C.-J. Zhong, J. E. Harris, R. W. Vachet, M. R. Clark, J. D. Londono, S. J. Green, J. J. Stokes, G. D. Wignall, G. L. Glish, M. D. Porter, N. D. Evans, R. W. Murray, *Langmuir*, **1998**, *14*, 17; (b) W. P. Wuelfing, A. C. Templeton, J. F. Hicks, R. W. Murray, *Anal. Chem.*, **1999**, *71*, 4069; (c) W. Chen, A. C. Templeton, R. W. Murray, *Langmuir*, **2000**, *16*, 3543.
14. S. Chen, R. W. Murray, *Langmuir*, **1999**, *15*, 682.
15. M. Brust, J. Fink, D. Bethell, D. J. Schiffrin, C. Kiely, *J. Chem. Soc., Chem. Commun.*, **1995**, 1655.
16. See *e.g.*: A. C. Templeton, W. P. Wuelfing, R. W. Murray, *Acc. Chem. Res.* **2000**, *33*, 27 and references therein.

Another important reaction that involved Au MPCs is the so-called "place-exchange reaction" developed by Murray and co-workers (see Figure 3.3).[17] With this reaction the target Au MPCs are synthesized through exchange of the organic shell of *n*-dodecanthiol-stabilized Au MPCs with the desired thiolated ligand. The driving force of this process is the large excess of the latter compound. This method is complementary with the previous ones and it has been successfully employed for the introduction of multiple functionalities in the MPC systems in a stepwise fashion. This method is very useful for the preparation of Au MPCs coated with an organic shell containing functional groups not compatible with the classic reduction condition ($NaBH_4$), such as aldehyde and ketones.

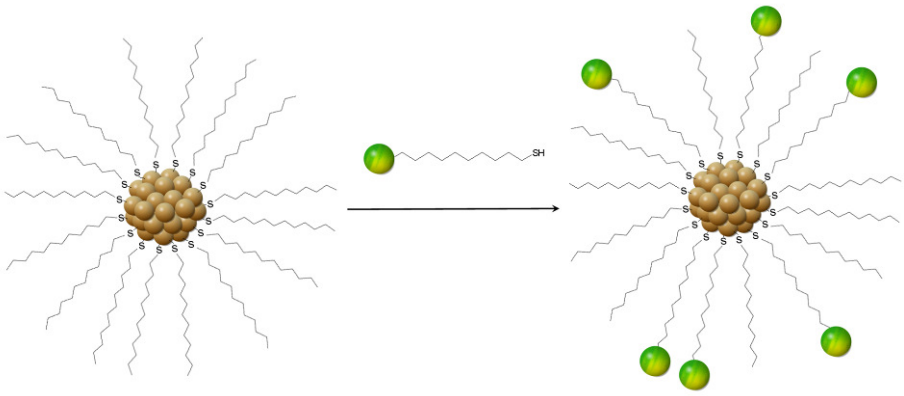

Figure 3.3 Schematic representation of the "place-exchange reaction" involving the organic shell of n-dodecanthiol-stabilized Au MPCs.

Another type of place-exchange reaction considers as starting material gold clusters stabilized by lipophilic organic salts such tetraalkylammonium salts $R_4N^+X^-$ where R is usually a long alkyl chain such as butyl or octyl. With this method, developed by Schiffrin in 1998,[18] the gold clusters are prepared as in the classical Brust-Schiffrin procedure, but the addition of the reducing agent is accomplished in absence of the thiolated ligand. In this way, the Au surface of the clusters is stabilized through electrostatic interactions with the bromide anion (see Figure 3.4), while the alkyl chains of the cation are used as surfactant to maintain the particles in solution. They alkyl chains also avoid the aggregation processes. This method allows the synthesis of Au clusters having a core size of 3-5 nm and characterized by high monodispersity and stability. The nanoparticles can be then exchanged with whatever thiolated ligands.

17. (a) A. C. Templeton, M. J. Hostetler, E. K. Warmoth, S. W. Chen, C. M. Hartshorn, V. M. Krishnamurthy, M. D. E. Forbes, R. W. Murray, *J. Am. Chem. Soc.*, **1998**, *120*, 4845; (b) A. C. Templeton, M. J. Hostetler, R. W. Murray, *Langmuir,* **1999**, *15*, 3782.
18. J. Fink, C. J. Kiely, D. Bethell, D. J. Schiffrin, *Chem. Mater.*, **1998**, *10,* 922.

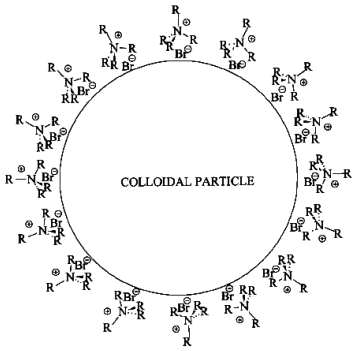

Figure 3.4 Schematic representation of the proposed arrangement of R_4N^+ and Br^- species adsorbed on the surface of Au particles.

3.1.2 Investigation tools for the characterization of MPCs

The recent emerging of the nanosciences as a new frontier science can be also strictly correlated with the concomitant development of several new investigation techniques that have helped the scientists to understand the phenomena at nanoscale level. In other words, the progressive ability to fabricate smaller structures has been followed by an improvement in their characterization.[19] The investigation tools used for the characterization of MPCs range from simple techniques such as elemental analysis and TGA, that allow the determination of the composition of the material, up to more sophisticated ones such as microscopy and photoemission spectroscopy. Several other techniques such as scanning tunnelling microscopy (STM), atomic force microscopy (AFM), small-angle X-ray scattering (SAXS) and powder X-ray diffraction have been largely used for the determination of the size of the MPCs cores.

High-Resolution Transmission Electron Microscopy (HRTEM)

The most common characterization technique for Au MPCs is the (HRTEM),[20] which gives a photograph of the gold core of the Au MPCs. TEM techniques involve a high voltage electron beam emitted by a cathode, usually a tungsten filament and focused by electrostatic and electromagnetic lenses. The electron beam that has been transmitted through a specimen that is in part transparent to electrons carries information about the inner structure of the specimen in the electron beam that reaches the imaging system of the microscope. The histogram providing the size distribution of the MPCs cores gives crucial information on the dispersity of the sample that is usually obtained from TEM pictures.

19. C. P. Poole Jr, F. J. Owens, *Introduction to Nanotechnology*, John Wiley & Sons, Hoboken New Jersey, 2003.
20. D. B. Williams, C. B. Carter, Transmission Electron Microscopy: A Textbook for Materials Science, Plenum Press, 1996.

X-ray Photoelectron Spectroscopy (XPS)

This spectroscopic technique provides information on the chemical state of the constituents of materials.[21] This technique is thus very useful for the characterization of Au MPCs because XPS spectra for the carbon and sulphur regions are consistent with the presence of alkanethiolate species in the clusters. XPS spectra are obtained by irradiating a material with a beam of X-rays while simultaneously measuring the kinetic energy (KE) and number of electrons that escape from the top 1 to 10 nm of the material being analyzed. XPS requires ultra-high vacuum (UHV) conditions (see figure 3.6). Because the energy of a particular X-ray wavelength correspond to a known quantity, we can determine the electron binding energy (BE) of each of the emitted electrons by using an equation that is based on the work of Ernest Rutherford (1914):

$$E_{\text{binding}} = E_{\text{photon}} - E_{\text{kinetic}} - \Phi$$

where E_{binding} is the energy of the electron emitted from one electron configuration within the atom, E_{photon} is the energy of the X-ray photons being used, E_{kinetic} is the kinetic energy of the emitted electron as measured by the instrument and Φ is the work function of the spectrometer (not the material).

A typical XPS spectrum is a plot of the number of electrons detected (Y-axis, ordinate) versus the binding energy of the electrons detected (X-axis, abscissa). Each element produces a characteristic set of XPS peaks at characteristic binding energy values that directly identify each element that exist in or on the surface of the material being analyzed. These characteristic peaks correspond to the electron configuration of the electrons within the atoms, e.g., 1s, 2s, 2p, 3s, etc. The number of detected electrons in each of the characteristic peaks is directly related to the amount of element within the area (volume) irradiated. To generate atomic percentage values, each raw XPS signal must be corrected by dividing its signal intensity (number of electrons detected) by a "relative sensitivity factor" (RSF) and normalized over all of the elements detected. To count the number of electrons at each KE value, with the minimum of error, XPS must be performed under ultra-high vacuum (UHV) conditions because electron counting detectors in XPS instruments are typically one meter away from the material irradiated with X-rays. It is important to note that XPS detects only

21. C. D. Wagner, W. M. Riggs, L. E. Davis, J. F. Moulder, G. E. Mullenberg, *Handbook of X-ray Photoelectron Spectroscopy*, Perkin-Elmer Corp, Eden Prairie, USA, **1979**.

those electrons that have actually escaped into the vacuum of the instrument. The photo-emitted electrons that have escaped into the vacuum of the instrument are those that originated from within the top 10 to 12 nm of the material. All of the deeper photo-emitted electrons, which were generated as the X-rays penetrated 1–5 micrometers of the material, are either recaptured or trapped in various excited states within the material. For most applications, it is, in effect, a non-destructive technique that measures the surface chemistry of any material.

UV/Vis Spectroscopy

A particular property of the MPCs known as the Surface Plasmon Band (SPB) is observable in the UV-visible spectral region. The SPB is due to the collective oscillations of the nanoparticles inorganic core surface electrons (6s electrons of the conduction band for AuMPCs). The surface plasmon band is correlated with the electromagnetic field of the incoming light, i.e., the excitation of the coherent oscillation of the conduction band.

The SPB is susceptible to changes when the dispersity state of the nanoparticles or the structural organisation of the organic layer is modified,[22] thus the SPB provides a considerable body of information on the development of the band structure in metals and has been the subject of extensive study of optical spectroscopic properties of gold nanoparticles.[23] From the Mie's theory it is possible to determine the average size of the gold nanoparticles through the evaluation of the position of the maximum of the SPB absorption band. Another important aspect of the SPB is that its steepest decrease reflects a high monodispersity of the corresponding nanoparticles.

The main characteristics of the SPB are: (i) its position around 520 nm; (ii) its sharp decrease with decreasing core size for AuNPs with 1.4-3.2 nm core diameters to the onset of quantum size effects that become important for particles with core sizes <3nm in diameter and also causes a slight blue shift. The SPB maximum and bandwidth are also influenced by: the particle shape, medium dielectric constant and temperature. The refractive index of the solvent has been shown to induce a shift of the SPB. The ligand shell alters the refractive index and causes either a red or blue shift, so that the spectroscopic data obtained often deviate from the prediction. Another influential parameter is the core charge. Formation of

22. (a) U. Kreibig, M. Vollmer: *Optical Properties of Metal Clusters*, Springer, Berlin, 1995; (b) P. K. Jain, W. Huang, M. A. El-Sayed, *Nano Letters* **2007**, *7*, 2080; (c) J. Schmitt, P. Mächtle, D. Eck, H. Möhwald, C. A. Helm, *Langmuir*, **1999**, *15,* 3256.
23. See *e.g.*: (a) W. Haiss, N. T. K. Thanh, J. Aveyard, D. G. Fernig, *Anal. Chem.*, **2007**, *79*, 4215; (b) J. Kimling, M. Maier, B. Okenve, V. Kotaidis, H. Ballot, A. Plech, *J. Phys. Chem. B*, **2006**, *110*, 15700; A. C. Templeton, J. J. Pietron, R. W. Murray, P. Mulvaney, *J. Phys. Chem. B*, **2000**, *104*, 564.

large aggregates caused also a reversible change in colour of the AuNPs suspension from red to violet due to coupling to surface plasmons in aggregated colloids. Unfortunately, nanoparticles having mean core diameter lower than 2.5 nm do not show an appreciable SPB: this is due to the low "concentration" of electrons at the surface. The solution of such nanoparticles thus appears as black colored.

Dynamic Light Scattering

DLS represents a powerful technique for the determination of the size distribution profile of small particles in solution.[24] When light hits small particles the light scatters in all directions (Rayleigh scattering) so long as the particles are small compared to the wavelength (<250 nm). If the light source is a laser, and thus is monochromatic and coherent, then one observes a time-dependent fluctuation in the scattering intensity. These fluctuations are due to the fact that the small molecules in solutions are undergoing Brownian motion and so the distance between the scatterers in the solution is constantly changing with time. This scattered light then undergoes either constructive or destructive interference by the surrounding particles and within this intensity fluctuation information is contained about the time scale of movement of the scatterers. The dynamic information of the particles is then derived from an autocorrelation of the intensity trace recorded during the experiment.

Characterization of the monolayer

The structure of the organic monolayers in MPCs has been probed by ^{13}C NMR[25] and transmission IR[26] spectroscopies. ^{13}C NMR focuses on the dependence of chemical shifts as a function of the carbon position relative to the gold–hydrocarbon interface. All the ^{13}C peaks are broadened in the cluster, attributed to the immobilization of the surfactant on the cluster surface. Going from the shorter to longer chain lengths, the peak width narrows, as the carbon is located further away from the thiol functionality. Other significant observations are that the resonances from carbon atoms closest to the Au core, those due to C_α, C_β and C_γ, are broadened into the baseline and that there is a systematic change in both the chemical shift and the line width with the carbon position relative to the Au–hydrocarbon interface. These are attributed to the discontinuity in the diamagnetic susceptibility at the Au–hydrocarbon interface and residual dipolar interactions in alkanethiolate monolayers. Broadening of the

24. B. Chu, Laser Light scattering: Basic Principles and Practice, 2nd Ed., Dover Publications, 2007.
25. R. H. Terril, T. A. Postlethwaite, C.-H. Chen, C.-D. Poon, A. Terzis, A. Chen, J. H. Hutchison, M. R. Clark, G. Wignall, J. D. Londono, R. Superfine, M. Falvo, C. S. Johnson, E. T. Samulski Jr, R. W. Murray, *J. Am. Chem. Soc.*, **1995**, *117*, 12537.
26. M. J. Hostetler, J. J. Stokes, R. W. Murray, *Langmuir* **1996**, *12*, 3604.

resonances as well as the disappearance of the carbons closest to the surface shows the immobilization of the alkyl chains and the strong interaction with the metal surface respectively.

IR spectroscopy shows that, as in 2D SAMs, the thiolate ligands of AuMPCs are essentially in all-trans zigzag conformations, with 5-25% of gauche defects at both inner and terminal locations.[27] IR and NMR spectroscopies allow, together with differential scanning calorimetry (DSC), the detection of order-disorder transitions in AuMPCs in the solid state. The temperature of the transition increases with the chain length, and FT-IR can show the increasing amount of gauche defects.

3.1.3 Au MPCs as Sensors

Au MPCs are endowed with properties mostly connected with the disposition of an insulator organic layer over a very small core (1-10 nm) of metal atoms that might give rise to quantum size effects.[28] A very attractive topological property of MPCs is the possibility to anchor onto the surface of the metallic core a discrete number of suitable receptors in a radial tri-dimensional arrangement. The combination of the typical features of MPCs with the recognition properties of synthetic receptors could lead in principle to the manufacturing of nanoscale devices with potential applications as sensors, switches and new materials having tuneable properties. Nevertheless, only few examples exist in the literature where Au MPCs have been employed as multivalent hosts and sensors.[29] Thiolated cyclodextrins (CDs) derivatives have been incorporated by Kaifer et al. into the monolayer of MPCs because of their ability to form inclusion complexes in aqueous media.[30] Wei et al. have employed *Resorcinarene* derivatives to encapsulate gold nanoclusters,[31] though no reports on the supramolecular applications of these MPCs were reported. Few studies report on the

---

27. T. Ung, M. L. Liz-Marzan, P. Mulvaney, *Colloids Surf. A: Physiochemical. Eng. Asp.,* **2002**, *202*, 119.
28. (a) Y. Volokitin, J. Sinzig, L. J. de Jongh, G. Schmid, M. N. Vargaftik, I. I. Moiseev, *Nature* **1996**, *384*, 621-622; (b) S. W. Chen, R. S. Ingram, M. J. Hostetler, J. J. Pietron, R. W. Murray, T. G. Schaaff, J. T. Khoury, M. M. Alvarez, R. L. Whetten, *Science* **1998**, *280*, 2098-2101.
29. For general reviews on this topic see *e.g.*: (a) U. Drechsler, B. Erdogan, V.M. Rotello, *Chem. Eur. J*., **2004**, 10, 5570; (b) Ana B. Descalzo, R. Martínez-Máñez, F. Sancenón, K. Hoffmann, K. Rurack, *Angew. Chem. Int. Ed*., **2006**, *45*, 5924; (c) P. K. Jain, X. Huang, I. H. El-Sayed, M. A. El-Sayed, *Acc. Chem. Res.* **2008**, *41*, 1578 and references therein.
30. (a) J.Liu, R. Xu, A. E. Kaifer, *Langmuir,* **1998**, *14*, 7337; (b) J. Liu, S. Mendoza, E. Roman, M. J. Lynn, R. Xu, A.E. Kaifer, *J. Am. Chem. Soc.,* **1999**, *121*, 4304; (c) J. Liu, W. Ong, E. Roman, M. J. Lynn, A. E. Kaifer, *Langmuir,* **2000**, *16*, 3000; (d) J. Liu, J. Alvarez, W. Ong, E. Roman, A. E. Kaifer, *J. Am. Chem. Soc.,* **2001**, *123*, 11148.
31. (a) B. Kim, M. A. Carignano, S. L. Tripp, A. Wei, *Langmuir*, **2004**, *20*, 9360; (b) R. Balasubramanian, B. Kim, S.L. Tripp, X. Wang, M. Lieberman, A. Wei, *Langmuir*, **2002**, *18*, 3676; (c) B. Kim, S. L. Tripp, A. Wei, *J. Am .Chem .Soc.*, **2001**, *123*, 7955; (d) K. B. Stavens, S.V. Pusztay, S. Zou, R. P. Andres, A. Wei, *Langmuir*, **1999**, *15*, 8337.

employment of thiolated calix[4]arene derivatives for the stabilization of Au MPCs.[32] We have recently shown that Au MPCs stabilised with dialkylthiolated calix[4]arene derivatives can be successfully employed as multivalent hosts for the recognition of organic salts both in organic[32b] and aqueous media.[32c] A study on the recognition of amino acids by *p*-sulfonatocalix[4]arene functionalized gold Au MPCs in aqueous solution has been recently published.[33]

3.2 Synthesis of Multipodand Calix[4]arene-protected Au MPCs

As seen in the previous paragraph, a very attractive property of MPCs is the possibility to anchor on their surface a discrete number of suitable receptors in a radial tri-dimensional arrangement. From this prospective it become possible to introduce different kinds of molecules or hosts on the same nanoparticles. In addition the recognition properties of the multivalent hosts obtained can be studied in solution.[32b] Therefore, in the following paragraphs, we report the one-pot synthesis and the detailed characterisation (TEM, NMR and XPS) of a series of Au MPCs protected with a series of multipodand thiolated calix[n]arene (n = 4 and 6) ligands. This study aims to disclose the role played by the host "sulphur denticity" on the core size of the resulting Au MPCs stabilized with the calix[n]arene ligands.

3.2.1 Synthesis of thiolated calix[n]arene derivatives.

As seen in section 3.1.1, the synthesis of lipophilic Au MPCs is usually obtained through the reduction of aurate salts in the presence of a thiolated ligand. The formation of the protected clusters could be considered as the result of two processes: growth of the metallic core and gold surface passivation due to the presence in solution of the thiols. The two processes are competitive and Tsukuda has proposed that the isolated MPCs correspond to kinetically trapped intermediates of the growing gold core.[34] Murray has indirectly supported such hypothesis since he shown that the core size of n-alkylthiol-stabilized Au MPCs is strongly affected by the concentration of the reactants, temperature and reductant rate addition.[13] In contrast, the effect of the capping agent, and in particular of the ligand "denticity", has not been systematically investigated yet. The data present in the literature

32. (a) X.-M. Li, M. R. de Jong, K. Inoue, S. Shinkai, J. Huskens, D. N. Reinhoudt, *J. Mater. Chem.*, **2001**, *11*, 1919; (b) A. Arduini, D. Demuru, A. Pochini, A. Secchi, *Chem. Commun.* **2005**, 645; (c) T. R. Tshikhudo, D. Demuru, Z. X. Wang, M. Brust, A. Secchi, A. Arduini, A. Pochini, *Angew. Chem. Int. Ed.* **2005**, *44*, 2913.
33. G. Patel, S. Menon, *Chem. Commun.*, **2009**, 3563.
34. Y. Negishi, Y. Takasugi, S. Sato, H. Yao, K. Kimura,T. Tsukuda, *J. Phys. Chem. B* **2006**, *110*, 12218.

evidences that multidentate thiolated ligands could promote the preparation of Au MPCs having improved stability.[35] Moving from these interesting findings, we have formulated the hypothesis that multidentate ligands could also exert a relevant kinetic effect on the gold core growth. Moreover, in the literature, there are few examples of synthetic protocols that allow the preparation of monodispersed Au MPCs with very small diameter (<1 nm).[36,37] This aspect could be of great importance considering that sub-nanometer MPCs are particularly enticing owing to their possible quantum size effects.[28]

To evaluate the effect of multidentate ligands on the gold core growth we decided to use a series of thiolated calix[n]arene derivatives in the *cone* conformation bearing a variable number of convergent undecanthiol chains onto their lower rim. Both rims of the receptor can be in principle used as scaffold for the insertion of the convergent thiol functionalities. Wei et al. have shown that resorcinarenes having SH groups onto their upper rim can be used for the stabilization of lipophilic Au MPCs.[31] However, the lower rim functionalization offers several advantages. First of all the calix[4]arene cavities, that represent the recognition units, are exposed toward the bulk and not toward the surface. The position of the recognition unit with the respect the gold surface can be likely varied using thiolated alkyl chain of variable length. Furthermore, the different acidity of the calix[n]arene phenolic OHs allows the regiochemical insertion of a variable number (up to 4) of thiolated alkyl chains. This is accomplished by varying the nature of the base employed during the alkylation process (see 2.1.4) and by choosing the appropriate molar ratio between the calix[4]arene and the alkylating agent, as well as the solvent and the temperature.

The thiolated calix[4]arene ligands **10a, 10b** and **13** characterized by the presence of one, two and four long ω-thiolated alkyl chains (C_{11}) onto the macrocycle lower rim were synthesized according to scheme 3.1 and fully characterized. In the dilakylated compound **10b**, the two chains were inserted in the 1,3 "distal" position to satisfy the requirements of host rigidity and preorganization discussed in 2.1.3. The use of the thiol group (SH), as the macrocycle anchoring point onto the metallic surface, was dictated by previous observations

35. (a) K. Wojczykowski, D. Meißner, P. Jutzi, I Ennen, A. Hütten, M. Fricke, D. Volkmer, *Chem. Commun.*, **2006**, 3693; (b) Z. Wang, B. Tan, I. Hussain, N. Schaeffer, M. F.Wyatt, M. Brust, A. I. Cooper, *Langmuir*, **2007**, *23*, 885; (c) S. Zhang, G. Leem, L. Srisombat, T. L. Lee, *J. Am. Chem. Soc.*, **2008**, *130*, 113.
36. Monodispersed alkylthiol-stabilized undecagold (Au_{11}) clusters can be obtained through ligand exchange reactions starting from the corresponding rather unstable phosphine-stabilized clusters, see *e.g.*: (a) G. H. Woehrle, M. G. Warner, J. E. Hutchinson, *J. Phys. Chem. B*, **2002**, *106*, 9979; (b) G. H. Woehrle, J. E. Hutchinson, *Inorg. Chem.*, **2005**, *44*, 6149; (c) M. F. Bertino, Z.-M. Sun, R. Zhang, L.-S. Wang, *J. Phys. Chem. B.* **2006**, *110*, 21416.
37. Special ligands such as glutathione also promote the formation of very small Au MPCs, see : Y. Negishi, K. Nobusada, T. Tsukuda, *J. Am. Chem. Soc.*, **2005**, *127*, 5261.

that such function yields RS-Au bonds energetically more stable than those formed i.e. by thioether functions (R_2S-Au).[32a]

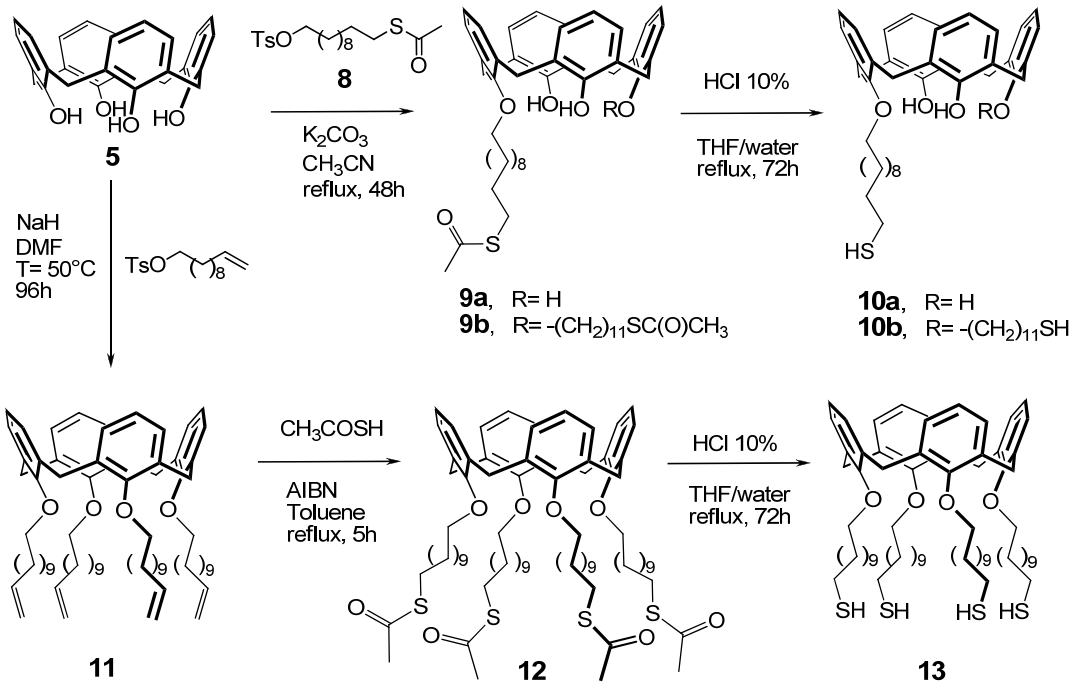

Scheme 3.1 Synthesis of thiolated calix[4]arenes **10a, 10b** and **13**.

For the preparation of monoalkylated ("monodentate") and dialkylated ("bidentate") thiolated ligands **10a** and **10b**, the anchoring group (S) was inserted in the alkyl chain before the alkylation of the macrocycle lower rim. To avoid oxidation problem, the thiolic functionality was inserted as thioester (-$SCOCH_3$). Initially, the alkylating agent S-11-(tosyloxy)undecyl ethanethioate was easly obtained throught anti-Markovnikov radicalic reaction[32b] of undec-10-enyl 4-methylbenzenesulfonate[38] with thioacetic acid in toluene for 5 hours. The reaction was promoted by the radical initiator AIBN. Calix[4]arene derivatives **9a** and **9b** were then obtained by refluxing calix[4]arene **5** in acetonitrile for 48h in presence of K_2CO_3 as base. Using a stochiometric defect (0.8 eq.) of both the alkylating agent and the base, **9a** was obtained in 80% yield. The dialkylated derivative **9b** was instead obtained in 85% yield employing 2 eq. of tosylate and of K_2CO_3. The successive hydrolysis reaction carried out with a 1:1 mixture of THF-HCl (10% w/v) lead to desired thiolated products **10a** (yield 95%) and **10b** (yield 92%). All compounds described in scheme 3.1 were characterized using NMR and mass spectroscopy (see experimental). The ^{1}H NMR spectrum of the monodentate **10a** in $CDCl_3$ has been depicted in figure 3.5. It shows two singlets at δ = 9.74 and 9.43 ppm in 1:2 integral ratio that are diagnostic for the three unsubstituted OH groups of

38. G. W. Kabalka, M. Varma, R. S. Varma, P. C. Srivastava, F. F. Knapp, *J. Org. Chem.*, **1986**, *51*, 2386.

the calix[4]arene lower rim. The monosubstitution of the lower rim induces a complex pattern of aromatic signals (in integral ratio 1:2:1). The protons of the bridging methylene groups give rise to a typical pattern of signals for a monosubstituted calix[4]arene derivative.[39] The four "axial" and the four "equatorial" protons resonate as two couple of doublets (with geminal coupling, J = 14 Hz) at δ = 4.37, 4.28, 3.47 and 3.46 ppm. The undecanyl chain yields several multiplet in the upfield region (2.2 – 0.8 ppm), though both the OCH_2 and CH_2SH methylene protons resonates as characteristic signals. The former is a triplet at δ = 4.15 ppm, while the latter is a *dt* (double-triplet) centered at δ = 2.55 ppm. The multiplicity of the latter signal reflects the coupling of the CH_2 protons with the proton of the SH group. The signal of the SH proton (δ ~ 1.5 ppm) is completely hidden by the pattern of signals of the aliphatic chain. Its presence was confirmed exclusively through 2D COSY experiments.

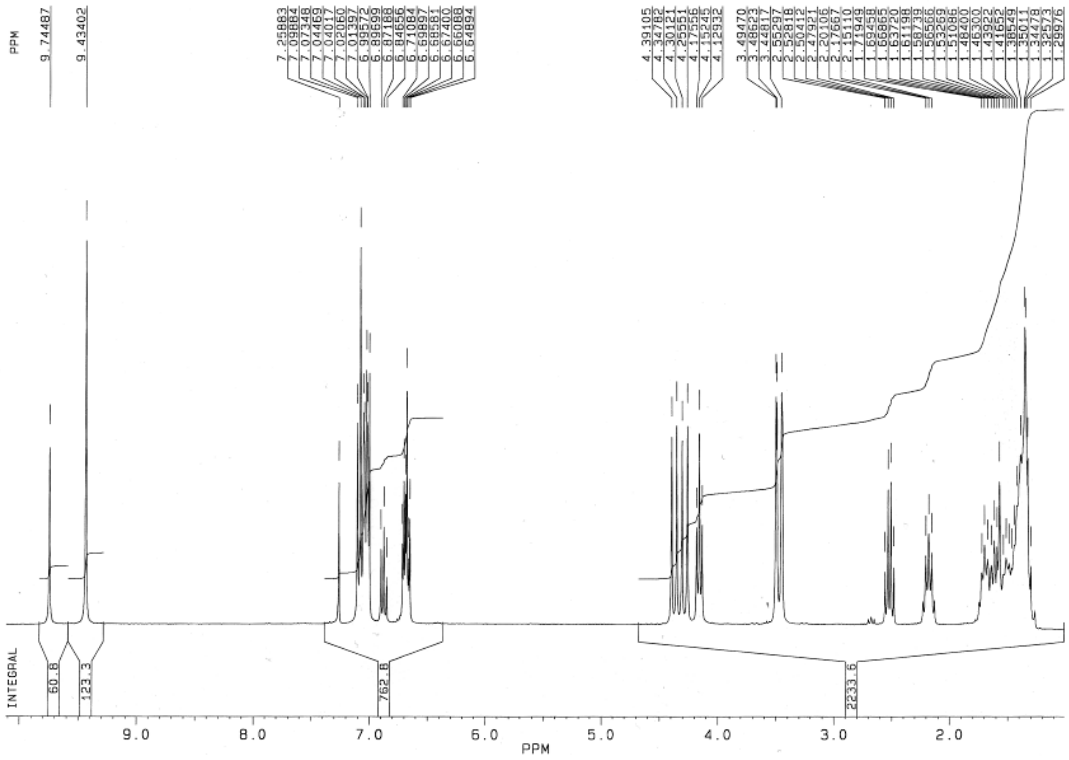

Figure 3.5 ^{1}H NMR spectrum of **10a** in $CDCl_3$ (300 MHz).

The ^{1}H NMR spectrum of **10b** taken in $CDCl_3$ (see Figure 3.6) is simpler than the spectrum originating from **10a**. Indeed, the structure of **10b** presents a C_{2v} symmetry that generates only a singlet for the two OH groups at δ = 8.29 ppm, two doublets and two triplets, respectively, for the two different *meta* and *para* protons of the aromatic nuclei. A unique AX system of two doublets at δ = 4.40 and 3.45 ppm for the axial and equatorial protons of the

39. For a detailed discussion on NMR spectra of calix[n]arene compounds see: C. J. Hawker, K. L. Wooley, *Science,* **2005**, *309*, 1200.

methylene bridging units (J =12 Hz). As seeen for **10a**, the protons of the methylene group in α to the SH resonates as multiplet centered at δ ~ 2.6 ppm, while the signal of the SH function is totally hidden by the resonances of the CH_2 groups of the undecanyl chain.

The synthesis of the "tetradentate" calix[4]arene **13** was carried out with a different synthetic approach because the exhaustive alkylation of the phenolic groups of **5** requires the use of strong bases, such as NaH, which are not compatible with the thioester group. In detail (see Scheme 3.1), **5** was salified in DMF with a 4 equivalents of NaH and then reacted with a slight excess of undec-10-enyl 4-methylbenzenesulfonate.[38]

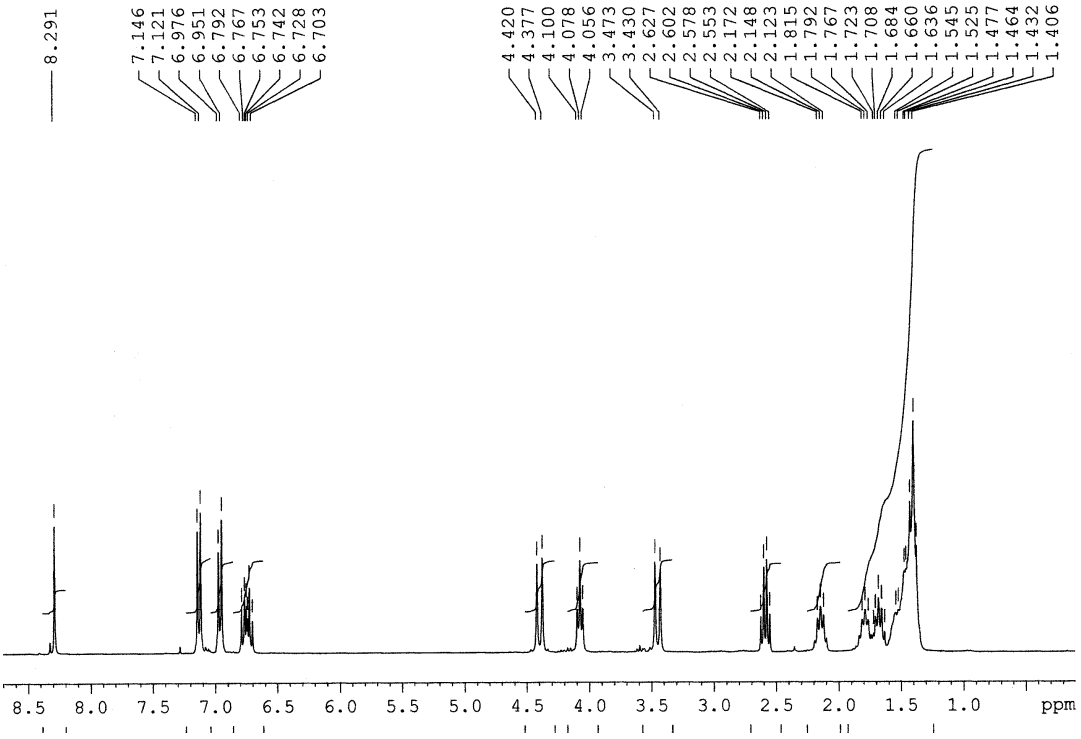

Figure 3.6 ^{1}H NMR spectrum of **10b** in $CDCl_3$ (300 MHz)

The resulting tetralkylated derivative **11** was then converted in **12** through an anti-Markovinkov addition of thioacetic acid. As before, the hydrolysis of the thioacetyl groups was accomplished in acid conditions with a 1:1 mixture of THF-HCl (10% w/v) to yield the "tetradentate" thiolated calix[4]arene **13** in very high yields (93%). The C_4 simmetry of **13** in cone conformation gives rise the ^{1}H NMR spectrum in $CDCl_3$ depicted in Figure 3.7. The aromatic protons are visible as a large multiplet at δ = 6.7-6.5 ppm, the axial and equatorial protons of the methylene bridging units generates a unique AX system of two doublets (δ = 4.43 and 3.14 ppm). Similar to the other thiolated calix[4]arenes, the protons of the methylene group in α to the SH resonates as a multiplet centered at δ ~ 2.5 ppm.

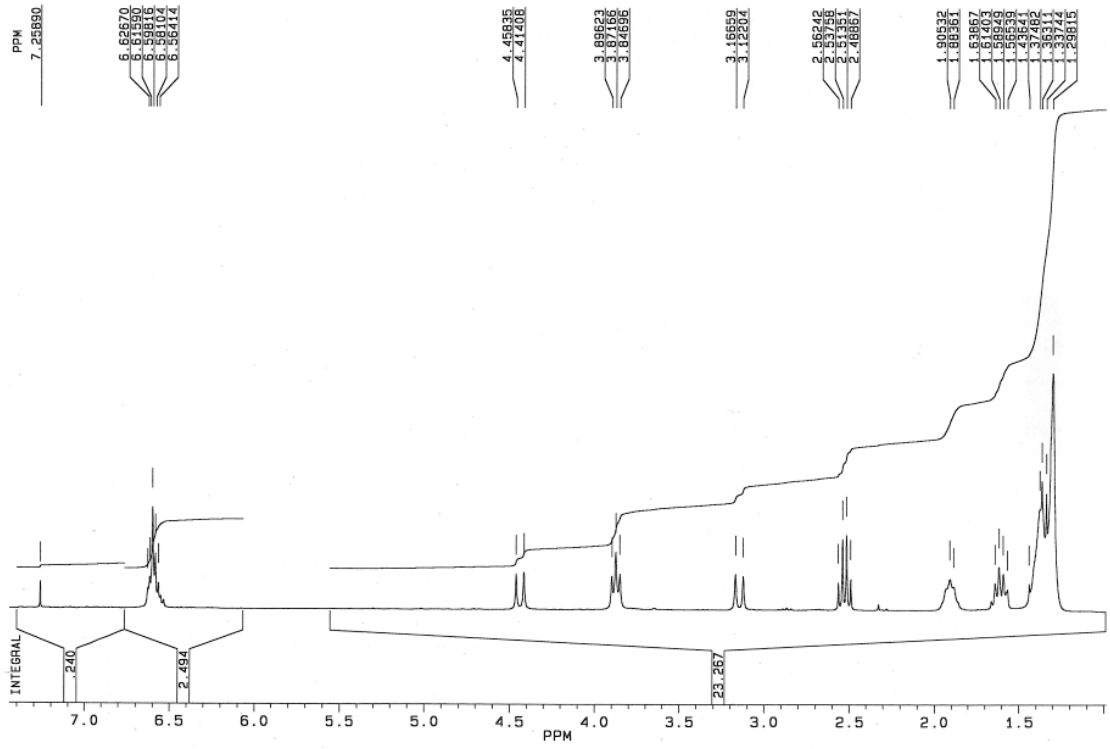

Figure 3.7 ^{1}H NMR spectrum of **13** in $CDCl_3$ (300 MHz)

In order to prepare a "tridentate" thiolated ligand, we employed the trimethoxy calix[6]arene **14**, which has the proper symmetry, as platform for the introduction of the three thiolated C_{11} alkyl chains onto the macrocycle lower rim (see scheme 3.2). Initially, compound **15** was synthesized through reaction of **14** with undec-10-enyl 4-methylbenzenesulfonate using acetonitrile as solvent and K_2CO_3 as base. Compounds **16** and **17** were synthesized using the same synthetic approach employed for the preparation of the tetradentate thiolated calix[4]arene **13**. The experimental details and characterization have been summarized in the experimental part. The ^{1}H NMR spectrum of **17**, taken in $CDCl_3$ (see Figure 3.8), shows two singlets at 7.28 ppm and at 6.64 ppm for the aromatic protons. Indeed, the phenolic rings are differently substituted and the macrocycle assumes on the NMR timescale a flattened cone conformation with three alternate aromatic rings almost parallel and three bended with the mothozy gropus oriented inward the cavity. The C_{3v} symmetry of **17** generates a AX system of two doublets (δ = 4.58 and 3.40 ppm) for the axial and equatorial protons of the methylene bridging units. As for the others thiolated compounds, the protons of the methylene group in α to the SH resonates as multiplet at $\delta \sim 2.5$ ppm.

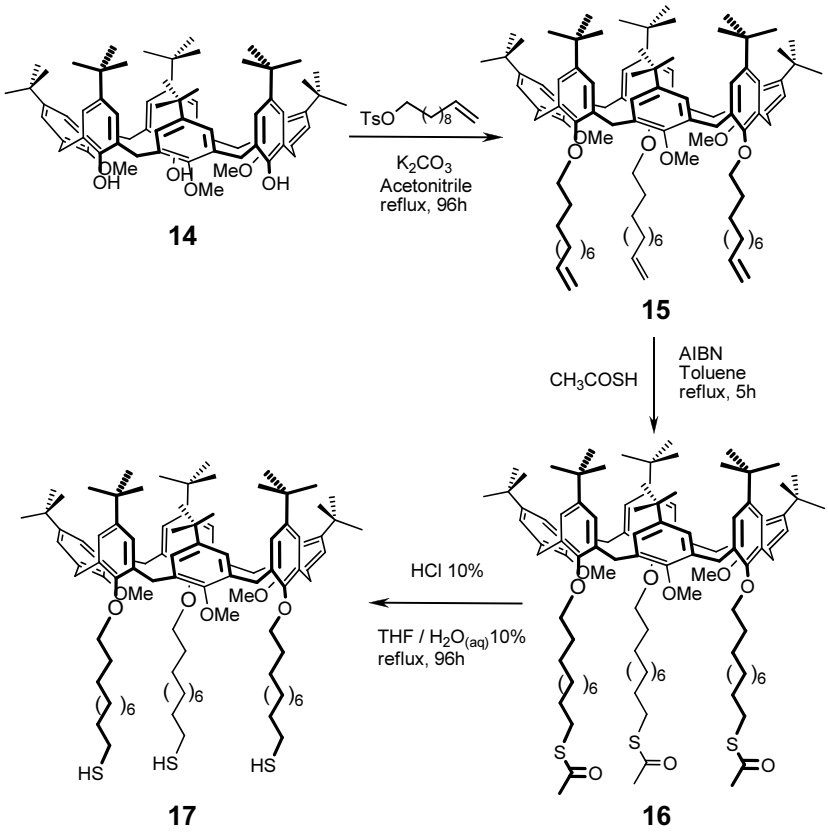

Scheme 3.2 Synthesis of the "tridentate" thiolated calix[6]arene **17**.

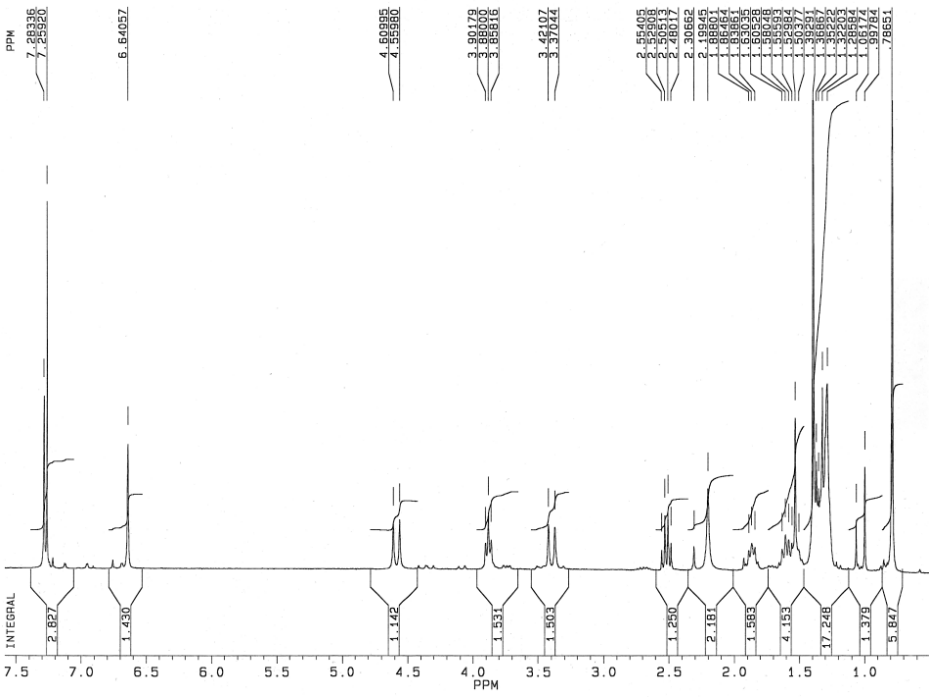

Figure 3.8 ^{1}H NMR spectrum of **17** in $CDCl_3$ (300 MHz).

3.2.3 Synthesis and characterization of the calix[n]arene-protected Au MPCs

Synthesis and purification

A series of novel Au MPCs was prepared using the thiolated calixarene ligands previously synthesized as capping agents. Taking advantage of the two-phase synthetic procedure reported by Brust,[12] the reduction of the aurate was accomplished with $NaBH_4$ in a toluene solution containing the thiolated calixarene ligand. For each calixarene ligand $Cx(SH)_n$, where n indicates the number of thiolated alkyl chains present on its lower rim, three samples of MPCs were prepared using the following $Cx(SH)_n$:Au molar ratios: 3:(1×n), 1:(3×n) and 1:(6×n). Regardless the multidentate nature of the ligand, these molar ratios always correspond to effective S(thiolated alkyl chain):Au ratios of 3:1, 1:3 and 1:6. The outcomes of the synthesis carried out using the same S:Au ratio become independent by the absolute amount of the calixarene employed (see Table 3.1) and directly comparable with the literature data on *n*-dodecanthiol-protected Au MPCs prepared by Murray et al.[13] using the same S:Au molar ratios.

The purification of the synthesized Au MPCs was a difficult task. Indeed, differently from the *n*-dodecanthiol-protected Au MPCs, the simple addition of acetonitrile to the reaction mixture did not afford a precipitate of the desired pure nanoclusters. The precipitate usually contained small amount of phase transfer catalyst TOABr and of the calix[n]arene ligand not bonded on the gold surface. The contamination of "free" calix[n]arene is mainly due to the low solubility experienced by these macrocycles in acetonitrile. In order to overcome this problem, we devised the two purification methods called A and B. With the method A, the toluene solution was evaporated and the resulting black precipitate was sonicated in presence of absolute ethanol. The filtered precipitate was then taken up with a 1:1 dichloromethane:ethanol and recovered by centrifugation. The two steps are used to remove TOABr and the excess of the not anchored calix[n]arene, respectively. This method was particularly effective for the purification of Au MPCs obtained using a molar defect of calix[n]arene (S:Au = 1:3 and 1:6, see Table 3.1). The method "B" consisted in a dilution of the reaction mixture in toluene with the same same volume of absolute ethanol. The desired nanoclusters were recovered from the resulting heterogeneous mixture through centrifugation at 5'000 rpm for 15 minutes. This method was generally effective for the purification of all Au MPCs synthesized. The nanoclusters prepared with a large excess of calix[n]arene ligand (S:Au = 3:1) may require a further chromatographic purification step using a mixture 9:1

dichloromethane:methanol as eluent. The effectiveness of these purification methods has been verified through elemental analysis and ^{1}H NMR measurements (see infra).

TEM measurements

After their purification the core size distribution of the synthesized Au MPCs was determined through TEM measurements. To simplify the nomenclature of the nanoclusters we used the designation [$C_m(S)_n$-Au] (**n*x***), where m identificates the calixarene macrocycle (m = 4 or 6), n is the ligand denticity (number of thiolated alkyl chains). We used also the index *x* (*x* = *s*, *m* or *l*) to classify, whitin each series of nanoclusters protected with the same type of ligand, the relative core size (*s* = small, *m* = medium and *l* = large) with respect the S:Au molar ratio used for the synthesis (3:1, 1:3 and 1:6).

Table 3.1. Composition and core diameter of the calix[n]arene-protected Au MPCs

Entry	Ligand denticity n	Ligand $C_m(SH)_n$	MPC designation	$C_m(SH)_n$/Au mole ratio	S:Au (theor)[a]	Org.fract. (%)[b]	d_{TEM} (nm)[c]
1	1	**10a**	[C_4(S)-Au] (**1s**)	3:1	3:1	53	1.5±0.4
2	1	**10a**	[C_4(S)-Au] (**1m**)	1:3	1:3	34	2.2±0.8
3	1	**10a**	[C_4(S)-Au] (**1l**)	1:6	1:6	23	3±1
4	2	**10b**	[$C_4(S)_2$-Au] (**2s**)	1.5:1	3:1	69	0.9±0.2
5	2	**10b**	[$C_4(S)_2$-Au] (**2m**)	1:6	1:3	38	1.6±0.4
6	2	**10b**	[$C_4(S)_2$-Au] (**2l**)	1:12	1:6	28	2.5±0.7
7	3	**17**	[$C_6(S)_3$-Au] (**3s**)	1:1	3:1	75	0.9±0.2
8	3	**17**	[$C_6(S)_3$-Au] (**3m**)	1:9	1:3	47	2.0±0.5
9	3	**17**	[$C_6(S)_3$-Au] (**3l**)	1:18	1:6	32	2.6±0.7
10	4	**13**	[$C_4(S)_4$-Au] (**4s**)	4:3	3:1	65	1.0±0.2
11	4	**13**	[$C_4(S)_4$-Au] (**4m**)	1:12	1:3	34	1.2±0.1
12	4	**13**	[$C_4(S)_4$-Au] (**4l**)	1:24	1:6	26	1.4±0.2
13	1	*n*-C_{12}SH	[C_{12}S-Au] (**1s**)	3:1	3:1	47[d]	1.6[d]
14	1	*n*-C_{12}SH	[C_{12}S-Au] (**1m**)	1:3	1:3	17[e]	2.8[e]
15	1	*n*-C_{12}SH	[C_{12}S-Au] (**1l**)	1:6	1:6	9[e]	4.4[e]

[a] equivalents of alkylthiol chains per aurate; [b] determined through TGA and elemental analysis; [c] core diameter determined by TEM measurements (mean ± std dev); [e] see ref. 13b; [d] see ref. 13a.

The analysis of the TEM images showed that for each ligand used, the mean core size (d_{TEM}) of the corresponding nanoclusters is inversely proportional to the S:Au ratio employed during the synthesis (cf. entries 1-3; 4-6; etc., Table 3.1). The effect of the ligand "denticity"

on the size of the nanocluster is well evidenced by comparing the d_{TEM} and the size distribution diagrams (see Figures 3.8 and 3.9) determined for samples obtained using the same S:Au molar ratios (cf. entries 1 and 4, 2 and 5 etc., Table 3.1). Indeed, the nanoclusters protected with the bidentate calix[4]arene **10b**, tridentate calix[6]arene **17** and the tetradentate calix[4]arene **13** show always a smaller mean size than those protected with the monodentate **10a** (see Table 3.1). The latter nanoclusters were characterised by d_{TEM} (entries 1-3) comparable to those reported for *n*-dodecanthiol-protected MPCs prepared using the identical S:Au ratios (entries 13-15).[13] Most important, the distribution analysis revealed that the use of a threefold excess of alkylthiol chains per aurate (S:Au = 3:1, entries 4, 7 and 10, Table 3.1) for the multidentate ligands **10b** , **13** and **17** induces the formation of very small clusters (see Figures 3.8b and 3.9a).

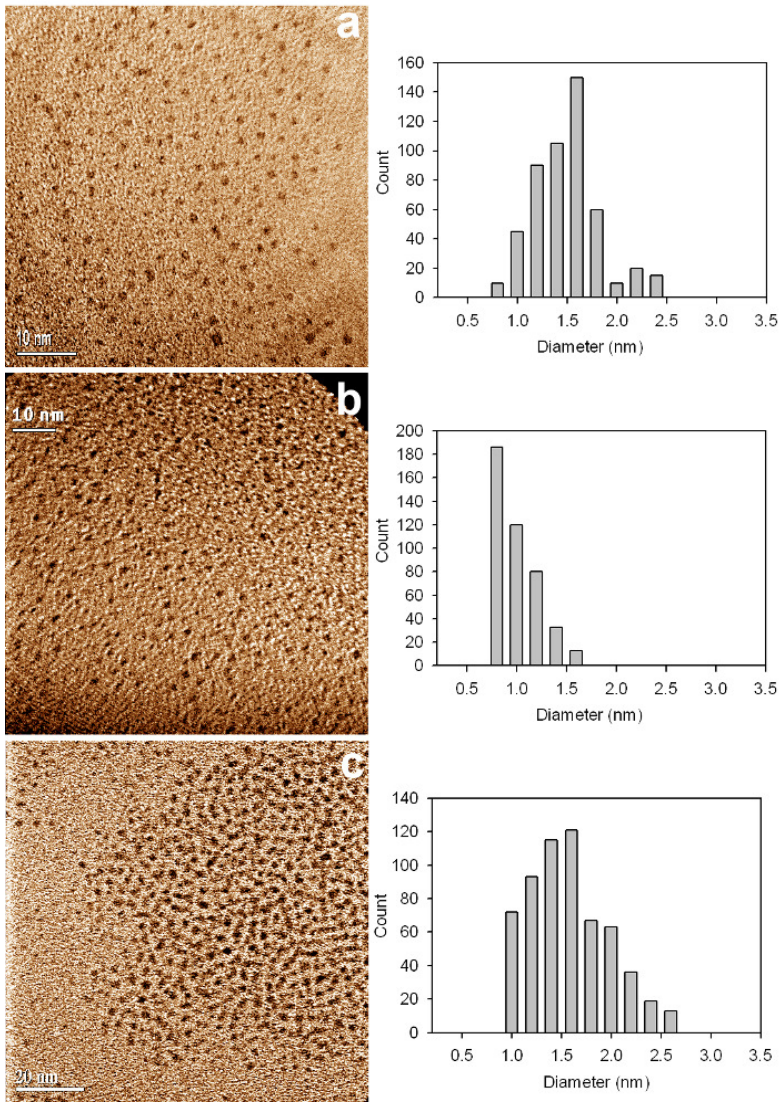

Figure 3.8. TEM images and core size distribution diagrams of the calix[4]arene-protected Au MPCs: a) $[C_4(S)$-Au] (**1s**) (d = 1.5±0.4 nm), b) $[C_4(S)_2$-Au] (**2s**) (d = 0.9±0.2 nm) and c) $[C_4(S)_2$-Au] (**2m**) (d = 1.6±0.4 nm).

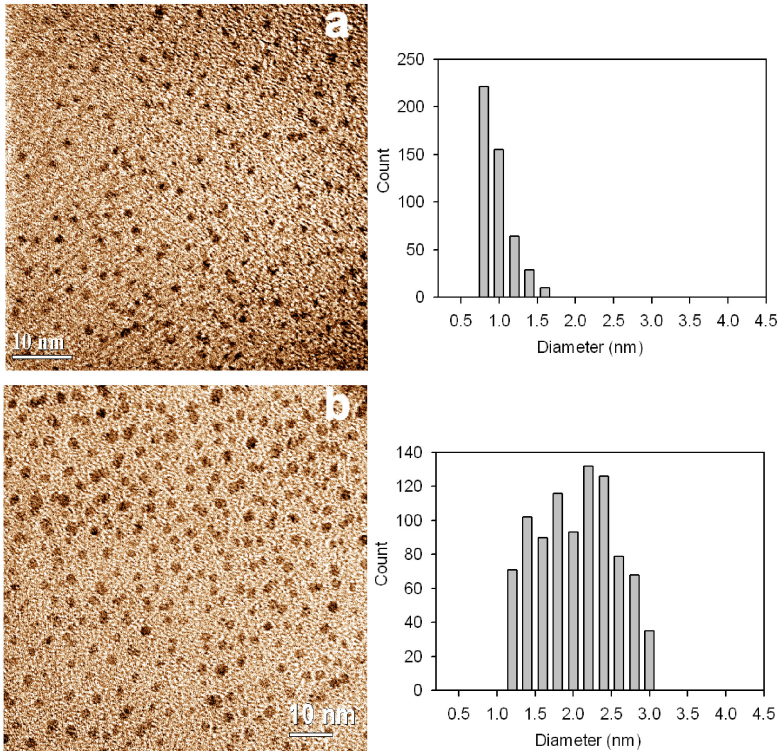

Figure 3.9 TEM images and core size distribution diagrams of the calix[6]arene-protected Au MPCs: a) $[C_6(S)_3$-Au] (**3s**) (d_{TEM} = 0.9±0.2 nm); and b) $[C_6(S)_3$-Au] (**3m**) (d_{TEM} = 2.0±0.5 nm).

These results support the hypothesis that the size distribution of the calix[n]arene-protected Au MPCs is affected by the "denticity" of the ligand. The formation of small nanoclusters from the multidentate ligands could be a consequence of the convergent arrangement of the thiolated chains that, because of their proximity and thus elevated effective molarity, might increase the passivation rate of the growing gold core after the formation of the first Au-S bond.

To exclude a possible role of the calixarene cavity in the stabilization of the small nanoclusters, as found for instance with resorcinarene derivatives,[31] the MPCs synthesis was repeated using a 1,3-bis(ω-undecenyl)calix[4]arene **18**, which is structurally analogous to **10b** but lacking of the thiol group on the two alkyl chains (see Scheme 3.3). The gold colloids obtained after the reduction step, however, collapsed after the reaction work up.

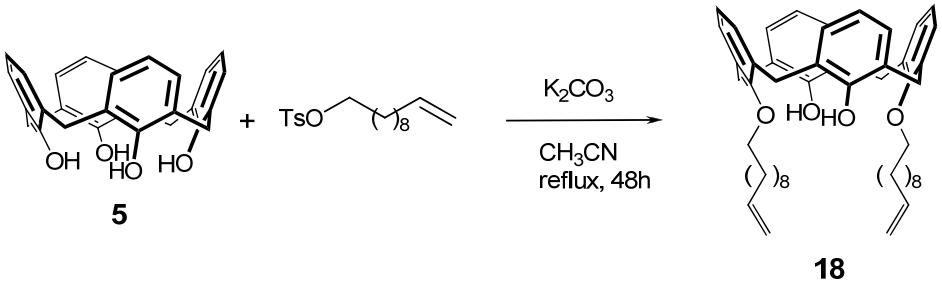

Scheme 3.3 Synthesis of the calix[4]arene **18**.

Elemental analysis

The composition of the synthesized nanoclusters was initially inferred by elemental analysis. The data summarized in Table 3.1 show that the percentage of organic fraction present in the nanoclusters is directly proportional to the amount of calix[n]arene ligand used during the synthesis. A particular large contribution of organic fraction (69, 75 and 65%) was found in the nanoclusters [$C_4(S)_2$-Au] (**2s**), [$C_6(S)_3$-Au] (**3s**) and [$C_4(S)_4$-Au] (**4s**) obtained by reducing the aurate salt in the presence of a threefold excess of alkylthiol chains derived from the bidentate **10b**, the tridentate **17** and the tetradentate **13** ligands, respectively (see Table 3.1). In all three cases the organic fractions were larger than those reported for the nanoclusters stabilized with the monodentate ligands **10a** (53%) and *n*-C_{12}SH (47%) and prepared with the same S:Au ratio of 3:1 (see Table 3.1). These findings suggest, as verified by TEM measurements, the formation of nanoclusters with the very small sizes (< 1 nm).

XPS Measurements

As seen in section 3.1.2, XPS spectroscopy is a powerful technique that provides qualitative and quantitative information on the chemical state of the constituents of nanoclusters. The following XPS measurements are the results of a collaboration we started with the research group of Prof. Robertino Zanoni of the Dipartimento di Chimica of the University "La Sapienza" of Rome.

In Table 3.2 the Au $4f_{7/2}$ and S $2p_{3/2}$ binding energy (BE) values determined for all synthesized calix[n]arene-protected Au MPCs have been summarized. These XPS regions generally appear as complex peaks and require curve-fitting procedures. Due to the (static) charging under X-rays of the nanoclusters coated by an organic layer, the BE experimentally determined (columns with heading "Obsvd." in Table 3.2) have been in some cases referenced to the C 1s signal of the calixarene taken at 285.0 eV (columns with heading "Norm." in Table 3.2see Table 3.2).

The relative quantitative S:Au ratios have been determined by comparing the intensity of the peaks relative to S 2p and Au 4f, respectively. As expected, within of series of MPCs obtained using the same calixarene ligand the S:Au ratios are always inversely proportional to the size of the nanoclusters. For example, in the series of MPCs obtained using the bidentate **10b** as capping agent (entries 4-6), the nanoclusters characterized by core size of 0.9, 1.6 and 2.5 nm have corresponding values of the S:Au ratios of 1, 0.6 and 0.3. The first ratio should imply that, on the average, all the gold atoms of the [$C_4(S)_2$-Au] (**2s**) core are involved in bonding with sulphur groups.

Table 3.2 Au $4f_{7/2}$ and S $2p_{3/2}$ binding energies determined for the series of calix[n]arene-protected Au MPCs.

Entry	MPC designation	S:Au (theor)[a]	S:Au (exp)[b]	d_{TEM} (nm)	Au $4f_{7/2}$ (eV) [c] Obsvd.	Au $4f_{7/2}$ (eV) [c] Norm.	S $2p_{3/2}$ (eV) [d] Obsvd.	S $2p_{3/2}$ (eV) [d] Norm.
1	[C_4(S)-Au] (**1s**)	3:1	0.7	1.5±0.4	87.2 88.5 90.1	83.2 84.5 86.1	166.8 - -	162.8 - -
2	[C_4(S)-Au] (**1m**)	1:3	0.5	2.2±0.8	84.3 86.0 87.0	83.2 84.9 86.9	163.7 - -	162.6 - -
3	[C_4(S)-Au] (**1l**)	1:6	0:2	3±1	86.6 88.3 -	82.9 84.6 -	166.4 167.2 -	162.7 163.5 -
4	[$C_4(S)_2$-Au] (**2s**)	3:1	1:0	0.9±0.2	87.4 88.7 90.4	83.5 84.8 86.5	167.1 169.2 -	163.2 165.3 -
5	[$C_4(S)_2$-Au] (**2m**)	1:3	0.6	1.6±0.4	85.7 87.8 88.5	82.8 84.1 85.6	165.3 - -	162.4 - -
6	[$C_4(S)_2$-Au] (**2l**)	1:6	0:3	2.5±0.7	84.0 88.5 86.8	84.0 88.5 86.8	162.3 - -	162.3 - -
7	[$C_6(S)_3$-Au] (**3s**)	3:1	1.5	0.9±0.2	85.8 87.1 88.4	82.8 84.1 85.4	165.3 166.6	162.3 163.6
8	[$C_6(S)_3$-Au] (**3m**)	1:3	0.5	2.0±0.5	86.7 88.0 89.4	82.8 84.1 85.5	166.3 167.6 -	162.4 163.7 -
9	[$C_6(S)_3$-Au] (**3l**)	1:6	0.4	2.6±0.7	84.0 84.9 86.3	82.5 83.4 84.8	163.0 164.1 -	161.5 162.6 -
10	[$C_4(S)_4$-Au] (**4s**)	3:1	1.8	1.0±0.2	86.5 87.7 89.3	83.3 84.5 86.1	166.4 - -	163.2 - -
11	[$C_4(S)_4$-Au] (**4m**)	1:3	0.9	1.2±0.1	84.1 85.3 86.7	84.1 85.3 86.7	162.8 164.8 -	162.8 164.8 -
12	[$C_4(S)_4$-Au] (**4l**)	1:6	0.4	1.4±0.2	85.1 86.5 87.5	85.1 86.5 87.5	162.8 164.7	162.8 164.7
13	[$C_4(S)_2$-Au] (**2ex**)[e]	-	1.0	-	87.2 88.5 91.0	83.3 84.6 87.1	166.9 - -	166.9 - -

[a] equivalents of alkylthiol chains per aurate during the synthesis; [b] quantitative S:Au ratios determined through XPS measurements (associated uncertainty of ±10%); [c]; components in the Au 4f deconvoluted peak referenced to aromatic carbon the C 1s (from calixarene rings) taken at 285.0 eV; from low to high energies: Au(0), Au(I) and Au(III); [d] components in the S 2p deconvoluted peak referenced to aromatic carbon the C 1s (from calixarene rings) taken at 285.0 eV; from low to high energies: S-Au and S-S; [e] Au MPCs prepared from undecagold $Au_{11}(PPh_3)_8Cl_3$ nanoclusters through ligand exchange reaction with **10b**.[36a]

As far as the composition of the gold core is concerned, the XPS measurements have shown that in most cases the gold is present in the core at different chemical state. In Figure 3.10a has been depicted, for example, the Au 4f region of the subnanometric Au MPCs obtained using an excess of bidentate ligand **10b** ([$C_4(S)_2$-Au] (**2s**), entry 4, table 3.2). Au 4f peak deconvolution evidenced the presence of at least three components indicated with blue,

red and green lines. The ratio of the low-BE (red line, corrected BE = 83.5 eV) to the major peak component (blue line, corrected BE = 84.8 eV) was found to be 1:10. The third component (green line, corrected BE = 86.5 eV) is in a much less definite ratio to the main one. To identify these components we considered that, as previously verified by TEM measurements, these nanoclusters have a mean diameter of ~0.9 nm (see entry 4, Table 3.2), consistent with a core composed of ca. 11-13 gold atoms.[36,40] On this basis, we may assign the major component in Figure 3.10a to Au(I) species bonded with the S groups. The BE shift between the minor peak component (red line) and the major one (blue line) amounts to a –1.3 eV. The minor component is thus compatible for a gold species having a –1 oxidation state.

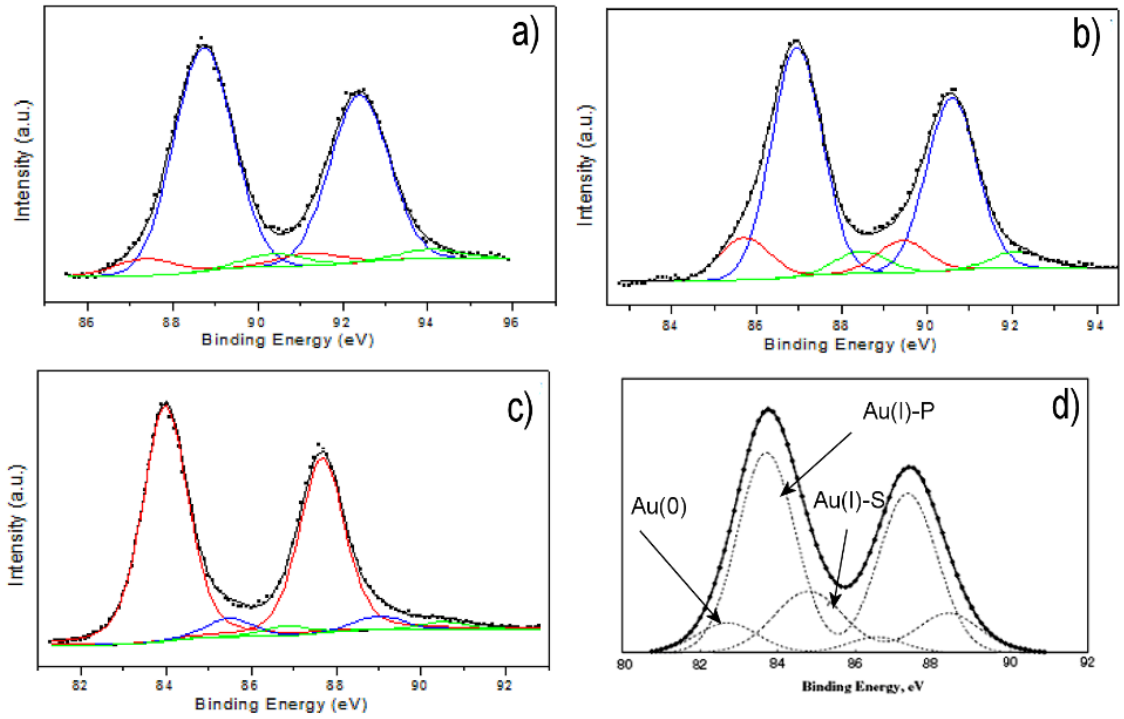

Figure 3.10 Au 4f XPS spectrum of a) $[C_4(S)_2\text{-Au}]$ (**2s**), b) $[C_4(S)_2\text{-Au}]$ (**2m**) and c) $[C_4(S)_2\text{-Au}]$ (**2l**). Experimental curve (dots) and Au $4f_{7/2,\ 5/2}$ curve-fitted components: Au(I) (blue line), Au(0) (red line), and Au(III) (green line). d) $Au_{11}(S\text{-}4\text{-}NC_5H_4)_3(PPh_3)_7$ (*Reproduced by permission of the Elsevier B.V.*,). Binding energy in figures are not scaled, see table 3.2 for scaled values (eV) of binding energy.

Finally, the high-BE minor component (green line) is likely due to Au(III) species deriving from impurities of $AuCl_4^-$. It is important to observe that the presence of a Au 4f component at a BE lower than the characteristic value for bulk gold (84.0 eV) has been already reported in the literature.[41]. In the literature is also present a XPS study of undecagold

40. The application of the "spherical model" to Au_{11} clusters yields a core size of 0.7 nm, see ref. 25. This size is unfortunately beyond the resolution limit of the TEM measurements we carried out. Therefore, the core size of our nanoclusters is probably overestimated.
41. (a) K. Nunokawa, S. Onaka, M. Ito, M. Horibe, T. Yonezawa, H. Nishihara, T. Ozeki, H. Chiba, S. Watase, M. Nakamoto, *J. Organometallic Chem.*, **2006**, *691*, 638; (b) B. J. Auten, B. P. Hahn, G. Vijayaraghavan,

cluster $Au_{11}(S\text{-}4\text{-}NC_5H_4)_3(PPh_3)_7$ having a core size < 1 nm. The three gold components (see Figure 3.10d) have been assigned by the authors in following way: the low energy component to a gold central atom at 82.8 eV, while the two high energy components to two gold bounded to PPh_3 and sulphur groups (S-py) at 83.8 and 84.8 eV, respectively.

In Figures 3.10b and 3.10c have been depicted the XPS spectra of the Au MPCs protected with **10b** having core size of 1.6 and 2.5 nm ($[C_4(S)_2\text{-Au}]$ (**2m**) - entry 5, $[C_4(S)_2\text{-Au}]$ (**2l**) - entry 6, see Table 3.2). It is easily observable that an increase of the core size corresponds to an increase of the Au(0) component (red line). The larger nanoclusters (**2l**) (see Figure 3.10c) are composed in high proportion by Au(0) species (see red line). This trend was observed also in the other series of Au MPCs protected with the monodentate **10a**, tridentate **17** and tetradentate **13** ligands (see experimental). These findings are in agreement with the observation that larger clusters present a lower percentage of superficial gold species interacting with the sulphur ending of the ligand.

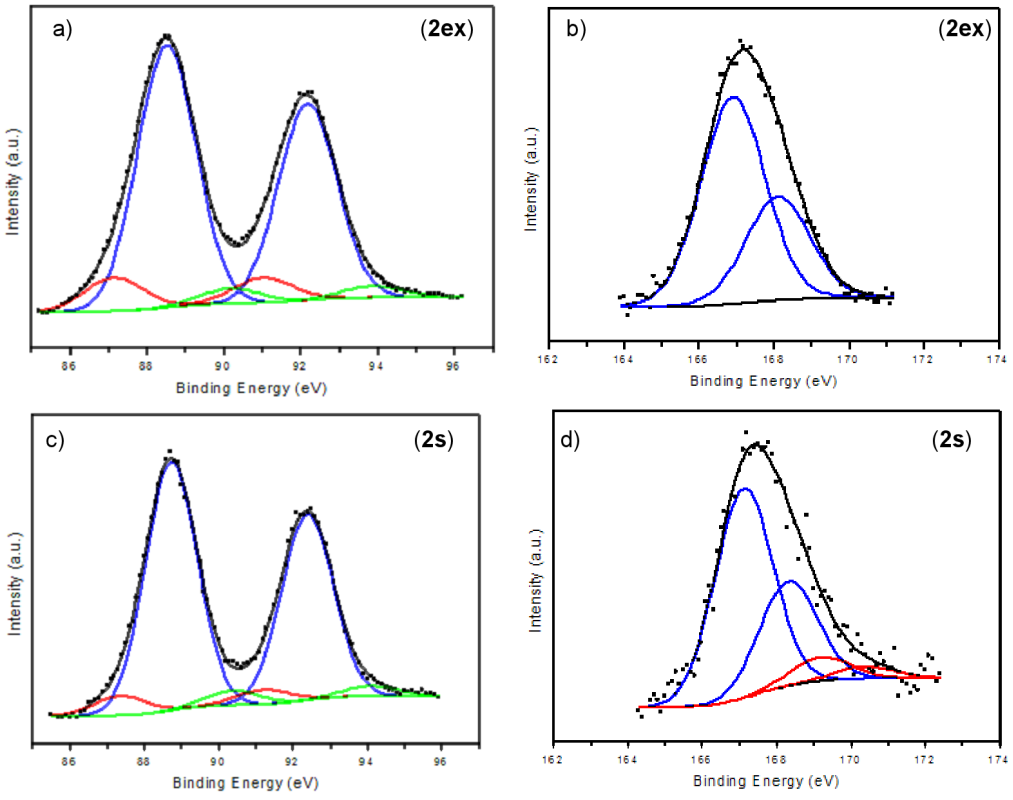

Figure 3.11 XPS regions of a) Au 4f (**2ex**), b) S 2p) (**2ex**), c) Au 4f (**2s**) and d) S 2p (**2s**). Experimental curves (dots). Au $4f_{7/2,\ 5/2}$ curve-fitted components: Au(I) (blue line), Au(0) (red line), and Au(III) (green line). S $2p_{3/2,\ 1/2}$ curve-fitted components: S-Au (blue line), S-S (red line).

K. J. Stevenson, B. D. Chandler, *J. Phys. Chem. C*, **2008**, *112*, 5365; (c) H. Tsunoyama, N. Ichikuni, H. Sakurai, T. Tsukuda, *J. Am. Chem. Soc.* **2009**, *131*, 7086.

To confirm the composition of the subnanometric Au MPCs [$C_4(S)_2$-Au] (**2s**) derived by bidentate **10b**, we carried out a simple experiments. Undecagold $Au_{11}(PPh_3)_8Cl_3$ nanoclusters[36a] were exchanged in toluene with an excess **10b**. After chromatographic purification, the nanoclusters obtained (**2ex**) were submitted to XPS analysis (see entry 13, Table 3.2). The Au 4f and S 2p regions of the (**2s**) and (**2ex**) nanoclusters depicted in figure 3.11 show a very similar pattern of peak components and relative abundance. The only marked difference is the presence of a little components due to S-S bonds in the sample of (**2s**) (red line of Figure 3.11d). For the S 2p peak, we compared the energy distances found in this study between the components of peaks Au $4f_{7/2}$ and S $2p_{3/2}$ with the analogous values for different thiolates already reported in the literature.[42] The experimentally determined distance between the major components of the peak for Au 4f and S 2p (78.3 eV), is characteristic for Au-thiolate[42] and it evidences the formation of a covalent S-Au chemical bond in all synthesized Au MPCs. As an example in Figure 3.12 has been depicted the XPS S 2p region relative to [$C_4(S)_2$-Au] (**2s**) nanoclusters and the major components (unmarked areas) were attributed to S-Au thiolate species. A 2 eV larger distance is characteristic either for an unbound thiol (SH) and a disulphide (S-S) species.[42c] The minor components of the S 2p peak (hatched areas) of figure 3.12 can be accordingly interpreted as due to either free SH terminations or to disulphide bridges connecting two distinct calixarenes chains (Au-S-CX-S-S-CX-S-Au).[43]

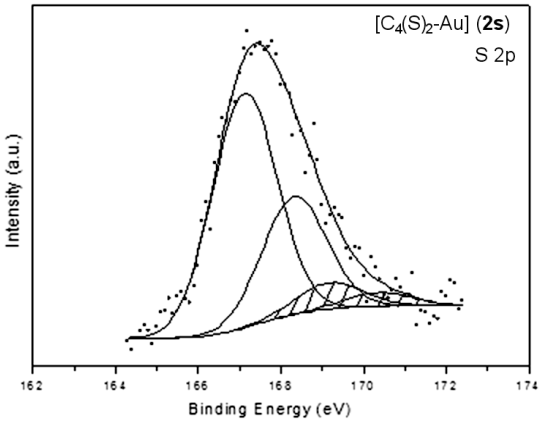

Figure 3.12 S 2p XPS spectrum of [$C_4(S)_2$-Au] (**2s**). Experimental curve (dots) and S $2p_{3/2,\ 1/2}$ curve-fitted components: S-Au major components (unmarked areas), disulphide bridges (hatched areas).

42. (a) D. G. Castner, K. Hinds, D. W. Grainger; *Langmuir*, **1996**, *12*, 5083; (b) M. C. Bourg, A. Badia, R. B. Lennox, *J. Phys. Chem. B*, **2000**, *104*, 6562; (c) F Demoisson, M. Mullet, B. Humbert, *J. Colloid Interf. Sci*, **2007**, *316*, 531.
43. (a) S. W. Joo, S. W. Han, K. Kim, *J. Phys. Chem. B*, **1999**, *103*, 10831; (b) S. W. Joo, S. W. Han, K. Kim, *Langmuir*, **2000**, *16*, 5391; (c) S. W. Joo, S. W. Han, K. Kim, *J. Phys. Chem. B*, **2000**, *104*, 6218; (d) S. W. Joo, S. W. Han, K. Kim, *J. Colloid Interf. Sci*, **2001**, *240*, 391.

NMR measurements

All synthesized Au MPCs were submitted to NMR analysis. However, according with previous findings reported in the literature, the ^{1}H NMR spectra are quite broad due to the different positions of the calix[4]arene derivatives around the Au core.[13a,44] In figure 3.13 has been depicted the ^{1}H NMR stack plot in $CDCl_3$ (300MHz) of Au MPCs **2s**, **2m** and **2l** that are protected with calix[4]arene **10b**. The comparison of the spectrum of the free bidentate ligand (see Figure 3.6) with those of the nanoclusters evidenced as expected a general broadening of the calixarene resonances. As reported in the literature,[13a] the anchoring process of the thiolated groups SH on the surface of the metal induces the disappearing of the diagnostic signal of the methylene protons of the CH_2 group adjacent to the S atom directly attached on gold. This signal is visible instead in the free ligands as a multplet centred at ca. 2.5 ppm (see Figure 3.6).

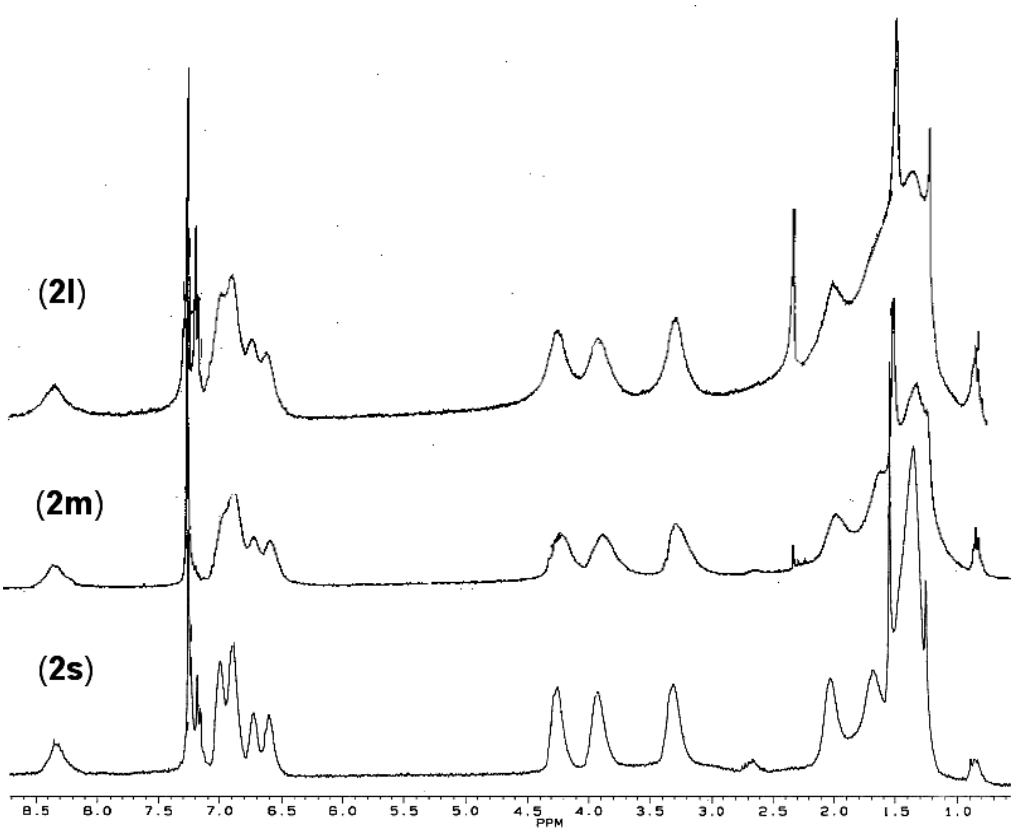

Figure 3.13 ^{1}H NMR stack plot in $CDCl_3$ (300 MHz) of Au MPCs **2s**, **2m** and **2l** protected with bidentate calix[4]arene ligand **10b**.

44. The broadening of the nanoclusters resonances can be related with the T_2* relaxation time (that reflects the contribution of transverse relaxation time T_2 and instrumental field inhomogeneity). Short T_2* increases the resonance linewidth ($\nu_{FWHM} = 1/\pi T_2$*) and it is usually correlated with slow rotating molecules in solution. See A. Badia, R. B. Lennox, L. Reven, *Acc. Chem. Res.*, **2000**, *33*, 475.

Even though the increase of the clusters passing from **2s** to **2l** enhance the broadening of the NMR signals, in all the three spectra are still recognisable the typical pattern of signals of a calix[4]arene blocked in the cone conformation. Indeed, the bridging methylene groups generate two broad signals at δ at 3.2 and 4.4 ppm, the CH_2 linked to the phenolic oxygen is visible as broad signal at δ 3.9 ppm. The long undecanyl chains give rise to a huge and complex ensemble of aliphatic resonaces between 1.1-2.1 ppm. In the subnanometric Au MPCs **2s**, the aromatic protons are splitted in at least four more solved signals. The not alkylated OH groups give rise in all cases to a well recognisable broad signal at δ ~8.4 ppm. All the other series of calix[n]arene-protected Au MPCs give rise to similar spectroscopic characteristic (see experimental).

In summary, the synthesis and the characterisation of a series of Au MPCs protected with calix[n]arene derivatives functionalised with alkylthiol chains on their lower rim has been reported. The particular multidentate structure of the calix[n]arene derivatives introduce a new control element in the preparation of the resulting clusters that allows, in particular experimental conditions, to obtain structures of subnanometric core size.

3.3 Guest Controlled Assembly of Calix[4]arene-protected Au MPCs

3.3.1 Introduction

As seen in the general introduction of this chapter, a very attractive topological property of Au MPCs is the possibility to insert in the organic layer a discrete number of "effectors" disposed in a radial tri-dimensional arrangement. Upon the application of external stimuli the effectors could promote an extensive networking of nanoparticles.[45] When the effectors are molecular receptors, the networking process could be triggered through the recognition of proper guests and being driven by non covalent interactions it is usually reversible. The latter approach could thus benefit of the principles and methods of supramolecular chemistry for the development of nanoscale devices, sensors, switches and nanostructured materials endowed with reversible and tuneable properties.

The idea to self-assemble gold nanoparticles through molecular recognition processes has been documented in the literature by few authors who showed the feasibility of these

45. See, for example: (a) S. I. Lim, C.-J. Zhong, *Acc. Chem. Res.*, **2009**, *42*, 798; (b) F. Westerlund, T. Bjørnholm, *Current Opinion in Colloid & Interface Science*, **2009**, *14*, 126; (c) B. L. V. Prasad, C. M. Sorensen, K. J. Klabunde, *Chem. Soc. Rev.*, **2008**, *7*, 1871 and references therein.

processes in solutions.[30b,46] To the best of our knowledge, however, the possibility to exploit the cavity of calix[n]arenes for assembly and networking processes of Au MPCs remains unexplored. On the other hand, we have previously seen in the introduction of this chapter that calix[4]arene-based receptors can be used as "active" protecting layer for Au MPCs able to recognize organic ion pairs in low polar media.[32b] These binding properties have also been transferred to aqueous media using water soluble Au MPCs bearing calix[4]arene hosts which were able to self-assemble onto flat gold surfaces covalently coated with N-alkyl pyridinium cationic guests.[32c] In this paragraph we thus present a study in which Au MPCs having a mean core size of ~6 nm and coated with the thiolated calix[4]arene derivative **10b** (see Figure 3.14) are able to self-assemble through supramolecular interactions with bifunctional guests based on the dialkyl bipyridinium salts **G5** and **G10** (see Figure 3.14) to yield aggregates whose sizes and solubility can be controlled by the length and rigidity of the bifunctional guest used as linker between the nanoparticles.

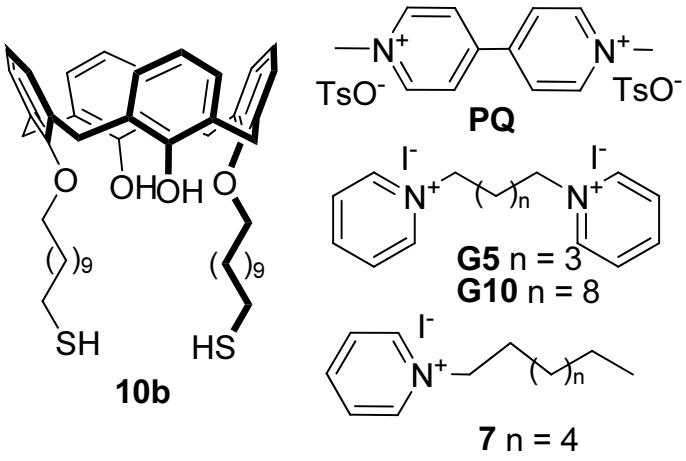

Figure 3.14. Structural formulae of the lower rim thiolated calix[4]arene host (**10b**) used for the stabilization of the Au MPCs and of the organic salts used as monofunctional (**7**) and bifunctional guests (**PQ**, **G5**, and **G10**) for the networking of the nanoparticles.

3.1 Synthesis and characterization of the calix[4]arene-coated nanoparticles.

Samples of Au MPCs protected with the calix[4]arene **10b** [NP(**10b**)] were prepared through a ligand exchange reaction[17] (see Figure 3.15) starting from a toluene solution of freshly prepared Au MPCs stabilized with tetraoctyl ammonium bromide[47] [NP(TOABr)] and having a mean core size of 6±1 nm (see experimental).

46. (a) S. S. Kinge, M. Crego-Calama, D. N. Reinhoudt, *Langmuir*, **2007**, *23*, 8772; (b) Z. Liu, M. Jiang, *J. Mater. Chem.*, **2007**, *17*, 4249.
47. M. Brust, D. Bethell, C. J. Kiely, D. J. Schiffrin, *Langmuir*, **1998**, *14*, 5425.

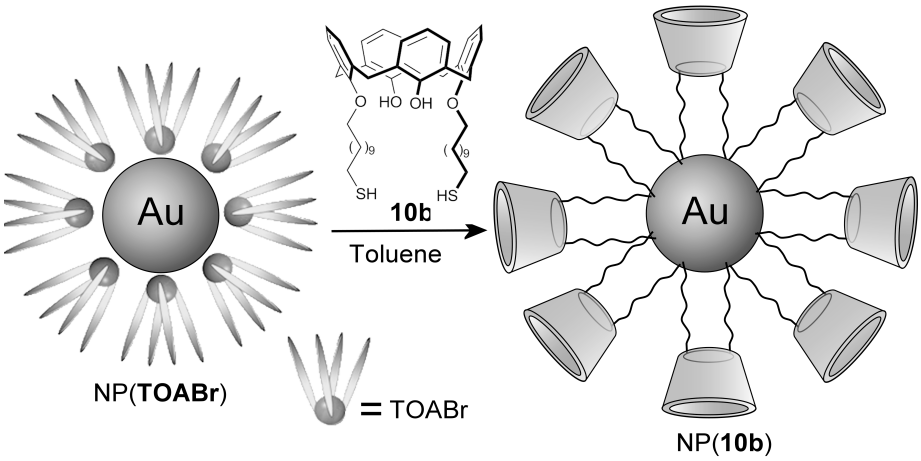

Figure 3.15. Schematic representation of the synthesis through ligand exchange reaction of the calix[4]arene-protected MPCs NP(**10b**) starting from tetraoctyl ammonium-stabilized ones NP(**TOABr**).

Thiolated calix[4]arene **10b** was chosen as stabilizer of these nanoclusters because, as seen in section 3.2, it promotes the formation of stable Au MPCs and its affinity for pyridinium-based organic ion pairs has been already investigated in chapter 2. **10b** can be anchored on the gold surface of the nanoclusters through its two long ω-thiolated alkyl (C11) chains. This anchoring mode has the advantage to maintain the receptor binding site oriented toward the bulk and thus retaining its potential recognition properties.[32b]

After exchange, the size dispersion of the novel calix[4]arene-protected Au MPCs was determined through TEM measurements. The analysis of several TEM images collected on the NP(**10b**) sample showed that, as expected, the exchange of the organic layer did not significantly affect the core size of the resulting nanoclusters. As shown in Figure 3.16, the mean diameter of the nanoclusters present in NP(**10b**) still remains about 6 nm. As expected for nanoclusters of this size, their optical properties are very informative. Indeed, UV/Vis spectroscopy mainly detects the plasmon resonance surface band (SPB) of NP(**10b**).

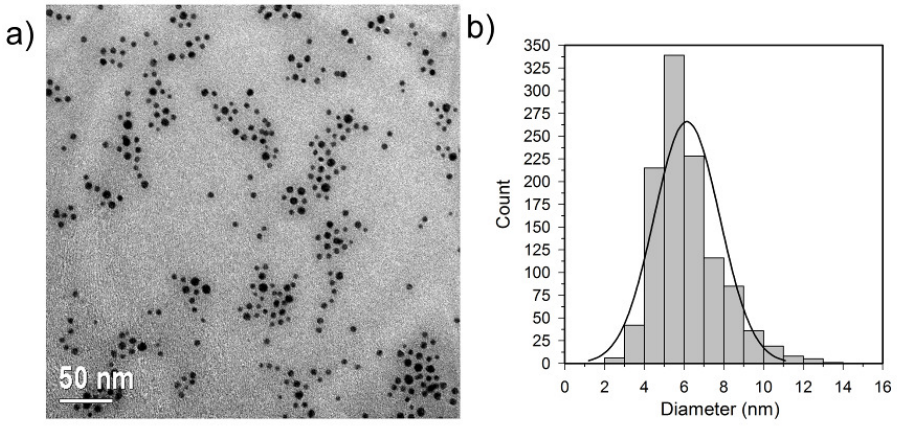

Figure 3.16. a) TEM image and b) core size distribution diagram of the nanoclusters [NP(**10b**)]

The maximum of the SPB for the NP(TOABr) nanoclusters is found around 526 nm in toluene solution and a slight shift is observed upon ligand exchange with **10b** (see Figure 3.17). In chloroform, however, there is also a narrow band at λ ~270 nm visible, which stems from to the absorption of the calix[4]arene phenolic nuclei of **10b**. The presence of this band was an indication that several calix[4]arene units were inserted as stabilizing layer on the surface of the nanoclusters.

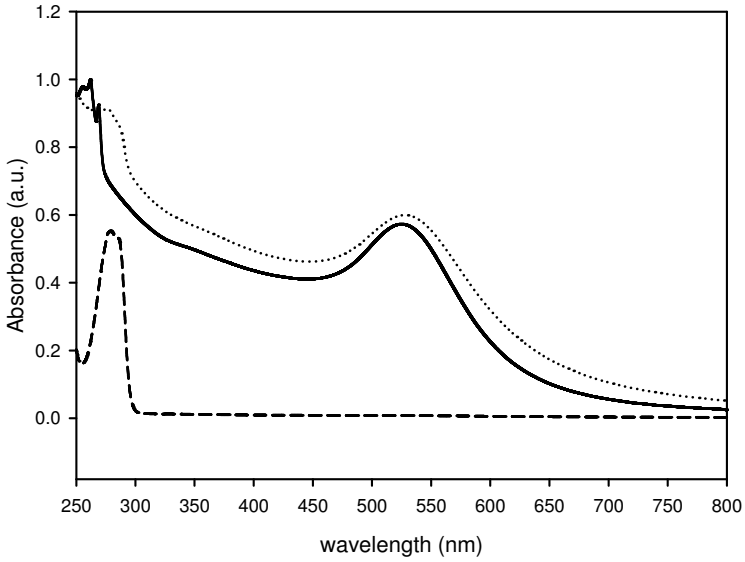

Figure 3.17 UV/Vis spectra of NP(TOABr) in toluene (continuos line), NP(**10b**) in $CHCl_3$ (dotted line) and of free **10b** in $CHCl_3$ ($c = 10^{-4}$ M, dashed line).

The elemental analysis carried out on NP(**10b**) gave us further evidences of the attainment of the exchange reaction. The percentage of organic matter present in the nanoclusters was 21.7% with a sulphur content of 0.7%. From these data it is possible to calculate a gold sulphur ratio (Au/S) of ~18, that is in good agreement with the achievement of ~6 nm nanoclusters approximately decorated with 250-300 calix[4]arene units. The Au/S ratio of ~18 also accounts for nanoclusters where the "footprint" for each thiolated alkyl chain of ranges between 0.25 and 0.3 nm^2.[48]

3.3.2 Guest-induced self-assembly experiments.

UV-Vis titration experiments were carried out monitoring the variation of SPB of NP(**10b**). The maximum of this band is sensitive to the size of the particles as well as to particle-particle electromagnetic coupling.[22] The first guest used to promote the self-assembly process between the nanoclusters was the rigid dimethylviologen ditosilate **PQ** (see Figure

48. For the determination of the "footprint" of thiolated ligands see for example: L. Fabris, S. Antonello, L. Armelao, R. L. Donkers, F. Polo, C. Toniolo, F. Maran, *J. Am. Chem. Soc.*, **2006**, *128*, 326.

3.14). The addition of 10µl of 1×10^{-5} M solution of **PQ** in chloroform to a solution of 0.1% w/v NP(**10b**) in chloroform initially determines a red-shift of the main absorption band (λ~530 nm) of the clusters up to 550 nm (see Figure 3.18).

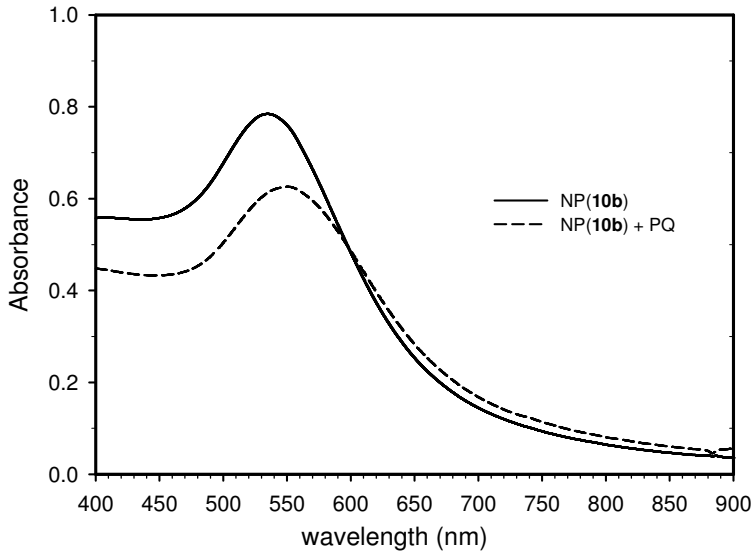

Figure 3.18 UV-Vis spectra of a chloroform solution of NP(**10b**) before (continuos line) and after (dashed line) the addition of a 10 µl of a 10^{-5} M chloroform solution of **PQ**.

This red-shift was indicative for the formation of aggregates of the nanoclusters, in which **PQ** acts as "supramolecular linker" between calix[4]arene cavities resident on the surface of different nanoclusters. The solubility of the aggregates formed upon the addition of **PQ** was poor and the colloid tends to precipitate from the solution as a black solid material. This phenomenon is probably ascribed to the high structural rigidity and directionality of **PQ** that generates the formation of an extensive rigid 3D-network of self-assembled nanoparticles. The solid filtered-off from the solution was insoluble even in very polar solvents such as DMF and DMSO.

In order to reduce the collapsing of the nanoparticles, the assembly experiments were carried out using the dipyridinium diiodides 1,1'-(pentane-1,5-diyl)dipyridinium diiodide **G5** and 1,1'-(decane-1,10-diyl)dipyridinium diiodide **G10** (see Figure 3.14). Both salts were synthesized in high yields (> 90%) by reaction of pyridine with the corresponding alkyl diodide in refluxing acetonitrile (see experimental section). With respect to **PQ**, both salts are endowed with an higher structural flexibility and experience an appreciable solubility in chloroform solution.

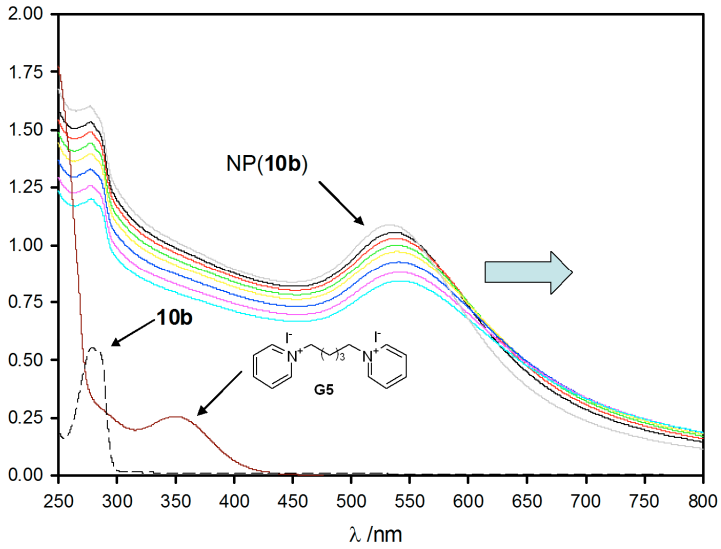

Figure 3.19 UV-Vis spectroscopic titration of NP(**10b**) with a 1×10^{-4}M solution of **G5** in chloroform (free NP(**10b**) gray line, last guest addition point: azure line).

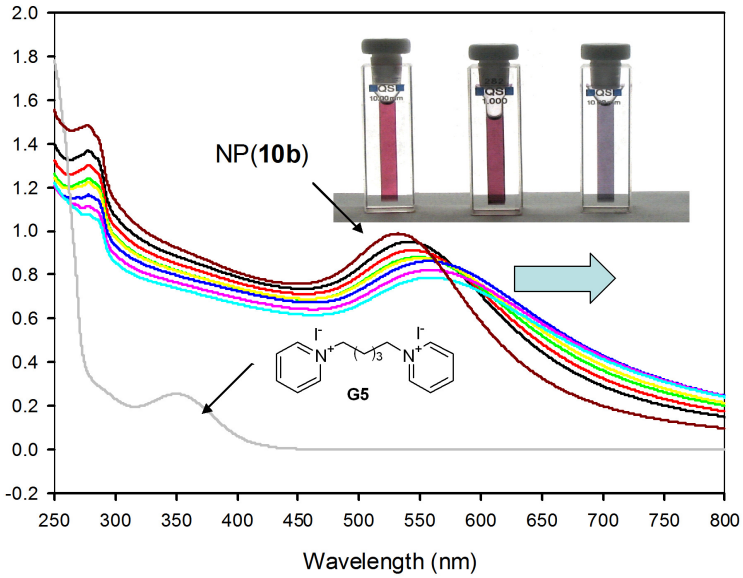

Figure 3.20 UV-Vis spectroscopic titration of NP(**10b**) with a 1×10^{-5}M solution of **G5** using chloroform as solvent (free NP(**10b**) brown line, last guest addition point: azure line).

The addition of a 10^{-5} M solution of **G5** in $CHCl_3$ to the solution of NP(**10b**) in the same solvent induces an intensity decrease with a very slight red-shift of the SPB (λ ~545 nm, see Figure 3.19). A new titration experiment was thus carried out by adding a tenth time more concentrated solution of **G5** (10^{-4} M). The results of the titrations experiments have been depicted in figure 3.20.[49] Upon guest addition, the SPB undergoes a red-shift until λ ~ 560 nm

49. It should be observed that an estimate of the average number of recognition sites present onto the surface of the clusters is still under progress. Therefore, the evaluation of the clusters aggregation induced by the guest should be exclusively considered as semiqualitative.

with a concurrent decreasing of absorbance. During the titration the colour of solution variate from ruby-red to dark-blue (see figure 3.20).

This information tell us that when the concentration of the guest in solution is sufficient to create a nanoparticles aggregate a change occurs in the UV-Vis spectra resulting in a red-shift of the SPB. It is also interesting to notice that the addition of a large amounts of **G5** induces the collapsing of the aggregates with the formation of a black precipitate. However, differently from what observed with **PQ**, the aggregation induced by such flexible supramolecular linkers is reversible. The original uncomplexed NP(**10b**) could be restored through treatment of the solid with a polar solvent such as methanol. In other words, the treatment with methanol destroy, as expected, the aggregates through the solvation of the difunctional guest. Indeed, the recovered nanoclusters show again their typical UV spectrum.

The guest-induced aggregation experiment was then repeated using guest **G10** (see Figure 3.14), characterized by a longer alkyl chain linking the two pyridine units with respect **G5**. The addition of a 10^{-5} M chloroform solution of this difunctional guest to the 0.1% w/v solution of NP(**10b**) in chloroform induced a similar red-shift of the SPB as previously observed with a solution of **G5** of the same concentration. An increase of the titrating solution (10^{-4} M) induced a bigger red-shift. The UV-Vis data depicted in figure 3.21 show the trend of the titration. Also in this case it was possible to observe a red-shift of the SPB from λ = 530 nm to λ = 560 nm. The addition of the difunctional guest determines the broadening of the SPB. Therefore, as found for **G5**, **G10** is able to drive the aggregation of the uncomplexed clusters.

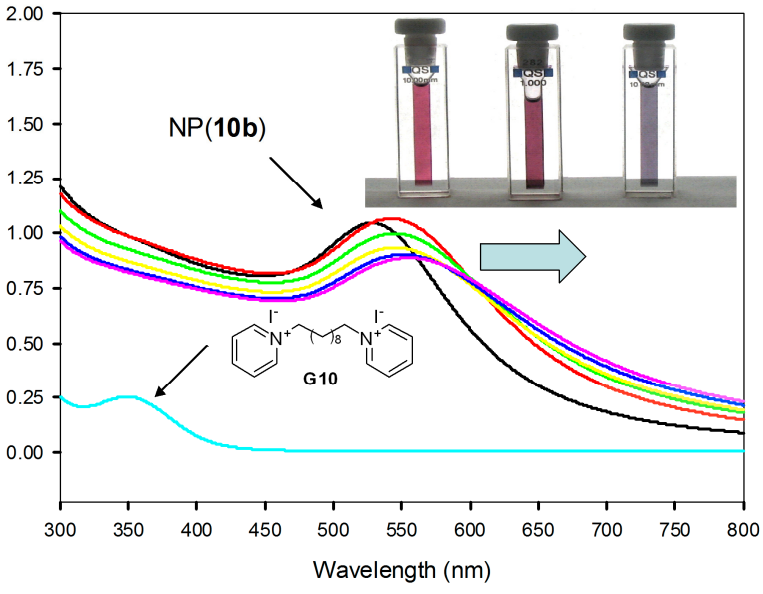

Figure 3.21 UV-Vis spectroscopic titration of NP(**10b**) with a 10^{-4}M solution of **G10** using chloroform as solvent (free NP(**10b**) black line, last guest addition point: fuchsia line).

In this case, however, it is important to observe that just after the first guest addition the SPB increases its intensity and shift to 542 nm (red line in figure 3.21). Afterward, the further addition of **G10**, induces the typical decrease of the SPB intensity together with a red-shift up to 560 nm. The different aggregation behaviour experienced by NP(**10b**) observed with **G5** and **G10**, can be tentatively explained considering that the first addition of the longer **G10** deos not generate the progressive intermolcular aggregation of the nanoclusters, but thanks to its larger flexibility, **G10** may surround the nanoclusers surface complexing simultaneously two close calix[4]arene cavity of **10b** present on the clusters surface (see Figure 3.22). Differently from **G5**, the addiction of a large amount of **G10** does not induce the total collapsing of the aggregates. This information suggests that longer difunctional guests improve the solubility of the aggregates.

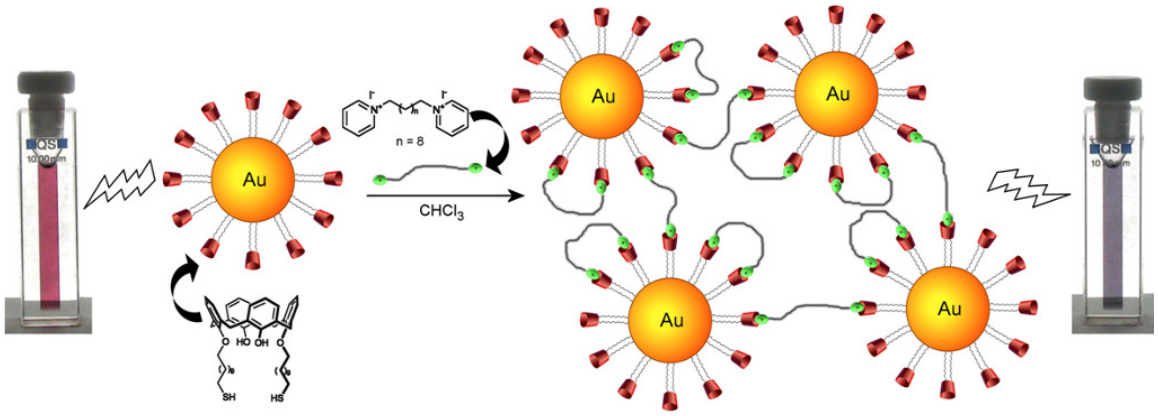

Figure 3.22 Schematic representation of interaction between NP(**10b**) and guest **G10**

In order to confirm that the observed aggregation processes are effectively due to the complexation of the bifunctional guests **G5** and **G10** through the aromatic cavity of calix[4]arene **10b** localized on different nanoclusters we repeated the titration experiments using *n*-dodecanthiol-protected nanoclusters NP(**C12**) having the same core size of NP(**10b**). In Figure 3.23a, it has been depicted the collection of UV/vis spectra recorded during the titration of these nanoclusters with **G10** in chloroform solution. It is easily observed the the addition of the difunctional guest only determines a decrease of the SPB intensity without any shift to longer wavelength. This is an expected result because **G10** cannot act as a bridge between nanoclusters which have not receptors on the surface. A further piece of evidence, was finally found titrating a 0.1% w/v solution of NP(**10b**) in chloroform with a 10^{-3} M solution of *N*-octyl pyridinium iodide **7**, which was previously used in Chapter 2 as a monofunctional guest. The spectra of the titration experiment also in this case evidenced a diminishing of the SPB band of the calix[4]arene-proteced nanoclusters but not a significant

shift of its maximum. This is a reasonable result because **7**, being a monofunctional guest cannot promote the networking between the nanoclusters.

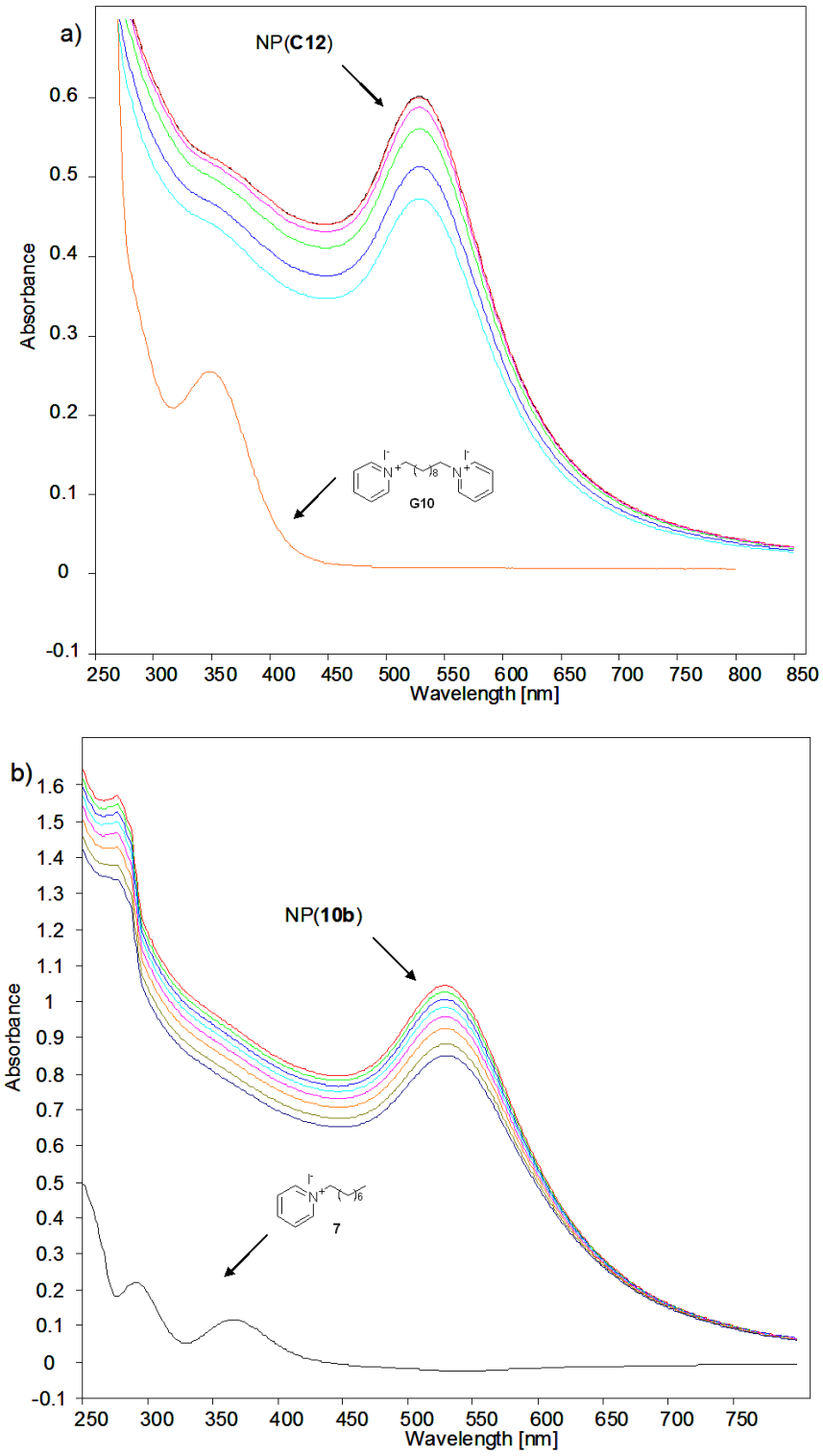

Figure 3.23 UV-Vis spectroscopic titration in $CHCl_3$ of : a) NP(**C12**) with a 10^{-4} M solution of **G10**, and b) NP(**10b**) with a 10^{-3} M solution of **7**.

The guest-induced aggregation of the NP(**10b**) clusters with **G10** was also studied through TEM measurements. From the TEM image depicted in figure 3.24, it is possible to

notice that aggregation effectively occurred. The Au MPCs are all close to each other forming a 3D packed system (see figure 3.24a). In fact, in some regions it is possible to notice where the aggregates changes from a 2D monolayer of clusters (see figure 3.24c) to a 3D network (see figure 3.24b) on the TEM grid.

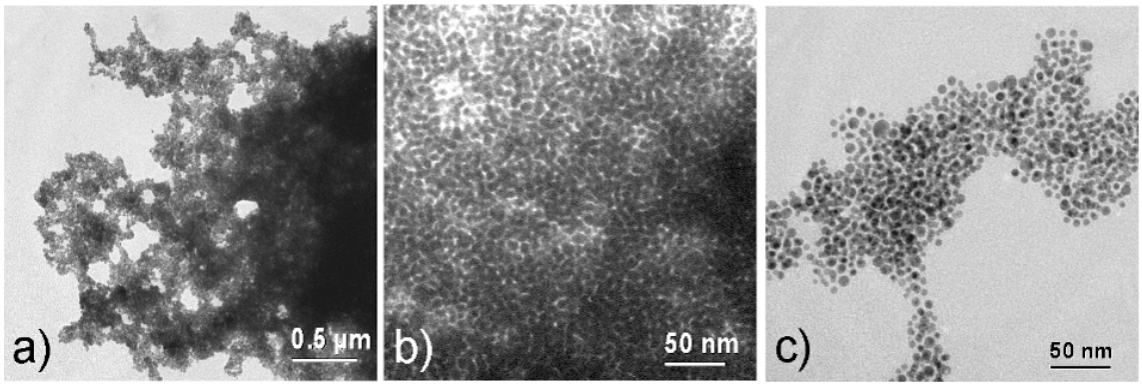

Figure 3.24 TEM images of self-assembled NP(**10b**) with G10**.**

Summarising, the guest-induced self-assembly process between nanoparticles protected with the thiolated calix[4]arene **10b** has been tackled and studied using UV/vis and TEM techniques. It has been shown that the aggregation process can be modulated by the nature of the difunctional supramolecular linker. In particular, the long and flexible **G10** gives rise to super-aggregates of nanoparticles that maintain solubility properties in common low polar solvents. Studies aimed to render these aggregation processes reversible through external (electro)chemical stimuli are in due course in our laboratories.

3.4 Experimental section

3.4.1 Materials and instrumentation

All reactions were carried out under nitrogen; all solvents were freshly distilled under nitrogen and stored over molecular sieves for at least 3h prior to use. ^{1}H and ^{13}C NMR spectra were recorded on BRUKER AC300 instrument operating at 300 and 75 MHZ, respectively. Chemical shift reported are referred to the tetramethylsilane (TMS) or residual solved resonances. ESI-MS spectra were recorded with Infusion Waters Acquity Ultra Performance LC instrument. UV-Visible spectra were recorded with a Lambda Bio 20 instrument. Melting points are uncorrected, and were recorded with Electrothermal instrument in sealed capillars under nitrogen atmosphere. Silica gel layers (SiO_2, MERCK 60 F_{254}) were used for thin layer chromatography (TLC). 60 Å silica gel (MERCK, 0.04-0.063 mm, 230-240 mesh) were used

for column chromatography. Compounds **5**,[50] undec-10-enyl 4-methylbenzenesulfonate,[38] and **14**[51] were synthesized according to reported procedures. The synthesis of **PQ**, and **NOPI,** were already reported in previous chapters. All other reagents were of reagent grade quality as obtained from commercial suppliers and were used without further purification.

3.4.2 Synthesis

S-11-(tosyloxy)undecyl ethanethioate (8): To a solution of undec-10-enyl 4-methylbenzenesulfonate (5 g, 15.4 mmol) and thioacetic acid (5.9 g, 77 mmol) in dry toluene (200 ml), a tip of spatula of AIBN was added. After refluxing for 5h, the reaction was quenched by addition of water (200 ml). The separated organic phase was dried over Na_2SO_4. After the removal of the solvent under reduced pressure, the solid residue was purified by column chromatography (eluent: hexane/ethyl acetate = 9/1) to afford the pure **8** as a yellow solid (95%). ^{1}H NMR (300 MHz, $CDCl_3$): δ (ppm) 7.78 (d, 2H, J = 8.3 Hz), 7.34 (d, 2H, J = 8.3 Hz), 4.01 (t, 2H, J = 6.6 Hz), 2.85 (t, 2H, J = 7.2 Hz), 2.44 (s, 3H), 2.32 (s, 3H), 1.8-1.5 (m, 4H), 1.4-1.1 (m, 14H). ^{13}C NMR (75 MHz, $CDCl_3$): δ (ppm) 195.0, 144.4, 140.3, 130.5, 128.3, 70.0, 32.5, 30.5, 29.7 (2 resonances), 29.5 (2 resonances), 29.3 (2 resonances), 28.8 (2 resonances), 25.8, 21.3. MS-ESI (m/z): 347 ($M+Na^+$, 100). Elemental Analysis for $C_{20}H_{32}O_4S$, calculated: C, 59.96; H, 8.05; S, 16.01, found: C, 59.57; H, 8.15; S, 16.23. M.p.: 28.0°C – 29.5°C.

Calix[4]arene 9a: a solution of calix[4]arene **5** (0.42 g, 1 mmol), K_2CO_3 (0.11 g, 0.8 mmol), and **8** (0.26 g, 0.8 mmol) in dry acetone (70 ml) was poured in a small glass autoclave filled with nitrogen. After sealing the autoclave, the reaction mixture was refluxed at 80 °C for 48h. After this period, the mixture was cooled at room temperature and the solvent evaporated to dryness under reduced pressure. The solid residue was taken up with a 10% solution of HCl (100 ml) and CH_2Cl_2 (100 ml). The separated organic phase was washed with water up to neutrality, dried over Na_2SO_4, and evaporated to dryness under reduced pressure. The crude product was purified by column chromatography (eluent: hexane/CH2Cl2 = 7/3) to afford the pure **9a** as a white solid (80%). ^{1}H NMR (300 MHz, $CDCl^3$): δ (ppm) 9.75 (s, 1H), 9.44 (s, 2H), 7.1-7.0 (m, 8H), 6.87 (t, 1H, J = 7.5 Hz), 6.7-6.6 (m, 3H), 4.37 (d, 2H, J = 13 Hz), 4.28 (d, 2H, J = 14 Hz), 4.16 (t, 2H, J = 7.2 Hz), 3.47 (d, 2H, J = 14 Hz), 3.46 (d, 2H, J = 13 Hz),

50. A. Arduini, A. Casnati in *Macrocycle Synthesis, A Practical Approach,* Ed.*:* D. Parker, OUP, Oxford, 1996, pp. 145-172.
51. R. G. Janssen, W. Verboom, D. N. Reinhoudt, A. Casnati, M. Freriks, A. Pochini, F. Ugozzoli, R. Ungaro, P. N. Nieto, M. Carramolino, F. Cuevas, P. Prados, J. de Mendoza, *Synthesis*, **1993**, 380.

2.86 (t, 2H, J = 7.2 Hz), 2.32 (s, 3H), 2.2-2.1 (m, 2H), 1.8-1.6, 1.6-1.5 and 1.5-1.3 (3m, 16H). ^{13}C NMR (75 MHz, $CDCl_3$): δ (ppm) 196.0, 151.4, 150.8, 149.2, 134.2, 129.2, 128.8, 128.7 (2 resonances), 128.3, 126.0, 121.9, 120.8, 77.2, 31.8, 31.4, 30.6, 29.8, 29.4 (2 resonances), 29.1, 28.8, 25.8. M.p. 53.0-54.0 °C. MS-ESI (m/z): 653 (M+1, 100), 675 (M+Na, 50). Elemental analysis for $C_{41}H_{48}O_5S$, calc: C, 75.43; H, 7.41; S, 4.91; found: C, 75.03, H, 7.41, S, 4.85.

Calix[4]arene 9b: A mixture of calix[4]arene **5** (3 g, 7 mmol), K_2CO_3 (0.97 g, 7 mmol), and **8** (6 g, 15 mmol) in CH_3CN (200 ml) was stirred and heated under reflux. After two days, the solvent was evaporated under vacuum and the solid residue taken up with CH_2Cl_2. The organic phase was washed with H_2O up to neutrality and dried over Na_2SO_4. After evaporation of the solvent under reduced pressure, the resulting crude product was purified by column chromatography (silica gel, hexane:ethyl acetate = 95:5) to give **9b** as white solid (70%). ^{1}H NMR (300 MHz, $CDCl_3$): δ (ppm) 8.22(s, 2H), 7.07 (d, 4H, *J* = 7 Hz), 6.91 (d, 4H, *J* = 7 Hz), 6.73 (t, 2H, *J* = 7 Hz), 6.66 (t, 2H, *J* = 7 Hz), 4.33 (d, 4H, *J* = 14 Hz), 4.02 (t, 4H, *J* = 6 Hz), 3.39 (d, 4H, *J* = 14 Hz), 2.88 (4H, *J* = 6 Hz), 2.32 (s, 6H), 2.1-2.0 (m, 4H), 1.8-1.7 (4H, m), 1.6-1.4 (2m, 28H); ^{13}C NMR (75 MHz, $CDCl_3$): δ (ppm) 153.3, 1520.0, 133.3, 128.8, 128.3, 128.1, 125.1, 118.9, 76.5, 31.4, 30.5, 29.9, 29.5, 29.4. MS-ESI (m/z): 904 ($M+Na^+$). Elemental analysis for $C_{54}H_{62}O_6S_2$, calculated: C, 73.51, H, 8.22, S, 7.27; found: C, 73.55, H, 8.14, S, 6.98.

Calix[4]arene 10a: A solution of calix[4]arene **9a** (0.4 g, 0.6 mmol) in a mixture of THF (20 ml) and HCl (10% v/v in H_2O, 20 ml) was refluxed for 3 days. After cooling to room temperature, the mixture was extracted with CH_2Cl_2 (30 ml). The resulting organic phase was separated, washed with water up to neutrality, dried over Na_2SO_4 and evaporated to dryness under reduced pressure. The oily residue was purified by column chromatography (eluent: hexane/CH2Cl2 = 7/3) to afford the pure product **10a** as a white solid (90%). ^{1}H NMR (300 MHz, $CDCl_3$): δ (ppm) 9.75 (s, 1H), 9.43 (s, 2H), 7.1-7.0 (m, 8H), 6.87 (t, 1H, J = 7.5 Hz), 6.7-6.6 (m, 3H), 4.37 (d, 2H, J = 13 Hz), 4.28 (d, 2H, J = 14Hz), 4.15 (t, 2H, J = 7.2 Hz), 3.47 (d, 2H, J = 14 Hz), 3.46 (d, 2H, J = 13 Hz), 2.6-2.5 (m, 2H), 2.2-2.1 (m, 2H), 1.8-1.6, 1.6-1.5 and 1.5-1.3 (3m, 16H). ^{13}C NMR (75 MHz, $CDCl_3$): δ (ppm) 151.4, 150.8, 149.2, 134.2, 129.3, 128.8, 128.7 (2 resonances), 128.4, 126.0, 121.9, 120.9, 77.4, 34.0, 31.9, 31.4, 29.9, 29.5 (2 resonances), 29.4, 29.1, 28.4, 25.9, 24.6. m.p. 87.0-88.0 °C. MS-ESI (m/z): 611 (M+1, 10), 634 (M+Na, 85), 650 (M+K, 60). Elemental analysis for $C_{39}H_{46}O_4S$, calculated: C, 76.68; H, 7.59; S, 5.25; found: C, 75.62, H, 7.46, S, 4.81.

Calix[4]arene 10b: A solution of calix[4]arene **9b** (1.5 g, 1.7 mmol) in a mixture of THF (50 ml) and HCl (10% v/v in H_2O, 50 ml) was refluxed for 3 days. After cooling to room temperature, the mixture was extracted with CH_2Cl_2 (30 ml). The resulting organic phase was separated, washed with water up to neutrality, dried over Na_2SO_4 and evaporated to dryness under reduced pressure. The oily residue was purified by column chromatography (eluent: hexane/CH_2Cl_2 = 7/3) to afford the pure **10b** as a white solid (80%). ^{1}H NMR (300 MHz, $CDCl_3$): δ (ppm) 8.29 (s, 2H), 7.13 (d, 4H, *J* = 7 Hz), 6.96 (d, 4H, *J* = 7 Hz), 6.8-6.7 (m, 4H), 4.40 (d, 4H, *J* =14 Hz), 4.07(t, 4H, *J* = 6 Hz), 3.45 (d, 4H, *J* =14 Hz), 2.7-2.5 (m, 4H), 2.2-2.1 (m,4H), 1.9-1.8 (m, 4H), 1.8-1.7 (m, 4H), 1.6-1.3 (m, 24H); ^{13}C NMR (75 MHz, $CDCl_3$): δ (ppm) 153.3, 133.4, 128.8, 128.3, 128.1, 125.2, 118.9, 75.6, 31.4, 31.3, 30.1, 29.9, 29.7, 29.5, 29.1, 29.0, 28.5, 26.1, 25.9. m.p. 300-302°C. MS-ESI (m/z): 818($M+Na^+$). Elemental analysis for $C_{50}H_{68}O_4S_2$, calculated: C, 75.33, H, 8.60, S, 8.05; found: C, 75.40, H, 8.32, S, 8.26.

Calix[4]arene 11: To a DMF mixture of calix[4]arene **5** (0.6 g, 1.4 mmol) previously degassed with nitrogen, was added NaH (0.15 g, 6.3 mmol). The mixture was salificated for 1h at 40°C, then compound **7** (2 g, 6.3 mmol) was added and mixture stirred and heated continuously at 40°C. After 4 days reaction was quenched adding methanol. The solvent was then removed under low pressure, HCl (10% v/v in H_2O, 50 ml) was added and the organic phase was extracted with CH_2Cl_2 (50ml). The resulting organic phase was separated, washed with water up to neutrality, dried over Na_2SO_4 and evaporated to dryness under reduced pressure. The oily residue was purified by column chromatography (eluent: hexane/ethyl acetate = 95/5) to afford the pure product **11** as a white solid (70%). ^{1}H NMR (300 MHz, $CDCl_3$): δ (ppm) 6.7-6.5 (m, 12H), 5.9-5.7 (m 4H), 5.1-4.9 (m 8H), 4.43 (d, 4H, *J* =13.5 Hz), 3.87 (t, 8H, *J* = 7.2 Hz), 3.14 (d, 4H, *J* =13.5 Hz), 2.2-2.0 (m, 8H), 2.0-1.8 (m, 8H), 1.5-1.2 (m, 48H); ^{13}C NMR (75 MHz, $CDCl_3$): δ (ppm) 156.6, 139.1, 135.1, 128.1, 121.8, 114.1, 75.1, 33.8, 31.0, 30.33, 29.9 (2 resonances), 29.7, 29.2, 29.0, 26.3. M.p. 35.5°C-36.5°C. MS-ESI (m/z): 1056($M+Na^+$, 100). Elemental analysis for $C_{72}H_{104}O_4$, calculated: C, 83.64, H, 10.07; found: C, 83.36, H, 10.42.

Calix[4]arene 12: To a solution of **11** (1.00 g, 0.97 mmol) and thioacetic acid (0.52 g, 6.79 mmol) in dry toluene (100 ml), a tip of spatula of AIBN was added. After refluxing for 5h, the reaction was quenched by addition of water (100 ml). The separated organic phase was dried

over Na_2SO_4. After the removal of the solvent under reduced pressure, the solid residue was purified by column chromatography (eluent: hexane/ethyl acetate = 95/5) to afford the pure **12** as a white solid (95%). ^{1}H NMR (300 MHz, $CDCl_3$): δ (ppm) 6.7-6.5 (m, 12H), 4.43 (d, 4H, *J* =13.5 Hz), 3.87 (t, 8H, *J* = 7.2 Hz), 3.14 (d, 4H, *J* =13.5 Hz), 2.86 (t, 8H, *J* =7.3 Hz), 2.32 (s, 12H), 2.0-1.8 (m, 8H), 1.7-1.5 (m, 8H), 1.5-1.2 (m, 14H); ^{13}C NMR (75 MHz, $CDCl_3$): δ (ppm) 195.9, 156.5, 135.1, 128.0, 121.8, 75.0, 30.9, 30.6, 30.2, 29.9 (2 resonances), 29.7, 29.6, 29.5, 29.2, 29.1, 28.9, 26.3. M.p. 56.0°C-57.0°C. MS-ESI (m/z): 1359($M+Na^+$, 100). Elemental analysis for $C_{80}H_{120}O_8S_4$, calculated: C, 71.86, H, 8.98, S, 9.58; found: C, 72.20, H, 8.78, S, 9.76.

Calix[4]arene 13: A solution of calix[4]arene **12** (0.8 g, 0.6 mmol) in a mixture of THF (20 ml) and HCl (10% v/v in H_2O, 20 ml) was refluxed for 3 days. After cooling to room temperature, the mixture was extracted with CH_2Cl_2 (30 ml). The resulting organic phase was separated, washed with water up to neutrality, dried over Na_2SO_4 and evaporated to dryness under reduced pressure. The oily residue was purified by column chromatography (eluent: hexane/ethyl acetate = 95/5) to afford the pure product **13** as a white solid (95%). ^{1}H NMR (300 MHz, $CDCl_3$): δ (ppm) 6.7-6.5 (m, 12H), 4.44 (d, 4H, *J* =13.5 Hz), 3.87 (t, 8H, *J* = 7.2 Hz), 3.14 (d, 4H, *J* =13.5 Hz), 2.52 (m, 8H), 2.0-1.8 (m, 8H), 1.7-1.5 (m, 8H), 1.5-1.2 (m, 14H); ^{13}C NMR (75 MHz, $CDCl_3$): δ (ppm) 156.5, 135.1, 128.0, 121.8, 75.0, 34.0, 30.9, 30.3, 29.9 (2 resonances), 29.7, 29.6, 29.2, 28.4, 26.3, 24.6. M.p. 48.0°C-49.0°C. MS-ESI (m/z): 1191($M+Na^+$, 100). Elemental analysis for $C_{72}H_{112}O_4S_4$, calculated: C, 73.97, H, 9.59, S, 10.96; found: C, 74.15, H, 9.31, S, 10.48.

Calix[6]arene 15: To a stirred solution of calix[6]arene **14** (1 g, 0.98 mmol) and K_2CO_3 (0.4, 3 mmol) in acetonitrile (200 ml), undec-10-enyl 4-methylbenzenesulfonate (0.96 g, 3 mmol) was added. The resulting heterogeneous mixture was refluxed for 4 days. After this period, the solvent was evaporated to dryness under reduced pressure. The solid residue was taken up with a 10% solution of HCl in water (100 ml) and ethyl acetate (200 ml). The organic phase was separated, washed with brine up to neutrality, dried over Na_2SO_4. After the removal of the solvent under reduced pressure, the solid residue was purified by column chromatography (eluent : n-hexane/CH_2Cl_2 = 8/2) to afford **15** as a white solid (55%). ^{1}H NMR (300 MHz, $CDCl_3$): δ (ppm) 7.33 (s, 6H), 6.70 (s, 6H), 6.0-5.8 (m, 3H), 5.1-4.8 (m, 6H), 4.63 (d, 6H, *J* = 14.1 Hz), 3.93 (t, 6H, *J* = 6.4 Hz), 3.44 (d, 6H, *J* = 14.1 Hz), 2.26 (s, 9H), 2.1-2.0 (m, 6H),

2.0-1.8 (m, 6H), 1.6-1.5 (m, 6H), 1.44 (s, 27H), 1.4-1.3 (m, 30H), 0.84 (s, 27H). ^{13}C NMR (75 MHz, $CDCl_3$): δ (ppm) 154.5, 152.1, 145.5, 145.2, 139.2, 133.6, 133.3, 127.9, 123.4, 114.1, 73.0, 60.2, 34.2, 33.9, 33.8, 31.6, 31.3, 31.2, 30.4, 29.7, 29.6, 29.5, 29.1, 28.9, 26.2. m.p. 133-135 °C. MS-ESI (m/z): 1495 (100, M+Na^+). Elemental analysis for $C_{102}H_{150}O_6$, calculated: C, 83.15; H, 10.32; found: C, 83.20, H, 10.52.

Calix[6]arene 16: To a solution of calix[6]arene **15** (1 g, 0.68 mmol) and thioacetic acid (0.37 g, 4.9 mmol) in dry toluene (100 ml), a tip of spatula of AIBN was added. After refluxing for 5h, the reaction was quenched by addition of water (100 ml). The separated organic phase was dried over Na_2SO_4. After the removal of the solvent under reduced pressure, the solid residue was purified by column chromatography (eluent: hexane/ethyl acetate = 95/5) to afford the pure **16** as a white solid (80%). ^{1}H NMR (300 MHz, $CDCl_3$): δ (ppm) 7.29 (s, 6H), 6.66 (s, 6H), 4.59 (d, 6H, *J* = 15.0 Hz), 3.88 (t, 6H, *J* = 6.5 Hz), 3.40 (d, 6H, *J* = 15.2 Hz), 2.87 (t, 6H, *J* = 7.3 Hz), 2.32 (s, 9H), 2.22 (s, 9H), 2.0-1.8 (m, 6H), 1.6-1.4 (m, 6H), 1.42 (s, 27H), 1.4-1.1 (m, 42H), 0.80 (s, 27H). ^{13}C NMR (75 MHz, $CDCl_3$): δ (ppm) 196.0, 164.4, 152.0, 145.6, 145.2, 133.8, 133.6, 133.2, 127.9, 126.8, 125.7, 124.7, 123.6, 123.3, 73.0, 60.1, 59.5, 34.2, 34.0, 33.9, 31.6, 31.4, 31.1, 30.6, 30.4, 29.6, 29.5, 29.4, 29.1, 28.8, 26.3, 26.2, 19.1. m.p. 125-127 °C. MS-ESI (m/z): 1723 (M+Na^+). Elemental analysis for $C_{108}H_{162}O_9S_3$, calculated: C, 76.23; H, 9.52; S, 5.65; found: C, 76.35; H, 9.43; S, 5.81.

Calix[6]arene 17: a solution of calix[6]arene **16** (0.6 g, 0.34 mmol) in a mixture of THF (20 ml) and HCl (10% v/v in H_2O, 20 ml) was refluxed for 4 days. After cooling to room temperature, the organic phase was extracted with CH_2Cl_2 (5 x 30 ml). The organic phases were collected, washed with water until neutrality, dried over Na_2SO_4 and evaporated to dryness under reduced pressure. The crude producte was purified through chromatography column (eluent hexane/ethyl acetate 95/5), to obtain **17** as white solid (85%). ^{1}H NMR (300 MHz, $CDCl_3$): δ (ppm) 7.29 (s, 6H), 6.64 (s, 6H), 4.59 (d, 6H, *J* = 15.0 Hz), 3.89 (t, 6H, *J* = 6.4 Hz), 3.40 (d, 6H, *J* = 15.0 Hz), 2.51 (q, 6H, *J* = 7.2 Hz), 2.20 (s, 9H), 2.0-1.8 (m, 6H), 1.7-1.2 (m, 81H), 0.79 (s, 27H); ^{13}C NMR (75 MHz, $CDCl_3$) δ (ppm) 154.4, 152.0, 145.6, 145.2, 133.8, 133.6, 133.5, 133.2, 127.9, 123.3, 73.0, 60.1, 34.2, 34.0, 33.9, 31.6, 31.4, 31.3, 31.2, 31.1, 30.6, 30.4, 29.6, 29.53, 29.50, 29.4, 29.0, 28.3, 26.2, 24.6. m.p. 69.5-70.5 °C. MS-ESI (m/z): 1597 (M+Na^+). Elemental analysis for $C_{102}H_{156}O_6S_3$, calculated: C, 77.76; H, 9.91; S, 6.10; found: C, 77.61; H, 10.10; S, 6.10.

Calix[4]arene 18: A mixture of calix[4]arene **5** (1.50 g, 3.5 mmol), K_2CO_3 (1.45 g, 10.5 mmol) and undec-10-enyl 4-methylbenzenesulfonate (3.5 g, 10.5 mmol) in CH_3CN (200 ml) was stirred and heated under reflux. After two days, the solvent was evaporated under vacuum and the solid residue taken up with CH_2Cl_2. The organic phase was washed with H_2O up to neutrality and dried over Na_2SO_4. After evaporation of the solvent under reduced pressure, the resulting crude product was purified by column chromatography (silica gel, hexane/ethyl acetate = 9/1) to give **18** as white solid (70%). ^{1}H NMR (300 MHz, $CDCl_3$): δ (ppm) 8.17 (s, 2H), 7.04 (d, 4H, *J* = 7 Hz), 6.91 (d, 4H, *J* = 7 Hz), 6.73 (t, 2H, *J* = 7 Hz), 6.64 (t, 2H, *J* = 7 Hz), 5.9-5.8 (m, 2H), 5.0-4.9 (m, 4H), 4.32 (d, 4H, *J* = 14 Hz), 3.99 (t, 4H, *J* = 6 Hz), 3.37 (d, 4H, *J* = 14 Hz), 2.1-2.0 (m, 8H), 1.7-1.6 (m, 4H), 1.5-1.3 (m, 20H); ^{13}C NMR ($CDCl_3$, 75 MHz): δ (ppm) 155.2, 150.8, 138.0, 132.3, 127.6, 127.2, 127.0, 124.0, 117.7, 112.9, 76.4, 32.6, 30.2, 28.8, 28.4, 28.3, 27.9, 24.8. m.p. 120-122 °C. MS-ESI (m/z): 729 (MH^+). Elemental analysis for $C_{50}H_{64}O_4$, calculated: C, 82.37, H, 8.85; found: C, 82.45, H, 8.52.

General procedure for the synthesis of calix[n]arene-protected Au MPCs

The clusters were synthesized according to the general procedure published by Murray[13] for *n*-dodecanthiol-coated Au MPCs.

Small-size nanoclusters (S:Au = 3:1) : 0.2 ml (0.29 mmol) of $HAuCl_4 \cdot xH_20$ (30%) (FW: 339.8) (d=1.637) were mixed with 8 ml of distilled water in a 100ml round bottomed flask. Under vigorous stirring were added 0.4g (0.73 mmol) of TOABr in 25ml of toluene. The two phase system was stirred until all the $AuCl_4^-$ was transfered into the organic phase, with the change of the solution colour to orange-red. After 15 minutes organic phase was separated and added with the opportune amount of stabilazing thiolated calixarene without variating the S/Au 3/1 ratio. The solution becomes colourless ($Au^{(III)} \rightarrow Au^{(I)}$). The solution was stirred continuously for 20 minutes at room temperature. Subsequently the roud bottomed flask was lipped in a ice bath and always under vigorous stirring were rapidly added (t < 10s) 0.11g (2.9mmol) of $NaBH_4$ in 4ml of distilled water. The solution changes to dark brown color ($Au^{(I)} \rightarrow Au^{(0)}$). The reaction was stirred for 1h at 0°C and for 4h at room temperature.

Purification (Method B): After this period 30 ml of distilled water were added. The organic phase was entracted and washed with 20ml of $H_2SO_{4(aq)}$ 5% and then with distilled water up to neutrality. 30ml of ethanol were then added to the organic phase. Subsequently the mixture was centrifuged at 5000 rpm for 15 minutes. The supernatant containig the excesses of

TOABr and calixarene was been settled away. The precipitated nano particles were recovered with toluene and dried under vacuum avoiding to heat the nanoparticles over 40°C (over this temperature decomposition or gold collapse phenomena can occur). Finally nano particles were purified through chromatographic column using dichloromethane:methanol 9:1 as eluent. During the elution the desired compound is well visible as a dark brown spot with Rf = 0.9. The purified nanoparticles were characterized with spectroscopic analysis like ^{1}H NMR, ^{13}C NMR, TEM, XPS, and elemental analysis.

1s: During the synthesis, 0.53g (0.87mmol) of 10a, were used as passivating agent, to afford product with a yield of ~ 40%. ^{1}H NMR (300MHz, $CDCl_3$), δ (ppm): 9.8 (bs, 1H), 9.4 (bs, 2H) , 7.2-6.5 (bm, 12H), 4.5-3.8 (bm, 6H), 3.4 (bs, 4H), 2.3-1.1 (18H). ^{13}C NMR (75MHz, $CDCl_3$), δ (ppm): 151.4, 150.7, 149.1, 134.1, 129.2, 128.7, 128.4, 126.0, 121.9, 120.9, 77.2, 31.8, 31.6, 31.4, 29.9, 28.9, 26.0. Organic fraction: 55%. Elemental analysis: C, 45.33; H, 4.03; S, 1.84, N, 0.35.

2s: During the synthesis, 0.35g (0.44mmol) of 10b, were used as passivating agent, to afford product with a yield of ~ 30%. ^{1}H NMR (300MHz, $CDCl_3$), δ (ppm): 8.3 (bs, 2H), 7.0 (bd, 4H) , 6.9 (bd, 4H), 6.7 (bt, 2H), 6.6 (bt, 2H), 4.3 (bd, 4H), 3.9 (bt, 4H) , 3.3 (bd, 4H), 2.7 (bm, 4H), 2.2-1.2 (36H). ^{13}C NMR (75MHz, $CDCl_3$), δ (ppm): 153.2, 151.8, 133.4, 128.8, 128.3, 128.1, 125.2, 118.9, 77.1, 31.6, 31.4, 30.1, 29.7, 29.1, 29.0, 26.4, 22.5, 22.3. Organic fraction: 61%. Elemental analysis: C, 48.87; H, 5.19; S, 3.54, N, 0.11.

3s: During the synthesis, 0.46g (0.29mmol) of 19, were used as passivating agent, to afford product with a yield of ~ 25%. ^{1}H NMR (300MHz, $CDCl_3$), δ (ppm): 7.3 (bs, 6H), 6.6 (bs, 6H) , 4.6 (bd, 6H), 3.9 (bt, 6H), 3.4 (bd, 6H), 2.7 (bm, 6H), 2.2 (bs, 9H) , 2.0-1.2 (bm, 81H), 0.8 (bs, 27H). ^{13}C NMR (75MHz, $CDCl_3$), δ (ppm): 154.4, 152.0, 145.6, 145.2, 133.6, 133.2, 127.8, 123.3, 77.1, 72.9, 34.2, 31.6, 31.3, 31.1, 29.9, 29.6, 29.2, 26.4, 22.5, 22.3. Organic fraction: 75%. Elemental analysis: C, 59.11; H, 7.40; S, 4.08; N, 0.15.

4s: During the synthesis, 0.26g (0.22mmol) of 13, were used as passivating agent, to afford product with a yield of ~ 25%. ^{1}H NMR (300MHz, $CDCl_3$), δ (ppm): 7.2-6.0 (bm, 12H), 4.5-4.2 (bd, 4H), 3.8 (bs, 8H), 3.2-3.0 (bd, 4H), 2.8-2.5 (bm, 8H), 2.1-1.0 (bm, 72H). ^{13}C NMR (75MHz, $CDCl_3$), δ (ppm): 156.5, 135.1, 128.0, 121.8, 77.1, , 31.7, 30.9, 30.3, 29.8, 29.5,

29.2, 28.2, 27.2, 26.6, 22.6. Organic fraction: 65%. Elemental analysis: C, 49.81; H, 6.39; S, 5.06, N, 0.17.

Medium-size nanoclusters (S:Au = 1:3): 0.2 ml (0.29 mmol) of $HAuCl_4 \cdot xH_20$ (30%) (FW: 339.8) (d=1.637) were mixed with 8 ml of distilled water in a 100ml round bottomed flask. Under vigorous stirring were added 0.4g (0.73 mmol) of TOABr in 25ml of toluene. The two phase system was stirred until all the $AuCl_4^-$ was transfered into the organic phase, with the change of the solution colour to orange-red. After 15 minutes organic phase was separated and added with the opportune amount of stabilazing thiolated calixarene without variating the S/Au 3/1 ratio. In this case the colour of solution didn't change because the $Au^{(III)}$ wasn't completely reduced to $Au^{(I)}$ by the thiol. The solution becomes colourless ($Au^{(III)} \rightarrow Au^{(I)}$). The solution was stirred continuously for 20 minutes at room temperature. Subsequently under vigorous stirring were rapidly added (t < 10s) 0.11g (2.9mmol) of $NaBH_4$ in 4ml of distilled water. The solution changes to dark brown color ($Au^{(I)} \rightarrow Au^{(0)}$). The reaction was stirred for 5h at room temperature.

Purification (Method A): After this period 30 ml of distilled water were added. The organic phase was entracted and washed with 20ml of $H_2SO_{4(aq)}$ 5% and then with distilled water up to neutrality. After this the organic phase recovered with CH_2Cl_2 was dried over Na_2SO_4 and evaporated with rotavapor avoiding to heat the nanoparticles over 40°C (over this temperature decomposition or gold collapse phenomena can occur). To the crude product were added 20ml of ethanol and then the subspesion was centrifuged at 5000rpm for 15 minutes. The precipitate was recovered with the minimum quantity of CH_2Cl_2 (and THF for 15-MPCs-M) and added again of ethanol. After this step the subspension was centrifuged again at 10000 rpm for 20 minutes. The nanoparticles obtained were characterized without further purification. The purified nanoparticles obtained, were characterized with spectroscopic analysis like ^{1}H NMR, ^{13}C NMR, TEM, XPS and elemental analysis.

1m: During the synthesis, 0.059g (0.096mmol) of 10a, were used as passivating agent, to afford product with a yield of ~ 65%. ^{1}H NMR (300MHz, $CDCl_3$), δ (ppm): 9.7 (bs, 1H), 9.4 (bs, 2H) , 7.2-6.4 (bm, 12H), 4.5-3.7 (bm, 6H), 3.3 (bs, 4H), 2.4-1.0 (18H). ^{13}C NMR (75MHz, $CDCl_3$), δ (ppm): 151.4, 150.7, 149.2, 134.1, 129.2, 128.7, 128.4, 126.0, 121.9, 120.8, 77.1, 31.9, 31.6, 31.4, 29.9, 29.5, 29.2, 28.3, 26.0. Organic fraction: 36%. Elemental analysis: C, 27.52; H, 2.74; S, 1.88, N, 0.00.

2m: During the synthesis, 0.038g (0.048mmol) of 10b, were used as passivating agent, to afford product with a yield of ~ 60%. ^{1}H NMR (300MHz, $CDCl_3$), δ (ppm): 8.3 (bs, 2H), 7.2-6.3 (bm, 12H), 4.3 (bs, 4H), 3.9 (bs, 4H) , 3.3 (bs, 4H), 2.3-1.0 (36H). ^{13}C NMR (75MHz, $CDCl_3$), δ (ppm): 153.1, 151.7, 133.5, 129.0, 128.8, 128.3, 128.2, 128.0, 125.2, 118.9, 76.9, 31.6, 31.4, 30.2, 29.7, 29.5, 29.1, 29.0, 28.5, 28.0, 26.3, 26.1, 22.5, 22.2. Organic fraction: 44%. Elemental analysis: C, 32.81; H, 3.45; S, 3.61, N, 0.14.

3m: During the synthesis, 0.050g (0.032mmol) of 19, were used as passivating agent, to afford product with a yield of ~ 50%. ^{1}H NMR (300MHz, $CDCl_3$), δ (ppm): 7.3 (bs, 6H), 6.6 (bs, 6H) , 4.5 (bs, 6H), 3.8 (bs, 6H), 3.3 (bs, 6H), 2.4-0.6 (bm, 117H). ^{13}C NMR (75MHz, $CDCl_3$), δ (ppm): 154.4, 152.0, 145.4, 145.2, 133.6, 133.2, 127.8, 123.3, 77.1, 72.9, 34.2, 31.5, 31.6, 31.0, 29.9, 29.5, 29.2, 26.5, 22.5, 22.3. Organic fraction: 48%. Elemental analysis: C, 36.78; H, 4.57; S, 3.08; N, 0.08.

4m: During the synthesis, 0.028g (0.024mmol) of 13, were used as passivating agent, to afford product with a yield of ~ 50%. TEM and XPS analysis were described previously in this chapter. ^{1}H NMR (300MHz, $CDCl_3$), δ (ppm): 7.3-6.0 (bm, 12H), 4.7-3.0 (bm, 16H), 2.3-1.0 (bm, 72H). ^{13}C NMR (75MHz, $CDCl_3$), δ (ppm): 156.4, 135.1, 128.0, 121.8, 77.1, 31.6, 30.8, 30.4, 29.7, 29.5, 29.1, 28.2, 27.3, 26.5, 22.6. Organic fraction: 35%. Elemental analysis: C, 25.62; H, 3.07; S, 3.78, N, 0.13.

Large-size nanoclusters (S:Au = 1:6): 0.2 ml (0.29 mmol) of $HAuCl_4 \cdot xH_20$ (30%) (FW: 339.8) (d=1.637) were mixed with 8 ml of distilled water in a 100ml round bottomed flask. Under vigorous stirring were added 0.4g (0.73 mmol) of TOABr in 25ml of toluene. The two phase system was stirred until all the $AuCl_4^-$ was transfered into the organic phase, with the change of the solution colour to orange-red. After 15 minutes organic phase was separated and added with the opportune amount of stabilazing thiolated calixarene without variating the S/Au 3/1 ratio. 0.030g (0.048mmol) for 10a, 0.019g (0.024mmol) for 10b, 0.014g (0.012mmol) for 13, 0.025g (0.016mmol) for 19. In this case the colour of solution didn't change because the $Au^{(III)}$ wasn't completely reduced to $Au^{(I)}$ by the thiol. The solution becomes colourless ($Au^{(III)} \rightarrow Au^{(I)}$). The solution was stirred continuously for 20 minutes at room temperature. Subsequently under vigorous stirring were rapidly added (t < 10s) 0.11g

(2.9mmol) of $NaBH_4$ in 4ml of distilled water. The solution changes to dark brown color ($Au^{(I)} \rightarrow Au^{(0)}$). The reaction was stirred for 5h at room temperature.

Purification (Method A): After this period 30 ml of distilled water were added. The organic phase was entracted and washed with 20ml of $H_2SO_{4(aq)}$ 5% and then with distilled water up to neutrality. After this the organic phase was dried over Na_2SO_4 and evaporated with rotavapor avoiding to heat the nanoparticles over 40°C (over this temperature decomposition or gold collapse phenomena can occur). To the crude product were added 20ml of ethanol and then the subspesion was centrifuged at 5000rpm for 15 minutes. The precipitate was recovered with the minimum quantity of toluene and added again of ethanol. After this step the subspension was centrifuged again at 10000 rpm for 20 minutes. Le nanoparticles obtained were characterized without further purification. The purified nanoparticles, were characterized with spectroscopic analysis like ^{1}H NMR, ^{13}C NMR, TEM, XPS and elementary analysis.

1l: During the synthesis, 0.030g (0.048mmol) of 10a, were used as passivating agent, to afford product with a yield of ~ 70%. ^{1}H NMR (300MHz, $CDCl_3$), δ (ppm): 9.7 (bs, 1H), 9.4 (bs, 2H) , 7.2-6.4 (bm, 12H), 4.5-3.7 (bm, 6H), 3.4 (bs, 4H), 2.4-1.0 (18H). ^{13}C NMR (75MHz, $CDCl_3$), δ (ppm): 151.3, 150.7, 149.1, 134.1, 129.2, 128.7, 128.4, 126.0, 121.9, 120.9, 77.1, 31.8, 31.4, 29.9, 26.0. Organic fraction: 25%. Elemental analysis: C, 18.60; H, 1.92; S, 1.29; N, 0.10.

2l: During the synthesis, 0.019g (0.024mmol) of 10b, were used as passivating agent, to afford product with a yield of ~ 80%.. ^{1}H NMR (300MHz, $CDCl_3$), δ (ppm): 8.3 (bs, 2H), 7.2-6.3 (bm, 12H), 4.3 (bs, 4H), 3.9 (bs, 4H) , 3.3 (bs, 4H), 2.3-1.0 (36H). ^{13}C NMR (75MHz, $CDCl_3$), δ (ppm): 153.3, 151.9, 133.5, 128.8, 128.3, 128.1, 125.2, 118.9, 77.1, 31.6, 31.4, 30.0, 29.7, 29.0, 27.2, 27.0, 26.4, 22.6, 22.2. Organic fraction: 30%. Elemental analysis: C, 22.65; H, 2.59; S, 2.41, N, 0.13.

3l: During the synthesis, 0.025g (0.016mmol) of 19, were used as passivating agent, to afford product with a yield of ~ 70%. ^{1}H NMR (300MHz, $CDCl_3$), δ (ppm): 7.2 (bs, 6H), 6.6 (bs, 6H) , 4.5 (bs, 6H), 3.8 (bs, 6H), 3.3 (bs, 6H), 2.5-0.5 (bm, 117H). ^{13}C NMR (75MHz, $CDCl_3$), δ (ppm): 154.4, 152.0, 145.4, 145.2, 133.6, 133.2, 127.8, 123.3, 77.2, 72.9, 34.3, 31.6, 31.4,

31.1, 29.8, 29.5, 29.3, 26.4, 22.5, 22.3. Organic fraction: 32%. Elemental analysis: C, 24.73; H, 3.28; S, 1.95; N, 0.14.

4l: During the synthesis, 0.014g (0.012mmol) of **13**, were used as passivating agent, to afford product with a yield of ~ 65%. ^{1}H NMR (300MHz, $CDCl_3$), δ (ppm): 7.3-6.0 (bm, 12H), 4.7-3.0 (bm, 16H), 2.3-0.9 (bm, 72H). ^{13}C NMR (75MHz, $CDCl_3$), δ (ppm): 156.5, 135.1, 128.0, 121.8, 77.1, 31.6, 30.9, 30.4, 29.6, 29.5, 29.2, 28.2, 27.3, 26.5, 22.6. Organic fraction: 26%. Elemental analysis: C, 19.57; H, 2.58; S, 2.71, N, 0.00.

Synthesis of NP(TOABr): these clusters were prepared following the Schiffrin method. Briefly: a 30 mM solution of $HAuCl_4$ in water (30 mL) was added to a 25 mM solution of tetraoctylammonium bromide in toluene (80 mL). The transfer of the gold salt to the toluene phase can be clearly seen visually within a few seconds. A 0.4 M solution of freshly prepared $NaBH_4$ (25 mL) was slowly added to the vigorous stirred mixture (30 minutes for the addiction), which caused an immediate reduction to occur. After 1h the two phases were separated and the toluene phase was subsequently washed with 0.1M H_2SO_4 and H_2O (five times), and then dried over anhydrous Na_2SO_4. ^{1}H NMR (300MHz, $CDCl_3$), δ (ppm): 3.3 (bm, 8H), 1.7 (bs, 8H), 1.5-1.2 (bm, 40H), 0.9 (bt, 12H). UV-spectra: SPB λ_{max} (toluene) = 523nm; SPB λ_{max} ($CHCl_3$) = 524nm. Organic fraction: 97%. Elemental analysis: C, 67.57; H, 12.90; N, 2.51.

Synthesis of NP(10b): to a 30 ml of TOABr-MPCs solution were added 130 mg of calix[4]arene **10b**. The mixture was stirred for 5 days at room temperature. After this period 30 ml of absolute ethanol were added and the solution was centrifugated at 5000 rpm for 20 minutes. After precipitation of nanoparticles the colourless liquid was removed and the precipitate redissolved in 40 ml of toluene and centrifugated again at 2000 rpm for 10 minutes in order to remove the colloidal gold. The surnatant containing the gold nanoparticles was recovered, added with 20ml of absolute ethanol and centrifuged again at 10000 rpm for 20 minutes in order to remove calixarene non bonded on gold surface. The precipitate was collected with CH_2Cl_2 and used without any other purification. ^{1}H NMR (300MHz, $CDCl_3$), δ (ppm): 8.3 (bs, 2H), 6.8 (bs, 12H) , 4.5-2.5 (bm, 12H), 2.4-1.0 (bm, 36H). ^{13}C NMR (75MHz, $CDCl_3$), δ (ppm): 153.3, 151.9, 133.5, 128.8, 128.3, 128.1, 125.2, 118.9, 77.1, 31.6, 31.4, 30.0, 29.6, 29.1, 29.0, 27.2, 26.4, 22.5, 22.3. UV-spectra: SPB λ_{max} (toluene) = 526nm; SPB

λ_{max} ($CHCl_3$) = 528nm. Organic fraction: 29%. Elemental analysis: C, 22.29; H, 1.89; S, 2.,52; N, 0.19. IR (KBr): 3432 (w), 2923 (s), 2852 (s), 1464 (w).

General procedure for the syntesis of **G5** and **G10**:

Pyridine (2.3 g, 30 mmol) and the proper amount of alkylating agent (5 mmol) were dissolved in acetonitrile (50 ml). The resulting homogeneous solution was refluxed for 24h. After cooling to room temperature, 150 mL of ethyl acetate were slowly added to the reaction mixture until a crystalline solid precipitated from the solution. The solid was recovered by suction filtration, washed with ethyl acetate (3 × 25 ml) and dried under vacuum. The recovered salt did not required further purification.

1,1'-(pentane-1,5-diyl)dipyridinium) iodide (G5): 1,5-diiodo pentane (1.62 g) was used as alkylating agent to afford 2.29 g of guest **G5** as a yellow solid (95%). ^{1}HNMR (CD_3OD, 300 MHz) δ (ppm): 9.11 (d, 4H, J = 5.6 Hz, Ar-H); 8.62 (t, 2H, J = 7.8 Hz, Ar-H); 8.2-8.1 (m, 4H, Ar-H); 4.73 (t, 4H, J = 7.6 Hz, N-CH_2-CH_2-); 2.2-2.1 (m, 4H, N-CH_2-CH_2-CH_2-); 1.6-1.5 (m, 2H, N-CH_2-CH_2-CH_2-). ^{13}CNMR (CD_3OD, 75 MHz) δ (ppm): 147.3; 146.4; 130.0; 62.8; 32.0; 24.0. ESI-MS(+) : m/z = 355.0 $[M-I]^+$. M.p = 144.5-145.3 °C. Elemental Analysis for $C_{15}H_{20}N_2I_2$: calc. C 37.37, H 4.18, N 5.81; obs. C 37.21, H 4.22, N 5.73.

1,1'-(decane-1,10-diyl)dipyridinium) iodide (G10): 1,10-diiodo decane (1.97 g) was used as alkylating agent to afford 2.57 g of guest **G10** as a yellow solid (93%). ^{1}HNMR (CD_3OD, 300 MHz) δ (ppm): 9.05 (d, 4H, J = 5.2 Hz, Ar-H); 8.60 (t, 2H, J = 7.8 Hz, Ar-H); 8.2-8.1 (m, 4H, Ar-H); 4.66 (t, 4H, J = 7.8 Hz, N-CH_2-CH_2-); 2.1-2.0 (m, 4H, N-CH_2-CH_2-); 1.4-1.3 (m, 12H, N-CH_2-CH_2-CH_2-CH_2-CH_2-). ^{13}CNMR (CD_3OD, 75 MHz) δ (ppm): 147.2; 146.2; 129.8; 63.4; 32.8; 30.5; 30.2; 27.4. ESI-MS(+) : m/z = 425.1 $[M-I]^+$. ESI-MS(-) : m/z = 126.6 $[I]^-$. M.p. = 172.5-173.7 °C. Elemental analysis for $C_{20}H_{30}N_2I_2$: calc. C 43.50, H 5.48, N 5.07; obs. C 43.12, H 5.61, N 5.12.

3.4.3 Products Characterization

NMR Spectra

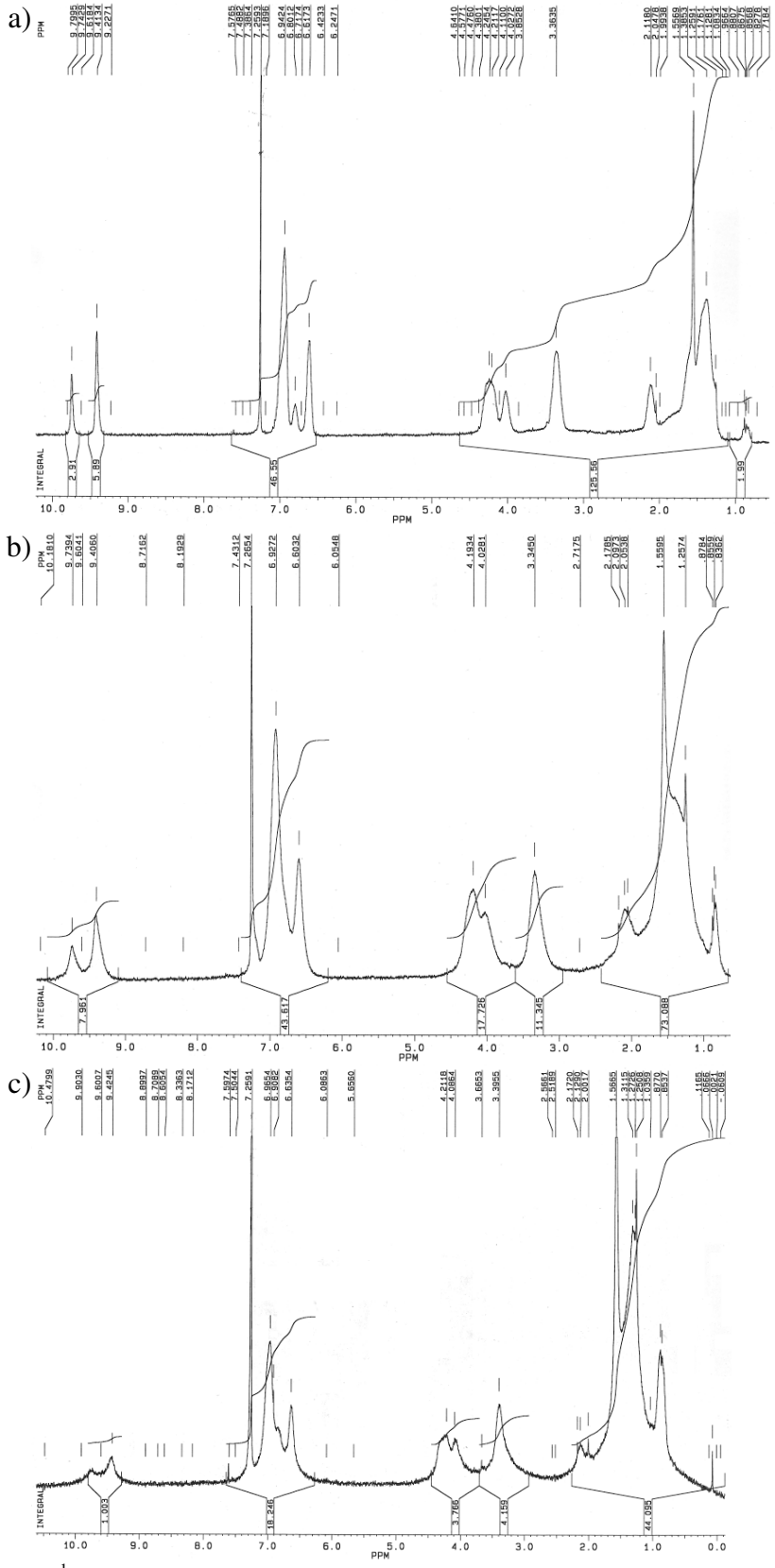

Figure 3.25 ^{1}H NMR spectra in $CDCl_3$ (300 MHz) of Au MPCs: a) **1s** b) **1m**, and c) **1l**.

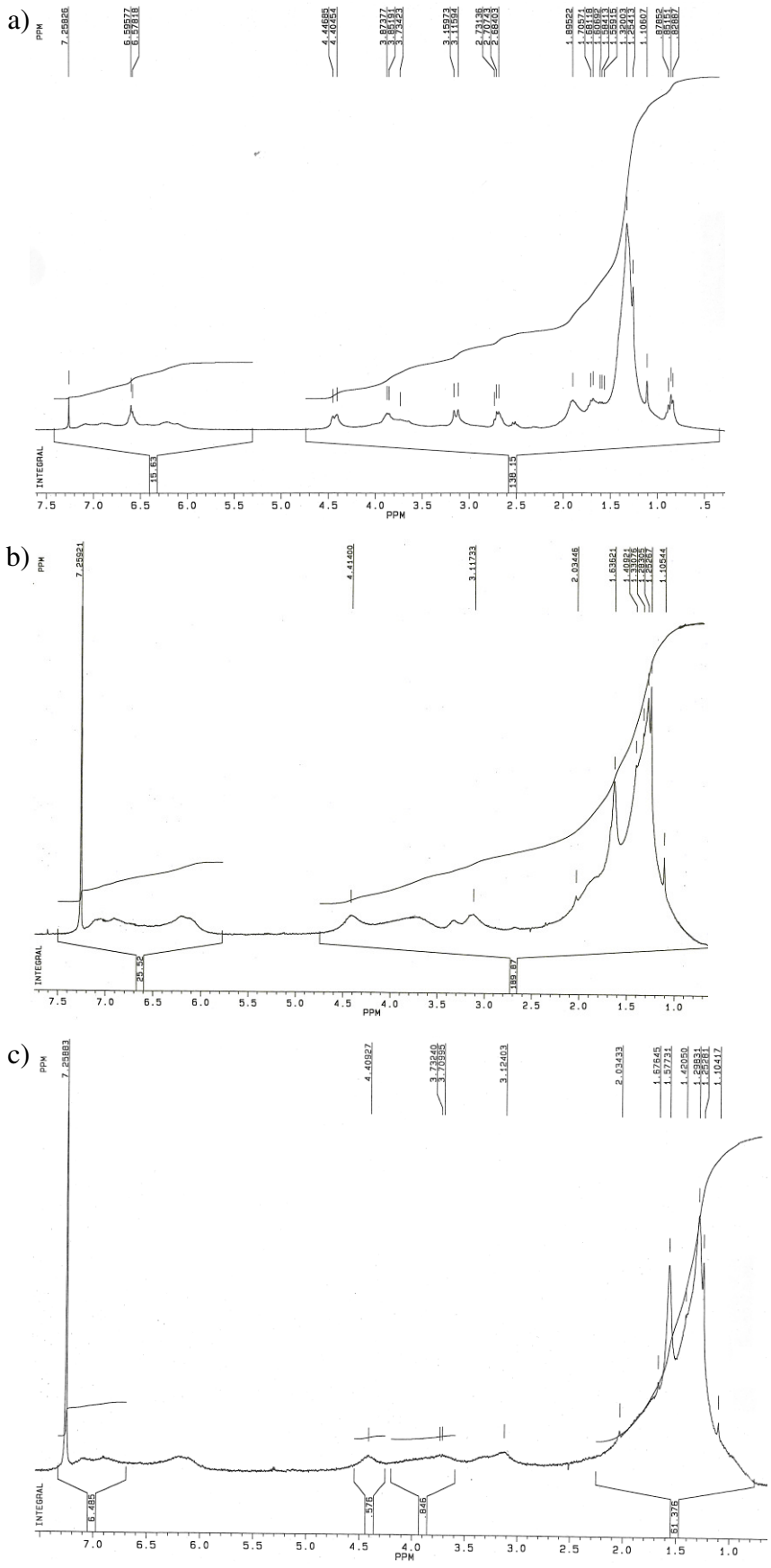

Figure 3.26 ^{1}H NMR spectra in $CDCl_3$ (300 MHz) of Au MPCs: a) **3s** b) **3m**, and c) **3l**

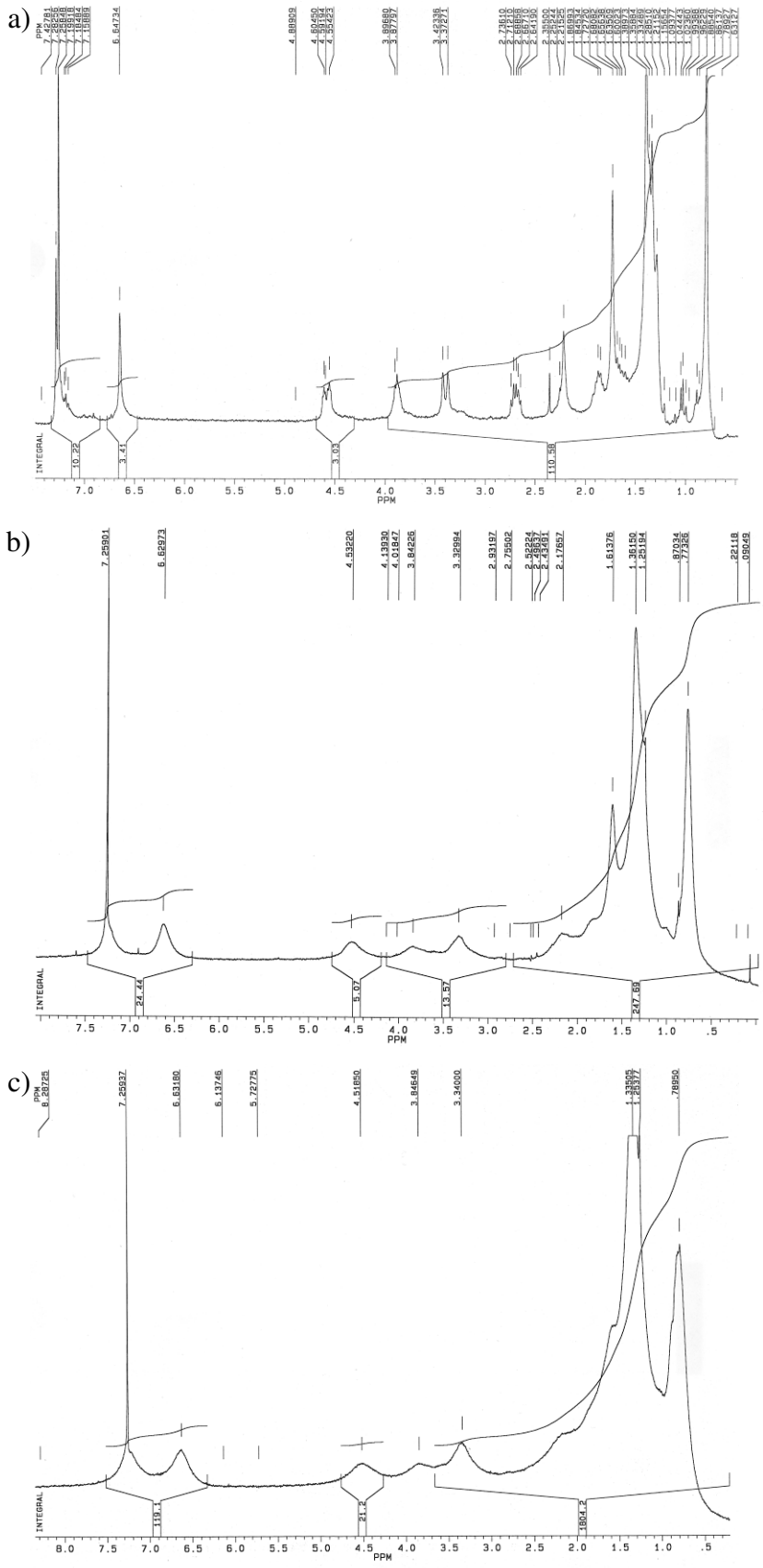

Figure 3.27 ^{1}H NMR spectra in $CDCl_3$ (300 MHz) of Au MPCs: a) **4s** b) **4m**, and c) **4l**

UV-Vis experiments:

UV-Vis experiments were performed at a T= 300K, using a quartz cuvette of 1 cm optical length. UV-Vis self-assembly experiments were performed titrating the chloroform solution of nanoparticles taken in exam, with a chloroform solution of the desired guest with variable concentration (see detailed description of each experiment in this chapter).

TEM Measurements

TEM measurements were carried out at CIGS of the University of Modena (Italy) on a Jeol JEM 2010 Microscope. The clusters size distribution was determined by statistical analysis of more than 300 clusters taken from at least three images for each sample. Clusters size was obtained by analysing each TEM images with the free UTHSCSA Image Tool program.[52]

XPS Measurements

XPS experiments were performed at the department of chemistry of the Univerisità "La Sapienza" Roma. The solid compounds were finely ground in an agate mortar and a small quantity of the resulting powder was homogeneously spread over a graphite tip attached to the XPS sample holder. Photoelectron spectra have been acquired with a modified Omicron NanoTechnology MXPS system equipped with various photon sources and an Omicron EA-127-7 energy analyzer. The experimental conditions adopted were as follows: excitation by Mg Kα photons (hν = 1253.6 eV), generated operating the anode at 14 kV, 16 mA. XPS atomic ratios for the investigated compounds have been estimated from experimentally determined area ratios of the relevant core lines. Correction for static charging (~3-4 eV) was performed by referencing all the BEs to the C 1s of ring carbons of calixarenes, taken at 285.0 eV. S 2p can be curve-fitted with two spin-orbit components, $2p_{3/2}$ e $2p_{1/2}$, with a 1.2 eV separation and a 2:1 area ratio.

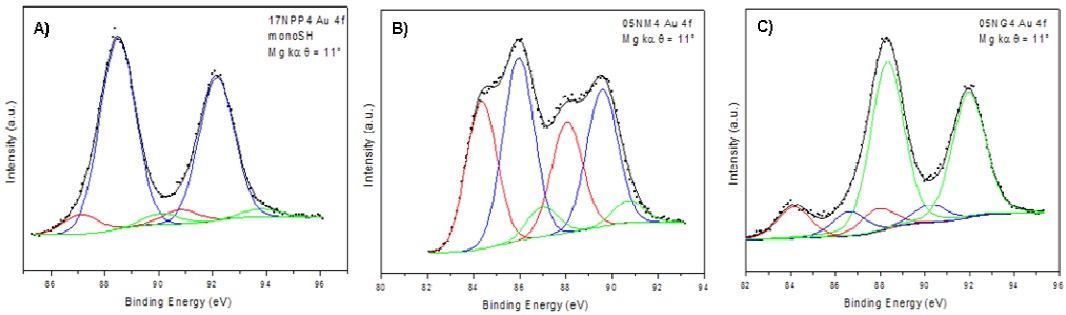

Figure 3.28. XPS region of Au 4f of: a) **1s**, b) **1m,** c) **1l**. Curve-fitted components: Au (0) (red line), Au (I) (blue line), Au (III) (green line). Binding energy in figures are not referenced to BE of C 1s (from calixarene rings).

52. UTHSCSA Image Tool program. Developed at the University of Texas Health Science Center at San Antonio, Texas and available from the internet by anonymous FTP from ftp://maxrad6.uthscsa.edu.

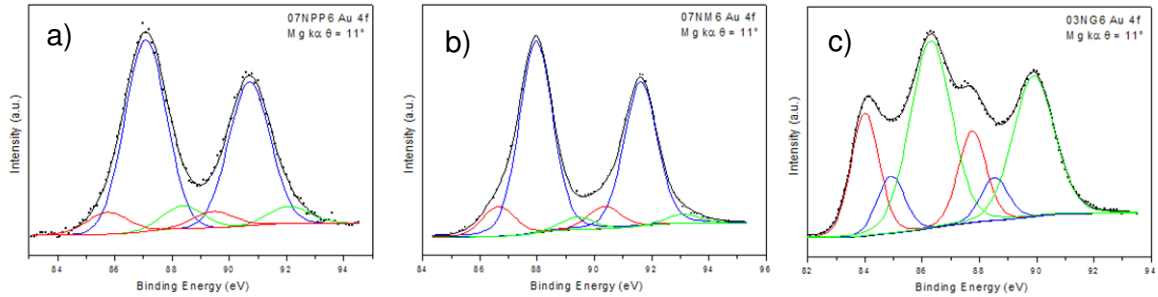

Figure 3.29. XPS region of Au 4f of: a) **3s**, b) **3m,** c) **3l**. Curve-fitted components: Au (0) (red line), Au (I) (blue line), Au (III) (green line). Binding energy in figures are not referenced to BE of C 1s (from calixarene rings).

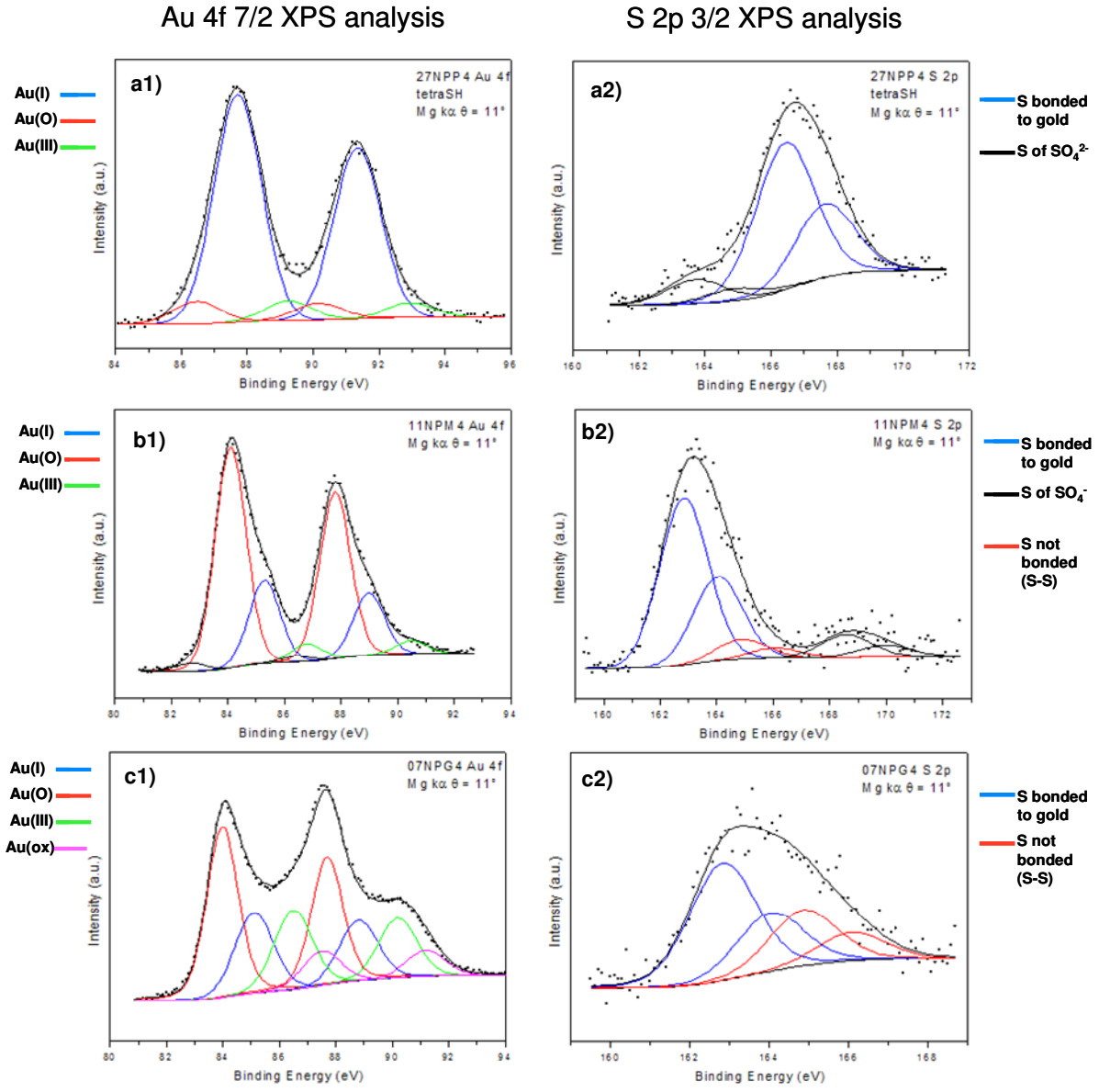

Figure 3.30. XPS region of: a1-2) **4s,** b1-2) **4m,** c1-2) **4l** (see legend). Binding energy in figures are not referenced to BE of C 1s (from calixarene rings).

Chapter 4:
Calix[n]arene-based 2D Self-Assembled Monolayers

Chapter 4. Calix[n]arene-based 2D Self-Assembled Monolayers

4.1 Introduction

In chapter 2 it has been shown that preorganized calix[n]arene compounds can be used as hosts for the complexation in low polar solvents of organic *N*-alkyl pyridinium-based salts. In the subsequent chapter, these recognition properties have been exploited to promote the guest-induced aggregation of calix[4]arene-protected Au MPCs. In this chapter we present our preliminary results on the reversible self-assembly of properly functionalized nanoclusters (3D SAM) on surfaces covered with complementary effectors (2D SAM). Calix[n]arene compounds can infact be inserted on the surface of the 2D SAM as the active protecting layer, while properly modified *N*-alkyl pyridinium units may be loaded on the 3D SAM (see Figure 4.1). Obviously, also the opposite approach is very likely feasible.

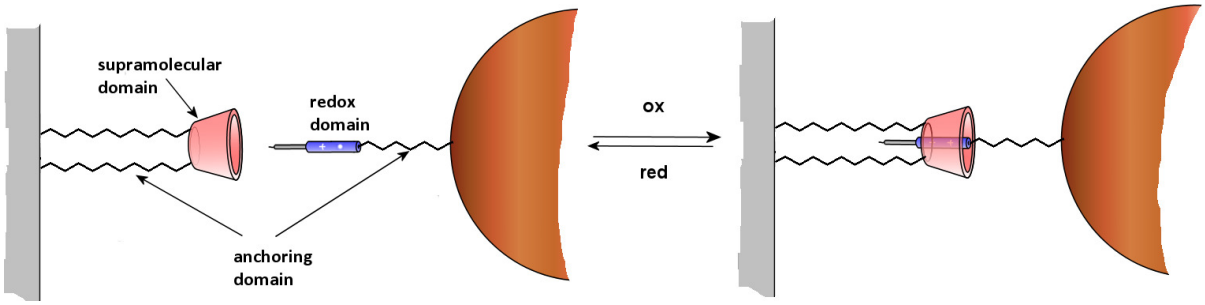

Figure 4.1 Schematic representation of a redox controlled self-assembly processes between a Si or Cu 2D SAM functionalized with calix[n]arene-based receptors and a Au 3D SAM functionalized with pyridinium or viologen salts. The reverse strategy (calix on 3D and salt on the 2D SAM) can be also devised.

Among the several flat inorganic surfaces so far used as substrates for the formation of 2D SAM, gold has as usual played a primary role because of its stability, facile handling and well documented affinity for thiolated derivatives.[1,2] Surely less explored are the 2D SAM based on copper or silicon. The difficult handling of silicon-based materials has very often limited the employment of this semiconductor as base for the development of novel 2D SAM.[3,4] On the other hand, copper has not been considered yet by the scientific community as

1. See e.g. : J. C. Love, L. A. Estroff, J. K. Kriebel, R. G. Nuzzo, G. M. Whitesides, *Chem. Rev.*, **2005**, *105*, 1103 and references therein.
2. Few studies are present in the literature in which calix[n]arene derivatives have been anchored on flat gold surfaces, see e. g.: (a) J. D. Faull, V. K. Gupta, *Langmuir*, **2001**, *17*, 1470; (b) J. D. Faull, V. K. Gupta, *Thin Solid Films*, **2003**, *440*, 129; J. D. Faull, P. J. Wissmann, V. K. Gupta, *Thin Solid Films*, **2004**, *457*, 292.
3. For the functionalization of Si(100) surfaces with organic compounds, see: (a) R. Zanoni, A. Aurora, F. Cattaruzza, C. Coluzza, E.A. Dalchiele, F. Decker, G. Di Santo, A. Flamini, L. Funari, A.G. Marrani, *Materials Science and Engineering C*, **2006**, *26*, 840; (b) M. Cossi, M.F. Iozzi, A.G. Marrani, T. Lavecchia,

a potent and cheaper alternative to gold as substrate for the formation of functional 2D SAM.[5] In this framework herein we report our studies aimed to the development of 2D SAM of Si(100) and polycrystalline Cu stabilized both by calix[n]arene derivatives. The recognition properties of these novel functional 2D SAM have been studied at the solid-liquid interface by using XPS spectroscopy as investigation tool. The good results obtained with the prototype systems were then used to self-assemble calix[6]arene-based rotaxane and pseudorotaxane structures on Si and Cu surfaces. The following research is the result of collaboration with the research group of Prof. Robertino Zanoni of the Dipartimento di Chimica of the University "La Sapienza" of Rome.

4.2 Calix[n]arene-based Si(100) 2D SAMs

4.2.1 Functionalization and characterization of Si(100) surface

Silicon is a semiconductor with an intrinsic conductivity of 4.3×10^{-6} Ω^{-1} cm^{-1}, and a band gap of 1.12 eV at 300 K. Silicon materials are usually used in electronics and they are generally doped with P or Al. For a single silicon crystal the superficial properties depend on the orientation of the crystal faces. The (111) surface has the highest atomic density and the lowest superficial energy, whereas the (100) surface has the highest superficial energy and the lowest atomic density. Among the several anchoring procedures developed for the functionalization of Si(100) surfaces, the photochemical one intially devised by Buriak et al.[3c,d] and improved by Zanoni et al.[3a,b] allows a non destructive anchoring of the organic layer, provided that the latter is constituted by molecules having in their structure insaturation functions such as alkenyl or alkynil.

Synthesis of calixarene derivatives for the Si(100) functionalization

In order to evaluate the feasibility of the Si surface functionalization with calixarene derivatives, we used two simple compounds which present on their lower rim proper "anchoring points" (see Figure 4.2). In particular calix[4]arene **19** and calix[6]arene **20** are characterized by the presence of two and three "ω-alkenyl" chains (see figure 4.2, blu circles)

P. Galloni, R. Zanoni, F. Decker, *J. Phys. Chem. B*, **2006**, *110*, 22961; (c) J.M. Buriak, *Chem. Rev*., **2002**, *102*, 5; (d) M.P. Stewart, J. M. Buriak, *Angew. Chem. Int. Ed.*, **1998**, *23*, 3257.

4. In the literature are also present few examples of Si surfaces functionalized with resorcinarenes, a class of macrocyclic compounds similar to calix[n]arenes, see: (a) G.G. Condorelli, A. Motta, M. Favazza, I.L. Fragalà, M. Busi, E. Menozzi, E. Dalcanale, L. Cristofolini, *Langmuir*, **2006**, *22*, 11126; (b) M. Busi, M. Laurenti, G.G. Condorelli, A. Motta, M. Favazza, I.L. Fragalà, M. Montalti, L. Prodi, E. Dalcanale, *Chem. Eur. J*., **2007**, *13*, 6891.
5. Polycrystalline copper surfaces have been very often covered with thiolated derivatives, see e.g : M. Beccari; S. Pomponio; V. Di Castro, *Superlattices and Microstructures,* **2009**, *46*, 25.

on their lower rim, respectively. Moreover, the two macrocycles present some hetero atoms in their structure. These heteroatoms indeed give rise to well codified signals in the corresponding XPS spectra (see infra), which are diagnostic for the characterization of the functionalized surface. **19** is characterized by the presence of two bromine atoms and **20** posses three nitro groups on its upper rim (see figure 4.2, red circles). Compound **20** was synthesized according to literature procedure,[6] whereas compound **19** has been synthesized through the synthetic pathway depicted in scheme 4.1.

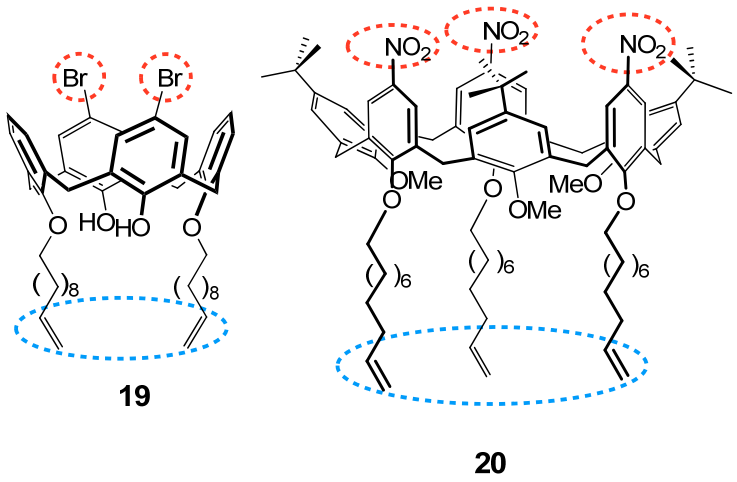

Figure 4.2 Calix[n]arenes used for the functionalization of Si(100) surface.

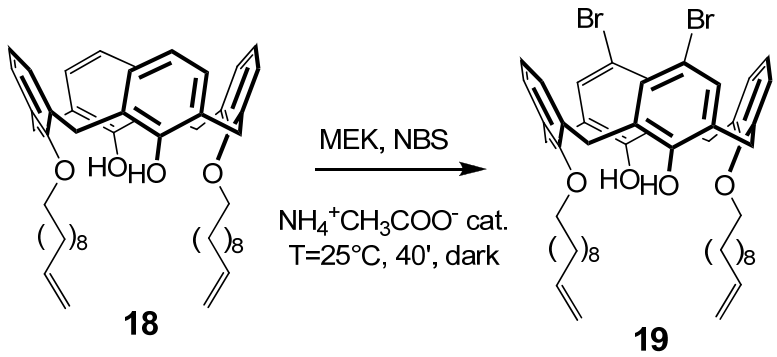

Scheme 4.1. Synthesis of calix[4]arenes **19**.

The dibromo-calix[4]arene **19** was obtained for reaction of **18** (see chapter 3) with *N*-bromo succinimide (NBS) using methyl ethyl chetone (MEK) as solvent in the presence of ammonium acetate as catalyst.[7] The reaction was carried out at room temperature for 40 minutes in the dark. After purification by column chromatography, **19** was obtained in 50% yield. In its ^{1}H NMR spectrum taken in $CDCl_3$ (see Figure 4.3), the singlet at δ = 7.16 ppm,

6. B. Gadenne, I. Yildiz, M. Amelia, F. Ciesa, A. Secchi, A. Arduini, A. Credi, F. M. Raymo, *J. Mater. Chem.*, **2008**, *18*, 2022.
7. B. Das, K. Venkateswarlu, A. Majhi, V. Siddaiah, K. R. Reddy, *J. Mol. Catal. A: Chem.*, **2007**, *267*, 30.

the doublet at δ =6.92 ppm and the triplet at δ =6.80 ppm are diagnostic for the effective distal functionalization with bromine atoms of the upper rim of the calixarene macrocycle.

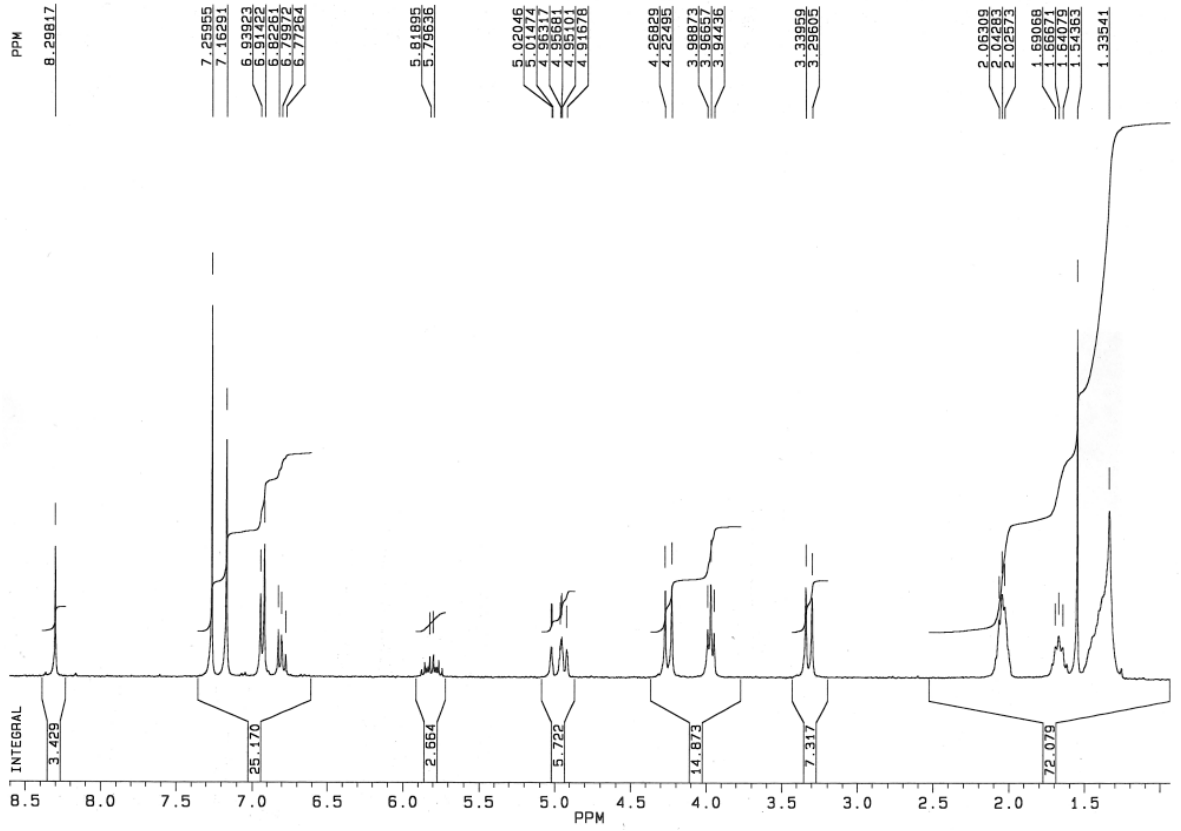

Figure 4.3 ^{1}H NMR spectrum of **19** in $CDCl_3$ (300 MHz).

Functionalization of the Si(100) surface

The functionalization of Si(100) surfaces is not a straightforward operation. Indeed, the formation of a chemical bond between the silicon of the surface and the molecules of the organic layer needs a careful preparation (activation) of the silicon surface. The following activation procedure aims to have a hydrogen terminated (Si-H) silicon surface ready to be functionalized. Initially the silicon substrate was cleaned with trichloroethylene and ethanol, followed by treatment with a mixture of $HCl:H_2O_2:H_2O$ = 1:2:8 and with a final rinsing with water. Then, the substrate was etched with a 10% solution of HF and rinsed again with water.

The covering of the Si(100) surface with calixarenes **19**, **20**, and **21** was then accomplished using an extra-mild photochemical activation with visible light. In particular, the silicon substrate was dipped in the calixarene solution (10 mM, toluene, 4-5h) followed by irradiation with visible light (I_2 quartz lamp: 35 mW cm^{-2}) (see Figure 4.4). Then, the silicon plate was rinsed with dichloromethane to remove the not anchored residual calixarene.

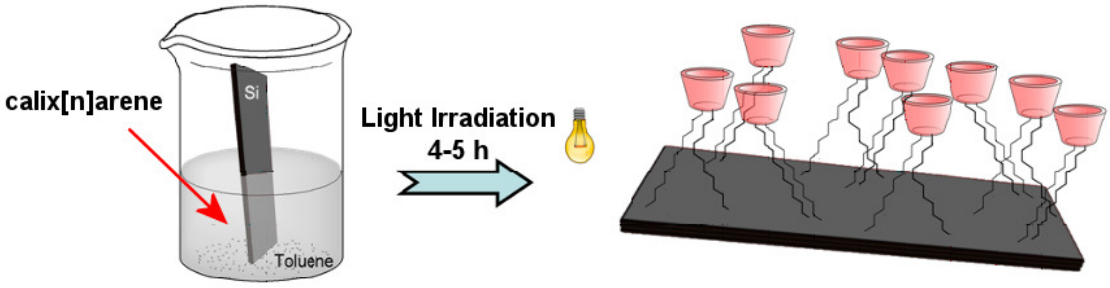

Figure 4.4 Schematic functionalization process of Si(100) surface with some calix[n]arenes derivatives, through photochemical activation of silicon.

Characterization of the functionalized Si(100) surface

The Si(100) surfaces functionalized with calix[n]arenes **19** and **20** were analyzed through XPS spectroscopy. The region of the XPS spectrum relative to Si 2p (see figure 4.5a) shows that after the functionalization process the surface does not present traces of oxidized silicon (blue arrow in Figure 4.5a). The deconvolution of the Si peak indeed shows: two signals for the bulk silicon (gray shaded areas) and two for the surface silicon (black areas).

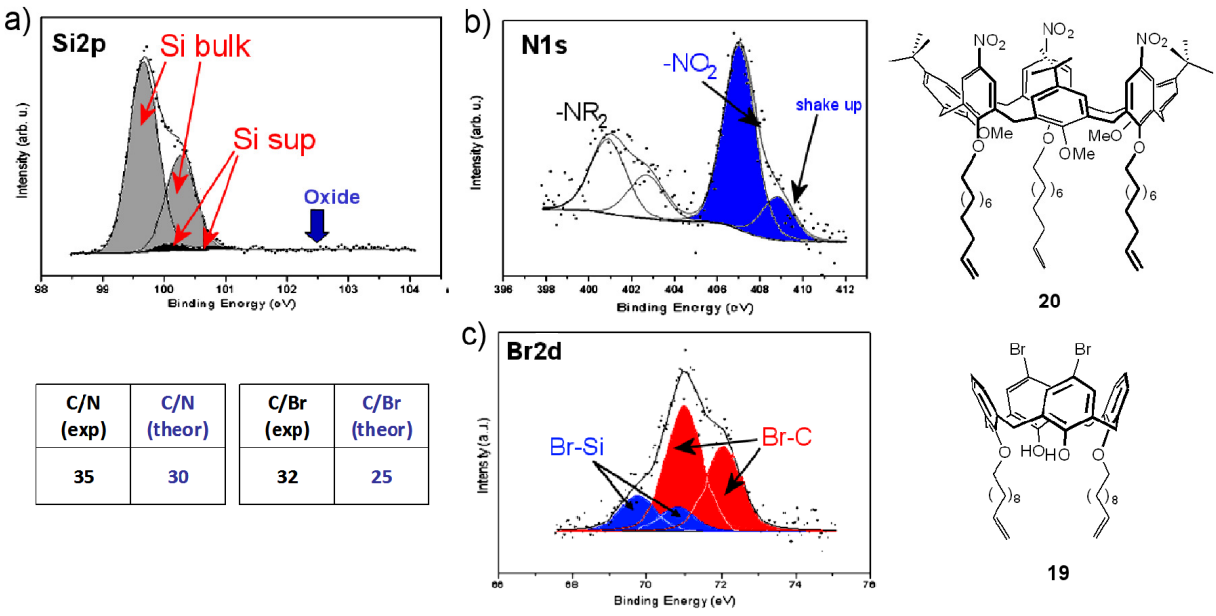

C/N (exp)	C/N (theor)	C/Br (exp)	C/Br (theor)
35	30	32	25

Figure 4.5 Regions of the XPS spectrum of the Si surface functionalized with **20**: a) Si 2p and b) N 1s. c) Br 2d region of the XPS spectrum of the Si surface functionalized with **19** and **20**. Binding energy in figures are not referenced to BE of C 1s (from calixarene rings).

The covalent attachment of calix[6]arene **20** on the Si surface was verified by analysing the region of the spectrum corresponding to N 1s (see Figure 4.5b, BE in figures are not referenced to the C 1s signal of the calixarene). One large peak at 407 eV (blue shaded area, see figure 4.5b) is attributable to the nitrogen of the NO_2 groups present on the calix[6]arene upper rim. In the spectrum it is also visible another signal at lower BE that could correspond

to a $-NR_2$ group. Latter group is not present in the calixarene macrocycle, and the impurities which have originated this signal were not established yer. The ratio between the signal of N 1s relative to the NO_2 group and the signal of C 1s is about 35 (error ±10%). This ratio is in good agreement with the theoretical C/N value of 30.

The silicon surface functionalized with the calix[4]arene **19** presents a large signal relative to Br 2d. After deconvolution, in Figure 4.5c it is possible to observe two kinds of diagnostic signals: a more intense one (red areas) assigned to the bromine atoms bonded to calix[4]arene unit and a less intense one (blue areas) ascrivable to the bromine atoms bonded on the silicon surface. The presence of the latter signal told us that during the photochemical functionalization, some Br migrated from the upper rim of the macrocycle to the activated silicon surface.[8] However, from these results, it was possible to obtain a C/Br integration ratio of ~32 that is still in good agreement with the theoretical ratio of 25.

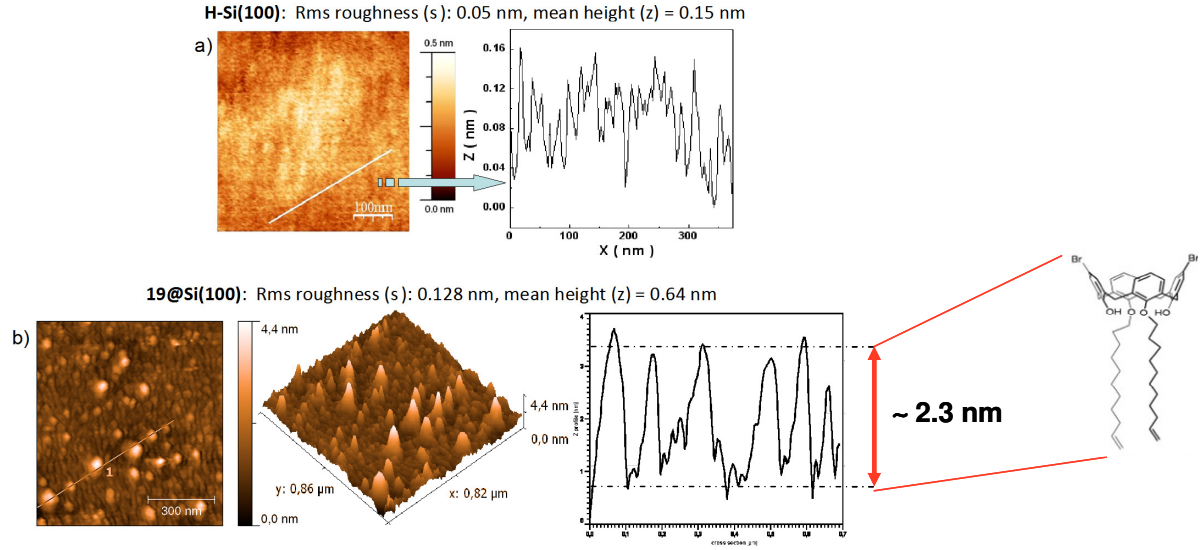

Figure 4.6 AFM images of the Si(100) surface a) before and b) after functionalization with calix[n]arene **19**.

In order to evaluate the coverage degree of the Si(100) surface, the uncovered plate and the one used for the functionalization with **19** were submitted to AFM measurements (see figure 4.6). The "blank" surface shows a low roughness with a mean height of 0.15 nm (see Figure 4.6a), while the covalent insertion of **19** increases both the roughness and the mean height in 0.128 and 0.64 nm, respectively. The picture of the latter covered surface (see Figure 4.6b) revealed the presence of "islands" of 2-2.5 nm high, which are consistent with the calix[4]arene units of **19** in a "standing up" conformation. The diameter of these structures (~30 nm) suggests that clusters of calixarene units are formed on Si.

8. This phenomenon was observed also by Fragalà et al. during the functionalization of Si(100) surfaces with resorcinarene derivatives, see Ref. 3.

Further AFM experiments will be conducted on Si surface functionalized with calix[6]arene 20.

4.2.2 Binding studies

As seen in the introduction, the main aim of this chapter is to study self-assembly processes between 2D and 3D SAMs properly functionalized with complementary host and guest compounds. To this aim, we initially tackled the problem to study the recognition processes at the solid-liquid interface using simpler models. We have designed to cover the Si(100) surface with a calix[n]arene host of proved recognition abilities using the functionalization conditions set up with **19** and **20**. Our choice was to use the heteroditopic calix[4]arene **21** functionalized at its lower rim with two ω-undecenyl" chains (see scheme 4.2). The structure of this compound is very similar to heteroditopic receptors **3** and **4** described in chapter 2 which have shown good recognition abilities toward *N*-alkylpyridinium ion pairs in low polar solvents

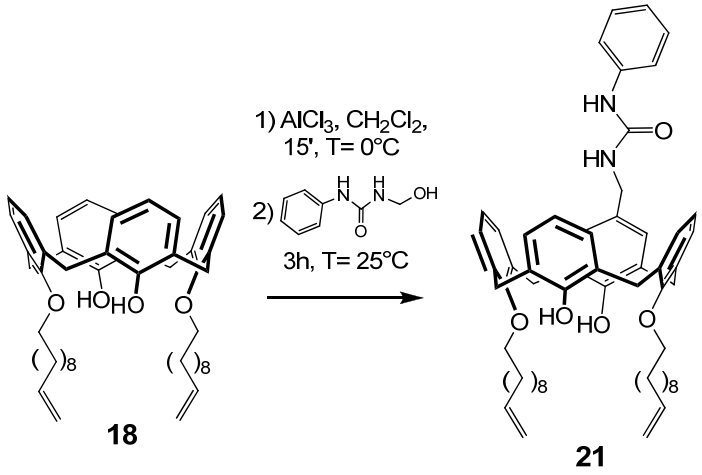

Scheme 4.2 Synthesis of **21**.

Compound **21** was synthetized through reaction of **18** with 1-(hydroxymethyl)-3-phenylurea (see experimental for details) in CH_2Cl_2 in the presence of $AlCl_3$ as catalysing agent. After purification by column chromatography, product **21** was isolated in 45% yield.

The ^1H NMR spectra in $CDCl_3$ of **21** (see figure 4.7) shows a complicated patter of signals due to the introduction on the upper rim of the phenylureido mojety that make not symmetric the whole macrocycle. As a consequence, the classic AX system of the bridging CH_2 protons is splitted and the not alkylated phenolic groups are visible as two singlets at 8.34 and 8.29 ppm. The insertion of methyl phenylureido group at the upper rim of the calixarene unit is easily recognisable for the corresponding signals falling in the aromatic region of the spectrum.

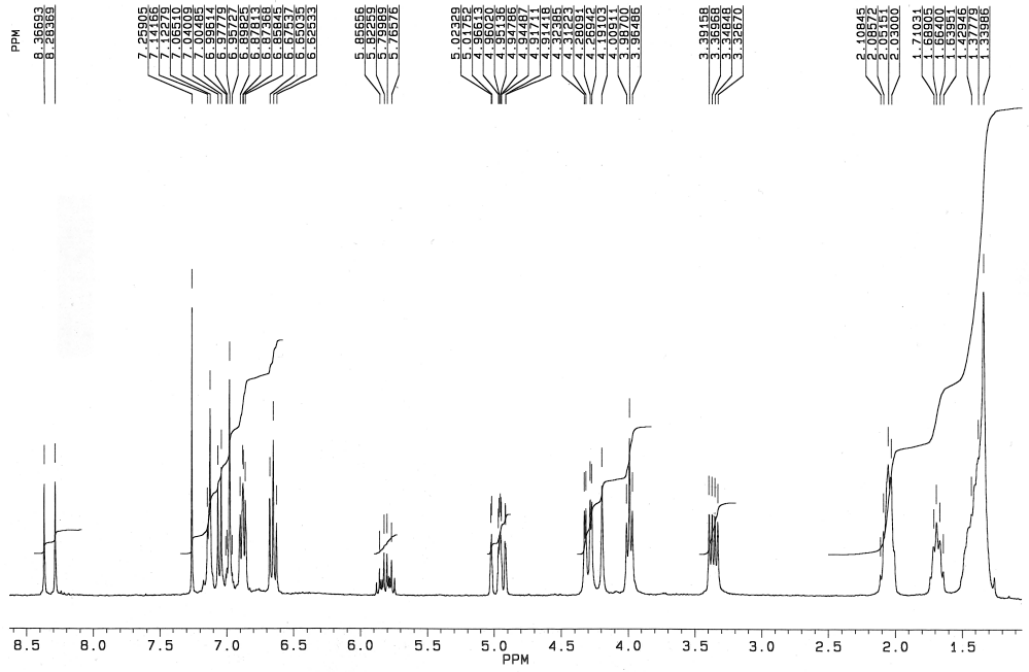

Figure 4.7 ^{1}H NMR spectrum of **21** in $CDCl_3$ (300 MHz).

The Si(100) surface functionalized with **21** was analyzed with XPS spectroscopy and then used for a binding study with *N*-methyl pyridium iodide (NMPI). The binding experiment was carried out by dipping the Si(100) functionalized plate in a chloroform solution containing NMPI. After extensive rinsing with dichloromethane and drying, the plate was submitted again to XPS analysis. In figure 4.8a it has been depicted the N 1s region of the XPS spectrum of the Si plate after the anchoring of **21**. The plate does not show any trace oxidized silicon. However, beside a large peak relative to the N atoms of the urea group (norm. BE = 403.3 eV), it is also present a smaller signal at lower BE (norm. BE = 401.1 eV). The normalized BE value of this signal (taking the BE of the C 1s signal as reference) was compatible with a positively charged nitrogen.[9] This result was quite unexpected because it could mean that **21** was already in a complexed form after its introduction on the Si surface. The calculated ratio between N(urea) and N+ was 7.4 (see entry 3 - Table 4.1), however the total absence of signals for iodine species supported the hypothesis that the origin of the N^+ signal is of adventitious ammonium salts taken from glassware. Unfortunately, several washings of the plate with different polar organic solvents did not improve this ratio.[10]

9. The Δ(N-C) values are in a good agreement with those present in literature for the same atom type F. Tao, M. H. Qiao, Z. H. Wang, G. Q. Xu, *J. Phys. Chem. B*, **2003**, *107*, 6384.
10. Water cannot be employed for the washing procedure because it promotes the oxidation of the Silicon surface not covered with the calixarene.

Table 4.1 Theoretical and XPS experimentally determined elemental ratios for the binding process between NMPI and Si (100) 2D SAM covered with **21**. (error ± 10%)

Entry	Designation	C/N[a]	NH/N+	N/I[a]	N+/I
1	**21**@Si (theor.)	29.0	-	-	-
2	**21**@Si + NMPI (theor)	21.3	2	3	1
3	**21**@Si (exp.) (a)	16.8	7.4	-	-
4	**21**@Si + NMPI (1st addition) (b)	28.5	4.8	44.5	7.6
5	**21**@Si (rinsed with MeOH) (c)	37.6	8.5	40.7	4.1
6	**21**@Si + NMPI (2nd addition) (d)	38.0	2.1	21.2	6.6

[a] Total amount of N species (NH and N^+)

The XPS spectrum of the Si plate recorded after its dipping in the chloroform solution of **21** (see Figure 4.8b and entry 4 - Table 4.1) shows an enhancement of the N+ signal. In the spectrum are also visible peaks relative to the presence of iodine species. The calculated N+/I ratio of 7.6 confirm the presence of ammonium species not originating from NMPI.

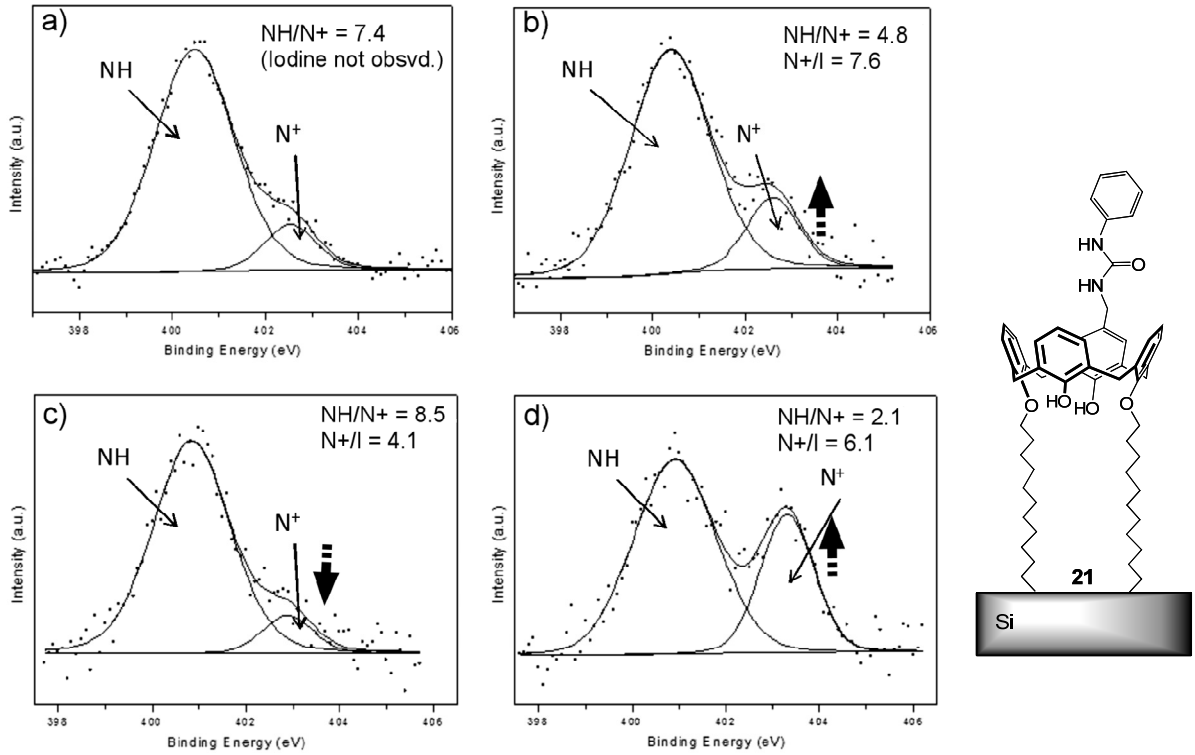

Figure 4.8. N 1s region of the XPS spectrum of a) the Si(100) surface functionalized with **21**; b) after complexation with NMPI; c) after rinsing with MeOH, and d) after 2nd treatment with NMPI. Binding energy in figures are not referenced to the signal of C 1s.

The following extensive rinsing with methanol is not effectively enough to remove all the ammonioum salts present on the surface either as complexed or physisorbed species. Nevertheless, the NH/N+ ratio slightly improved (8.5, see entry 5 – Table 4.1). The second

treatment of the plate with the NMPI solution finally determines a large enhancement of the N+ peak that is almost as large as the one of NH (NH/N+ = 2.1). In principle, this ratio is in perfect agreement with a 1:1 complexation between the cavity of **21** and NMPI. However, the corresponding N+/I ratio should be 1, instead of the calculated 6.6. This could mean that: a) the NH/N+ ratio is fortuitously 2 or more reasonably that b) the iodine present on the surface has been partially exchanged with other anions not evaluated (oxygenated anions are not visible by XPS). Further studies must be accomplished to totally disclose the effictiveness of these binding processes, even though this study represents a good starting point.

4.2.3 Calix[6]arene-based rotaxanes and pseudorotaxanes on Si(100) surface

In the recent years our research group has extensively used triphenylureido calix[6]arene derivatives as a "wheel" for the synthesis of rotaxanes and pseudorotaxanes[11] with axles based on 4,4'-bipyridinium salt which are known to have interesting redox properties[11b] (see paragraph 2.1.6). The possibility to transfer these achievements to silicon surfaces it is obviously enticing.[12] To this aim it becomes however necessary to introduce the proper anchoring points for the silicon surface in the structure of either the calix[6]arene "wheel "or the dialkyl viologen axle (see Figure 4.9).

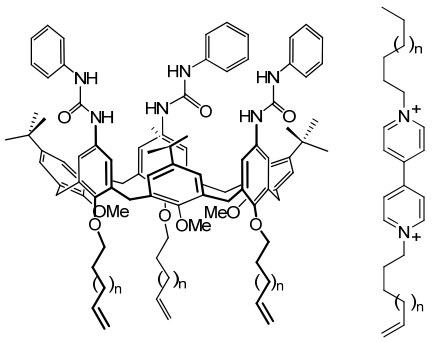

Figure 4.9 Calix[6]arene "wheel" and viologen-based "axle" for the functionalization of Si(100) surfaces.

As previously seen, ω-alkenyl chains represent good anchoring points for the Si(100) surfaces using the mild photoactivation procedure. However, the functionalization of the lower rim of the calix[6]arene wheel with ω-alkenyl chains is only apparently feasible owing to the compatibility problems between the insaturations of the alkyl chains and the series of

11. (a) A. Arduini, A. Credi, G. Faimani, C. Massera, A. Pochini, A. Secchi, M. Semeraro, S. Silvi, F. Ugozzoli, *Chem. Eur. J.*, **2008**, *14*, 98; (b) A. Credi, S. Dumas, S. Silvi, M. Venturi, A. Arduini, A. Pochini, A. Secchi, *J. Org. Chem.*, **2004**, *69*, 5881; (c) A. Arduini, F. Calzavacca, A. Pochini, A. Secchi, *Chem. Eur. J.*, **2003**, *9*, 793; (d) A. Arduini, R. Ferdani, A. Pochini, A. Secchi, F. Ugozzoli, *Angew. Chem. Int. Ed.*, **2000**, *39*, 3453.
12. For papers on rotaxanes structures anchored on inorganic surfaces see *e.g.*: (a) T. J. Hubin, D. H. Busch, *Coord. Chem. Rev.,* **2000**, *200-202*, 5; (b) A. R. Pease, J. O. Jeppesen, J. F. Stoddart, Y. Luo, C. P. Collier, J. R. Heath, *Acc. Chem. Res*., **2001**, 34, 433 and references therein.

reactions required for the introduction of the phenylurea groups on the upper rim of the macrocycle. The introduction of these insaturations on the alkyl chains of the viologen axle certainly requires less synthetic efforts and this strategy was thus adopted.

Synthesis of the viologen-based axle

We chosen to synthesize axle **24** that is characterized by redox-active bypridinium core alkylated with a pentyl and 10-undecenyl chains according to synthetic pathway described in scheme 4.3. Initially 4,4'-bipyridyl was refluxed in acetonitrile for 72h in the presence of a stoichiometric defect of 1-pentyl tosylate to afford the tosylate salt **23** in high yields. Successively, the viologen salt **24** was obtained in high yields by heating a solution of **23** in acetonitrile in the presence of an excess of undec-10-enyl 4-methylbenzenesulfonate (see experimental).

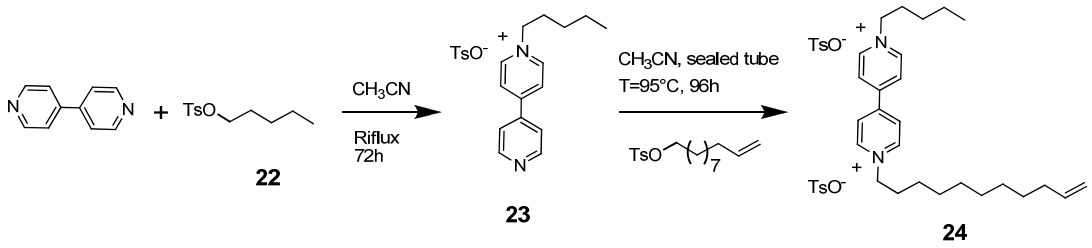

Scheme 4.3 Synthesis of the viologen based axle **24**.

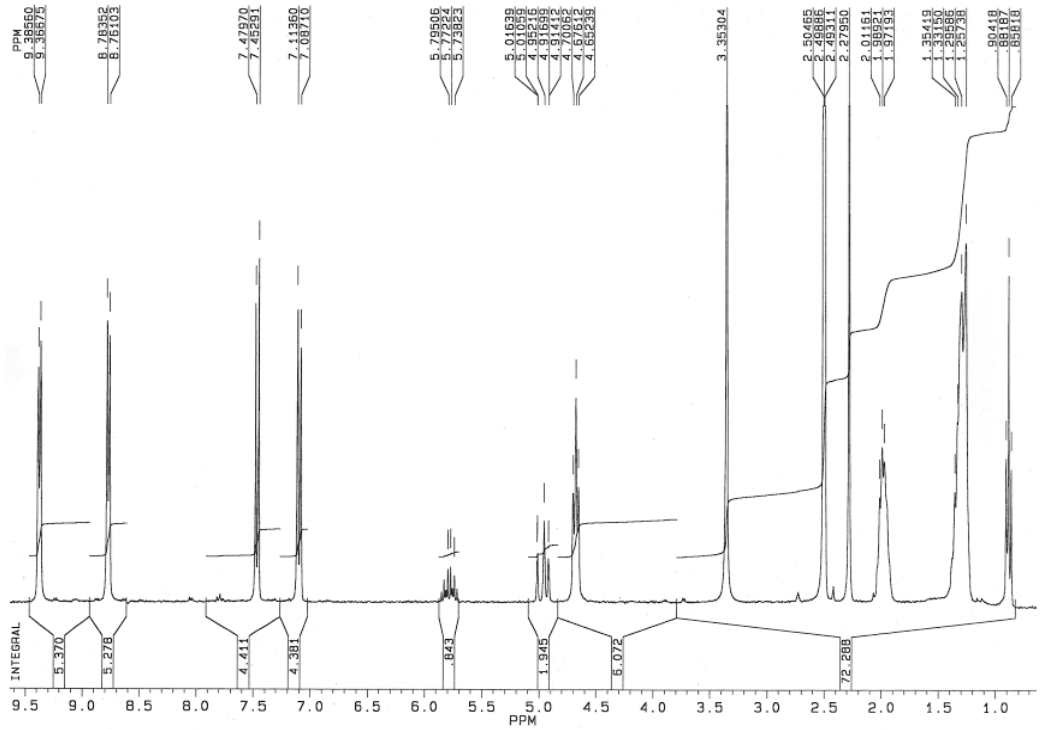

Figure 4.10 ^{1}H NMR spectra in 300MHz in DMSO-d_6 of axle **24**.

In the ^{1}H NMR spectrum of **24** in DMSO-d_6 (see figure 4.10) it is possible to observe the presence of several diagnostic signals: two doublets and one singlet at δ = 7.46, 7.10 and 2.28

ppm, respectively, corresponding to the two tosylate anions, and two doublets at δ = 9.38 and 8.77 ppm relative to the aromatic protons of the 4,4'-bipyridyl unit. The signals of the two CH_2 groups directly linked to the nitrogen atons are not distinguishable and visible as a unique triplet at δ = 4.67 ppm. The remnants CH_2 groups of the two alkyl chains give rise to a typical pattern of aliphatic signals of long alkyl chains. The ω-insaturation generates a typical pattern of multiplet signals at δ = 5.8-5.7 and 5.0-4.8 ppm

Functionalization of the Si(100) surface

The insertion of the pseudorotaxane system on the silicon surface was carried out using a simple strategy: a) dip coating of a silicon plate in a toluene solution containing equimolar amounts of axle **24** and triphenylureido-calix[6]arene **25**; b) irradiation of the system; c) extensive rinsing of the irradiated silicon plate with low polar solvents in order to remove all the material not covalently attached on the surface. Calix[6]arene **25** (see Figure 4.11) was chosen as the "wheel" because it has been extensively verified that **25** gives rise to the formation of stable pseudorotaxanes in apolar solvents (log$K$ > 6) with axles similar to **24**.[11]

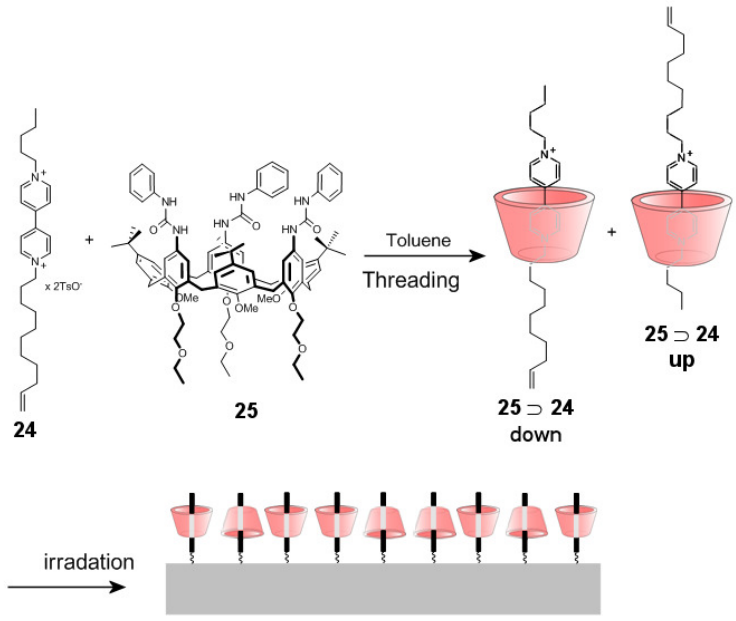

Figure 4.11 Synthesis of two isomers of the pseudorotaxane **25** ⊃ **24** and its anchoring on Si(100) surface

As described in 2.1.6, the lacking of control elements (stoppers) in the axle **24** generates the formation of a mixture of two pseudorotaxane isomers because the threading process can occur indifferently from both rims of the macrocycle. The two isomers (up and down, figure 4.11) differ for the relative position of the asymmetric axle **24** inside the asymmetric aromatic cavity of **25** which bears on its rims different substituents (see Figure 4.11).

XPS and electrochemical studies of the functionalized Si(100) surface.

The results of the XPS analysis carried out on the functionalized silicon surface were summarized in table 4.2 and in figure 4.12.

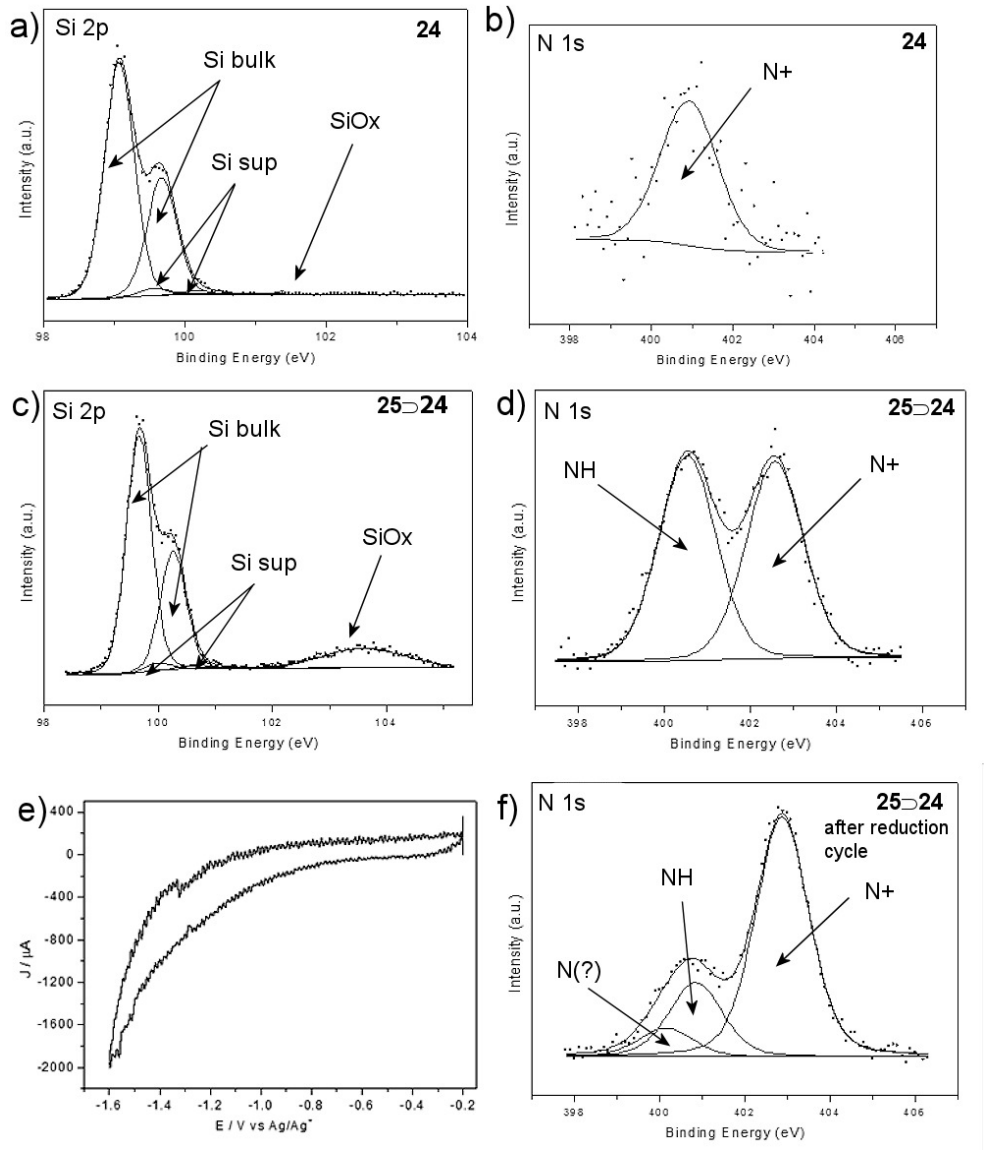

Figure 4.12 XPS spectral regions for **24**@Si: a) Si 2p and b) N 1s. XPS spectral region for **25⊃24**@Si: c) Si 2p and d) N 1s. e) Cyclic voltammetric curve of **25⊃24**@Si surface (scan rate, 200 mV/s, Ag/Ag^+ electrode used as reference) and f) N 1s XPS spectral region of the **25⊃24**@Si surface after the voltammetric cycle. Binding energy in figures are not referenced to BE of C 1s.

For comparison also a Si plate functionalized with axle **24** was analysed. The XPS spectral region relative to Si 2p shows that, after functionalization, the Si(100) surface does not present a relevant amount of oxidized silicon. (See Figures 4.12a and 4.12c, BE in figure are not referenced to the signal of C 1s of calixarene). The analysis of the N 1s region offers more interesting results: the surface functionalized with **24** (**24**@Si) gives rise to a unique signal with a binding energy (BE) typical for charged nitrogen (N+) species (see Figure

4.12b),[13] while the surface covered with the pseudorotaxanes (**25**⊃**24**@Si) presents two signals which were assigned to the NH of the urea groups (lower BE) and to the N+ of the bypyridinium unit (higher BE) (see Figure 4.12d).

Table 4.2 Theoretical and experimental elemental ratios of Si(100) surfaces functionalized with axle (**24**@Si) and with the mixture of pseudorotaxanes (**25**⊃**24**@Si) as determined by XPS spectroscopy (error ± 10%)

Entry	Designation	C/N (theor)	C/N (exp)	NH/N+ (theor)	NH/N+ (exp)
1	**24**@Si	20	22	-	-
2	**25**⊃**24**@Si	14.5	16.2	3	1
3	**25**⊃**24**@Si after reduction	20	14.9	-	0.3

The NH/N+ elemental ratio of ~1 (see table 4.2, entry 2) determined for **25**⊃**24**@Si evidences that this surface is still covered with a considerable amount of uncomplexed axle **24** since the expected ratio should be 3. This result could imply that: a) the anchoring reaction is faster than the threading process occurring in solution between the calixarene **25** and **24**, b) during the irradiation process the temperature of the toluene solution containing the pseudorotaxanes increases up to ~50 °C.

In a previous study we have demonstrated the possibility to electrochemically switch the threading-dethreading process of viologen-calix[6]arene based pseudorotaxane systems in solution of CH_2Cl_2.[11b] In particular, this study was conducted using cyclic voltammetry (see Figure 4.13) and revealed that the free axle (Figure 4.13a) shows two monoelectronic and reversible reduction processes ($E_{1/2}$ = -0.29 V, $E_{1/2}$ = -0.81 V vs SCE) characteristic of the viologen unit; the complexed axle shows instead a shift of the first reduction potential to more negative values, while the second potential remains equal to the one of the free axle. This confirmed that axle dethreading occurs after the first reduction event.

13. The experimental values of the BE of the N 1s signal were corrected as usual taking into account the value of the carbon taken as reference. The corrected values are in agreement with the reported literature data relative to charged N 1s species, see: (a) S.M. Mendoza, J. Berná, E.M. Pérez, E.R. Kay, A. Mateo-Alonso, C. De Nadaï, S. Zhang, J. Baggerman, P.G. Wiering, D.A. Leigh, M. Prato, A.M. Brouwer, P. Rudolf, *J. Electron .Spectrosc.,* **2008**, *165*, 42; (b) S. M. Mendoza, C. M. Whelan, J. P. Jalkanen, F. Zerbetto, F. G. Gatti, E. R. Kay, D. A. Leigh, M. Lubomska, P. Rudolf, *J. Chem. Phys.*, **2005**, *123*, 244708, (c) H. Suga, E. Koyama, H. Tokuhisa, K. Fujiwara, Y. Nagawa, T. Nakamura, Y. Nishioka, M. Kanesato, W. Mizutani, T. Ishida, *Surf. Sci.*, **2007**, *601*, 68.

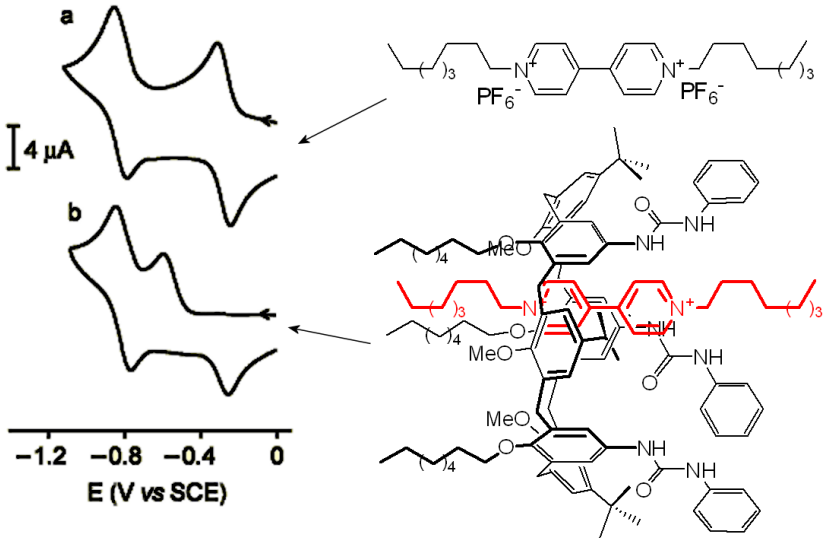

Figure 4.13 Cyclic voltammetric curves for the first and second reduction of the viologen unit in a) dioctyl violgen and in b) the pseudorotaxane formed between a trioctyltriphenylureido calix[6]arene and dioctyl viologen ($TBAPF_6$, 293 K; scan rate 0.2V/s, CH_2Cl_2).

Starting from these interesting results we did few attempts to study the threading-dethreading process of the **25⊃24**@Si surface using cyclic voltammetry techniques. This study was carried out to demonstrate the feasibility and reseversibily of the threading process also at the solid-liquid interface. However, differently from the studies in solution, this electrochemical experiment requires the use of the functionalized silicon surface (plate) as one of the electrodes and the current involved in the processes at the interface are sensibily lower than those recorded in homogeneous solution.

The cyclic voltammogram reported in Figure 4.12e is characterized by a very low signal to noise ratio that prevents the identification of possible reduction potentials of the viologen unit. Despite this disappointing result, we analyzed through XPS spectroscopy the silicon plate after the reduction cycle experiment (see Figure 4.12f). The N 1s spectral region evidences a clear decrease of the peak corresponding to the NH species. Indeed, NH/N^+ quantitative ratio decreases from 1 to 0.3 (see Table 4.2). The N 1s region of the XPS spectrum shows, after deconvolution, also the presence of a weak signal at lower BE. Even though the nature of this peak has not been assigned yet, it is reasonable to assume it originates from reduced nitrogen species deriving from either the reduced axle or reduced wheel. All the results obtained in this work are preliminary and more studies are in progress to disclose and improve these kind of systems.

4.3 Calix[n]arene-based polycrystalline Cu 2D SAMs

4.3.1 Functionalization and characterization of polycrystalline Cu surface

Copper is a red coloured metal with good electrical and termal conductivity properties. The main part of the recent studies on copper 2D and 3D SAM is related to its possible use in microelectronics. Owing to its low electrical resistivity and high electromigration resistance copper represents indeed the most important conducting metal used for conductor path and interconnection in microcircuits.[14] The introduction of calix[n]arenes on polycrystalline copper surfaces requires the functionalization of the calixarene macrocycle with appropriate "anchoring points". The high affinity of sulphur for copper has been largely documented,[15] therefore we chosen calix[n]arene derivatives **10b**, **17** and **27**, that are characterized by the presence of two or three ω-thiolated chains on their lower rim, for the functionalization of the surface of polycrystalline copper (see figure 4.14).

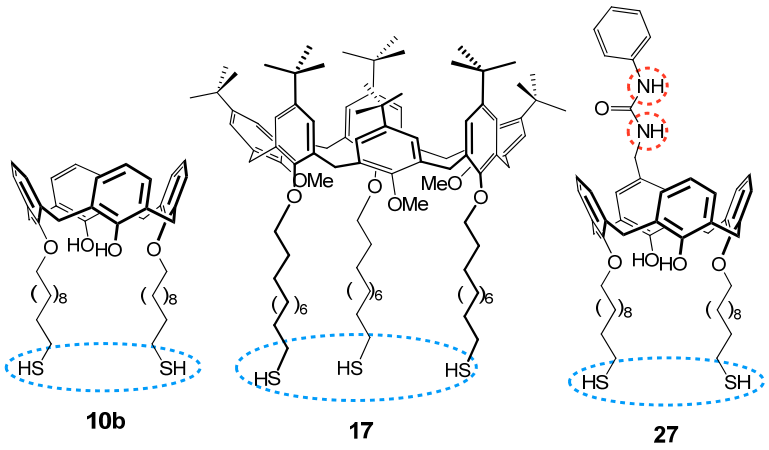

Figure 4.14 Calix[n]arenes used for the functionalization of polycrystalline copper surface.

The synthesis of calixarenes **10b** and **17** and their properties as protecting ligands of gold nanoclusters have been already described in Chapter 3. The heteroditopic calix[4]arene **27** has been synthesized following the procedure described in scheme 4.4. The insertion of the methyl phenylureido group on the calix[4]arene upper rim was accomplished for regiochemical problems on the thiol-protected derivative **9b** using *N*-methylolphenylurea as alkylating agent and $AlCl_3$ as the catalyst. After chromatographic purification compound **26** was obtained in good yields (80%). Compound **26** was characterized using NMR and mass

14. See e. g. : (a) T. Y. Dong, H. H. Wu, C. Huang, J. M. Song, I.G. Chen, T. H. Kao, *Appl. Surf. Sci.* **2009**, *255*, 3891;(b) K. Woo, D. Kim, J. S. Kim, S. Lim, J. Moon, *Langmuir* **2009**, *25*,429 and references therein.
15. H. Sellers, A. Ulman, Y. Shnidman, J. E. Eilers, *J. Am. Chem. Soc.*, **1993**, *115*, 9389.

spectroscopy (see experimental). The ^{1}H NMR spectrum of **26**, taken in $CDCl_3$, has been depicted in Figure 4.15.

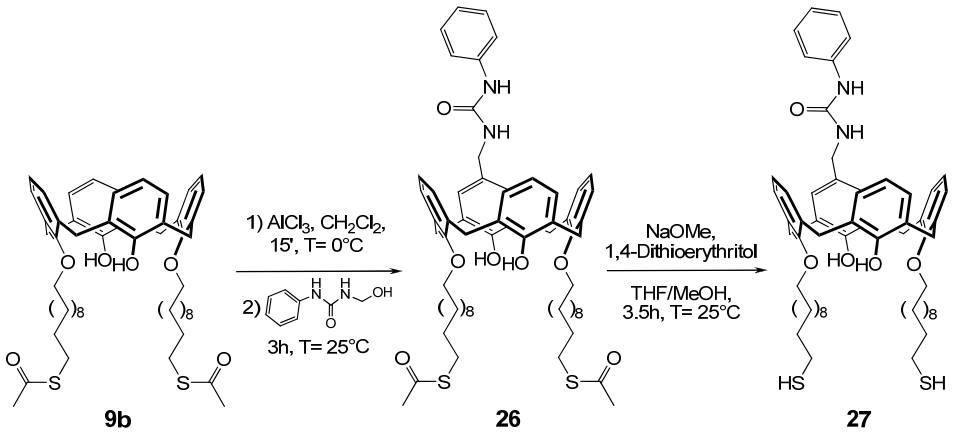

Scheme 4.4. Synthesis of thiolated heteroditopic calix[4]arene derivative **27**.

The spectrum of **26** shows two singlets at δ = 8.31 and 8.23 ppm in 1:1 ratio that are diagnostic for the two unsubstituted OH groups. The complicated pattern of the aromatic signals reflects the presence in the compound of three types of aromatic rings, in ratio 1:2:1, having different magnetic environment. The protons of the bridging methylene groups give rise to a typical pattern of signals for a not symmetric calix[4]arene derivative.

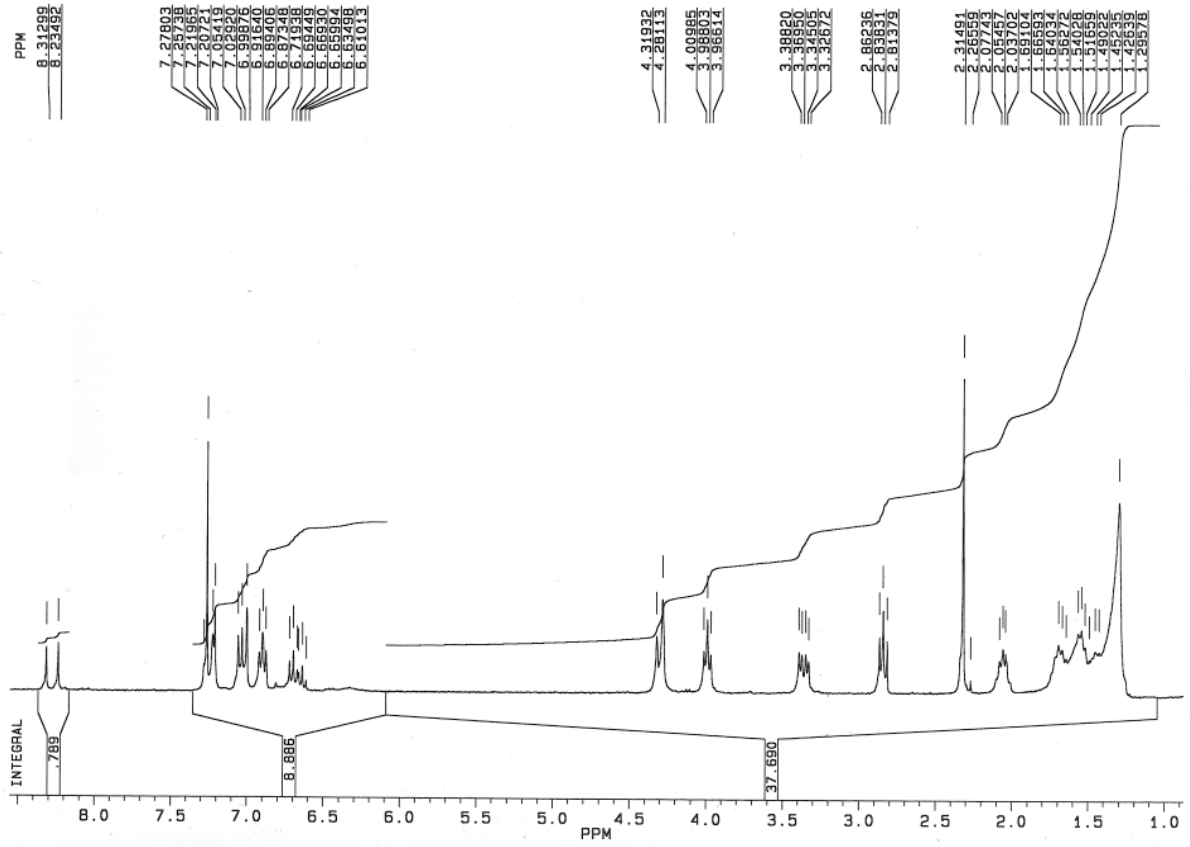

Figure 4.15 ^{1}H NMR spectrum of **26** in $CDCl_3$ (300 MHz).

Diagnostic for the presence of the methyl phenylureido group is the singlet at δ = 4.28 ppm overlapped with the doublet of the axial protons. This singlet is relative to the protons of the CH_2 group linking the phenylurea moiety to one calixarene aromatic ring. The presence of a triplet at δ = 2.83 ppm (CH_2-S, protons) and a singlet at δ = 2.31 ppm ($SCOCH_3$ protons) demonstrates that $AlCl_3$ catalyst did not affect the thioacetic protecting group.

In the following step, the thioacetic groups of **26** were removed using NaOMe in the presence of 1,4-dithioerythritol at room temperature in a 1:1 THF/MeOH, followed by quenching with Dowex-H^+. The 1,4-dithioerythritol is necessary to maintain in the reduced state the unprotected SH groups of the alkyl chains. After chromatographic purification, compound **27** was obtained in 70% yield. The compound was characterized using NMR and mass spectroscopy. The ^{1}H NMR spectrum of **27**, taken in $CDCl_3$, has been depicted in figure 4.16. It shows diagnostic signal of the deprotected product is the presence of a multiplet relative to methylenic protons near SH functionality centered at 2.51 ppm, and the presence of the tipical signal pattern of the ureidic unit.

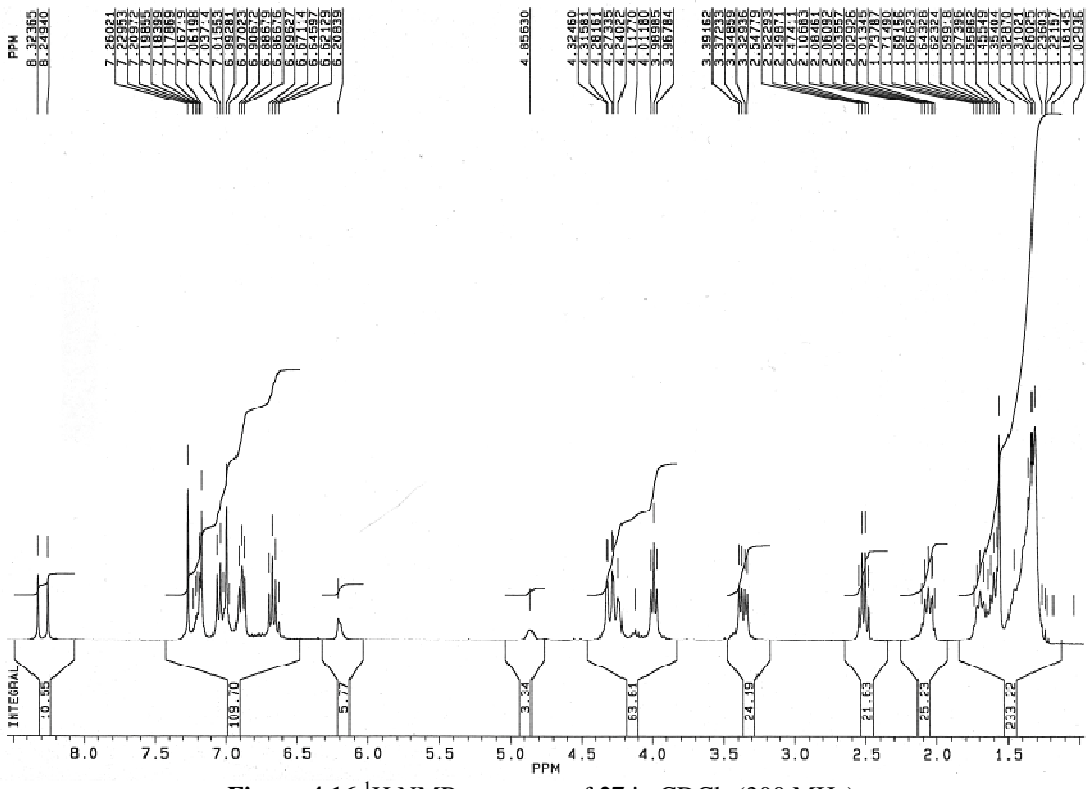

Figure 4.16 ^{1}H NMR spectrum of **27** in $CDCl_3$ (300 MHz).

Functionalization and characterization of the polycrystalline copper surface

The functionalization of the polycrystalline copper surface was carried out using a dip-coating procedure. Cleaned plates of polycrystalline copper were dipped for at least 4 hours in solutions of the calix[n]arene derivatives **10b**, **17** and **27** in toluene (see experimental for

details). After rinsing and drying procedures, the plates were submmitted to XPS analysis in order to evaluate the effective covalent anchoring of the calixarene derivatives on the copper surface. The results of the analysis carried out on the surfaces functionalized with calix[n]arenes **10b** (**10b**@Cu), **17** (**17**@Cu) and **27** (27@Cu) are depicted in figures 4.17 - 4.19. For reference, the XPS analysis was also accomplished on a polycrystalline copper surface covered with *n*-undecanthiol chains (C11S@Cu).

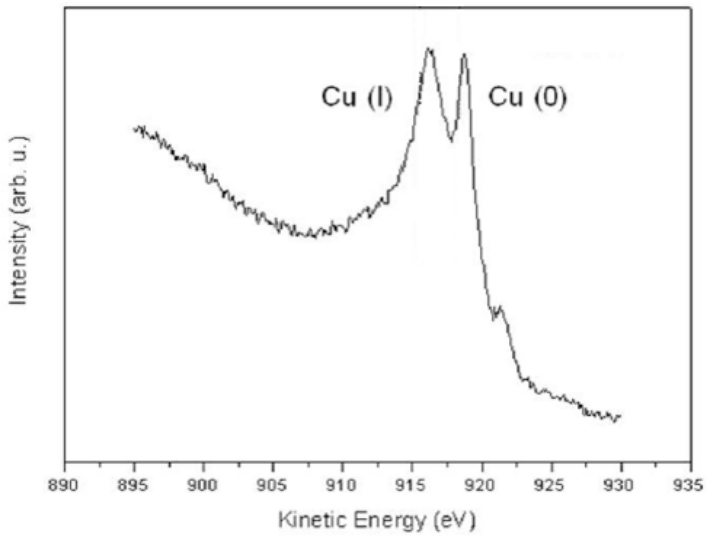

Figure 4.17 Cu 2p XPS spectra (not deconvoluted) of polycrystalline copper surface **10b**@Cu.

In Figure 4.17 it has been depicted the Cu 2p XPS spectral region originating from the **10b**@Cu surface. Two signals associated with Cu(I) and Cu(0) species are easily recognized, while no peaks attributable to traces of Cu(II) are found. The **17**@Cu and **27**@Cu surfaces afforded very similar patterns of signals. The lack of signals due to Cu(II) species indirectly confirmed the formation of the 2D SAM, since it has been reported that organic layer covalently attached on a copper surface effectively prevents its oxidation.[16]

The S 2p XPS spectral region evidences, after peak deconvolution, the presence of two types of sulphur species on the **10b**@Cu (Figure 4.18b), **17**@Cu (Figure 4.18c) and **27**@Cu (Figure 4.19c) surfaces. Two weak peaks at higher BE (~163 and 165 eV, not normalized) were assigned to sulphur atoms in free thiol groups, while the two very intense peaks at lower BE (~162 and 163.5 eV, not normalized) were assigned to sulphur atoms involved in S-Cu bonding. The C11S@Cu surface afforded a result very similar (see Figure 4.18a). These findings suggest that only negligible amounts of free thiolated calixarene are physisorbed on the copper surface.

16. P. E. Laibinis, G. M. Whitesides, *J. Am. Chem. Soc.*, **1992**, *114*, 9022.

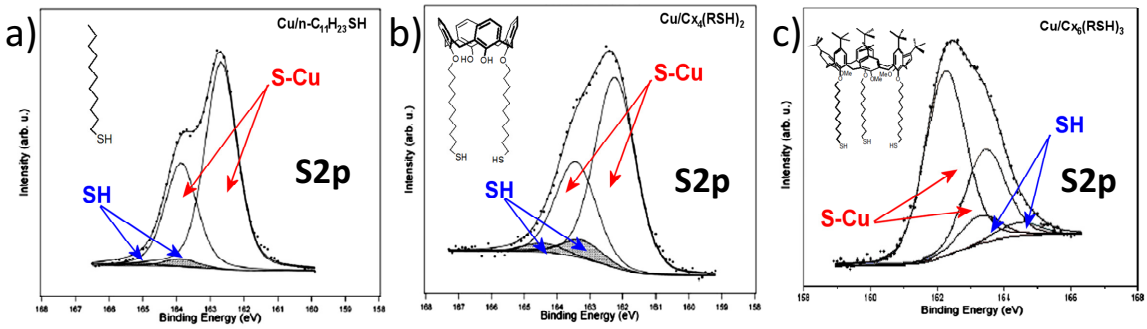

Figure 4.18 S 2p XPS spectral region of a) C11S@Cu, b) **10b**@Cu and c) **17**@Cu copper surfaces. The BE energy in figure are not referenced to the signal of C 1s of calixarene unit.

Other evidences for the covalent anchoring of the thiolated calixarene derivatives were obtained by evaluating the C/S and S/Cu elemental ratios calculated from the relative abundance of the peaks present in the XPS spectra of **10b**@Cu and **17**@Cu. For **27**@Cu, the C/N ratio was taken into account. The analysis of the C/S ratios (see table 4.3) reveals a good agreement between the theoretical and experimentally determined values. The S/Cu ratios calculated for surfaces **10b**@Cu and **17**@Cu (0.45 and 0.47, respectively) are slightly lower than the value determined for the C11S@Cu surface (0.51). This result suggests that the covering degree induced by the thiolated alkyl chains of calixarene derivatives is comparable with that of the less sterically demanding *n*-$C_{11}H_{23}SH$.

Table 4.3 Elemental ratios of Cu surfaces functionalized with calix[n]arenes **10b** (**10b**@Cu), **17** (**17**@Cu), **27** (**17**@Cu), and *n*-undecanthiol (C11S@Cu) as determined by XPS spectroscopy (error ± 10%)

Entry	Designation	S/Cu[a]	C/S (exp)	C/S (theor)	C/N (exp)	C/N (theor)	NH/N+ (exp)	NH/N+ (theor)
1	$C_{11}S$@Cu	0.51	12	12				
2	**10b**@Cu	0.45	28	25				
3	**17**@Cu	0.47	34	34				
4	**27**@Cu				27	29		
5	**27**@Cu + NMPI				24	21	2.6	2

[a] S is the sulphur species covalently linked to the copper surface.

4.3.2 Binding studies

The **27**@Cu copper surface was employed to obtain preliminary results on the binding processes occurring at the liquid-solid interface between the heteroditopic calix[4]arene host **27** and *N*-methyl pyridium iodide (NMPI) ion pairs. Similarly to the experiment carried with the Si(100) surface loaded with the same host, the copper plate was analyzed by XPS spectroscopy before and after its dipping in the chloroform solution of the guest.

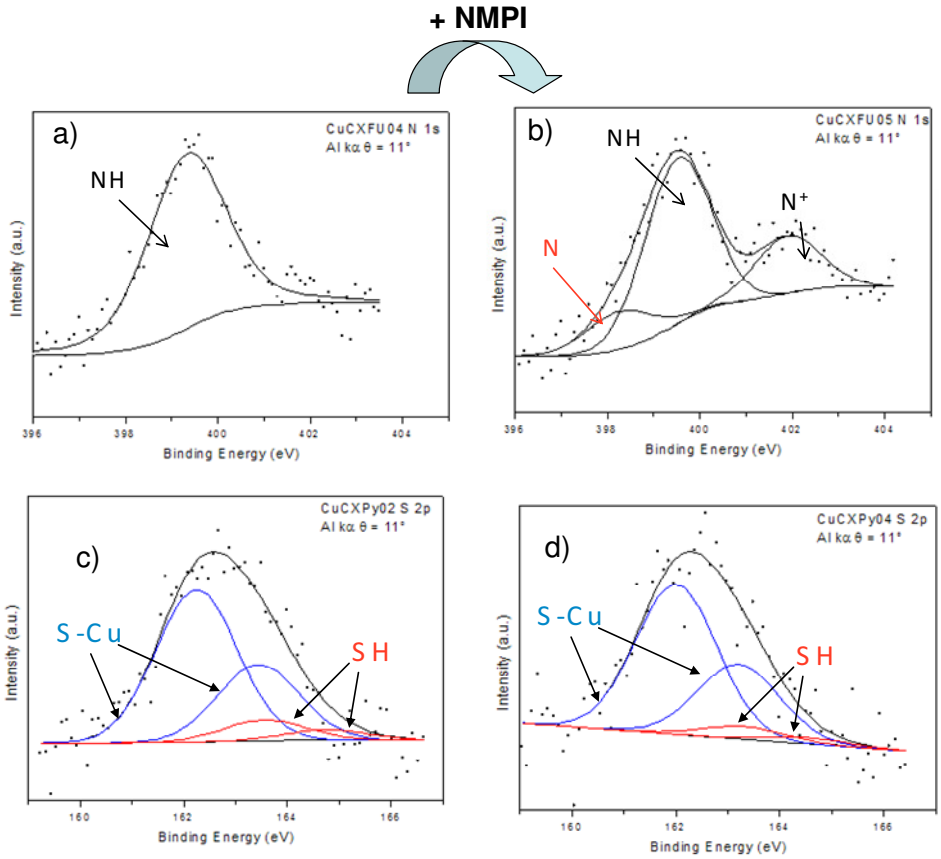

Figure 4.19 a) S 2p and b) N 1s XPS spectral regions of polycrystalline copper surface functionalized with calix[4]arene **27**. Spectra c) and d) depict the same regions after complexation of the **27**@Cu surface with NMPI. Binding energies are not normalized.

In Figure 4.19a it has been reported the N 1s XPS spectral region of the uncomplexed **27**@Cu surface. Only one signal is visible and its BE is compatible, as expected, with a nitrogen atom relative to a urea groups (NH). After the contact of the guest solution with **27**@Cu, more signals become visible in the same spectral region: a rather intense signal at higher BE (~402 eV, not normalized) is reasonably assignable to the nitrogen (N+) of the pyridinium cation interacting with the calix[4]arene cavity. The nature of the new weak signal present at lower BE (~398 eV, not normalized) with respect the signal of the NH has not been fully disclosed yet. Nevertheless, the appearance of this signal after the binding event and its high BE could be associated with more "negative" nitrogen species generated upon binding through the formation of strong hydrogen bonds between the NHs and the iodide ions. It should also be observed that the value of the NH/N+ ratio experimentally determined (2.6, see Table 4.3) is in good agreement with the theoretical value of 2 calculated considering the formation of a 1:1 complex between **27** and NMPI. These findings thus show the feasibility of XPS spectroscopy as monitoring technique of the complexation process occurring at the solid-liquid interface.

4.3.3 Calix[6]arene-based rotaxanes and pseudorotaxanes on Cu surface

Following the strategy adopted in paragraph 4.2.3 for the functionalization of Si(100) surfaces with viologen-calix[6]arene based pseudorotaxanes, we designed and used a monostoppered axle **31** and a not stoppered axle **33** (see figure 4.20) for the formation of pseudorotaxanes by threading reactions with the calix[6]arene "wheel" **25** (see Figure 4.23). Thanks to the thiol groups present on one ending of the axles, the respective pseudorotaxanes can be covalently anchored on the polycrystalline copper surface.

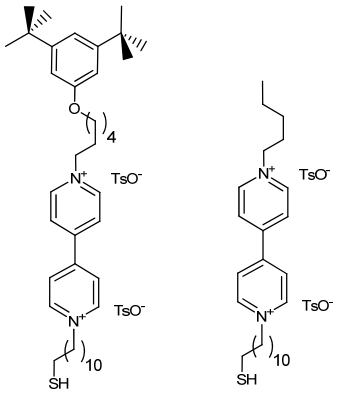

Figure 4.20 Viologen based axles **31**, **33**.

Synthesis of the viologen-based axle

The synthesis of the axles **31** and **33** is depicted in scheme 4.5. For the synthesis of axle **31**, compound **28** was prepared in 85% yield by refluxing 3,5-di-*tert*-butylphenol and 1,6-bis(toluene-4-sulfonyloxy)hexane in acetonitrile in the presence of K_2CO_3 as base. Successively, 4,4'-bipyridyl was refluxed with compound **28** in acetonitrile to obtain **29** in 65% yield after precipitation of the pure compound from ethyl acetate. After this step, compound **29** was reacted with S-11-(tosyloxy)undecyl ethanethioate **8** (already described in chapter 3) in acetonitrile to afford **30** in 50% yield. Finally the removing of the acetic protection group from the thiolic functionality was accomplished by refluxing **30** in ethanol in the presence of *p*-toluensulfonic acid. Pure **31**, was obtained in 70% yield after precipitation from ethyl acetate.

The ^1H NMR in $CDCl_3$ at 300MHz of **31** (see Figure 4.21) shows all the characteristic signals of an asymmetric 4,4'-bipyridinium compound. At δ = 9.19 and 8.79 ppm is possible to see the signals of the bipyridinium unit, in particular the peak at δ = 9.19 is not a doublet but a more complicated signals due to the asymmetry of compound **31**. The signals of the stoppers are visible at δ = 6.99 and 6.71 ppm. Diagnostic is also the presence of the multiplet at δ = 2.59 ppm due to the CH_2 in α position with respect to the thiol group.

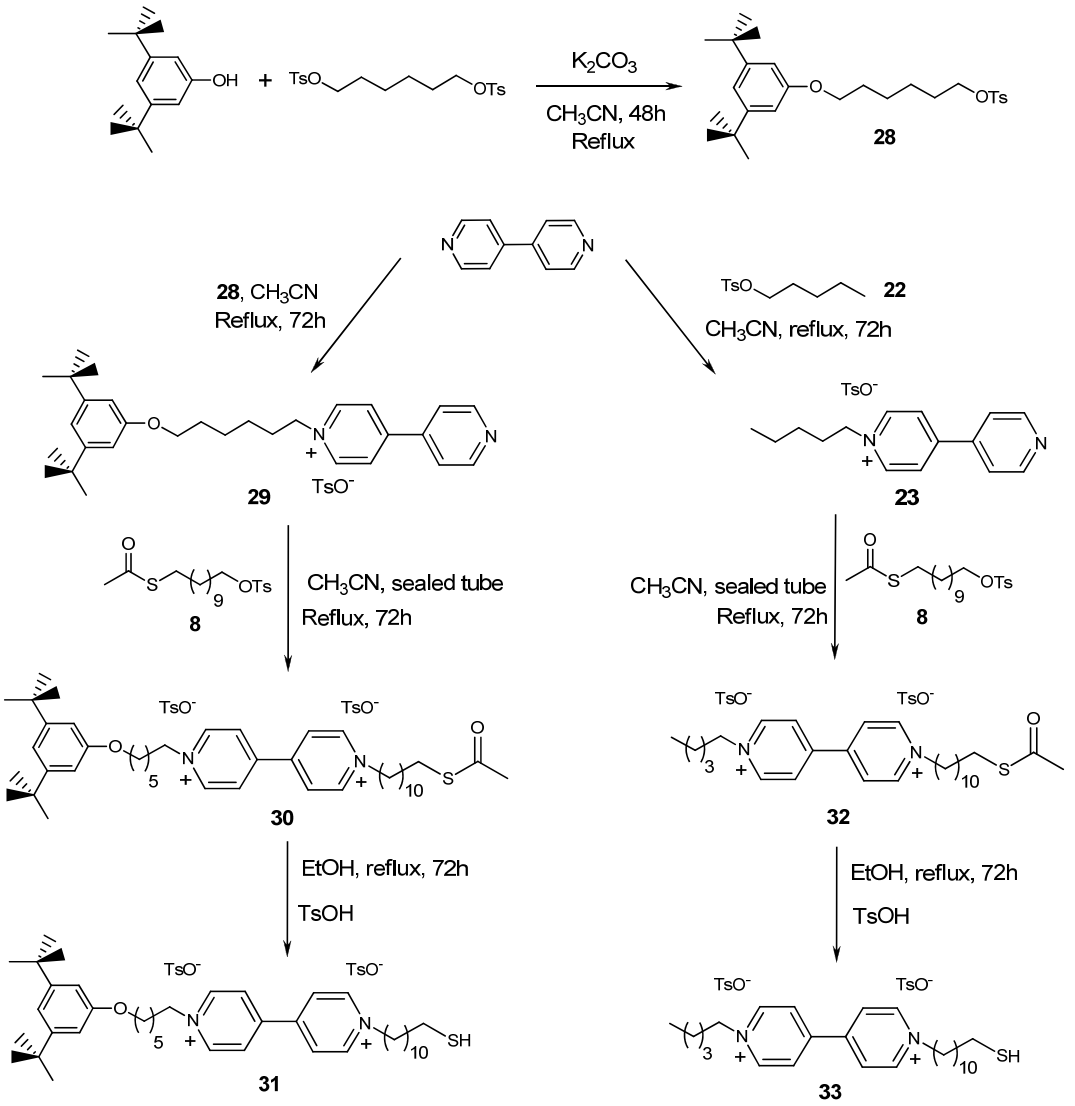

Scheme 4.5 Synthesis of the viologen based axles **31** and **33**.

Axle **33** was synthesized with a similar synthetic pathway used to synthesize **31** (see Scheme 4.5). Initially, 4,4'-bipyridyl was refluxed with 1-pentyl tosylate to afford the monoalkylated bipyridine **23** in 75% yield. Successively, **23** was reacted in a sealed tube with **8** using acetonitrile as solvent. After cooling, **32** crystallizes as pure product with 65% yield. As last step, the deprotection of thiol functionality was accomplished by refluxing **32** in ethanol in presence of *p*-toluenesulfonic acid. After precipitation from ethyl acetate, **33** was obtain as pure product in 65% yield.

Its ^{1}H NMR in $CDCl_3$ at 300MHz (see Figure 4.22) shows all the characteristic signals of a dialkylated viologen salt. At δ = 9.19 and 8.85 ppm is possible to see the signals of the bipyridinium unit and at δ = 7.74, 7.16 and 2.33 ppm are present the signals of protons attributable to tosilate anions. Diagnostic is the presence of the typical multiplet at δ = 2.52 ppm relative to the CH_2 in α position with respect to the SH group.

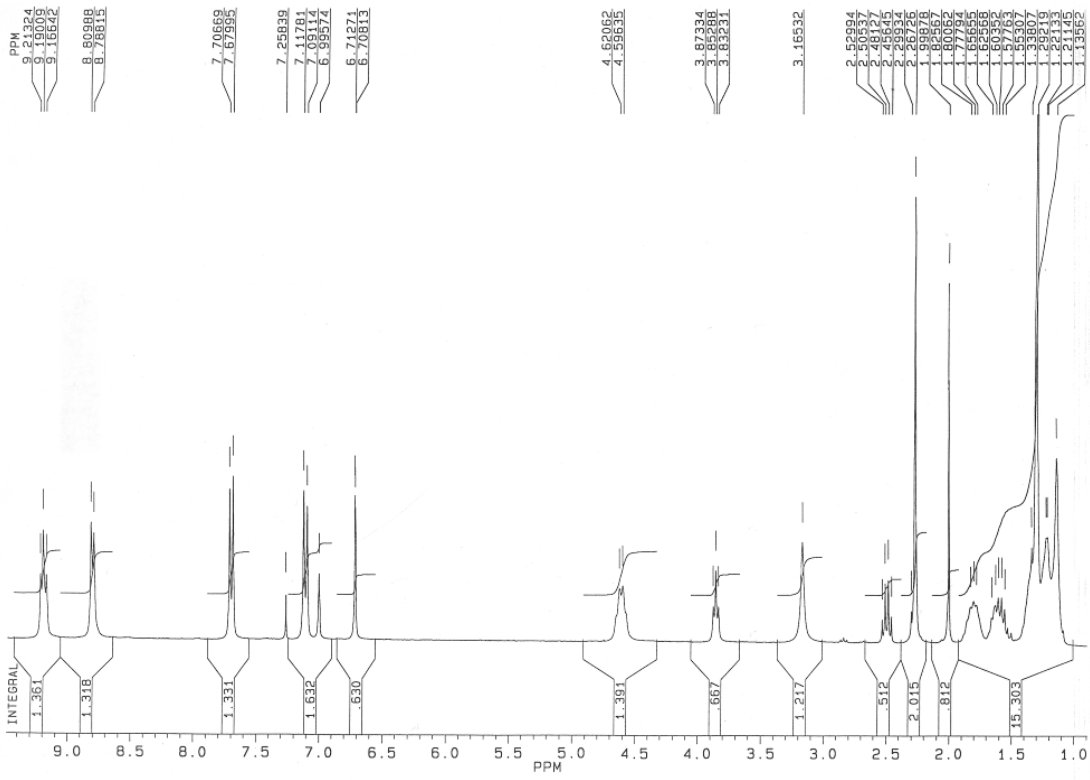

Figure 4.21 ^{1}H-NMR spectra in $CDCl_3$ at 300MHz of compound **31**.

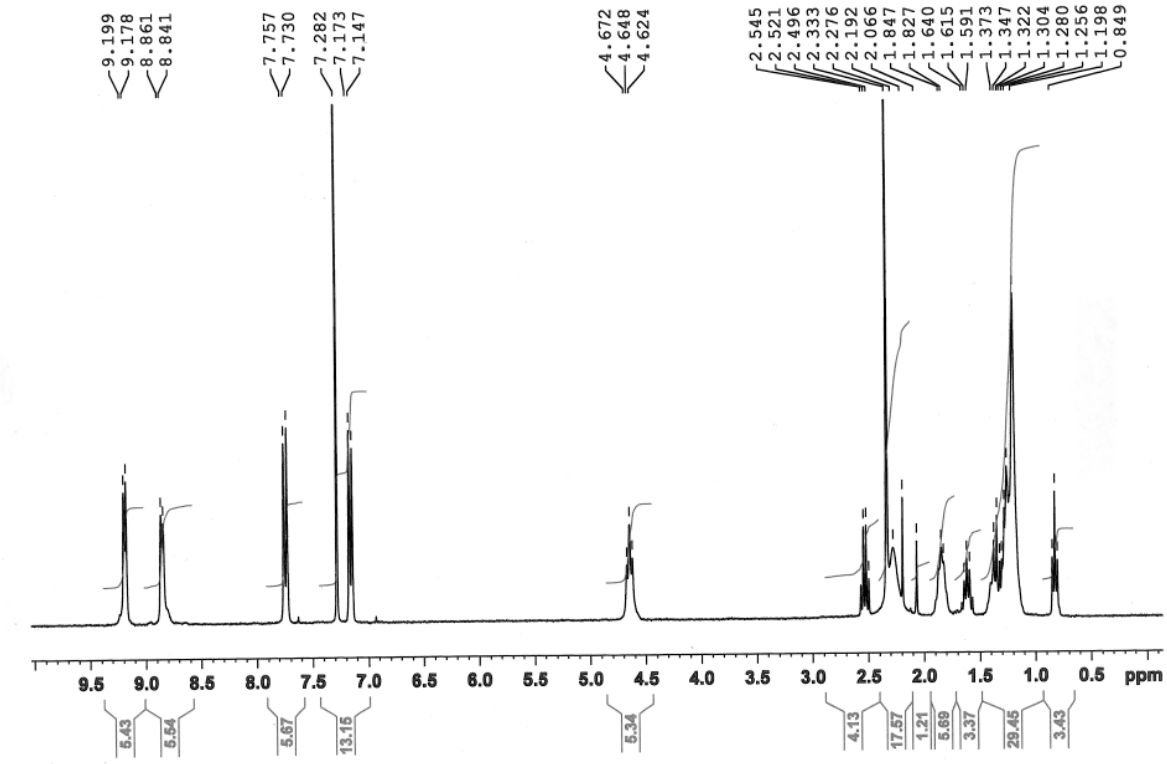

Figure 4.22 ^{1}H-NMR spectra in $CDCl_3$ at 300MHz of compound **33**.

Functionalization and characterization of the Cu surface functionalized with pseudorotaxanes

As reported for the functionalization of the Si(100) surfaces, the pseudorotaxanes were preformed in toluene solution and then anchored on the Cu surface through a dip-coating method (see figure 4.23). Using the "monostoppered" axle **31** and the wheel **25** the "oriented" pseudorotaxane **25⊃31** was obtained thanks to a selective threading process that, in low polar solvents, always occurs from the upper rim of the calix[6]arene with the axle having its stopper oriented above the cavity.[11] Using the not stoppered axle **33**, a mixture of the two isomers of pseudorotaxane **25⊃33** (up and down) was obtained.

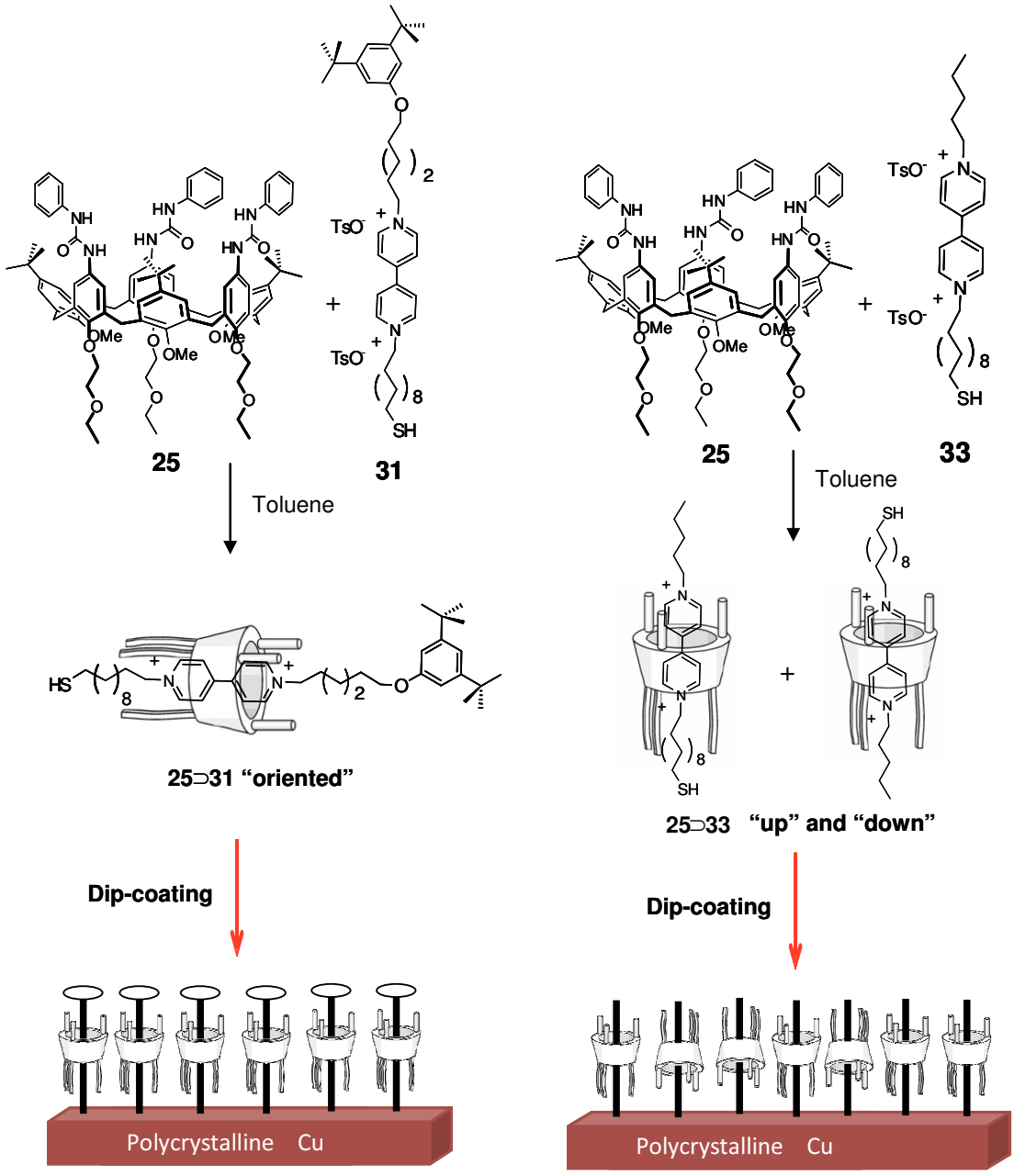

Figure 4.23 Synthesis of pseudorotaxane **25⊃31** and **25⊃33** and their covalent anchoring on the polycrystalline copper surface through dip-coating procedure.

The oriented pseudorotaxane **25⊃31** and the mixture of the two isomers **25⊃33** were used for the functionalization of the polycrystalline copper surface using the same dip-coating procedure adopted for the anchoring of thiolated calix[n]arene derivatives (see previous paragraph). After the coating, the two copper surfaces functionalized with pseudorotaxanes **25⊃31** (**25⊃31**@Cu) and **25⊃33** (**25⊃33**@Cu) were analyzed through XPS spectroscopy and the experimental results are depicted in figures 4.24 and 4.25 respectively.

In Figure 4.24a it has been depicted the XPS S 2p spectral region of the **25⊃31**@Cu surface. Two large S 2p signals are visible. After deconvolution the low BE signal is splitted in two pairs of peaks (blue and red lines in Figure 4.24a). The "blue" components, at lower BE, correspond to sulphur species bonded to copper (S-Cu), while the red components, at higher BE, correspond to sulphur atoms in not anchored SH groups (physisorbed pseudorotaxane). The large signal at high BE is composed by only two components (purple lines) and it was assigned to sulphate species, probably derived from the tosylate anions. The amount of this signal is high probably because an excess of tosylate is physisorbed on the copper surface. The N 1s region of the spectrum (figure 4.24b) shows the presence of two peaks: one at high BE which was assigned to the N^+ species present in the axle **31**, and one at lower BE attributable to the NH groups of the phenylureas of **25**. The BE of N 1s referenced to the signal of C 1s are 400.0 and 402.3 eV, respectively. The elemental ratios reported in table 4.4 evidences that the calculated C/N and NH/N^+ ratios are in good agreement with theoretical values.

Table 4.4 Elemental ratios of Cu surfaces functionalized with pseudorotaxanes **25⊃31** and **25⊃33** determined through XPS spectroscopy (error ± 10%).

Entry	Designation	C/N (exp)	C/N (theor)	NH/N^+ (exp)	NH/N^+ (theor)	N/Cu (exp)
1	**25⊃31**@Cu	13.7	18.1	3.5	3	1.5
2	**25⊃33**@Cu	11.6	14.5	2.8	3	0.09

The results obtained from the XPS study of the polycrystalline copper surface functionalized with the pseudorotaxane **25⊃33** are depicted in figure 4.24 c and d. Also in this case the deconvoluted of the S 2p signal shows that the amount of anchored pseudorotaxane (figure 4.24c, blue line) is lager than the physisorbed one (figure 4.24c, red line). In the same spectral region is also present a signal attributable to the sulphur specie of the tosylate anions. The deconvolution of the complex signal of the N 1s spectrum (figure 4.24d) shows the presence of three components: an higher BE signal attributable to the N^+ atoms of the axle **33**,

a halfway BE signal attributable to the NH groups of the phenylureas of **25** and a lower BE signal whose origin has not been fully disclosed yet. The BE of N 1s referenced to the signal of C 1s are 398.0, 399.6, and 401.8 eV, respectively. The elemental ratios reported in table 4.4 evidences that the calculated C/N and NH/N^+ ratios are in good agreement with theoretical values.

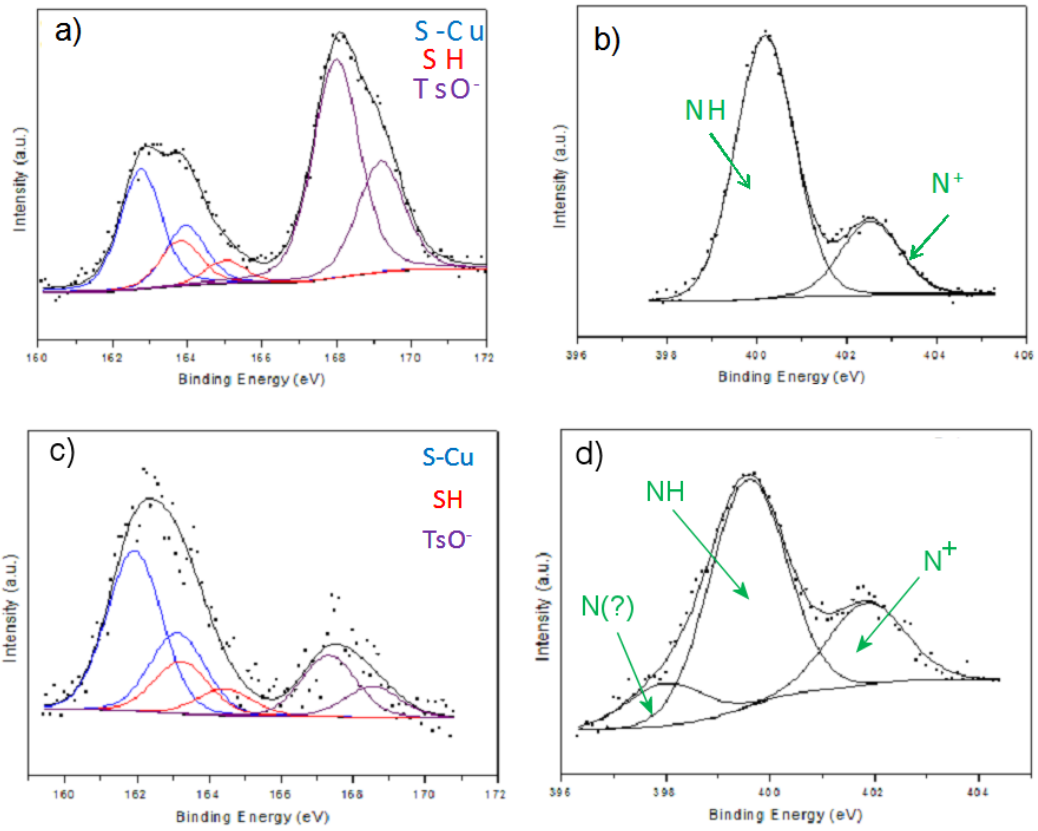

Figure 4.24 XPS spectral regions of the polycrystalline copper surface functionalized with the pseudorotaxane **25⊃31**: a) S 2p region and b) N 1s region and **25⊃33** : c) S 2p region and d) N 1s region.

The comparison of the N/Cu ratios reported in Table 4.4 can be used as an index of the covering degree of each copper surface. The high value calculated for **25⊃31**@Cu, that is 1.5, with respect the very low result obtained with **25⊃33**@Cu can be explained with a higher degree of covalent functionalization of the first surface. Works are in progess to understand which are the factors reducing the covalent anchoring of the pseudorotaxane mixtures.

4.4 Experimental section

All reactions were carried out under nitrogen; all solvents were freshly distilled under nitrogen and stored over molecular sieves for at least 3h prior to use. ^1H and ^{13}C NMR spectra were recorded on BRUKER AC300 instrument operating at 300 and 75 MHZ, respectively. Chemical shifts reported are referred to the tetramethylsilane (TMS) or residual solved

resonances. ESI-MS spectra were recorded with Infusion Waters Acquity Ultra Performance LC instrument. Melting points are uncorrected, and were recorded with Electrothermal instrument in sealed capillars under nitrogen atmosphere. Silica gel layers (SiO_2, MERCK 60 F_{254}) were used for thin layer chromatography (TLC). 60 Å silica gel (MERCK, 0.04-0.063 mm, 230-240 mesh) were used for column chromatography. Compounds **20**,[17] **22**,[18] **25**[19], 1-(hydroxymethyl)-3-phenylurea,[20] 1,6-Bis(toluene-4-sulfonyloxy)hexane[21] and undec-10-enyl 4-methylbenzenesulfonate[22] were synthesised according to reported procedures. The synthesis of *N*-methyl pyridinium iodide (NMPI) and **8**, **10b** and **17** were already reported in previous chapters. All other reagents were of reagent grade quality as obtained from commercial suppliers and were used without further purification.

4.4.1 Synthesis

Calix[4]arene 19: amixture of calix[4]arene **18** (0.2 g, 0.27 mmol), N-bromo succinimide (0.1 g, 0.56 mmol) and catalytic amount of ammonium acetate in methyl ethyl chetone (70 ml) was stirred in the dark at room temperature. Reaction is monitored through TLC (eluent hexane:ethyl acetate 95:5). After 40 minutes dichloromethane (50ml) and acqeous solution satured with N_2SO_3 (50ml) were added. Organic phase was separated and dried over Na_2SO_4. After evaporation of the solvent under reduced pressure, the resulting crude product was purified by column chromatography (silica gel, hexane:ethyl acetate = 95:5) to give **19** as white solid (50%). ^{1}H NMR (300 MHz, $CDCl_3$): δ (ppm) 8.30 (s, 2H), 7.16 (s, 4H), 6.92 (d, 4H, *J* = 7.5 Hz), 6.80 (t, 2H, *J* = 8.1 Hz), 5.9-5.7 (m, 2H), 5.1-4.9 (m, 4H), 4.24 (d, 4H, *J* = 13 Hz), 3.97 (t, 4H, *J* = 6.6 Hz), 3.32 (d, 4H, *J* = 13 Hz), 2.2-2.0 (m, 8H), 1.8-1.6 (m, 4H), 1.5-1.2 (m, 20H); ^{13}C NMR ($CDCl_3$, 75 MHz): δ (ppm) 155.4, 151.9, 139.1, 132.7, 130.6, 130.0, 129.1, 125.4, 114.1, 110.3, 76.8, 33.7, 31.1, 29.9, 29.6, 29.5, 29.4, 29.1, 28.9, 25.8. M.p. 172.5-173.5 °C. MS-ESI (m/z): 909 ($M+Na^+$, 100). Elemental analysis for $C_{50}H_{62}O_4Br_2$, calculated: C, 67.72, H, 6.99; found: C, 67.60, H, 6.92.

17. B. Gadenne, I. Yildiz, M. Amelia, F. Ciesa, A. Secchi, A. Arduini, A. Credi, F. M. Raymo, *J. Mater. Chem.*, **2008**, *18*, 2022
18. S. Oae, H. Togo, Bullettin of the Chemical Society of Japan, **1983**, 56(12), 3813.
19. J. J. Gonzalez, R. Ferdani, E. Albertini, J. M. Blasco, A. Arduini, A. Pochini, P. Prados, J. de Mendoza, *Chem. Eur. J.*, **2000**, *6*, 73.
20. G. Zigeuner, K. Voglar, R. Pitter, *Monatshefte für Chemie*, **1954**, *85*, 1196.
21. V. Pejanovic, V. Piperski, D. Ugljesic-Kilibarda, J. Tasic, M. Dacevic, L. Medic-Mijacevic, E. Gunic, M. Popsavin, V. Popsavin, *European Journal of Medicinal Chemistry*, **2006**, *41*, 503.
22. G. W. Kabalka, M. Varma, R. S. Varma, P. C. Srivastava, F. F. Knapp, *J. Org. Chem.*, **1986**, *51*, 2386.

Calix[4]arene 21: asolution of calix[4]arene **18** (0.5 g, 0.69 mmol) and 1-(hydroxymethyl)-3-phenylurea (0.11 g, 0.66 mmol) in dry CH_2Cl_2 (100ml) was stirred at 0°C for 15 minutes. After this period $AlCl_3$ (0.18 g, 1.35 mmol) was added to the mixture. The reaction was stirred for 30 minutes at 0°C, and then for 2.5h at room temperature. The reaction was monitored through TLC (hexane/ethyl acetate 7/3). After 2.5h reaction was quenched with 100ml of water. The resulting organic phase was separated, washed with water up to neutrality, dried over Na_2SO_4 and evaporated to dryness under reduced pressure. The residue was purified by column chromatography (eluent: hexane/ethyl acetate = 7/3) to afford the pure product **21** as a white solid (45%). ^{1}H NMR (300 MHz, $CDCl_3$): δ (ppm) 8.34 (s, 1H), 8.28 (s, 1H), 7.2-6.8 (m, 12H), 6.65 (t, 4H, *J* = 7.5 Hz), 5.9-5.7 (m, 2H), 5.1-4.9 (m, 4H), 4.4-4.2 (dd, 4H, *J* = 3.5 Hz, *J* = 12.9 Hz), 4.19 (s, 2H), 3.99 (t, 4H, *J* = 6.5 Hz), 3.36 (dd, 4H, *J* = 6.5 Hz, *J* = 12.9 Hz), 2.2-2.0 (m, 8H), 1.8-1.6 (m, 4H), 1.5-1.2 (m, 20H); ^{13}C NMR (75 MHz, $CDCl_3$): δ (ppm) 196.5, 155.9, 153.3, 152.7, 151.8, 139.1, 138.5, 133.4, 133.2, 128.9, 128.8, 128.7, 128.5, 128.4, 128.1, 128.0, 125.2, 123.1, 120.2, 118.9, 114.1, 76.8, 43.9, 33.8, 31.4, 31.3, 30.0, 29.6 (2 resonances), 29.5, 29.2, 28.9, 25.9. M.p. 67.5°C-68.5°C. MS-ESI (m/z): 899 ($M+Na^+$, 100). Elemental analysis for $C_{58}H_{72}N_2O_5$, calculated: C, 79.45; H, 8.21; N, 3.19; found: C, 79.23; H, 8.14; N, 3.16.

Compound 23: pentyl tosylate (2.4 g, 10 mmol) and 4,4'-bipyridile (2 g, 12.5 mmol) were dissolved in CH_3CN (300 ml) and the resulting mixture was refluxed with stirring for 72h. After cooling to room temperature, the solvent was completely evaporated under vacuum. The solid residue was then purified by precipitation from ethyl acetate to affort **23** as a white solid. Yield 75%. ^{1}H NMR (CD_3OD, 300 MHz, ppm): δ 9.08 (d, 2H, J=6.8 Hz), 8.79 (d, 2H, J=5.9 Hz), 8.46 (d, 2H, J=6.7 Hz), 7.96 (d, 2H, J=6.2 Hz), 7.66 (d, 2H, J=8 Hz), 7.19 (d, 2H, J=8 Hz), 4.65 (t, 2H, J=7.6 Hz), 2.33 (s, 3H), 2.2-2.0 (m, 2H), 1.5-1.3 (m, 4H), 0.94 (t, 3H, J=6.6 Hz), ^{13}C NMR (CD_3ODCl_3, 75 MHz, ppm): δ 155.1, 152.1, 146.8, 144.0, 143.9, 142.0, 130.2, 128.5, 127.4, 127.2, 123.8, 63.0, 32.5, 32.4, 29.6, 23.5, 21.6, 14.5. ESI-MS (m/z): 227(M^+, 100). M.p.: 155.5-156.5 °C. Elemental analysis for $C_{22}H_{26}N_2O_3S$, calculated: C, 66.30, H, 7.58, N, 7.03, S, 8.05; found: C, 66.62, H, 7.68, N, 6.91, S, 8.14.

Compound 24: compounds **23** (1.2 g, 3 mmol) and undec-10-enyl 4-methylbenzenesulfonate (1.6 g, 5 mmol) were dissolved in CH_3CN (70 ml). The mixture was heated at 95°C in a sealed tube and stirred for 96h. After this period the solvent was completely removed under vacuum and the white pure solid **24** was obtained by crystallization from CH_3CN. Yield 70%. ^{1}H NMR (DMSO d_6, 300 MHz, ppm): δ 9.38 (d, 4H, J=5.7 Hz), 8.77 (d, 4H, J=6.7 Hz), 7.46

(d, 4H, J=8 Hz), 7.10 (d, 4H, J=8 Hz), 5.9-5.7 (m, 1H), 5.1-4.9 (m, 2H), 4.68 (t, 4H, J=7 Hz), 2.28 (s, 6H), 2.1-1.9 (m, 4H), 1.5-1.2 (m, 18H), 0.88 (t, 3H, J=6.7 Hz), ^{13}C NMR (DMSO d_6, 75 MHz, ppm): δ 148.4, 145.7, 145.6, 138.6, 137.4, 127.9, 126.4, 125.3, 114.5, 60.8, 33.0, 30.6, 30.3, 28.6, 28.3, 28.2, 28.1, 27.4, 25.3, 21.4, 20.6, 13.6. ESI-MS (m/z): 190 (M^{2+}/2, 100). M.p.: 180.5-181.5 °C. Elemental analysis for $C_{40}H_{54}N_2O_6S_2$, calculated: C, 66.45, H, 7.53, N, 3.87, S, 8.87; found: C, 66.82, H, 7.31, N, 3.79, S, 9.02.

Calix[4]arene 26: a solution of calix[4]arene **9b** (1.2 g, 1.4 mmol) and 1-(hydroxymethyl)-3-phenylurea (0.23 g, 1.4mmol) in dry CH_2Cl_2 (100ml) was stirred at 0°C for 15 minutes. After this period $AlCl_3$ (0.37 g, 2.8 mmol) was added to the mixture. The reaction was stirred for 30 minutes at 0°C, and then for 2.5h at room temperature. The reaction was monitored through TLC (hexane/ethyl acetate 7/3). After 2.5h reaction was quenched with 100ml of water. The resulting organic phase was separated, washed with water up to neutrality, dried over Na_2SO_4 and evaporated to dryness under reduced pressure. The residue was purified by column chromatography (eluent: hexane/ethyl acetate = 7/3) to afford the pure product **26** as a white solid (40%). ^{1}H NMR (300 MHz, $CDCl_3$): δ (ppm) 8.33 (s, 1H), 8.27 (s, 1H), 7.3-6.6 (m, 16H), 6.3 (bs, 1H), 4.9 (bt, 1H), 4.4-4.2 (m, 6H), 3.99 (t, 4H, *J* = 6.5 Hz), 3.36 (dd, 4H, *J* = 6.4 Hz, *J* = 12.9 Hz), 2.84 (t, 4H, *J* = 7.2 Hz), 2.30 (s, 6H), 2.2-2.0 (m, 4H), 1.8-1.2 (m, 32H); ^{13}C NMR (75 MHz, $CDCl_3$): δ (ppm) 196.5, 156.1, 153.3, 152.6, 151.9, 138.9, 133.4, 133.3, 129.1, 128.9, 128.7, 128.4, 128.1, 128.0, 125.2, 122.7, 119.7, 119.0, 76.7, 43.9, 31.4, 31.3, 30.4, 30.0, 29.6, 29.5 (2 resonances), 29.2, 28.8, 25.9. M.p. 45.5°C-46.5°C. MS-ESI (m/z): 1051(M+Na^+, 100). Elemental analysis for $C_{62}H_{80}N_2O_7S_2$, calculated: C, 72.37; H, 7.78; N, 2.72; S, 6.22; found: C, 72.10; H, 7.59; N, 2.69; S, 6.06.

Calix[4]arene 27: to a solution of calix[4]arene **26** (0.4 g, 0.39 mmol) in a mixture of CH_3OH : THF 1:1 under argon atmosphere was added CH_3ONa (0.2g, 3.9 mmol), after 15 minutes 1,4-dithioerythrytol (0.36 g, 2.34 mmol) was added. The reaction was stirred at room temperature for 3h. After this period the reaction was quenched with the addiction of activated DOWEX H^+. Then the solution was filtered and dried under reduced pressure. The residue was finally purified through chromatography column (eluent CH_2Cl_2/ethyl acetate 95/5) to obtain product **27** as a white solid (70%). ^{1}H NMR (300 MHz, $CDCl_3$): δ (ppm) 8.32 (s, 1H), 8.25 (s, 1H), 7.3-6.6 (m, 16H), 6.2 (bs, 1H), 4.9 (bt, 1H), 4.4-4.2 (m, 6H), 3.99 (t, 4H, *J* = 6.5 Hz), 3.36 (dd, 4H, *J* = 6.4 Hz, *J* = 12.9 Hz), 2.51 (m, 4H), 2.2-2.0 (m, 4H), 1.8-1.2 (m, 16H); ^{13}C NMR (75 MHz, $CDCl_3$): δ (ppm) 155.6, 153.3, 152.7, 151.9, 138.4, 133.4, 133.2, 129.0, 128.9, 128.7, 128.5, 128.4, 128.1, 128.0, 125.1, 123.5, 120.6, 119.0, 76.7, 44.1, 34.0, 31.4,

31.3, 29.9, 29.6 (2 resonances), 29.5, 29.4, 29.1, 28.3, 25.9, 24.6. M.p. 67.5°C-68.5°C. MS-ESI (m/z): 967 ($M+Na^+$, 100). Elemental analysis for $C_{58}H_{76}N_2O_5S_2$, calculated: C, 73.72; H, 8.05; N, 2.97; S, 6.78; found: C, 73.53; H, 8.30; N, 2.86; S, 6.71.

Compound 28: 1,6-Bis(toluene-4-sulfonyloxy)hexane (10 g, 24 mmol), 2,4-di-*tert*-butylphenol (4.4 g, 24 mmol) and K_2CO_3 (3.2 g, 24 mmol) in CH_3CN (200 ml) were heated and stirred at reflux for 48h. After this period the solvent was completely evaporated under vacuum and the solid residue was taken up with CH_2Cl_2 and H_2O. The separated organic layer was then washed with H_2O, dried over Na_2SO_4, and evaporated to dryness. The pure product **28** was obtained by chromatography column (silica gel, hexane 70%-ethyl acetate 30%) as a white solid (yield 85%). ^1H NMR ($CDCl_3$, 300 MHz, ppm): δ 7.79 (d, 2H, J=8.3 Hz), 7.33 (d, 2H, J=8.3 Hz), 7.01 (t, 1H, J=1.5 Hz), 6.73 (d, 2H, J=1.5 Hz), 4.04 (t, 2H, J=6.4 Hz), 3.92 (t, 2H, J=6.4 Hz), 1.8-1.6 (m, 4H), 1.5-1.3 (m, 4H), 1.30 (s, 18H). ^{13}C NMR ($CDCl_3$, 75 MHz, ppm): δ 152.1, 129.7, 127.8, 114.8, 108.7, 70.5, 67.3, 34.9, 31.4, 28.7, 29.2, 25.5, 25.1, ESI-MS (m/z): 473 ($M+Na^+$, 100). M.p.: 79-80 °C. Elemental analysis for $C_{27}H_{40}O_4S$, calculated : C, 70.39, H, 8.75, S, 6.96; found: C, 70.77, H, 8.42, S, 7.22.

Compound 29: compound **28** (5.5 g, 12.5 mmol) and 4,4'-bipyridile (2 g, 12.5 mmol) were dissolved in CH_3CN (300 ml) and the resulting mixture was refluxed with stirring for 72h. After cooling to room temperature, the solvent was completely evaporated under vacuum. The solid residue was then purified by precipitation from ethyl acetate to affor **29** as a white sticky solid. Yield 65%. ^1H NMR ($CDCl_3$, 300 MHz, ppm): δ 9.21 (d, 2H, J=6.5 Hz), 8.73 (d, 2H, J=5.4 Hz), 8.18 (d, 2H, J=6.5 Hz), 7.73 (d, 2H, J=8 Hz), 7.55 (d, 2H, J=8 Hz), 7.08 (d, 2H, J=8 Hz), 6.99 (t, 1H, J=1.5 Hz), 6.70 (d, 2H, J=1.5 Hz), 4.75 (t, 2H, J=6 Hz), 3.87 (t, 2H, J=6 Hz), 2.25 (s, 3H), 2.0-1.9 (m, 2H), 1.7-1.6 (m, 2H), 1.5-1.4 (m, 2H), 1.28 (s, 20H), ^{13}C NMR ($CDCl_3$, 75 MHz, ppm): δ 158.4, 153.1, 152.1, 151.2, 150.6, 145.7, 143.5, 140.9, 139.4, 128.7, 125.8, 125.6, 121.4, 114.8, 108.6, 67.0, 61.5, 34.9, 31.4, 31.1, 29.5, 25.6, 25.4, 21.2, ESI-MS (m/z): 445(M^+, 100). M.p.: 59-60 °C. Elemental analysis for $C_{37}H_{48}N_2O_4S$, calculated: C, 72.04, H, 8.11, N, 4.24, S, 4.89; found: C, 71.84, H, 7.84, N, 4.54, S, 5.20.

Compound 30: compounds **29** (2 g, 3.3 mmol) and **8** (1.4 g, 3.3 mmol) were dissolved in CH_3CN (70 ml). The mixture was heated and stirred at 95°C in a sealed tube for 72h. After this period the solvent was completely eliminated under vacuum and the white pure solid **30** was obtained by crystallization from CH_3CN. Yield 50%. ^1H NMR (CD_3OD, 300 MHz, ppm): δ 9.27 (dd, 4H, J_1=2 Hz J_2=4.8 Hz), 8.66 (d, 4H, J=6.6 Hz), 7.70 (d, 4H, J=8 Hz), 7.23 (d, 4H, J=8 Hz), 7.03 (t, 1H, J=1.5 Hz), 6.70 (d, 2H, J=1.5 Hz), 4.75 (q, 4H, J=7 Hz), 3.99 (t,

2H, J=6 Hz), 2.86 (t, 2H, J=7 Hz), 2.38 (s, 6H), 2.31 (s, 3H), 2.2-2.0 (m, 4H), 1.9-1.7(m, 2H), 1.7-1.3(m, 38H). ^{13}C NMR ($CDCl_3$, 75 MHz, ppm): δ 158.5, 152.0, 148.7, 146.1, 143.3, 139.6, 128.8, 127.3, 125.7, 114.8, 108.6, 67.2, 61.9, 34.9, 31.4, 30.6, 29.4, 29.3, 29.2, 29.0, 28.9, 28.7, 26.0, 25.9, 25.5, 21.2. ESI-MS (m/z): 674 (M^+, 30), 337 (M^{2+}/2, 100). M.p.: 160-162 °C. Elemental analysis for $C_{57}H_{80}N_2O_8S_3$, calculated: C, 67.23, H, 8.65, N, 2.75, S, 9.45; found: C, 67.55, H, 8.53, N, 2.99, S, 9.10.

Compound 31: compound **30** (2 g, 2 mmol) was dissolved in EtOH (150 ml), then a solution of toluene-4-sulfonic acid (0.5 g, 2.5 mmol) in EtOH was added and the resulting mixture was heated at reflux and stirred for 72h. The solvent was evaporated under vacuum and the pure white product **31** was obtained by precipitation from ethyl acetate. Yield 70%. ^{1}H NMR ($CDCl_3$, 300 MHz, ppm): δ 9.21 (d, 4H, J=4.8 Hz), 8.79(d, 4H, J=6.6 Hz), 7.70 (d, 4H, J=8 Hz), 7.10(d, 4H, J=8 Hz), 6.71(d, 2H, J=1.5 Hz), 6.99 (t, 1H, J=1.5 Hz), 4.61 (q, 4H, J=7 Hz), 3.85 (t, 2H, J=6 Hz), 2.6-2.4 (m, 2H), 2.26 (s, 6H), 1.9-1.8 (m, 4H), 1.7-1.5(m, 4H), 1.5-1.0 (m, 36H). ^{13}C NMR ($CDCl_3$, 75 MHz, ppm): δ 158.5. 152.1, 148.7, 145.8, 143.3, 139.6, 128.9, 127.3, 125.7, 114.8, 108.7, 67.2, 61.9, 34.9, 29.6, 29.4, 29.1, 29.0, 28.9, 28.7, 26.0, 25.9, 25.7, 25.5, 21.2. ESI-MS (m/z): 632 (M^+, 50), 316 (M^{2+}/2, 100). M.p.: 189-191 °C. Elemental analysis for $C_{55}H_{78}N_2O_7S_3$, calculated: C, 67.72, H, 8.06, N, 2.90, S, 9.86; found: C, 67.91, H, 7.85, N, 3.18, S, 10.13.

Compound 32: compounds **23** (1.2 g, 3 mmol) and **8** (1.84 g, 5 mmol) were dissolved in CH_3CN (70 ml). The mixture was heated at 95°C in a sealed tube and stirred for 72h. After this period the solvent was completely eliminated under vacuum and the white pure solid **32** was obtained by crystallization from CH_3CN. Yield 65%. ^{1}H NMR (DMSO d_6, 300 MHz, ppm): δ 9.38 (d, 4H, J=5.7 Hz), 8.77 (d, 4H, J=6.7 Hz), 7.46 (d, 4H, J=8 Hz), 7.10 (d, 4H, J=8 Hz), 4.68 (t, 4H, J=7 Hz), 2.80 (t, 2H, J=7.2 Hz), 2.31 (s, 3H), 2.28 (s, 6H), 2.1-1.9 (m, 4H), 1.6-1.2 (m, 20H), 0.88 (t, 3H, J=6.7 Hz), ^{13}C NMR (DMSO d_6, 75 MHz, ppm): δ 195.1, 148.3, 145.6, 145.5, 137.5, 127.9, 126.4, 125.3, 60.7, 33.2, 30.7, 30.4, 30.3, 29.0, 28.7, 28.6, 28.4, 28.3, 28.2, 28.0, 27.6, 27.4, 25.3, 23.6, 21.4, 20.6, 13.6. ESI-MS (m/z): 228 (M^{2+}/2, 100). M.p.: 145.0-146.0 °C. Elemental analysis for $C_{42}H_{58}N_2O_7S_3$, calculated: C, 63.13, H, 7.32, N, 3.51, S, 12.04; found: C, 63.07, H, 7.12, N, 3.44, S, 11.87.

Compound 33: compound **32** (1.6 g, 2 mmol) was dissolved in EtOH (150 ml), then a solution of toluene-4-sulfonic acid (0.5 g, 2.5 mmol) in EtOH was added and the resulting mixture was heated at reflux and stirred for 72h. The solvent was evaporated under vacuum and the pure white product **33** was obtained by precipitation from ethyl acetate. Yield 70%.

^{1}H NMR ($CDCl_3$, 300 MHz, ppm): δ 9.19 (d, 4H, J=6.3 Hz), 8.85 (d, 4H, J=6 Hz), 7.74 (d, 4H, J=8.1 Hz), 7.16 (d, 4H, J=7.9 Hz), 4.65 (bt, 4H), 2.5 (m, 2H), 2.33 (s, 6H), 2.0-1.8 (m, 4H), 1.7-1.5 (m, 2H), 1.5-1.1 (m, 18H), 0.85 (t, 3H, J=6.7 Hz), ^{13}C NMR (CD_3OD, 75 MHz, ppm): δ 151.5, 147.3, 144.0, 142.0, 130.2, 128.6, 127.2, 63.5, 40.0, 35.5, 32.9, 32.5, 30.9 (2 resonances), 30.8, 30.6, 30.5, 29.7 (2 resonances), 29.6, 27.5, 25.2, 23.5, 21.6, 14.5. ESI-MS (m/z): 207 (M^{2+}/2, 100). M.p.: 236.0-237.0 °C. Elemental analysis for $C_{40}H_{56}N_2O_6S_3$, calculated: C, 63.46, H, 7.46, N, 3.70, S, 12.71; found: C, 63.32, H, 7.51, N, 3.60, S, 12.46.

General procedure for the synthesis of psudorotaxane

To a stirred solution of calixarene **25** (0.01g, 0.007mmol) in toluene (10 ml), were added an excess of desired axle (0.015mmol). In few minutes the colour of solution changes to orange-red. The mixture was stirred at room temperature for 30 minutes. After this period the solution was filter and the solvent was evaporated. The pseudorotaxane obtained was used without any further purification.

4.4.2 2D SAMs analysis

AFM mesurements

Mesurements were conducted in UHV, "non-contact" conditions, with a VT-STM/AFM microscope purchased from Omicron Nanotechnology. This apparatus was a part of the XPS-AFM/STM e PEEM system. Since the images obtained with this instrument are three-dimensional mapping of the surface analysed, the most important data for AFM mesurements is the thikness distributions (Z coordinate) of points (pixels) that compose each acquired region.

XPS mesurements

Si(100) surface

Hybrid systems are produced via photochemical functionalization. The photochemical approach is considered to be the mildest for functionalization of H-terminated Si surfaces via hydrosilylation reactions of terminal alkenes and alkynes. H-Si is prepared following wet chemistry procedure. Silicon wafers were cut in sample of 1 cm^2 approximate areas. Samples were first washed in boiling 1,1,2-trichlorethane for 10 min and subsequently in ethanol at room temperature, with sonication for 5". Then were oxidized in H_2O_2/HCl/H2O (2:1:8) at 353 K for 15", rinsed copiously with ultra-pure de-ionized water (Water PLUS). These solutions are used to clean surface from organic and metallic contaminations. Si wafers were etched with 10% aqueous HF for 10" thoroughly purging the solution with dry N_2 in order to

keep the solution deoxygenated. After samples were rinsed with water again, dried under a stream of dry N_2 and immediately used in the functionalization process. The opportune calixarene or pseudorotaxane was dissolved in toluene (10 mM concentration for calixarene, 5 mM concentration for pseudorotaxane instead). H-Si is dipped in the molecular solution previously deoxygenated through 3 freezing-pumping-annealing cycles and kept under dinitrogen N_2, to preserve silicon from surface oxidation. The sample is subjected to a 35 mW/cm^2 visible irradiation for 4 h from a quartz-iodine lamp. Then it is rinsed with dichloromethane for 2x5', with sonication, to eliminate physisorbed molecules. Care has been taken in order to reduce all sources of O_2 and H_2O contamination in the preparation steps.

Polycrystalline Cu surface

The preliminary cleaning of polycrystalline Cu (Cu 99.99%) plate (18x15x1 mm^3) was performed through this steps:

1) 15' sonicated in acetone, to eliminate organic contaminations;
2) 30" HNO_3 (32.5%), to oxidize surface and eliminate eventually adsorbed species;
3) 2x5" in distilled water;
4) 30" in HCl (3.7%), to dissolve oxides;
5) 3'30" in distilled water;
6) 30" in acetone.

Successively the opportune calixarene or pseudorotaxane were dissolved in toluene (0.2 mM concentration for calixarene, 0.4 mM concentration for pseudorotaxane instead). Cu plate is dipped in molecular solution at room temperature for controlled time (4 hours). Functionalized sample is rinsed with toluene for 2x5', with sonication, to eliminate physisorbed molecules, and dried under a stream of dry N_2. Concentration and immersion time were optimized in order to obtain a monolayer coverage and to limit physisorption and copper oxidation at the same time.

The Author

Luca Pescatori was born in Parma (Italy) on the 25th of March 1982. In 2001 he obtained his diploma in food technologies at the ITIS "Leonardo da Vinci" in Parma. In July 2006, he graduated in Chemistry, at the Department of Organic and Industrial Chemistry of the University of Parma, under the supervision of Dr. Andrea Secchi and Prof. Andrea Pochini with a thesis entitled "Synthesis of anionic receptors as organic monolayers for the preparation of gold nanoparticles". In January 2007, he started a Ph.D. research project at the Department of Organic and Industrial Chemistry of the University of Parma, under the supervision of Dr. Andrea Secchi. During this period, he joined as Ph.D. Visiting student, for three months the group of Prof. Zanoni and for two months to the group of Prof. Dallacort, both at the Department of Chemistry of the University "La Sapienza" in Rome (Italy). The results of the research conducted during the period 2007-2009 are described in this thesis.

Acknowledgements

Finalmente!!!!!!!

Ringrazio tutti coloro che hanno permesso la realizzazione di questo lavoro di tesi e che mi hanno sopportato ma soprattutto aiutato durante tutto questo tempo trascorso nel Laboratorio 49. Un sincero grazie al Dr. Andrea Secchi, Prof. Andrea Pochini ed al Prof. Arturo Arduini. Senza di voi e soprattutto te Andrea non avrei imparato tutto ciò che conosco ora. Grazie a voi questa è stata una esperienza fondamentale per la mia crescita professionale.

Ringrazio anche tutti coloro che con la loro intensa collaborazione hanno contribuito alla realizzazione di questo lavoro di tesi: il Prof. Zanoni, la Dottoressa Alice Boccia, la Professoressa Di Castro e la Dottoressa Valeria Lanzillotto, del dipartimento di chimica dell'Università La Sapienza di Roma… grazie ancora per tutto il lavoro svolto, per gli eccellenti risultati ottenuti e per avermi ospitato presso di voi. Un sincero grazie anche alla Prof.sa Dallacort, al Prof Mandolini (Università La Sapienza) e tutto il team per avermi cordialmente ospitato presso il loro laboratorio durante il mio periodo di tesi.

Ringrazio inoltre il Prof. Ugozzoli e la Dr. Massera per l'eccellente lavoro svolto nella risoluzione di tutti i cristalli da me inviatogli.

Un eterno grazie è per Mamma e Papà con tanto tantissimo affetto e riconoscenza. Finalmente sono riuscito a concludere tutto questo lungo percorso… sperò possiate essere orgogliosi di me! Ringrazio anche il resto della famiglia, Caterina, Lisa, Fabrizio e anche per te nonna...un bacione!

Eli, GRAZIE INFINITAMENTE per ogni cosa!!! Senza di te non avrei potuto fare niente di tutto ciò che sono riuscito a realizzare. Sei stata accanto a me in ogni momento, e mi hai sempre donato un immenso affetto, tantissimo supporto e incoraggiamento. Hai sopportato con me la lunga distanza e mi hai regalato sempre un grande sorriso nei momenti difficili. Grazie per tutte le cose che hai detto e fatto per rendermi una persona migliore e per aver, in fin dei conti, sempre creduto in me. Grazie a te ho imparato a vivere, e voglio che questo splendido cammino iniziato più di 5 anni fa, continui sempre assieme a te…

Ora posso passare ai ringraziamenti di tutti coloro mi hanno trascorso con me parte del tempo passato nel LAB. 49: Rocco in primis (quante ne abbiamo sparate!), Cristina (mi raccomando… fai sempre il contrario di tutto ciò che ti dico, lo sai che ogni molecola ha la sua storia… come le nanoparticelle del resto!), Federica (mi raccomando impara bene da Rocco), Mara, Dany, Mary, Mirella, Daniele, Federico (Giunta), Emiliano, Davide, Jessica, e gli ormai non più presenti, Mister Ciesa, Fabio Rosati, il Chiarissimo Faimani, il mitici Fra Davide (che noia sarebbe stata senza di voi e il calcetto infrasettimanale). Ringrazio i vicini di laboratorio del LAB 48 (Marti docet!), e LAB 50 (Ac, Alle e Alex).

Ringrazio infine anche tutti gli amici di ormai lunga data di Madregolo city: Fruttolo, Rizza, Sommi, Alle, Alex, Denti, Gubbo, Marina, Luca, Francesca e tutto il resto della ciurma che non ho nominato.

Se ho dimenticato qualcuno lo ringrazio ora: GRAZIE A TUTTI!!!!!!!!